

JAERI-M  
9 4 2 1

ANNUAL REPORT OF THE FUSION RESEARCH  
AND DEVELOPMENT CENTER FOR THE PERIOD  
OF APRIL 1, 1979 TO MARCH 31, 1980

March 1981

Fusion Research and Development Center

日 本 原 子 力 研 究 所  
Japan Atomic Energy Research Institute

この報告書は、日本原子力研究所が JAERI-M レポートとして、不定期に刊行している研究報告書です。入手、複製などのお問い合わせは、日本原子力研究所技術情報部（茨城県那珂郡東海村）あて、お申しこしください。

JAERI-M reports, issued irregularly, describe the results of research works carried out in JAERI. Inquiries about the availability of reports and their reproduction should be addressed to Division of Technical Information, Japan Atomic Energy Research Institute, Tokai-mura, Naka-gun, Ibaraki-ken, Japan.

Annual Report  
of  
the Fusion Research and Development Center  
for the period of April 1, 1979 to March 31, 1980

Fusion Research and Development Center

Tokai Research Establishment, JAERI

(Received March 12, 1981)

Research and development activities of the Fusion Research and Development Center (Division of Thermonuclear Fusion Research and Division of Large Tokamak Development) from April 1979 to March 1980 are described.

In Plasma physics research two experiments both related to radio-frequency power injection into tokamak plasmas are to be noted. One is the demonstration of current drive by lower hybrid waves in JFT-2 and the other high efficiency ICRF heating at two-ion hybrid resonance in JFT-2a/DIVA. A multi-MW neutral beam injection system was installed and tested at JFT-2 with heating experiments expected to start shortly. JFT-2a/DIVA was shutdown to make space for the injector. A new ingredient in this area is the initiation of deuterium plasma experiments in Doublet III at San Diego, USA by JAERI team under US-Japan cooperation agreement. Progress was rapid achieving all experimental objectives planned for this period. In theoretical area emphasis was placed on high beta tokamak plasmas. Development of the TRITON computer code system is in progress.

Construction of JT-60 is in progress as planned. Major components of the device were ordered by the end of this period. A Mukoyama site where JT-60 and other new facilities will be located was procured in October 1979, which was followed by the construction starts of JT-60 buildings. The completion of JT-60 is expected in fall 1984. A design study of JFT-2M was carried out. The device is a modification of JFT-2, whose main objective is experimental studies of advanced concepts in tokamak research.

In heating technology efforts are focussed on the development of

neutral beam and radiofrequency heating systems for JT-60. In the former area three injector test stands were fully utilized for the above purpose. A notable achievement is the demonstration of high power hydrogen ion beam at 65 keV, 4 A and 30 sec with a maximum output energy of 7.8 MJ. In the latter area the improvement of plasma-wave couplers were pursued together with a heating experiment in JFT-2. Design studies of JT-60 and JT-60 prototype heating systems are in progress.

In superconducting magnet technology a major development is the installation of the cluster testing facility with two 1.5 m diameter NbTi field coils. In conjunction with the IEA LCT agreement a JAERI's LCT coil was ordered together with its test facility to be used before its shipment to ORNL.

In tritium technology development experiments were carried out on basic technologies using hydrogen and deuterium. A simulation study of a reactor tritium facility and a design study of a tritium handling facility were conducted.

In surface technology hydrogen and helium bombardment studies on low Z materials and Mo were made as well as plasma-wall interaction studies in JFT-2. In association with the JT-60 program studies of low Z first wall of JT-60 were initiated and test facilities JVX were ordered.

Activities in reactor design studies were shifted from those on JXFR and PETF to INTOR studies, which is an international joint studies under the auspice of IAEA. Its first stage called the Phase Zero was completed.

Keywords: Annual Report, Plasma Confinement, Plasma Physics, JFT-2 Tokamak, JFT-2a(DIVA) Tokamak, Diagnostics, Neutral Beam Injector, RF Heating, Surface Study, Superconducting Magnet, Reactor Design, JT-60 Tokamak, Doublet III, Impurity Emission, Tritium Production, INTOR.



核融合研究開発推進センター年報（昭和 54 年度）

日本原子力研究所 東海研究所  
核融合研究開発推進センター

（1981 年 3 月 12 日受理）

核融合研究開発推進センター（核融合研究部および大型トカマク開発部）における研究開発の現況とその成果をとりまとめた。<sup>\*</sup>概要は次のとおりである。

プラズマ物理の研究において、トカマク・プラズマへの高周波電力入射に関連した 2 つの実験が注目される。ひとつは JFT-2 における低域ハイブリッド波（LHW）によるプラズマ電流駆動の実証であり、他のひとつは、JFT-2 a/DIVA における 2 種イオン・ハイブリッド共鳴における高い効率の ICRF 加熱である。JFT-2 における MW 級の中性粒子入射装置の組立てと試験が完了しており、加熱実験は近い将来に開始の予定である。この入射装置の設置用スペースを確保するために JFT-2 a/DIVA の研究を終了した。この分野における新しい要素は、日米核融合研究協力協定のもとで、JAERI チームによる米国・サンディエゴのダブレット III における D 型プラズマの実験が始まったことである。この期間における進歩は急速であり、当初予定の目標はすべて達成された。

JT-60 の建設は計画どおり進行している。本年度の終りまでに、JT-60 の主要設備が発注された。JT-60 および他の核融合研究施設が設置される向山サイトは 10 月に入手され、続いて JT-60 各建家の建設が始まった。JT-60 の完成は、1984 年秋を予定している。JFT-2 M の設計研究が進展している。この装置は、JFT-2 の改造であり、その主な目的はトカマク研究における新しい概念に関する実験的研究である。

加熱技術では、JT-60 のための中性粒子入射加熱装置および高周波加熱装置の開発に集中して努力が払われている。前者の面では、3 台の入射テストスタンドが上記目的のために駆使されている。注目すべき成果は、7.8 MJ の最大出力エネルギーを持ち、65 keV、4 A、30 秒という高出力の水素イオンビームを実現したことである。後者の面では、プラズマと高周波の結合系の改良研究が、JFT-2 における加熱実験と共に引き続き行なわれた。JT-60 加熱装置および JT-60 加熱装置および JT-60 加熱装置原型ユニットの設計研究が進められた。

超電導磁石の技術における主な開発は、直径 1.5 m の 2 個のニオブ・チタンコイルを有するク

---

<sup>\*</sup> 既刊されている年報は、昭和 45 年度以降、それぞれ JAERI-M 4654, 5029, 5564, 5888, 6359, 6926, 7479, 8059 および 8661 である。

ラスター・テスト装置の据付である。一方、国際エネルギー機関（IEA）のLCT協定に関連して、原研のLCTコイルおよびオークリッジ国立研究所（ORNL）への発送の前に用いる国内試験装置の発注を行った。

トリチウム技術の開発においては、水素および重水素を用いた基礎技術に関する実験が行なわれた。核融合炉のトリチウム施設のシミュレーション研究およびトリチウム取扱施設の設計研究が行なわれた。

表面技術においては、低Z材およびモリブデンに関して水素およびヘリウムの照射研究およびJFT-2におけるプラズマ-壁相互作用の研究が行なわれた。JT-60計画に関連して、JT-60の低Z材の第1壁の研究が開始され、試験装置JVXが発注された。

核融合炉設計研究における活動は、JXFRおよびPETRの研究に関する活動から、国際原子力機関（IAEA）の傘下における国際共同研究であるINTORの活動に主力を移行させた。

## CONTENTS

|   |     |
|---|-----|
| PREFACE .....   | xix |
| I. PLASMA THEORY AND COMPUTATION .....  | 1   |
| 1. Introduction .....   | 1   |
| 2. Stability and Transport .....  | 1   |
| 2.1 Evolution of stable high beta tokamak equilibria .....  | 1   |
| 2.2 Beta-limit of large tokamaks .....  | 1   |
| 2.3 Anomalous ion loss due to low-frequency instabilities .....   | 2   |
| 2.4 Toroidal effects on nonlocal collisionless drift<br>instability .....   | 2   |
| 2.5 A scaling law for high density tokamaks and its<br>application to J.I.P.P. T-II device .....  | 2   |
| 2.6 Critical conditions for drift, drift-Alfvén and drift-<br>tearing instabilities of finite- $\beta$ plasma in shered<br>magnetic field ..... | 3   |
| 2.7 Radio-frequency flux control of toroidal plasma .....   | 3   |
| 2.8 Spatial structure of toroidal drift instability .....   | 3   |
| 3. Computing .....  | 6   |
| 3.1 Particle simulation of scrape-off layer .....   | 6   |
| 3.2 Nonlinear Monte Carlo simulation for NBI heating .....  | 6   |
| 3.3 Numerical study on multichannel MEM .....   | 7   |
| 4. TRITON .....   | 8   |
| 4.1 Introduction .....  | 8   |
| 4.2 Convergence of solutions of the MHD stability code ERATO ..   | 8   |
| 4.3 Optimization of the ERATO code with respect to I/O<br>operations and for an array processor .....   | 8   |
| 4.4 Two-dimensional tokamak code APOLLO .....   | 9   |
| 4.5 Finite-n and $\omega_*$ corrections on ballooning mode .....  | 9   |
| 4.6 High-speed numerical code AEOLUS-R1 for resistive MHD<br>instability with single helicity .....   | 10  |
| 4.7 Numerical code AEOLUS-P for the analysis of positional<br>instability .....   | 10  |
| 4.8 Graphic I/O subsystem ARGUS-V2 .....  | 11  |
| 4.9 Supervisor of the TRITON system and utility code<br>packages .....  | 12  |

|  |    |
|--|----|
| II. TOROIDAL CONFINEMENT EXPERIMENT .....  | 16 |
| 1. Introduction .....  | 16 |
| 2. JFT-2 .....   | 16 |
| 2.1 Modified JFT-2 tokamak and plasma position control .....   | 16 |
| 2.2 Lower hybrid heating .....   | 18 |
| 2.3 Observation of the RF-driven current by the lower<br>hybrid wave .....                                       | 20 |
| 2.4 High power density heating experiment .....  | 22 |
| 2.5 Summary .....  | 23 |
| 3. JFT-2a .....  | 33 |
| 3.1 ICRF heating experiment .....  | 33 |
| 3.1.1 Majority and minority heatings .....   | 33 |
| 3.1.2 Increase of the heating efficiency .....   | 35 |
| 3.1.3 Power balance in the optimum heating conditions .....  | 36 |
| 3.2 Carbon limiter and wall experiment .....   | 42 |
| 3.2.1 Sputtering characteristics of carbon surfaces .....  | 42 |
| 3.2.2 Properties of obtained C-wall .....  | 43 |
| 3.2.3 Low-q discharges in C-wall .....   | 43 |
| 3.3 Role of runaway electrons in the formation of arcing<br>on the electrically isolated target in tokamak ..... | 49 |
| 4. JFT-2M .....  | 53 |
| III. OPERATION AND MAINTENANCE .....   | 55 |
| 1. Introduction .....  | 55 |
| 2. Operation and Maintenance .....   | 55 |
| 3. Development of Equipment and Instrument .....   | 55 |
| IV. JOINT EXPERIMENTS IN DOUBLET III .....   | 62 |
| 1. Joint Program .....   | 62 |
| 2. Experimental Results .....  | 63 |
| V. DEVELOPMENT OF PLASMA HEATING SYSTEM .....  | 70 |
| 1. Introduction .....  | 70 |
| 2. Neutral Beam Injection System .....   | 70 |
| 2.1 Ion source development .....   | 70 |
| 2.1.1 Long pulse beam extraction .....   | 70 |

|       |   |     |
|-------|---|-----|
| 2.1.2 | Impurity measurement .....  | 71  |
| 2.1.3 | Beam focusing by aperture displacement .....  | 72  |
| 2.1.4 | Lambdatron ion source .....   | 72  |
| 2.1.5 | Coaxial DuoPIGatron ion source .....  | 73  |
| 2.1.6 | Hollow cathode .....  | 74  |
| 2.2   | Development of the JT-60 neutral beam injection system ....   | 84  |
| 2.3   | The neutral beam injection system for the JFT-2 .....   | 88  |
| 2.3.1 | DuoPIGatron ion source for JFT-2 neutral beam<br>injector .....   | 88  |
| 2.3.2 | Beam line .....   | 88  |
| 2.3.3 | Power supply system .....   | 89  |
| 3.    | Radiofrequency Heating System .....   | 92  |
| 3.1   | Development of waveguide coupler .....  | 92  |
| 3.2   | Lower hybrid heating system in JT-60 .....  | 95  |
| 3.2.1 | Introduction .....  | 95  |
| 3.2.2 | The oscillation excited amplifier .....   | 95  |
| 3.2.3 | High power klystrons .....  | 96  |
| 3.2.4 | Controlling system .....  | 97  |
| VI.   | SURFACE SCIENCE AND VACUUM TECHNOLOGY .....   | 104 |
| 1.    | Introduction .....  | 104 |
| 2.    | Instrumental Development .....  | 105 |
| 2.1   | Construction of medium energy sputtering testing<br>accelerator with high current, light ion source ..... | 105 |
| 3.    | Sputtering Experiments with Low Energy Hydrogen Ions .....  | 105 |
| 3.1   | Chemical sputtering of various types of carbon .....  | 105 |
| 3.2   | Total erosion of SiC coatings on molybdenum .....   | 106 |
| 4.    | Surface Erosion Experiments with High Energy Helium Ions .....  | 107 |
| 5.    | Unipolar Arcs in JFT-2 Tokamak .....  | 108 |
| 6.    | Particle Induced Desorption from Molybdenum by Low<br>Energy Hydrogen Ions .....                          | 109 |
| 7.    | Some Considerations on Helium Pumping by Cryopumps .....  | 109 |
| VII.  | SUPERCONDUCTING MAGNET DEVELOPMENT .....  | 118 |
| 1.    | Introduction .....  | 118 |
| 2.    | Cluster Test Program .....  | 118 |

|  |     |
|--|-----|
| 2.1 Construction of cluster test facility .....                | 118 |
| 2.2 Test module coil .....                                     | 119 |
| 3. Large Coil Task of IEA .....                                | 123 |
| 3.1 LCT coil .....   | 123 |
| 3.1.1 Design concept .....                                     | 123 |
| 3.1.2 Conductor design and development .....                   | 123 |
| 3.1.3 Stress analysis and verification .....                   | 124 |
| 3.1.4 Coil protection .....                                    | 125 |
| 3.2 Domestic test facility .....                               | 126 |
| 4. High Field Superconducting Magnet Development .....         | 134 |
| 5. Pulse Field Magnet Development .....                        | 136 |
| VIII. TRITIUM .....  | 139 |
| 1. Development of Tritium Process Technology .....             | 139 |
| 1.1 Gas chromatographic measurement of hydrogen isotopes ..... | 139 |
| 1.2 Hydrogen recovery experiment .....                         | 139 |
| 1.3 System analysis .....                                      | 140 |
| 2. A Conceptual Design of Tritium Handling Facility .....      | 146 |
| 2.1 Introduction .....   | 146 |
| 2.2 Multiple barrier containment systems .....                 | 147 |
| 2.3 The other systems .....                                    | 149 |
| IX. DESIGN STUDY OF FUSION REACTOR SYSTEM .....                | 153 |
| 1. Introduction .....  | 153 |
| 2. Preliminary Design of JXFR .....                            | 153 |
| 3. Design of Repair and Maintenance .....                      | 153 |
| 4. Design Study of a Fusion Power Reactor .....                | 154 |
| 5. Development of Design Techniques .....                      | 154 |
| 5.1 Plasma design .....  | 154 |
| 5.2 Nuclear design .....                                       | 155 |
| X. DEVELOPMENT OF LARGE TOKAMAK — JT-60 .....                  | 159 |
| 1. Introduction .....  | 159 |
| 2. Outline of the Progress of JT-60 .....                      | 159 |
| 3. Status of Tokamak Machine .....                             | 168 |

|        |   |     |
|--------|---|-----|
| 3.1    | Time schedule and major activity .....  | 168 |
| 3.2    | Status of machine components .....  | 169 |
| 3.2.1  | Vacuum vessel .....   | 169 |
| 3.2.2  | First wall .....  | 170 |
| 3.2.3  | Toroidal field coils .....  | 171 |
| 3.2.4  | Poloidal field coils .....  | 172 |
| 3.2.5  | Support structures .....  | 174 |
| 3.2.6  | Vacuum pumping system .....   | 174 |
| 3.2.7  | Primary cooling system .....  | 176 |
| 3.2.8  | Fast movable limiter .....  | 176 |
| 3.2.9  | Adjustable movable limiter .....  | 176 |
| 3.2.10 | Gas feed system .....   | 177 |
| 3.2.11 | Preionization system .....  | 177 |
| 3.2.12 | Machine control system .....  | 177 |
| 3.3    | Related studies .....   | 177 |
| 3.3.1  | Dynamic response analysis of the vacuum vessel .....                              | 177 |
| 3.3.2  | Studies of eddy currents induced on the vacuum<br>vessel .....                    | 178 |
| 3.3.3  | Wire type strain gauge under high temperatures<br>and strong magnetic field ..... | 179 |
| 4.     | Status of Power Supplies .....  | 195 |
| 4.1    | Poloidal Field Power Supply .....   | 195 |
| 4.2    | Toroidal Field Power Supply .....   | 196 |
| 4.3    | Control System of Power Supplies .....  | 196 |
| 4.4    | System Design of JT-60 Electrical Power System .....                              | 196 |
| 5.     | Status of Control and Diagnostic Systems .....                                    | 209 |
| 5.1    | Major activities of control and diagnostic systems .....                          | 209 |
| 5.2    | Present design of control system .....  | 209 |
| 5.2.1  | System design .....   | 209 |
| 5.2.2  | Man-machine interface .....   | 210 |
| 5.2.3  | CAMAC system .....  | 212 |
| 5.2.4  | Timing system .....   | 213 |
| 5.2.5  | Safety and Protection system .....  | 213 |
| 5.2.6  | Plasma control .....  | 215 |
| 5.3    | Present design of diagnostic system .....   | 217 |
| 5.3.1  | System design .....   | 217 |
| 5.3.2  | Electron density and temperature measuring systems ....                           | 218 |

|            |   |     |
|------------|---|-----|
| 5.3.3      | Ion temperature and impurity measuring systems .....            | 219 |
| 5.3.4      | Radiation flux and peripheral plasma measuring<br>systems ..... | 221 |
| 5.3.5      | Data processing and diagnostic support systems .....            | 222 |
| 5.3.6      | Phase II diagnostics (B Group) .....                            | 223 |
| 6.         | Status of Auxiliary Systems .....                               | 245 |
| 6.1        | Secondary cooling system .....                                  | 245 |
| 6.2        | Power distribution system .....                                 | 245 |
| 7.         | Vacuum Technological Development for JT-60 .....                | 246 |
| 8.         | JT-60 Experimental Planning and Plasma Considerations .....     | 248 |
| 8.1        | Experimental program and schedule .....                         | 248 |
| 8.2        | Plasma considerations .....                                     | 252 |
| 8.2.1      | Predictions of plasma parameters .....                          | 252 |
| 8.2.2      | Operation scenarios .....                                       | 253 |
| 8.2.3      | Neutral beam injection heating .....                            | 254 |
| 8.2.4      | Radio frequency heating .....                                   | 257 |
| 8.2.5      | Impurity control .....  | 259 |
| 8.2.6      | One-dimensional transport simulation .....                      | 262 |
| XI.        | DEVELOPMENT OF THE NEXT LARGE TOKAMAK MACHINE .....             | 278 |
| 1.         | INTOR Activity .....  | 278 |
| 2.         | Study of INTOR Reactor Plasma .....                             | 279 |
| 2.1        | Particle and energy confinement .....                           | 279 |
| 2.2        | Impurity control, fueling and exhaust .....                     | 279 |
| 2.3        | Heating .....   | 280 |
| 2.4        | Stability control .....   | 280 |
| 2.5        | Start-up, burn and shutdown .....                               | 280 |
| 3.         | Design Study of INTOR-J .....                                   | 280 |
| 4.         | Related Technologies .....                                      | 283 |
| 4.1        | Materials .....   | 283 |
| 4.2        | Power supply and transfer .....                                 | 283 |
| 4.3        | Tritium .....   | 283 |
| 4.4        | Vacuum .....  | 283 |
| 4.5        | Diagnostics, data acquisition and control .....                 | 284 |
| APPENDIXES |   |     |
| A1.        | Publication List .....  | 285 |



|      |  |     |
|------|--|-----|
| A1.1 | List of JAERI-M Report .....                             | 286 |
| A1.2 | List of Papers Published in Journals .....               | 291 |
| A1.3 | List of Papers Published in Conference Proceedings ..... | 295 |
| A2.  | Personnel of the Center .....                            | 301 |
| A2.1 | Number of the Staff of the Center .....                  | 301 |
| A2.2 | List of Scientific Staffs and Officers .....             | 301 |
| A3.  | Budget of the Center .....                               | 309 |

## 目 次

|  |     |
|--|-----|
| まえがき .....   | xix |
| I. 理論および計算 .....   | 1   |
| 1. はじめに .....  | 1   |
| 2. 安定性および輸送 .....  | 1   |
| 2.1 安定な高ベータ・トカマク平衡の推移 .....  | 1   |
| 2.2 大型トカマクの限界ベータ値 .....  | 1   |
| 2.3 低周波不安定性によるイオンの異常損失 .....   | 2   |
| 2.4 非局所的無衝突ドリフト不安定性に対するトロイダル効果 .....                                   | 2   |
| 2.5 高密度トカマクに対する比例法則とそのJIPP TII装置への適用 .....                             | 2   |
| 2.6 シェアのある磁場中の有限プラズマにおけるドリフト、ドリフト-アルフ<br>ヴェン、ドリフト-テアリング不安定性の安定条件 ..... | 3   |
| 2.7 トロイダル・プラズマ中での高周波輸送制御 .....   | 3   |
| 2.8 トロイダル・ドリフト不安定性の空間構造 .....  | 3   |
| 3. 計 算 .....   | 6   |
| 3.1 スクレイプ・オフ層の粒子シミュレーション .....   | 6   |
| 3.2 NBI加熱の非線形モンテ・カルロ・シミュレーション .....                                    | 6   |
| 3.3 多チャンネルMEMに関する数値的研究 .....   | 7   |
| 4. TRITON .....  | 8   |
| 4.1 はじめに .....   | 8   |
| 4.2 MHD 安定性解析コードERATO の解の収束性 .....                                     | 8   |
| 4.3 ERATO コードの入出力過程およびアレイ・プロセッサに関する最適化 .....                           | 8   |
| 4.4 2次元トカマク・コードAPOLLO .....  | 9   |
| 4.5 バルーン・モードに対する有限 $n$ および $\omega_*$ 補正 .....                         | 9   |
| 4.6 単一ヘリシティ抵抗性MHD 不安定性解析のための高速<br>計算コードAEOLUS-R1 .....                 | 10  |
| 4.7 位置不安定性解析のための計算コードAEOLUS-P .....                                    | 10  |
| 4.8 図形入出力サブシステムARGUS-V2 .....  | 11  |
| 4.9 TRITON システムの管理コードと各種共用コード .....                                    | 12  |
| II. トロイダル系の閉じ込め実験 .....  | 16  |
| 1. はじめに .....  | 16  |
| 2. JFT-2 .....   | 16  |
| 2.1 改造されたJFT-2 トカマクとプラズマの位置制御 .....                                    | 16  |
| 2.2 低域混成波加熱の最近の結果 .....  | 18  |

|  |    |
|--|----|
| 2.3 低域混成波による電流維持の観察 .....                  | 20 |
| 2.4 高加熱密度実験 .....                          | 22 |
| 2.5 まとめ .....                              | 23 |
| 3. JFT-2a .....                            | 33 |
| 3.1 イオンサイクロロン加熱実験 .....                    | 33 |
| 3.1.1 多数派および少数派粒子の加熱 .....                 | 33 |
| 3.1.2 加熱効率の上昇 .....                        | 35 |
| 3.1.3 最適加熱条件でのパワーバランス .....                | 36 |
| 3.2 炭素リミターおよび壁実験 .....                     | 42 |
| 3.2.1 炭素表面のスパッタリング特性 .....                 | 42 |
| 3.2.3 形成された炭素壁の特性 .....                    | 43 |
| 3.2.3 炭素壁における低q放電 .....                    | 43 |
| 3.3 電氣的に絶縁されたターゲット上のアーク発生における逃走電子の役割 ..... | 49 |
| Ⅲ. 装置の運転・保守と技術開発 .....                     | 55 |
| 1. はじめに .....                              | 55 |
| 2. 運転・保守 .....                             | 55 |
| 3. 装置の技術開発 .....                           | 55 |
| Ⅳ. ダブレットⅢにおける協同実験 .....                    | 62 |
| 1. 協力計画 .....                              | 62 |
| 2. 実験結果 .....                              | 63 |
| Ⅴ. プラズマ加熱装置の開発 .....                       | 70 |
| 1. はじめに .....                              | 70 |
| 2. 中性粒子入射加熱装置 .....                        | 70 |
| 2.1 イオン源の開発 .....                          | 70 |
| 2.1.1 長パルスビームの引出し .....                    | 70 |
| 2.1.2 ビーム中の不純物測定 .....                     | 71 |
| 2.1.3 電極孔のずれによるビームの収束 .....                | 72 |
| 2.1.4 ラムダトロニオン源 .....                      | 72 |
| 2.1.5 同軸デュオピガトロニオン源 .....                  | 73 |
| 2.1.6 ホローカソード .....                        | 74 |
| 2.2 JT-60 粒子入射加熱装置の開発 .....                | 84 |
| 2.3 JFT-2 用粒子入射加熱装置 .....                  | 88 |
| 2.3.1 イオン源 .....                           | 88 |
| 2.3.2 ビームライン .....                         | 88 |
| 2.3.3 電源システム .....                         | 89 |

|                                      |     |
|--------------------------------------|-----|
| 3. 高周波加熱装置 .....                     | 92  |
| 3.1 導波管結合系の開発 .....                  | 92  |
| 3.2 JT-60 における低域ハイブリッド波加熱システム .....  | 95  |
| 3.2.1 はじめに .....                     | 95  |
| 3.2.2 励振増巾部 .....                    | 95  |
| 3.2.3 大電力クライストロン .....               | 96  |
| 3.2.4 制御系 .....                      | 97  |
| VI. 表面現象と真空技術 .....                  | 104 |
| 1. はじめに .....                        | 104 |
| 2. 装置の製作 .....                       | 105 |
| 2.1 大電流軽イオン引出装置 .....                | 105 |
| 3. 低エネルギー水素イオンによるスパッタリングの実験 .....    | 105 |
| 3.1 各種炭素材料の化学的スパッタリング .....          | 105 |
| 3.2 モリブデン上炭化珪素皮膜の侵食速度 .....          | 106 |
| 4. 高エネルギーヘリウムイオンによる表面侵食の実験 .....     | 107 |
| 5. JFT-2 トカマクにおける単極性アーク .....        | 108 |
| 6. モリブデンからの水素イオンによる粒子衝撃脱離 .....      | 109 |
| 7. クライオポンプを用いたヘリウム排気に関する二、三の考察 ..... | 109 |
| VII. 超電導磁石の開発 .....                  | 118 |
| 1. はじめに .....                        | 118 |
| 2. クラスタ・テスト・プログラム .....              | 118 |
| 2.1 クラスタ・テスト装置の製作 .....              | 118 |
| 2.2 テスト・モジュール・コイル .....              | 119 |
| 3. IEA-LCT .....                     | 123 |
| 3.1 LCT コイル .....                    | 123 |
| 3.1.1 設計の概要 .....                    | 123 |
| 3.1.2 導体の設計と開発 .....                 | 123 |
| 3.1.3 応力解析とその実証 .....                | 124 |
| 3.1.4 コイル保護 .....                    | 125 |
| 3.2 国内試験装置 .....                     | 126 |
| 4. 高磁界超電導磁石の開発 .....                 | 134 |
| 5. パルス磁石の開発 .....                    | 136 |
| VIII. トリチウム .....                    | 139 |
| 1. トリチウム・プロセス技術の開発 .....             | 139 |
| 1.1 水素同位体のガスクロマトグラフ分析 .....          | 139 |

|        |                  |     |
|--------|------------------|-----|
| 1.2    | 水素回収実験           | 139 |
| 1.3    | システム解析           | 140 |
| 2.     | トリチウム取扱施設の概念設計   | 146 |
| 2.1    | はじめに             | 146 |
| 2.2    | 多重隔壁格納システム       | 147 |
| 2.3    | 実験装置および附帯設備      | 149 |
| X.     | 核融合炉のシステム設計      | 153 |
| 1.     | はじめに             | 153 |
| 2.     | 実験炉 (JXFR) の予備設計 | 153 |
| 3.     | 炉体分解修理           | 153 |
| 4.     | 動力炉の設計研究         | 154 |
| 5.     | 設計手法の開発          | 154 |
| 5.1    | プラズマ設計           | 154 |
| 5.2    | 核設計              | 155 |
| X.     | 大型トカマク JT-60 の開発 | 159 |
| 1.     | はじめに             | 159 |
| 2.     | JT-60 計画の概況      | 159 |
| 3.     | 本体の現状            | 168 |
| 3.1    | 工程および主な活動        | 168 |
| 3.2    | 構成機器の現状          | 169 |
| 3.2.1  | 真空容器             | 169 |
| 3.2.2  | 第1壁              | 170 |
| 3.2.3  | トロイダル磁場コイル       | 171 |
| 3.2.4  | ポロイダル磁場コイル       | 172 |
| 3.2.5  | 架 台              | 174 |
| 3.2.6  | 真空排気設備           | 174 |
| 3.2.7  | 1次冷却設備           | 176 |
| 3.2.8  | 可動リミタ            | 176 |
| 3.2.9  | 半固定リミタ           | 176 |
| 3.2.10 | ガス注入装置           | 177 |
| 3.2.11 | 予備電離装置           | 177 |
| 3.2.12 | 本体制御設備           | 177 |
| 4.     | 電源の現状            | 195 |
| 4.1    | ポロイダル磁場コイル電源     | 195 |
| 4.2    | トロイダル磁場コイル電源     | 196 |
| 4.3    | 電源制御設備           | 196 |

|                                       |     |
|---------------------------------------|-----|
| 4.4 JT-60 電力システム設計 .....              | 196 |
| 5. 制御系及び計測系の現状 .....                  | 209 |
| 5.1 制御系および計測系の主な活動 .....              | 209 |
| 5.2 制御系の設計現状 .....                    | 209 |
| 5.2.1 システム設計 .....                    | 209 |
| 5.2.2 マン・マシン・インターフェイス .....           | 210 |
| 5.2.3 CAMAC システム .....                | 212 |
| 5.2.4 タイミング・システム .....                | 213 |
| 5.2.5 保護インターロック・システム .....            | 213 |
| 5.2.6 プラズマ制御 .....                    | 215 |
| 5.3 計測系の設計現状 .....                    | 217 |
| 5.3.1 システム設計 .....                    | 217 |
| 5.3.2 電子密度測定システムおよび電子温度測定システム .....   | 218 |
| 5.3.3 イオン温度測定システムおよび不純物挙動診断システム ..... | 219 |
| 5.3.4 放射損失測定システムおよび周辺プラズマ監視システム ..... | 221 |
| 5.3.5 データ処理設備および共通設備 .....            | 222 |
| 5.3.6 新計測器群 (B グループ) .....            | 223 |
| 6. 附属設備の現状 .....                      | 245 |
| 6.1 2次冷却設備 .....                      | 245 |
| 6.2 操作用配電設備・非常用電源 .....               | 245 |
| 7. JT-60 の真空技術の開発 .....               | 246 |
| 8. JT-60 の実験計画およびプラズマに関する考察 .....     | 248 |
| 8.1 実験計画およびスケジュール .....               | 248 |
| 8.2 プラズマに関する考察 .....                  | 252 |
| 8.2.1 プラズマ・パラメータの予測 .....             | 252 |
| 8.2.2 運転のシナリオ .....                   | 253 |
| 8.2.3 中性粒子入射加熱 .....                  | 254 |
| 8.2.4 高周波加熱 .....                     | 257 |
| 8.2.5 不純物制御 .....                     | 259 |
| 8.2.6 1次元輸送シミュレーション .....             | 262 |
| XI. 次期大型トカマク装置の開発 .....               | 278 |
| 1. INTOR の活動 .....                    | 278 |
| 2. INTOR 炉心プラズマの研究 .....              | 279 |
| 2.1 粒子閉じ込めおよびエネルギー閉じ込め .....          | 279 |
| 2.2 不純物制御, 燃料注入および排気 .....            | 279 |
| 2.3 加熱 .....                          | 280 |
| 2.4 安定性の制御 .....                      | 280 |
| 2.5 点火, 燃焼および停止 .....                 | 280 |

|                          |     |
|--------------------------|-----|
| 3. INTOR-J の設計研究 .....   | 280 |
| 4. 関連技術 .....            | 283 |
| 4.1 材 料 .....            | 283 |
| 4.2 電源および輸送 .....        | 283 |
| 4.3 トリチウム .....          | 283 |
| 4.4 真 空 .....            | 283 |
| 4.5 計測, データ処理および制御 ..... | 284 |

# PREFACE

A brief summary of activities in the Fusion Research and Development Center during the fiscal year 1979 is as follows:

## Procurement of the Naka site:

A new site for fusion activities at JAERI was procured in October 1979. The site is located 6 km west of the Tokai Research Establishment.

## JT-60:

This is the second year since JT-60 entered the construction phase. Its tokamak machine, power supplies, and central control system are under fabrication. Construction of the experimental and the power supplies buildings has begun.

## JFT-2:

Remodelling work of JFT-2 was completed in July 1979. Emphasis was placed on the following two experiments. One on the current drive by lower hybrid waves showed an efficiency of 110 A/kW. The other on the multi-MW neutral beam injection heating experiment will begin early in the next fiscal year.

## JFT-2a/DIVA:

An ICRF heating experiment by the two-ion hybrid resonance process was completed showing an absorption of coupled power into the plasma at 85 % and an efficiency of 8.2 eV/kW normalized to the plasma density of  $10^{13} \text{ cm}^{-3}$ . JFT-2a/DIVA was dismantled in September to evacuate the space for neutral beam injectors for JFT-2.

## Doublet III:

US-Japan cooperation in Doublet III was initiated in August 1979. A team of Japanese physicists mainly composed of JAERI's started deuterium plasma experiments using the upper lobe of the vacuum chamber. The progress made since then was rewarding in that all target values of the density, current, elongation and others were attained or surpassed.

## JFT-2M:

As a timely successor to the aging JFT-2, JFT-2M was conceived, and its definition and design studies were carried out. Emphasis is placed on the operational flexibility combined with the experimental objectives of simplified divertor, ICRF heating and current



drive, among others.

Plasma Heating Technology:

The activities in this area were primarily focussed on the development of heating technologies for JT-60. In neutral beam technology a two-stage hydrogen ion source of 65 keV and 4 A was operated for a duration of 30 sec compared to 0.1 sec achieved in the previous year. For the lower hybrid heating the power density in the coupler in the JFT-2 experiment was raised to 2 kW/cm<sup>2</sup> from 1.2 kW/cm<sup>2</sup> in the last year.

Surface Science and Vacuum Technology:

Works are conducted on three activities, surface bombardment studies by means of accelerators, observations of first-wall surfaces in tokamaks, and development of low-Z first wall materials for JT-60. JVX, test facilities for JT-60, are under construction.

Superconducting Magnet Technology:

A cluster testing facility is being installed, which is made of two NbTi coils of 1.5 m in bore. A LCT coil, JAERI's contribution to the IEA LCT program was ordered together with an associated facility for a domestic test before shipment to ORNL.

Tritium Technology:

Experimental studies were carried out on basic processes using hydrogen and deuterium. A simulation study of a reactor tritium system and a design of a tritium handling facility were performed.

Reactor Design:

Activities in this area focussed on JXFR and PETF in the preceding years were shifted to the INTOR studies, an international effort under IAEA. Its first stage, Phase Zero, was completed.

Yasuhiko ISO

# I. PLASMA THEORY AND COMPUTATION

## 1. Introduction

The main theoretical and computational works in this period were devoted to understand, comprehensively, evolutions of a tokamak plasma to stable high beta equilibria. For this purpose MHD stability problems were solved from the viewpoint of kinetic theory. As for computational study on this problem a linearized ideal MHD code ERATO was investigated minutely and it was applied to analyze stability of an INTOR-like plasma.

Toroidal drift mode, drift Alfvén mode, and collisional tearing mode were studied in detail. An idea of RFFC was proposed and investigated. Characteristics of a scrape-off layer were studied computationally by a particle model simulation code.

The first versions of almost all codes in TRITON system were brought into completion. These are the ballooning mode analysis code BOREAS, nonlinear MHD code AEOLUS-R, and several supporting codes PARIS, ARGUS, HARMONIA, PLUTO, and EOS. They are being used very effectively to solve practical problems.

## 2. Stability and Transport

### 2.1 Evolution of stable high beta tokamak equilibria<sup>1)</sup>

The pressure limitation due to MHD instabilities in an INTOR-like plasma is investigated. An equilibrium-transport calculation yields attainable  $\beta$  realizing the marginally ballooning stable pressure profile. The dependence of critical- $\beta$  on the plasma parameters is studied. For typical INTOR parameters, the critical- $\beta$  is about 4 %. The finite larmor radius effects stabilize the high- $n$  ballooning modes, and give the higher  $\beta$  state. Low- $n$  internal modes are also investigated numerically and the results are consistent with the high- $n$  mode analyses. The low- $n$  kink modes are stabilized completely by the shell placed near the plasma (Fig. I.2-1).

### 2.2 Beta-limit of large tokamaks<sup>2)</sup>

The dependence of stabilizing effect of a conducting shell on a poloidal beta value ( $\beta_p$ ) is investigated as to instabilities with low

toroidal mode numbers ( $n = 1$  and  $2$ ) for tokamaks such as JT-60 and INTOR. The  $n = 1$  mode is completely stabilized by the conducting shell which is located at a practically possible position and the critical position of the shell becomes closer to the plasma surface with increasing  $\beta_p$ . The stabilizing effect on the  $n = 2$  mode is remarkable for higher  $\beta_p$  when the shell is placed sufficiently close to the plasma surface but the shell far from the plasma surface has hardly an effect on the stability property of a higher  $\beta_p$  plasma.

It is concluded that critical  $\beta$  of about 2 % is attainable even in a standard circular tokamak such as JT-60 and higher  $\beta$  value is also expected by taking advantage of the closely located conducting shell.

### 2.3 Anomalous ion loss due to low-frequency instabilities<sup>3)</sup>

An ambipolarity formula for the cross-field flux in non-uniform plasma in the presence of low-frequency electromagnetic fluctuations is derived. It is shown that, owing to the ion polarization drift, ions are pulled out by diffusing electrons.

### 2.4 Toroidal effects on nonlocal collisionless drift instability<sup>4)</sup>

Toroidal curvature effects on the electrostatic collisionless drift instability in a sheared magnetic field is investigated. The magnetic curvature drift of ions causes the reduction of the shear convective damping and the mode ballooning. It is found that the universal mode is stable so long as the convective damping remains finite, and the critical current density for the current-driven drift instability becomes lower.

### 2.5 A scaling law for high density tokamaks and its application to J.I.P.P. T-II device<sup>5)</sup>

A scaling law for high density and high current tokamaks is presented on the basis of the nonlocal theory of electrostatic current-driven drift instability in both collisionless and collisional regimes with the assumption of quasilinear saturation level. It is shown that the energy confinement time scales as  $\tau_E \propto nq/\sqrt{T}$  ( $n$  and  $T$  are the averaged density and temperature) in relatively lower density region and  $\tau_E \propto B/\sqrt{n}$  ( $B$  is the toroidal magnetic field) in higher density region where a combined effect of the electron collisions and of a plasma current works. Trapped particle effects are assumed to be negligible and no magnetic

fluctuation is considered. A test experiment of the scaling law on the J.I.P.P. T-II device where both tokamak operation and the operation with superposition of helical fields are possible is proposed.

## 2.6 Critical conditions for drift, drift-Alfvén and drift-tearing instabilities of finite- $\beta$ plasma in sheared magnetic field<sup>6)</sup>

Kinetic theory on low frequency instabilities of current carrying finite- $\beta$  plasma in a sheared magnetic field is investigated. Drift mode, drift-Alfvén mode and drift-tearing mode are identified and stability boundary is discussed. It is shown that in the absence of the plasma current, any electromagnetic localized mode which is propagating in the direction of the electron diamagnetic drift is stable in the collisionless limit. For collisional mode, stability holds if  $\omega > \omega_*$  (electron diamagnetic frequency). The critical conditions for the drift, drift-Alfvén and drift-tearing instabilities are obtained for collisionless and collisional plasmas.

## 2.7 Radio-frequency flux control of toroidal plasma<sup>7)</sup>

A new method to reduce the cross field plasma loss in magnetic confinement device by use of a radio-frequency (RF) field is proposed. An RF field with momentum density in the direction of the electron diamagnetic drift appreciably reduces the cross field loss, if  $\omega > \omega_*$  ( $\omega_*$  is the electron diamagnetic drift frequency) and the wave is absorbed by electrons.

## 2.8 Spatial structure of toroidal drift instability<sup>8)</sup>

Nonlocal electrostatic drift mode in a toroidal plasma is investigated. The growth rate as well as the two dimensional mode structure is obtained. The stabilization effect of the magnetic shear is complete in a slab geometry but is reduced or even annihilated in a toroidal geometry. It has been shown, with the aid of strong coupling approximation, that the reduced shear stabilization is still enough to suppress universal mode unless completely annihilated. We give a growth rate in  $1/n \rightarrow 0$  limit, and further develop the two dimensional (2D) variational principle method to obtain the eigenvalues as well as mode structure of toroidal mode, confirming the results from the strong coupling limit.

References

- 1) Azumi, M., et al., "Evolution of stable high beta tokamak equilibria", Proceedings of the 8th International Conference on Plasma Physics and Controlled Nuclear Fusion Research, Brussels 1-10 July 1980, IAEA-CN-38/K-1-1.
- 2) Takeda, T., et al., "IAEA INTOR workshop report, Group 11 — Stability control —", JAERI-M 8624 (Jan. 1980).
- 3) Inoue, S., Tange, T., Itoh, K., and Tuda, T., Nucl. Fusion 19 (1979) 1252.
- 4) Itoh, K., Tuda, T., and Inoue, S., J. Phys. Soc. Japan 48 (1980) 258.
- 5) Inoue, S., Itoh, K., and Terashima, Y., J. Phys. Soc. Japan, 48 (1980) 264.
- 6) Inoue, S., Itoh, K., and Yoshikawa, S., J. Phys. Soc. Japan, 48 (1980) 973.
- 7) Itoh, K., and Inoue, S., Comments Plasma Phys. Cont. Fusion, 5 (1979) 203.
- 8) Tuda, T., Itoh, K., and Inoue, S., "Spatial structure of toroidal drift instability", Proceedings of International Conference on Plasma Physics (Nagoya, 1980) vol.1 p.256.

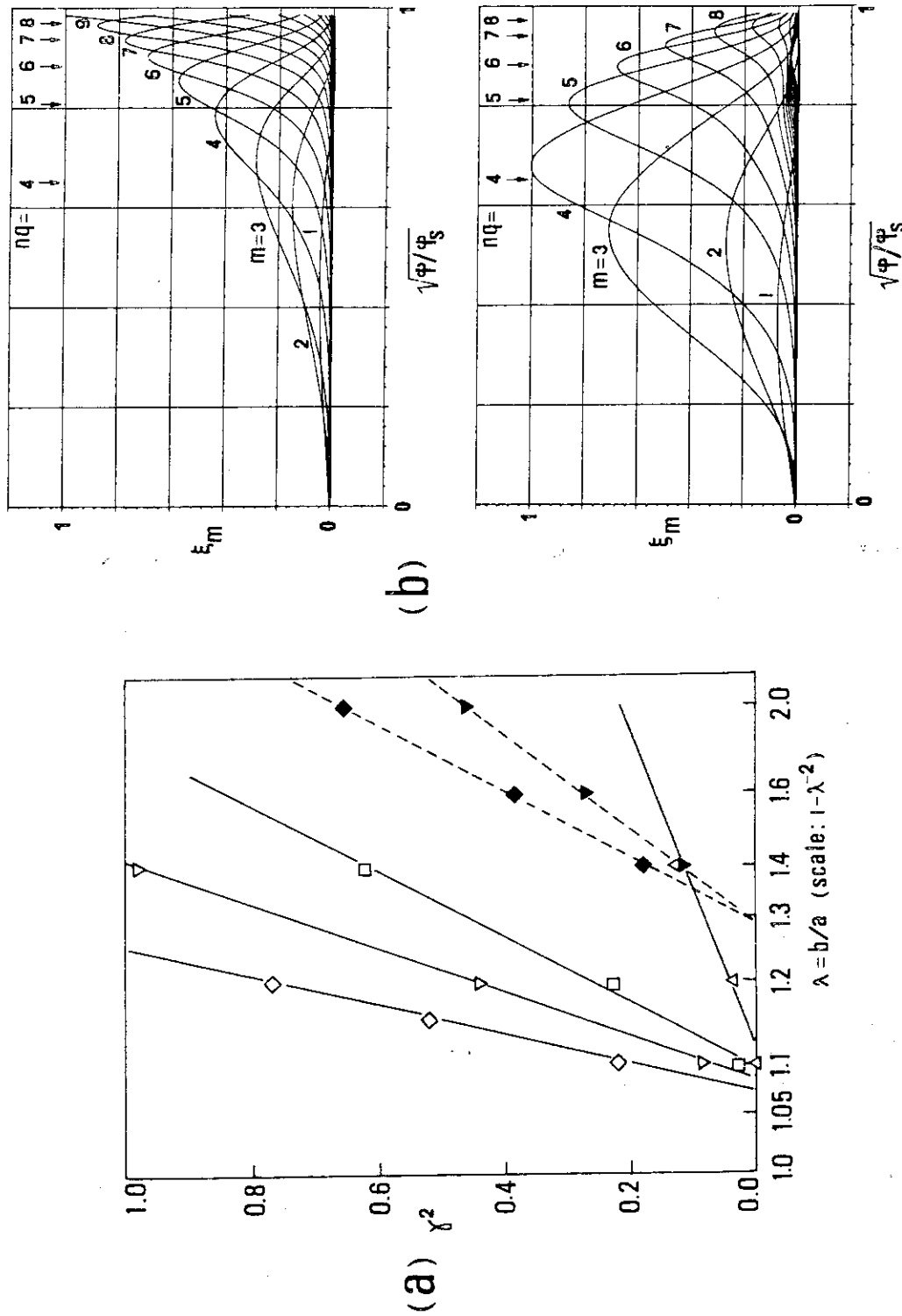


Fig. 1.2-1 (a)  $\gamma^2$  versus the shell position  $\xi_m(\sqrt{\psi})$  for the cases of an  $n = 3$  kink ( $b/a = 1.1$ , upper figure) and internal (lower figure) modes of the equilibrium with  $\beta = 22.6\%$ . Symbols,  $\Delta$ ,  $\square$ ,  $\nabla$ , and  $\diamond$  denote the cases with  $\beta = 8.4, 15.8, 22.6$ , and  $28.8\%$  for  $n = 1$  (black symbol) and  $n = 3$  (open symbol), respectively.

### 3. Computing

#### 3.1 Particle simulation of scrape-off layer<sup>1)</sup>

In order to understand the characteristics of the scrap-off plasma in a large tokamak with the poloidal divertor, a two-dimensional electrostatic particle simulation code is developed.

We consider a device with a rectangular cross-sectional metallic wall. The one-component plasma is confined by the magnetic field  $\vec{B}$ , which consists of the strong solenoidal field and the poloidal field produced by a line current  $I_p$  and by a divertor current  $I_d$ . The particle motions parallel to the magnetic lines of force and the electric field  $\vec{E} = -\nabla\phi$  are self-consistently calculated by using the PIC method.

Effects of the external electric field and of the gradient of the magnetic field are neglected. On the other hand, the cross-field diffusion of particles is simulated by using the Monte Carlo methods. The particles reaching the wall are absorbed there, and the reflection and secondary emissions are not taken into account.

Results of a simulation are obtained for the case of the system size  $L = 64\lambda_D$  ( $\lambda_D$  denotes the Debye length in the main plasma) and the mass ratio  $m_i/m_e = 100$ . The ions are assumed to be cold, and the diffusion coefficient is chosen as  $D_{\perp} = 10^{-3}LCs$  ( $Cs = \sqrt{T_e/m_i}$ ). The potential  $\phi$  and ion flow velocity  $V_f$  along a magnetic line in the scrape-off region are shown in Fig. I.3-1. The loss flux along a magnetic line in the scrape-off layer is balanced by the diffusion flux from the main plasma. The density profile perpendicular to the magnetic field is of the form  $\exp(-r/\ell)$  with  $\ell \approx 0.03L$ , which agrees with the expected value  $\sqrt{D_{\perp}L/Cs}$ .

#### 3.2 Nonlinear Monte Carlo simulation for NBI heating

A nonlinear Monte Carlo simulation code is developed in order to understand the slowing-down process of beam ions and the heating of main plasma in high-power neutral beam injection of tokamak plasmas. We consider only the velocity space  $(v_{\parallel}, v_{\perp})$  with orbit-loss region. Classical collisions are described by using a binary collision model<sup>2)</sup>. Electrons are treated as field particles with shifted Maxwell distribution. Effects of the toroidal electric field and charge-exchange reactions are also simulated.

The results shows that the slowing-down of beam ions agrees with that for the case of linear calculation, while the energy spread is

much faster than that for the linear case. The back-ground ions are effectively heated without significant tail formation.

### 3.3 Numerical study on multichannel MEM<sup>3)</sup>

A new spectral analysis method, the maximum entropy method (MEM), has been investigated numerically by applying to plasma simulations. The results show that both power and cross-spectral estimates obtained by MEM from a short data record length yield much higher resolution and accuracy than the conventional method.

#### References

- 1) Takizuka, T., et al., "Poloidal divertor study in tokamak", Proceedings of the 8th International Conference on Plasma Physics and controlled Nuclear Fusion Research, Brussels 1-10 July 1980, IAEA-CN-38/X-2-1.
- 2) Takizuka, T. and Abe, H., J. Comp. Phys. 25 (1977) 205.
- 3) Tokuda, S., "Numerical study on multichannel MEM", Proceedings of International Conference on Plasma Physics (Nagoya, 1980) vol.1 p.198.

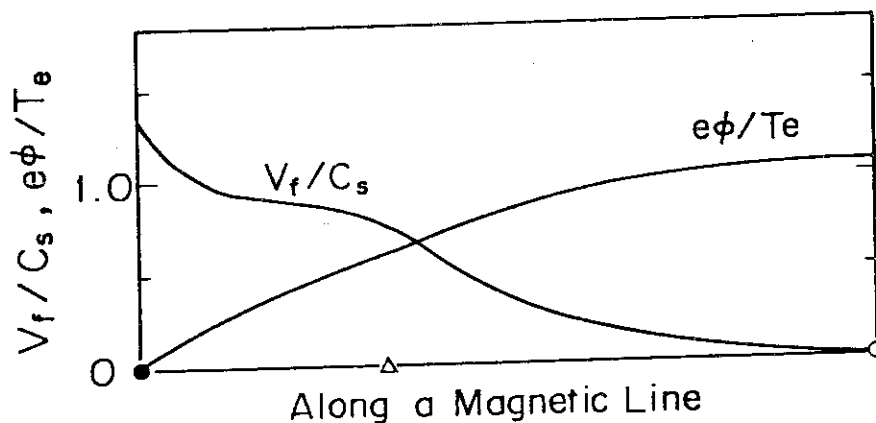


Fig.I.3-1 The potential  $\phi$  and the ion flow velocity  $V_f$  along a magnetic line in the scrape-off region.



## 4. TRITON<sup>1)</sup>

### 4.1 Introduction

As for the project TRITON we are now making efforts on detailed investigation of the codes, necessary improvement of them, and application of them to actual problems. In this year and the next, one of the most important objectives of the project TRITON is to establish the method to analyze the linear and nonlinear MHD system comprehensively, and most efforts are devoted to understand and improve the linear MHD codes ERATO<sup>2,3)</sup>, BOREAS and nonlinear MHD codes AEOLUS. An APOLLO code was combined with BOREAS and equilibria optimized with respect to the ballooning instability were searched (see also 2.1).

The following supporting codes were also developed in parallel with the above.

- (1) An eigenvalue and linear equation solvers in the PARIS subsystem for large-scale asymmetric matrices were developed, which are to be used for the AEOLUS codes.
- (2) The second version of the ARGUS subsystem (ARGUS-V2) was developed.
- (3) Supervising code of the TRITON system (HARMONIA), code analyzer (PLUTO), and a preprocessor for OLYMPUS-like programs with extended Fortran statements (EOS) were developed and they are being used very effectively to manage, analyze, and run codes.

### 4.2 Convergence of solutions of the MHD stability code ERATO<sup>4)</sup>

Convergence of solutions of the ERATO code is studied numerically. Some irregularities of data on a convergence curve are observed in our investigation. It is conjectured that the irregularities are due to inaccuracy of the equilibrium or inappropriate choice of the equilibrium calculation meshes.

### 4.3 Optimization of the ERATO code with respect to I/O operations and for an array processor<sup>5)</sup>

Optimization with respect to I/O operations is very important for codes with large-scale matrix handling. Improvement by rewriting basic I/O routines reduces the USE time considerably. For the ERATO code we succeeded to reduce the I/O time by factor 4.

In order to demonstrate the full effectiveness of the vector computers, it is required to optimize the codes for vector operations.

We started to optimize several codes for an array processor (FACOM 230-75 APU) by taking account of;

- (1) rewriting of Fortran source program in vector-operation-oriented Fortran language.
- (2) separation of arithmetic operation blocks and I/O operation blocks.
- (3) separation of scalar operation blocks and vector operation blocks.
- (4) efficient use of "vector temporaries" (vector registers) for temporarily obtained results.

Among the above items, (2)-(4) are important in the case of FACOM 230-75 APU because of its hardware architecture. For the ERATO calculation 3-4 times faster speed has been attained compared with calculations by the conventional FACOM 230-75 CPU.

#### 4.4 Two-dimensional tokamak code "APOLLO"

In order to study the evolution of a tokamak to high beta, the two-dimensional tokamak code APOLLO has been developed. The basic structure of this code is the combination of the transport step and the equilibrium step, and these two steps are solved alternatively. In the transport step, the surface-averaged transport equations are solved by the finite element method and the implicit time-integrating scheme. The former makes it easier to introduce the variable mesh without reducing the accuracy, while the latter guarantees the numerical stability. In the equilibrium step, the Grad-Shafranov equation is solved under the adiabatic conditions:  $\mu(\psi) = p(\psi) \left( \frac{dV}{d\psi} \right)^\gamma$  and  $q(\psi)$ . We developed two kinds of equilibrium solvers with high speed and high accuracy. The one, SELENE-30, employs the finite element method and the mesh structure based on the constant  $\psi$  surface. The other one, SELENE-40, solves the free boundary equilibrium, by using the Buneman solver of the Poisson type equation and the method of the surface Green function, which gives the magnetic flux on the artificial boundary of the Buneman solver. Both equilibrium modules automatically check the localized modes.

Using this code, the adiabatic compressions and the FCT heating scheme are tested and the numerical results are in good agreement with the theoretical predictions.<sup>6)</sup> Figure I.4-1 shows an example of the FCT heating of JT-60.

#### 4.5 Finite-n and $\omega_*$ corrections on ballooning mode

The  $\beta$  limit obtained from the infinite-n ballooning mode analysis

is too restrictive. The growth rates of the modes are reduced by decreasing  $n$  number. In order to estimate the reduction in the growth rate due to the finite  $n$  effect, we employed the W.K.B. method<sup>7)</sup>, because the correction derived by Conner et al. is too stabilizing. Another stabilizing effect is expected from the kinetic effects. The finite ion larmor radius can be included in the MHD eigenmode equation simply by replacing  $\omega^2$  to  $\omega(\omega + \omega_{*i})$ , where  $\omega_{*i}$  is the ion diamagnetic frequency. Taking account of these two effects, we can write the growth rate in the form  $\gamma^2(n) = \gamma_\infty^2 - \gamma_{fn}^2 - \omega_{*i}^2/4$ , where  $\gamma_\infty^2$  is the growth rate for infinite  $n$ ,  $\gamma_{fn}^2$  the finite- $n$  correction and the last term corresponds the stabilization due to the finite ion larmor radius, respectively. It must be noted that this formula gives the  $n$ -value and the corresponding growth rate for the most unstable mode because  $\gamma_{fn}^2$  scales as  $n^{-1}$ , while  $\omega_{*i}^2/4 \propto n^2$ . We applied this theory to the critical beta analysis of the standard INTOR parameters, which gives the critical beta value of 5 % and the corresponding  $n$  number of  $(k_{\perp} \rho_i)^2 \sim 0.2$ .

#### 4.6 High-speed numerical code AEOLUS-R1 for resistive MHD instability with single helicity<sup>8)</sup>

The nonlinear resistive MHD code AEOLUS-R1 solves a set of 2-dimensional equation with helical symmetry, which is derived from full MHD equations. Finite difference method for radial direction and Fourier expansion with respect to angular variable are employed. Combination of Crank-Nicolson implicit method and leapfrog method are used for the time integration. This numerical scheme reduces CPU time to  $1/10 \sim 1/15$  that by simple explicit method. Using this code, sawtooth oscillation due to  $m=1/n=1$  mode and island formation due to  $m=2/n=1$  mode are recovered.

#### 4.7 Numerical code AEOLUS-P for the analysis of positional instability

Before a fully three-dimensional nonlinear code we are developing a two-dimensional axisymmetric one to investigate the nonlinear behavior of the tokamak with a poloidal divertor such as JT-60. The Arbitrary Lagrangian-Eulerian grid<sup>9)</sup> is adopted. We construct the meshes under the constraint where the Jacobian is spatially constant<sup>10)</sup>. We represent the grid point in the polar coordinate  $(\rho, \theta)$  in a poloidal plane, where  $\rho$  is the distance between the magnetic axis and the grid point. For convenience we introduce the parameters  $r$  and  $\chi$  by

$$\rho = \rho_0(\theta)f(r) \quad , \quad (1)$$

$$\theta = \theta(r, \chi) \quad , \quad (2)$$

$$0 \leq r \leq 1 \quad \text{and} \quad 0 \leq \theta \leq 2\pi \quad , \quad (3)$$

where  $f(r)$  is the monotonously increasing function with  $f(0) = 0$  and  $f(1) = 1$ . The equation  $\rho = \rho_0(\theta)$  gives the plasma surface which is deformed by perturbation and the function  $\rho_0(\theta)$  is obtained by dividing the poloidal cross-section in equal area. Using the relations (1)-(3), the constraint that the Jacobian is spatially constant yields the differential equation

$$\rho_0(\theta) \frac{d\theta}{d\chi} = C / \left( \frac{df}{dr} \right) \quad , \quad (4)$$

where

$$C = \frac{1}{2\pi} \int_0^{2\pi} \rho_0(\theta) d\theta \left. \frac{df}{dr} \right|_{r=1} \quad . \quad (5)$$

Equations (1) and (4) give the mesh points  $(\rho_j, \theta_j)$  for the equi-intervals of  $\Delta r$  and  $\Delta\chi$ . The simplest choice of  $f(r)$  is  $f(r) = r$  where  $\theta$  depends only  $\chi$ .

The ideal MHD equations are expressed in a weak form by the finite element method and the resultant equations are in conservative form. All equations are solved by the explicit scheme.

#### 4.8 Graphic I/O subsystem ARGUS-V2

In the process of development and utilization of large-scale computer codes it is very effective to use graphic I/O functions of computer system.

The ARGUS subsystem of the TRITON is developed for efficient writing of fusion codes which include both graphic input and output processes. This subsystem is subdivided into three groups, i.e., ARGUS-V (a basic graphic output subsystem), ARGUS-W (an advanced graphic output subsystem which includes an option to produce a motion picture), and ARGUS-I (a graphic input subsystem). Presently, the first version of ARGUS-V (ARGUS-V1) was developed and used efficiently for development and utilization of the TRITON codes.

In this year a new subsystem ARGUS-V2 was developed as an extended version of ARGUS-V1. The ARGUS-V2 has several new functions and it can be used on the new computer system (FACOM M200) of JAERI computer center.

#### 4.9 Supervisor of the TRITON system and utility code packages

The TRITON system is not a conventional closed modular code system but a growing open system which has no definite boundaries. This is a natural consequence of the fact that production of new fusion codes are progressing and they are being improved rather constantly. In order to maintain these code effectively we applied the following concept to the TRITON. In this concept rules which define relations between constituent codes are first prepared, and actual codes and relations between them are put into the system according to the rules. This is the marked difference between this system and conventional modular code systems in which a set of constituent codes are first prepared, and relations between the elements of the system are looked for by considering the structure of original codes.

To realize this kind of code systems we are developing three types of supporting codes for manageable maintenance and easy development of numerical codes.

#### HARMONIA

HARMONIA is the supervisor code of the TRITON system. This code manages a set of complete programs, subprograms, job control programs, series of input data, and series of output data. Each element of the set is related, doubly, to other elements by a longitudinal tree structure (a family line of the codes) and by horizontal functional relations.

When one would like to analyze a certain phenomenon by using some computer codes in the TRITON, one can find most appropriate codes by sorting codes in the longitudinal tree structure and after that retrieve a group of elements (programs, job control programs, input data, and so on) which are connected each other by the horizontal functional relation. Relations between the elements and attribute of the elements are stored in INDEX FILE defined on a magnetic disk and the elements of the set are stored in magnetic tapes serially.

PLUTO

To facilitate maintenance, improvement, and adaptation of codes PLUTO was developed. The main functions of the PLUTO are semi-automatic documentation of a code, and extraction of necessary parts of a large-scale computer code. By using the former function of the PLUTO exchange of computer codes with other researchers becomes very easy and by using the latter function one can write a new code easily by reconstructing parts obtained from other codes.

EOS

EOS is a code which facilitate development of new codes. Originally the EOS was designed to be similar to the Olympus System<sup>11)</sup>. Present version of the EOS is, however, different from the Olympus System in that the EOS has no rule which defines the program structure. The EOS code has functions of insertion and extraction of COMMON blocks and evaluation of algebraic expressions in declaration statements.

References

- 1) Azumi, M., et al., "A fluid model numerical code system for tokamak fusion research", Proceedings of the Fourth International Symposium on Computing Methods in Applied Sciences and Engineering, 10-14 Dec., 1979, Versailles.
- 2) Gruber, R., et al., Comput. Phys. Commun. to be published.
- 3) Tanaka, Y., et al., "MHD stability analysis code ERATO-J — Users' manual of the JAERI-version ERATO —", JAERI-M 9040 (Aug. 1980).
- 4) Tsunematsu, T., et al., Comput. Phys. Commun. 19 (1980) 179.
- 5) Tsunematsu, T., et al., "Stability analysis by ERATO code" JAERI-M 8616 (Dec. 1979).
- 6) Azumi, M. and Nelson, O.B., "FCT heating of free boundary equilibria", 1979 Sherwood Meeting (April 1979, Mount Pocono) 1C32.
- 7) Dewar, R.L., et al., "WKB theory for high-n modes in axisymmetric toroidal plasma", PPPL-1587.
- 8) Tanaka, Y., et al., "High-speed numerical code AEOLUS-R1 for resistive MHD instability with single helicity", JAERI-M 8656 (Dec. 1979).
- 9) Brackbill, J.B. and Pracht, W.E., J. Comp. Phys. 13 (1973) 455.

- 10) Jardin, S.C., et al., J. Comp. Phys., 29 (1978) 101.
- 11) Roberts, K.V., Comput. Phys. Commun. 7 (1974) 237.

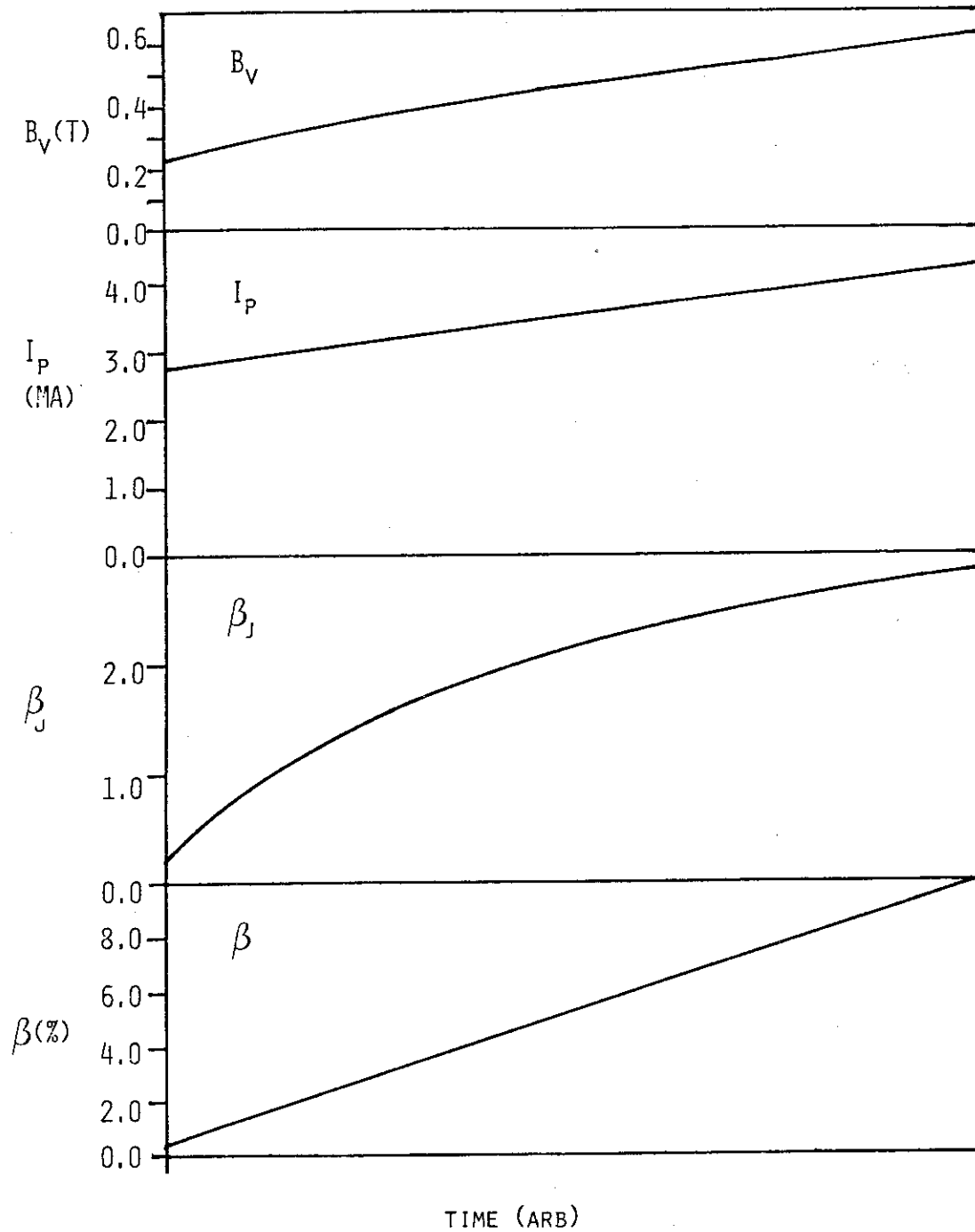


Fig.I.4-1 Numerical results of the FCT heating of JT-60; the major radius is 3 m, the minor radius 0.95 m, the toroidal field 4.5 T and the safety factor 3 on the surface and 1 at the magnetic axis, respectively.



## II. TOROIDAL CONFINEMENT EXPERIMENT

### 1. Introduction

JFT-2 (a conventional circular tokamak) has been operated with relevant development on diagnostics. The high power neutral beam injection system was installed to JFT-2 and the experiments were commenced, in addition to the RF heating experiments. JFT-2a/DIVA was shutdown on September 1979.

Succeeding the promising first result of lower hybrid heating in 1978, the ion heating efficiency of  $2 \sim 3$  ev/kW at the plasma density in the range of  $10^{13} \text{ cm}^{-3}$  was demonstrated with detailed diagnostics. Another important result of RF scheme is the demonstration of current drive of 110 A/kW by 125 kW net input of lower hybrid wave, as is described in section 2.3. This agrees well with a theoretical prediction and suggests the capability of steady state operation with realistic RF power in future tokamak reactors.

The high power neutral beam injection experiment on JFT-2 was started April 1980 and characteristics of high beta tokamak plasma of circular cross section were investigated. The result is described in section 2.4, with recent experimental results of additional heating by ICRF obtained in JFT-2a/DIVA.

The design of JFT-2M (a medium-sized noncircular tokamak) had been advanced expecting its operation by the end of 1982. The main objectives of the device is reactor-relevant optimization of tokamaks such as, optimized RF heating, current drive by LHW, high beta plasma with profile control, low-q discharge, helium exhaust with simple divertor, fueling etc.

### 2. JFT-2

#### 2.1 Modified JFT-2 tokamak and plasma position control<sup>1)</sup>

The JFT-2 tokamak was converted to a circular shell-less tokamak with a active control system of plasma position. Vacuum chamber consists of 14 sectorial cylinders (9 mm thick) which are connected by bellows (1.2 mm thick) and one turn resistance is 2.6 m $\Omega$ . The cylinders have 40 large ports including two tangential ports for neutral beam injection

and stainless steel O-ring seals are used to be bakable up to 350 °C. The ultimate pressure of  $3 \times 10^{-9}$  Torr was obtained after the bakeout with two turbomolecular pumps accompanied by a 18 °K cryo-trap. Surface conditionings under operation are a low power discharge cleaning ( $\sim 10$  KA,  $\sim 1$  pulse/sec) and a in-situ titanium coating (two RF-sputter system and one Ti-ball set). These equipments offer a clean plasma free from both light impurities and metal impurities. A circular fixed limiter of SUS with minor radius of 28 cm and a movable rail-type limiter of Mo are installed customarily, but limiters made of other materials are also usable. Basic parameters of the modified JFT-2 are listed in Table II.2-1.

A stable tokamak plasma requires a external vertical magnetic field for equilibrium  $B_{eq}$  ( $B_{eq} \sim 300$  G / 100 kA in our case) and a suitable decay index  $n$  ( $0 < n < 1.5$ ). In tokamaks with an iron core like JFT-2, a vertical field more than half of the  $B_{eq}$  is supplied from the iron core ( $\sim 200$  G/100 kA). The large attraction force of it and its direct proportionality to a discharge current are favorable to obtain a plasma equilibrium, but the large decay index of it ( $n \sim 2.0$ ) is unfavorable from the destabilizing effect. Then the decay index of vertical field from primary windings was decreased to be negative so that total decay index may satisfy the condition. The total vertical field from the iron core and the primary windings was chosen to be a little less than the  $B_{eq}$  and the residual field was fed from a control vertical field  $B_{vc}$  installed inside the toroidal coils. Precise control of plasma position is conducted by the active control system composed of magnetic probes, a digital computer for calculation of plasma position and control command, a microprocessor as pulse phase shifter and a thyristor rectifier. The sampling time is 1.67 ms, the total processing time is 2.3 ms and the time constant of the  $B_{vc}$  circuit is nearly 5 ms. The obtainable  $B_{vc}$  field is 0 - 480 G and its decay index is 1.0. On the other hand, a time constant of the vacuum chamber for a vertical field is about 0.5 ms, which resulted in a fast plasma shift of about 1 cm/ms. The gap between two time constants was covered by a passive circuit consisted of a inductance (0.7 mH) and a resistance (15 m $\Omega$ ). Each value has nearly the double of the  $B_{vc}$  coil and they are inserted parallel to the active circuit. So the passive circuit wastes one third of active circuit current, but the long time constant ( $\sim 40$  ms) of it plays a more important role to obtain a plasma equilibrium. Owing to above mentioned arrangements,

a stable plasma similar to one with a shell was obtained. Moreover adjustment of the reference position and the feedback gain (PID control) and the preprogramming enabled us to obtain a stable high density plasma ( $\bar{n}_e = 6 \times 10^{13} \text{ cm}^{-3}$ ,  $q_a = 2.5$ ), which is sufficient as a target plasma for MW neutral beam injection. Typical plasma parameters in JFT-2 are listed in Table II.2-1.

## 2.2 Lower hybrid heating<sup>2)</sup>

Previous results of lower hybrid heating<sup>3)4)</sup> have indicated that a good coupling efficiency of 90 % is obtainable with a 4 waveguide launcher and the efficient ion heating ( $\Delta T_i/T_i = 50 - 60 \%$  or  $\sim 1 \text{ eV/kW}$ ) on application of 135 kW RF power is possible and the high energy ion tail observed on perpendicular CX spectra correlates with parametric decay instabilities at the boundary plasma region. In the recent experiments, the RF power source has been increased from 200 kW to 320 kW ( $4 \times 80 \text{ kW}$  klystron). As a coupling system we employed the array of 4 rectangular waveguide and its size was changed from  $1.4 \text{ cm} \times 29 \text{ cm}$  to  $3.3 \text{ cm} \times 29 \text{ cm}$  to obtain a favorable refractive index  $N_z$  spectrum. The  $N_z$  spectrum calculated from the Brambilla theory peaks at  $N_z = 5$  with the half width of  $\Delta N_z = 3$  at the phase difference  $\Delta\phi = 180^\circ$ . This spectrum must be effective for ion heating. Another improvement of the launcher is that the inner surface was coated by titanium to reduce the breakdown at the front edge. Typical target plasma used for ion heating experiment is as follows;  $B_t = 16 \text{ kG}$ ,  $I_p = 110 \text{ kA}$ ,  $a = 25 \text{ cm}$ ,  $\bar{n}_e = 1 - 3 \times 10^{13} \text{ cm}^{-3}$  and  $V_1 = 1.5 - 2.0 \text{ V}$ . Main diagnostics are two CX neutral analysers tangential and perpendicular to  $B_t$  and a VUV spectroscopy to measure Doppler broadening of impurity lines (OVII, CV). They are shown in Fig. II.2-1 together with usual ones.

Good coupling efficiency of 70 - 90 % was obtained up to input RF power of 320 kW with a optimized launcher, so net RF power more than 200 kW was launched into a plasma at  $\Delta\phi = 180^\circ$ . Duration time of RF pulse used is 15 - 30 ms.

Tangential CX spectra with and without RF power are shown in Fig. II.2-2. Thermal ion temperature tangential to  $B_t$  was in good agreement with that perpendicular to  $B_t$ . Noticeable point of tangential CX spectra is the existence of the high energy ion tail and this is in contrast to other experimental observations in which the high energy ion tail has not been distinguished<sup>5)6)</sup>. But the decay time of the high energy ions

was 1 - 2 ms, which is longer than that of perpendicular spectra of about 0.3 ms and is comparable to the slowing time of energetic ions near the plasma center. Therefore these energetic ions existing near the plasma center must be responsible for the bulk ion heating.

Time evolution of various ion temperatures at RF power of 200 kW and  $\bar{n}_e = 1.9 \times 10^{13} \text{ cm}^{-3}$  is shown in Fig. II.2-3. Tangential ion temperature at the plasma center increased from 400 eV to 700 eV, Doppler ion temperatures from OVII and CV increased from 220 eV to 330 eV and from 130 eV to 170 eV respectively. From these data radial profile of ion temperature was determined, where the radial position of Doppler temperature was deduced from the radial distribution of each line intensity. It is noted that the central ion temperature during RF pulse is nearly the same as the electron temperature by the laser scattering.

One-turn voltage was rather decreased within 10 %, this decrease corresponds to the increase of electron temperature from 630 eV to 690 eV by the laser scattering. The increase of electron temperature seems not due to the direct electron heating by RF power, but due to the decrease of energy transfer from electrons to ions, because the deposited power to electrons may be a little from the optimized  $N_2$  spectrum for ion heating. Electron density was not changed in almost cases with Ti-gettering, still more in cases with intense Ti-gettering it decreased by 10 - 20 % during RF pulse<sup>7)</sup>. On the other hand, in cases without Ti-gettering it increased by 20 - 30 %. Light impurities (O,C) and metal impurities (Fe, Ti, Mo) both increased to some extent, but it is not serious because of originally low impurity level.

Ion heating efficiency calculated at a steady state under assumption of the neoclassical transport reached to 50 - 60 % as shown in Table II.2-2. Dependence of ion temperature increment on normalized RF power is shown in Fig. II.2-4 together with the previous data. Improvement of ion heating efficiency by more than 2 times of previous one is clearly demonstrated. This result confirms the importance of the  $N_2$  spectrum. Electron density dependence of ion heating efficiency was also investigated and showed that at a density less than  $\bar{n}_e = 1.0 \times 10^{13} \text{ cm}^{-3}$  the efficiency decreased abruptly and this critical density agrees well with the requirement to the turning point to exist in a plasma. Above the critical density the efficiency keeps almost constant and decreases only a little even at  $\bar{n}_e = 3 \times 10^{13} \text{ cm}^{-3}$ , where the turning point exists in the outer region of plasma. These features of ion heating efficiency

can not be explained only by the linear theory of LH heating and some non-linear processes take an important role in the bulk ion heating. This wide density window of ion heating efficiency is very favorable for LH heating itself.

Perpendicular CX spectra have shown the existence of high energy ion tail with the fast decay time (0.3 ms in our case) and their counts correlated with the intensity of lower side band of electro-static wave spectra. Therefore parametric decay instabilities excited at the outer region of plasma are responsible for the production of the high energy ion tail and it seems to be a major loss channel of RF power. Fast loss channels through parametric decay instabilities are a resistive loss of the accumulated decay waves, a ripple loss or an orbit loss of energetic ions accelerated by the decay waves, and the conduction and convection loss of the power deposited near the surface. We do not have any detector to measure these losses separately, but a bolometric detector to measure total wall loss power showed sudden increase of loss power of 30 - 70 kW on application of 200 kW RF power. Further investigations are necessary to reveal fast loss of RF power.

In present experiments, it was observed that the electron temperature of peripheral plasma has a large effect on the bulk ion heating. At a comparatively high electron temperature, the efficient ion heating was observed. So this result suggests that more efficient ion heating may be possible by increasing the peripheral electron temperature which affects the parametric decay instabilities. From this point of view, hybrid heating experiment with neutral beam injection of about 500 kW was carried out. Preliminary data showed decrease of the side band intensity with increase of peripheral electron temperature coming from the neutral beam heating. This result is also favorable to LH heating in future large tokamaks.

### 2.3 Observation of the RF-driven current by the lower hybrid wave<sup>8)</sup>

The experimental setup and the discharges were reported in detail in ref. 4, hence will be described briefly here. In the present experiment, the following discharge was used as a magnetohydrodynamically stable operation; toroidal magnetic field  $B_t = 14$  kG, plasma current  $I_p = 30$  kA, mean-line-of-sight electron density  $\bar{n} \approx 3 \times 10^{12} \text{ cm}^{-3}$ , central electron temperature  $T_{e0} \approx 250$  eV and effective ionic charge  $Z_{\text{eff}}$  of 2 to 5. The working gas was deuterium.

Data from a typical plasma experiment for applied rf power of  $P_{rf} = 100$  kW and  $\Delta\phi = 90^\circ$  are shown in Fig. II.2-5. The dotted curves of Fig. II.2-5 correspond to no rf conditions. The rf pulse is found to produce a marked decreases in the loop voltage  $V_1$  and the hard X-ray emission  $H_x$ , a dramatic enhancement of the electron cyclotron emission  $I_c$  and no effect on the electron density and the plasma current. The cyclotron emission was detected by a heterodyne radiometer having the local oscillator with frequency corresponding to the second harmonic cyclotron frequency at the major radius of  $R \approx 101$  cm. The hard X-ray emission, which radiates from the limiter bombarded by accelerated electrons, was measured by a NaI scintillator. The detectable energy range was 10-100 keV. The loop voltage falls to nearly its time-asymptotic level in about 0.6 msec after the rf pulse is turned on. The cyclotron radiation increases linearly in time until sudden increase is seen in intensity, which is accompanied by a rise of the loop voltage, and then the cyclotron radiation saturates soon after this sudden increase. Note that the emissivity of the electron cyclotron radiation is proportional to a mean-perpendicular energy, which increases linearly in the time in a plasma with anisotropic distribution function of electrons because of pitch angle scattering. The abrupt increases in the loop voltage and cyclotron emission seem to result from an anomalous diffusion in perpendicular velocity space which is driven by unstable plasma waves. The signal decay time of the cyclotron emission is about 20 msec which is very long compared to the electron energy confinement time. Figure II.2-6 shows the relative changes in the loop voltage  $\Delta V_1/V_{10}$ , the cyclotron emission  $\Delta I_c/I_{c0}$  and the hard X-ray emission  $\Delta H_x/H_{x0}$  versus the phase difference. The subscript 0 denotes the value for the discharge with no rf pulse and  $\Delta$  the difference with the rf pulse. The experimental points were obtained from data just before the termination of the rf pulse, having a width of  $t_d = 10$  msec, during which the sudden increase in the cyclotron emission was not observed. In this case the decreased loop voltage relaxed in about 0.2 msec to its level for the discharge without the rf pulse.

The effective linear Landau damping to heat the bulk electrons with  $T_e = 250$  eV would require  $v_{pz}/v_e \lesssim 3$  or  $n_z \gtrsim 15$ , which is far above the expected one where  $v_{pz}$  is the parallel phase velocity of the waves and  $v_e$  is the thermal velocity of electrons. Therefore, the decrease of the loop voltage seems to result from the generation of the rf-driven current

carried by the suprathermal electrons rather than from the bulk electron heating. This is because the decay time of the total plasma current,  $L/R \approx 100$  msec (where  $L$  and  $R$  are plasma inductance and resistance, respectively), is so long compared with the duration of the rf pulse that the total current does not change during the rf pulse, although the inductive electric field is effectively shut off. The rf interaction with the suprathermal electrons is also supported by the time evolution of the cyclotron emission. As a result, the rf-driven current  $I_{rf}$  can be estimated as  $I_{rf} = I_p \Delta V_1/V_{10}$ . It is also expected theoretically, from the viewpoint of the calculated power spectrum, that the waves excited at  $\Delta\phi = 90^\circ$  should couple more effectively with the electrons producing the rf-driven current than the waves at  $\Delta\phi = -90^\circ$ . This agrees well with the experimental results shown in Fig. II.2-6. This agreement strongly suggests that the waves having a power spectrum nearly equal to the calculated one are excited in the plasma. The relative changes of the loop voltage, the cyclotron emission and the hard X-ray emission as a function of the applied rf power for  $\Delta\phi = 90^\circ$  are shown in Fig. II.2-7. All relative changes are found to saturate at the applied rf power of 120 kW. When the applied rf power is 125 kW a rf-driven current of 15 kA is obtained.

#### 2.4 High power density heating experiment

In order to study a high- $\beta$  tokamak and develop high power heating technology, NBI of 2.5 MW and ICRF of 1 MW experiments in JFT-2 are being prepared.

The NBI system was developed and prepared by Plasma Heating Engineering Laboratory and Facility Operation and Engineering Section from April 1979 to March 1980 and was installed to JFT-2. Major parameters of the system are as follows:

Power supply : 40 kV, 2.5 MW  $\times$  2, 200 ms

Ion source : 30 kV, 25 A  $\times$  4 1980  
40 kV, 30 A  $\times$  4 1981

NBI power into Torus : 1  $\sim$  1.5 MW 1980  
2  $\sim$  2.5 MW 1982

A few days experiment with 1 MW was successfully done in March and the major results are as follows: Max.  $T_i = 1.1$  keV, Max. Volume average  $\beta = 2\%$ .

The ICRF system has been designed and will be completed at the beginning of 1981. The major parameters are as follows:

Generator : 1 MW, 20 MHz, 50 ms

Antenna : all metal, outside & inside

## 2.5 Summary

Recent results obtained in the modified JFT-2 are summarized as follows;

- (1) Plasma position control in a shell-less tokamak was successfully achieved by adjustment of primary windings and by addition of the passive circuit to the active control system.
- (2) A stable high density plasma of  $\bar{n}_e = 6 \times 10^{13} \text{ cm}^{-3}$  was obtained at  $B_t = 10 \text{ kG}$ ,  $q_a = 2.5$ . This plasma is sufficient as a target plasma for MW neutral beam injection.
- (3) Efficient ion heating of  $2 - 3 \text{ eV/kW} \cdot 10^{13} \text{ cm}^{-3}$  was obtained with the optimized launcher on application of 200 kW RF power.
- (4) Tangential CX spectra showed the existence of high energy ions with the decay time of 1 - 2 ms at the plasma center, which must be responsible for the bulk ion heating.
- (5) It was found that the electron temperature of peripheral plasma plays an important role for the bulk ion heating. Preliminary results of hybrid heating experiments with neutral beam injection showed a possibility of suppression of parametric decay instabilities at the outer region of plasma.
- (6) It was observed that the waves launched from a phased array antenna of four waveguides couple effectively with electrons under the condition of  $\omega_0/\omega_{1h}(0) \geq 2.0$ .
- (7) The coupling generates a rf driven current, rather than heating of the bulk electrons, and the current/rf-power ratio of 110 A/kW was obtained with a rf power of 125 kW radiated into a plasma which included appreciable suprathermal electrons.

## References

- 1) MATSUZAKI, Y., et al., in Proc. of the 8th Symp. on Engineering Problems in Fusion Research, San Francisco, Nov. 1979.
- 2) SUZUKI, N., et al., in the 8th Int. Conf. Brussels, 1980, EAIA-CN-38-T-2-3.



- 3) NAGASHIMA, T. and FUJISAWA, N., in Proc. of the Joint Varenna-Brenoble Int. Symp. on Heating in Toroidal Plasma, Grenoble France, 1978.
- 4) FUJII, T. et al., in Proc. of the 7th Int. Conf. Innsbruck, 1978, IAEA-CN37-A-4-2.
- 5) PACHER, H.D., et al., ibid. IAEA-CN37-A-4-3.
- 6) FUJITA, J., et al., in Proc. of the 9th European Conf., Oxford, England, 1979.
- 7) SUZUKI, N., et al., in Proc. 4th Int. Conf. on Plasma Surface Interaction in Controlled Fusion Devices, Germisch, Apr. 1980.
- 8) YAMAMOTO, T., et al., to be published in Phys. Rev. Letters.

Table II.2-1 Parameters of the modified JFT-2 and RF  
(lower hybrid wave) system.

Modified JFT-2 Machine Parameters

|                                |                              |
|--------------------------------|------------------------------|
| Major Radius                   | $R_0 = 90 \text{ cm}$        |
| Minor Radius                   | $a_L \leq 28 \text{ cm}$     |
| Minor Wall Radius              | $a_w = 31 \text{ cm}$        |
| Toroidal Magnetic Field        | $B_t \leq 16 \text{ kG}$     |
| Time Constant of Control Field | $5 \text{ ms}$               |
| Bakable Temperature            | $350 \text{ }^\circ\text{C}$ |

Typical Plasma Parameters

|                              |  |
|------------------------------|--|
| Plasma Current               | $I_p \leq 170 \text{ kA}$                          |
| Loop Voltage                 | $V_L = 1.5 - 2.5 \text{ V}$                        |
| Central Electron Temperature | $T_{eo} = 0.5 - 1.0 \text{ keV}$                   |
| Central Ion Temperature      | $T_{io} = 0.25 - 0.5 \text{ keV}$                  |
| Mean Electron Density        | $\bar{n}_e = 1 - 6 \times 10^{13} \text{ cm}^{-3}$ |
| Effective Z                  | $Z_{eff} = 1.0 - 5.0$                              |

RF Heating System

|                        |   |
|------------------------|---|
| RF Frequency           | $f_0 = 650 \text{ \& } 750 \text{ MHz}$ |
| RF Power               | $P_{RF} \leq 320 \text{ kW}$            |
| Coupling System        | Phased Array of Four Waveguides         |
| Size of Each Waveguide | $3.3 \text{ cm} \times 29 \text{ cm}$   |

Table II.2-2 Energy balance with and without the RF power.  $P_D$  is the deposited RF power. Heating efficiency  $\eta = P_D/P_{RF}$ .

|                                     | Without RF           | With RF<br>$P_{RF} = 200 \text{ kW}$ |
|-------------------------------------|----------------------|--------------------------------------|
| $\bar{n}_e \text{ (m}^{-3}\text{)}$ | $1.9 \times 10^{19}$ | $1.9 \times 10^{19}$                 |
| $L_V \text{ (V)}$                   | 2.1                  | 1.9                                  |
| $I_p \text{ (kA)}$                  | 110                  | 110                                  |
| $P_\Omega \text{ (kW)}$             | 231                  | 209                                  |
| $T_{e0} \text{ (eV)}$               | 630                  | 690                                  |
| $T_{i0} \text{ (eV)}$               | 400                  | 700                                  |
| $W_e \text{ (J)}$                   | 985                  | 1010                                 |
| $W_i \text{ (J)}$                   | 540                  | 870                                  |
| $Q_{e-i} \text{ (kW)}$<br>(e)       | 53                   | 6                                    |
| $\tau_E \text{ (ms)}$<br>(i)        | 5.5                  | 5.0                                  |
| $\tau_E \text{ (ms)}$               | 10.2                 | 7.5                                  |
| $\tau_E \text{ (ms)}$               | 6.6                  | 5.9                                  |
| $P_D \text{ (kW)}$                  | -                    | 110                                  |

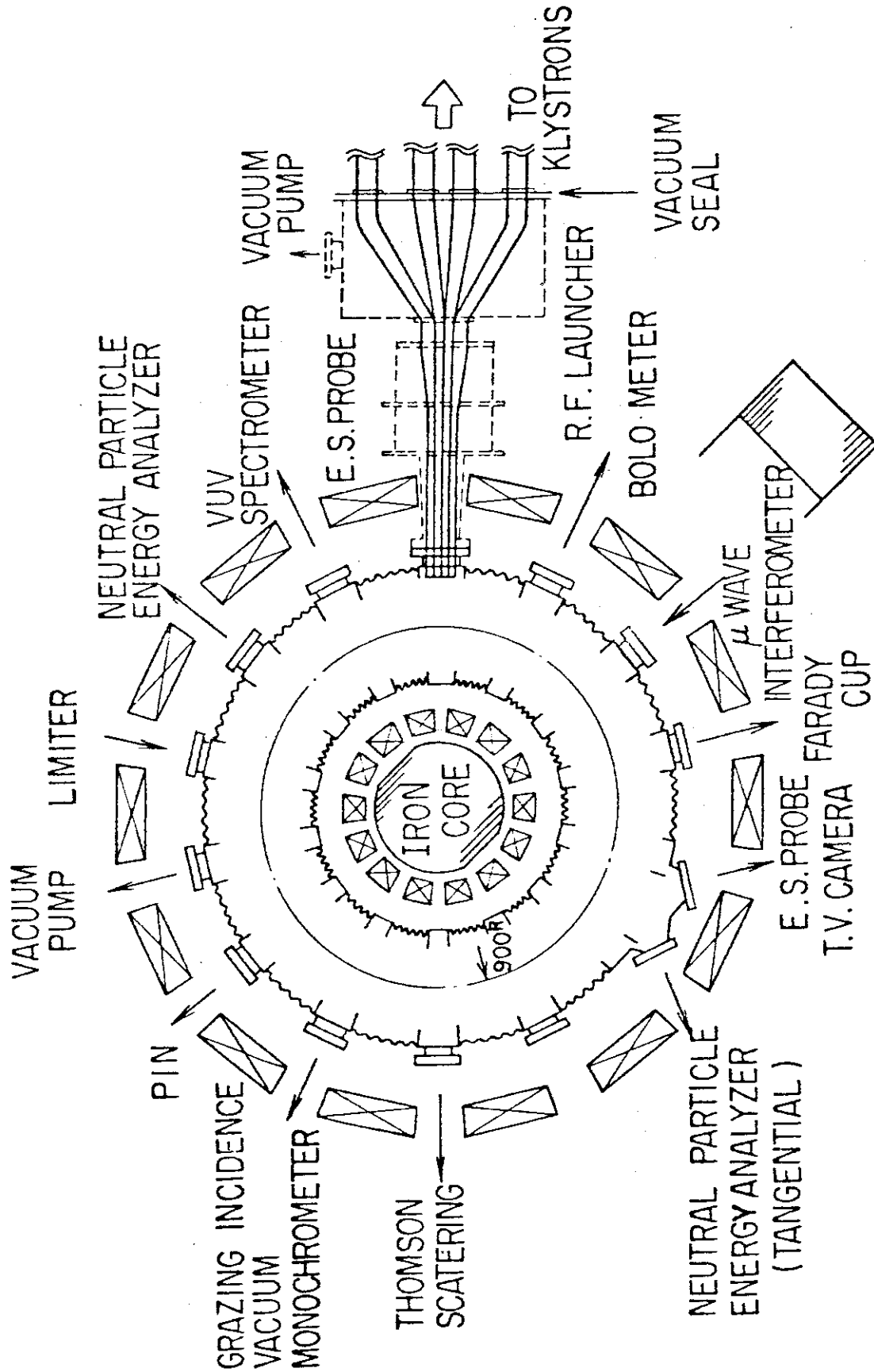


Fig. II.2-1 Top view of the modified JFT-2 tokamak and RF (lower hybrid wave) system. Diagnostics equipped are also shown.

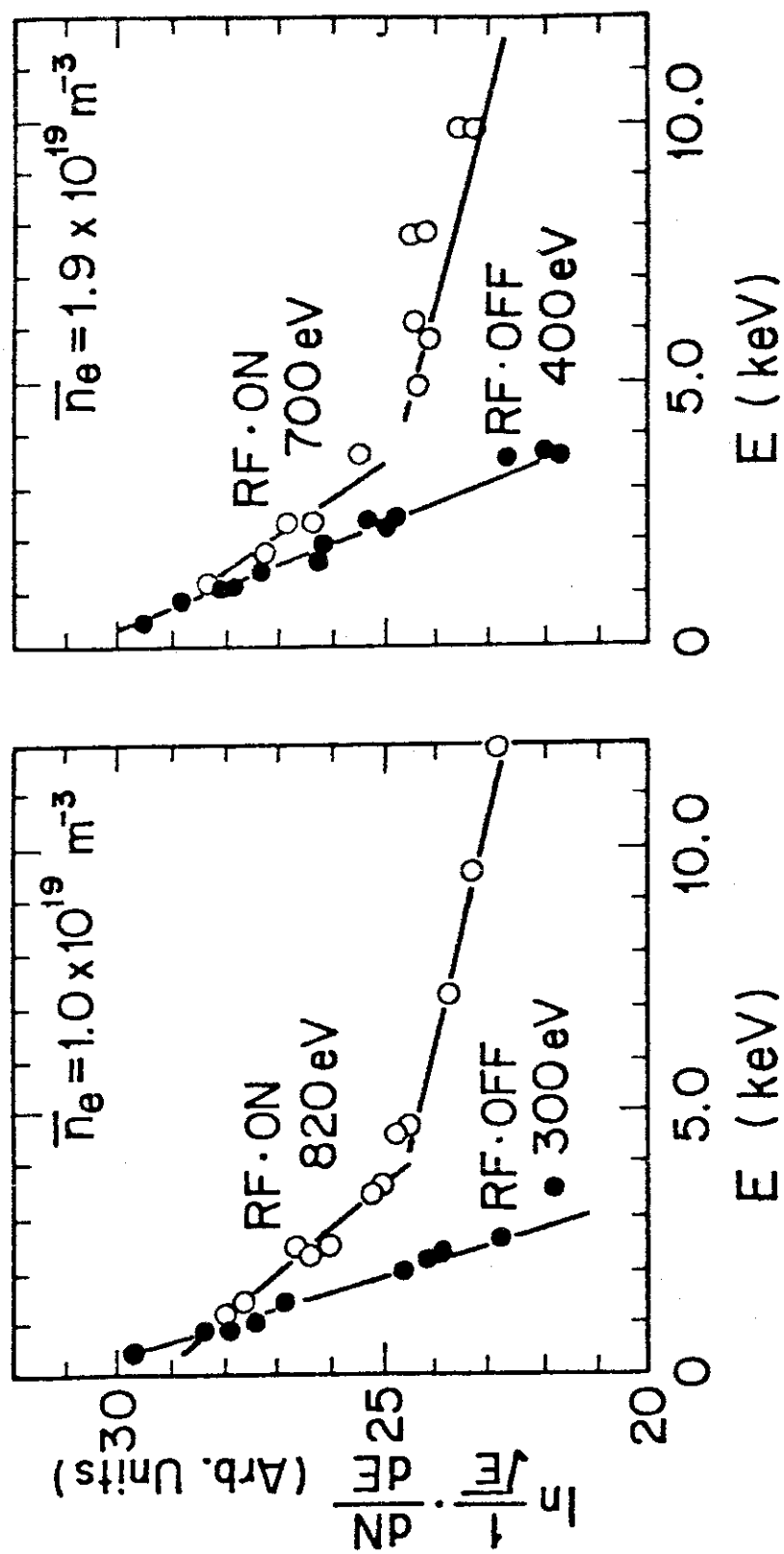


Fig. II.2-2 Tangential CX spectra with and without RF power. High energy ion tail is seen as well as in the perpendicular CX spectra.

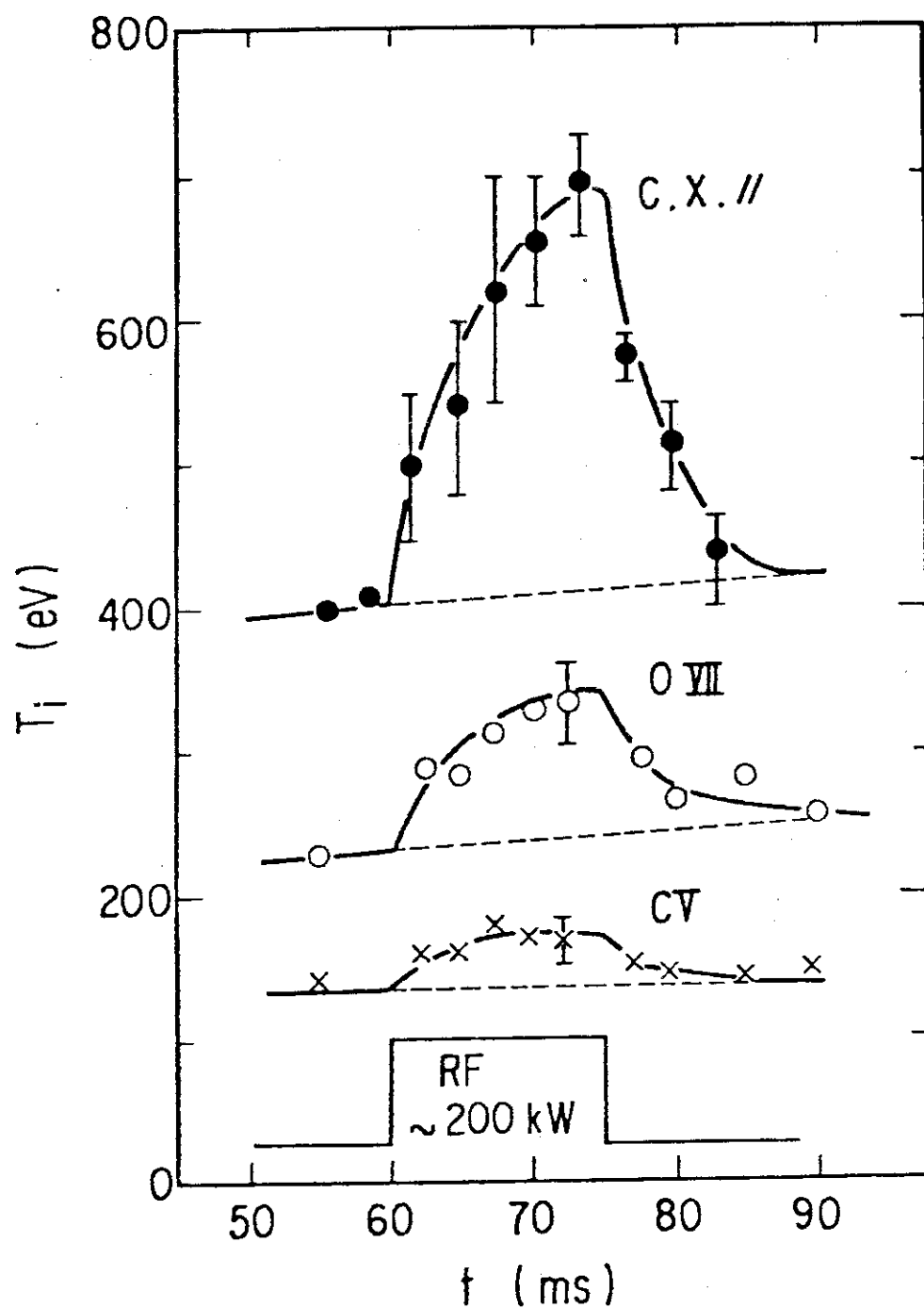


Fig. II.2-3 Time evolution of various ion temperature. Tangential ion temperature at  $r = 0$  cm, Doppler ion temperatures O VII at  $r \approx 10$  cm and CV at  $r \approx 17$  cm.

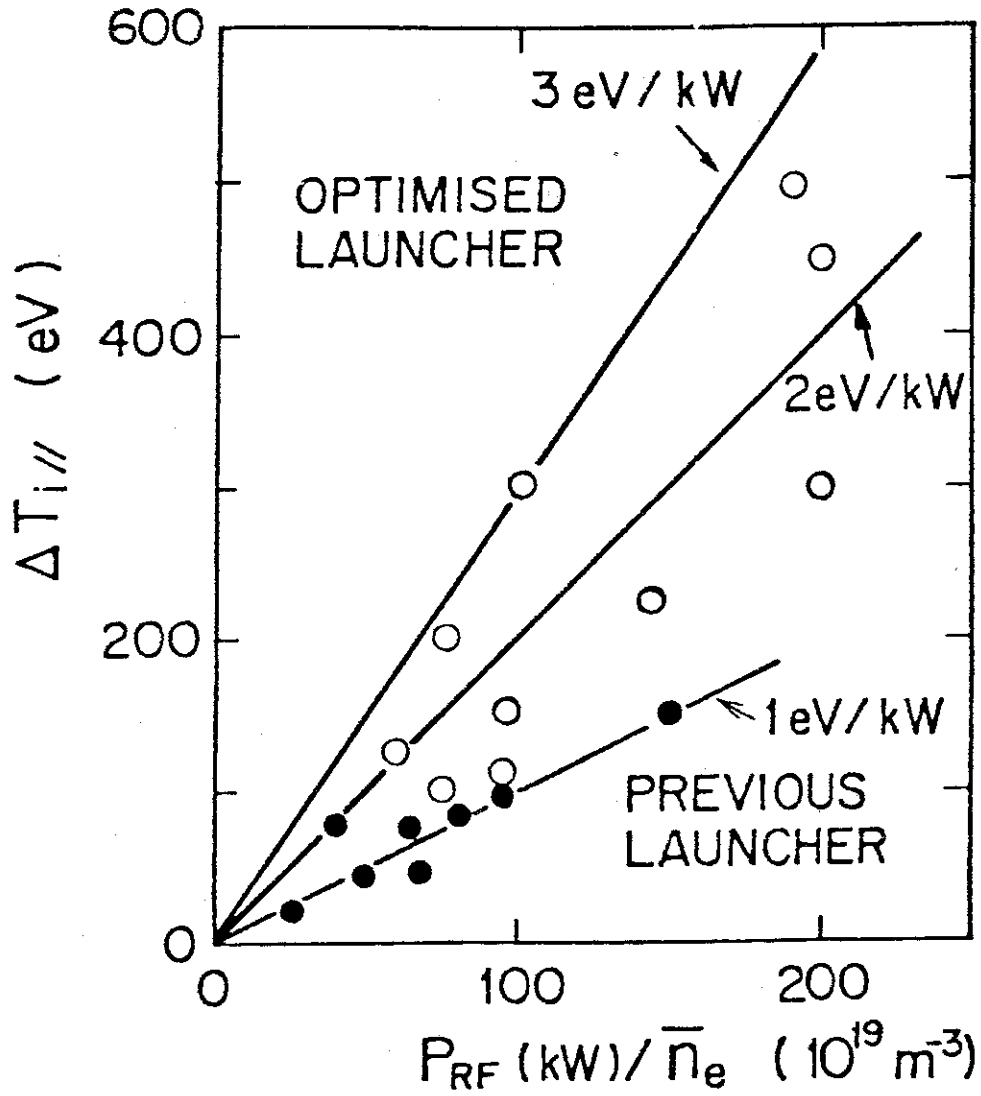


Fig. II.2-4 Ion temperature increase versus normalized RF power. Previous results are also shown and improvement of ion heating efficiency by more than 2 times is clear.

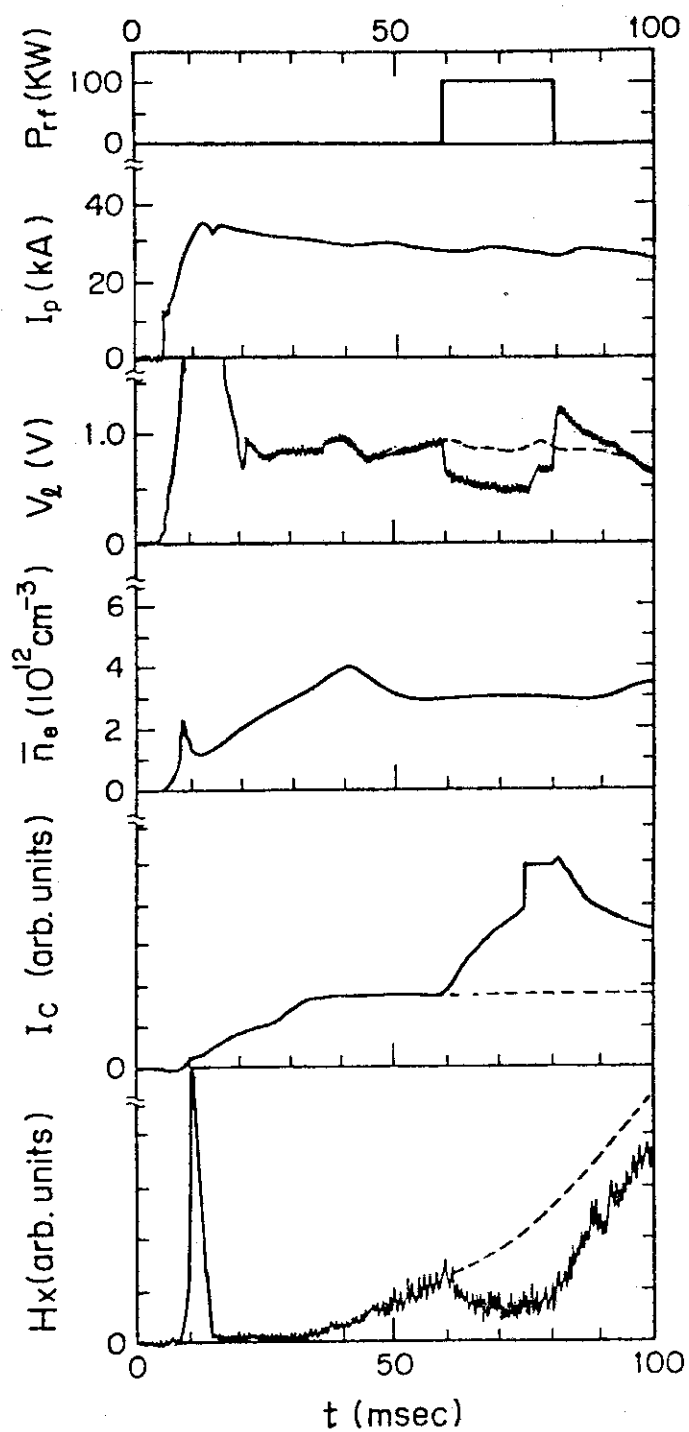


Fig. II.2-5 Typical plasma shot:  $B_t = 14$  kG and  $\Delta\phi = 90^\circ$ ; the solid lines show the shot with the rf pulse and the dotted lines with no rf pulse.



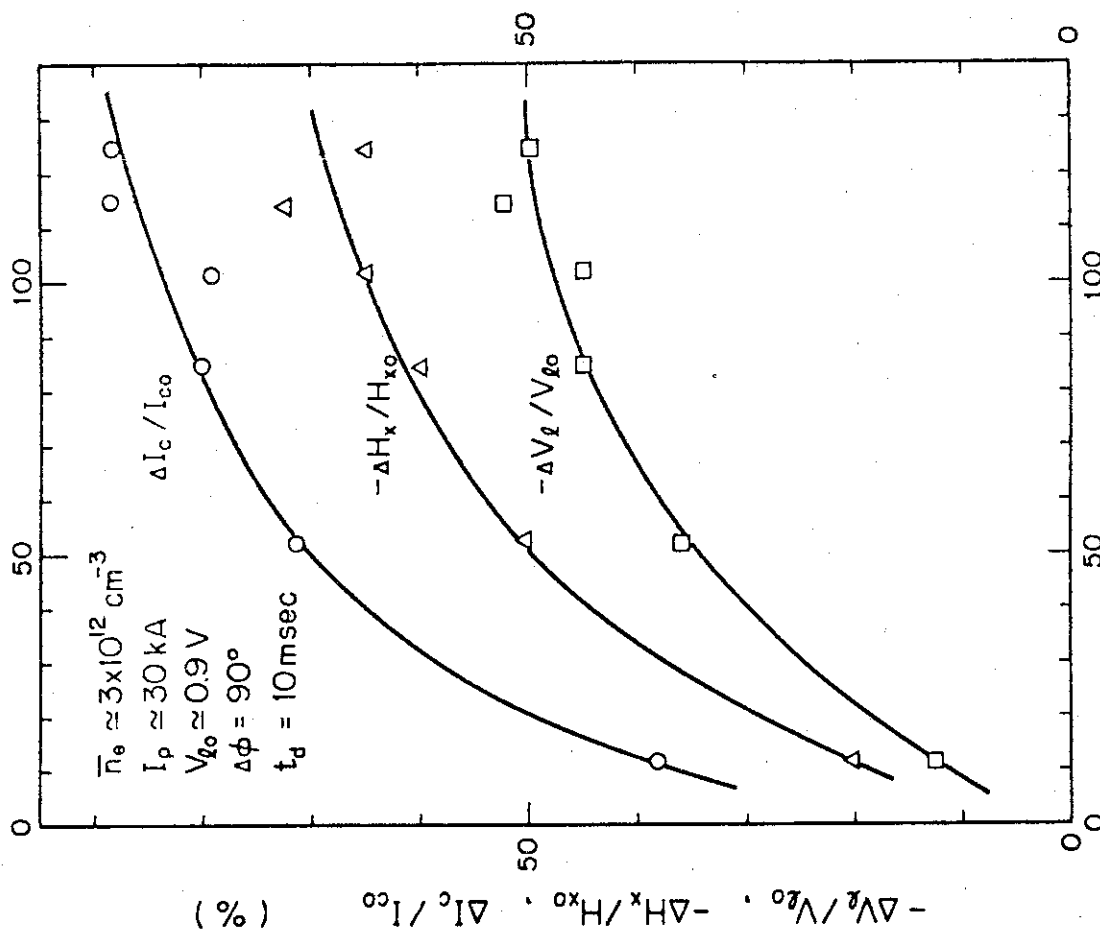


Fig. II.2-7 Relative changes of the loop voltage, the cyclotron emission and the hard X-ray emission as a function of the applied RF power.

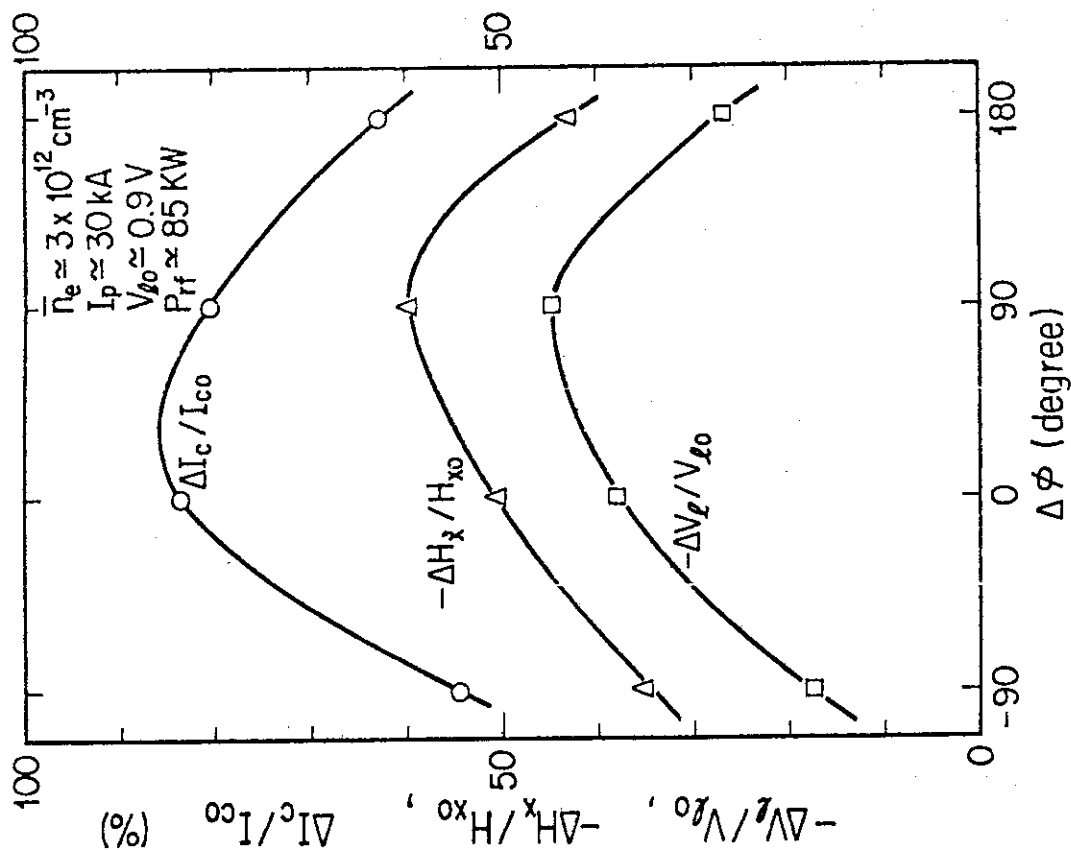


Fig. II.2-6 Relative changes in the loop voltage, the cyclotron emission and the hard X-ray emission versus the phase difference.

### 3. JFT-2a

#### 3.1 ICRF Heating Experiment

In the early experiment [1], we obtained the ion heating efficiency,  $\eta_i (\equiv P_{rf}^i / P_{Net}) \lesssim 40\%$  even for the optimum majority heating conditions, where  $P_{rf}^i$  and  $P_{Net}$  are respectively the RF power absorbed by ions in the plasma core and one excluding the circuit loss. In that case, a Faraday shield was not used. Later, a full Faraday shield was installed to cancel the potential gap between the antenna and the wall (the photograph of the Faraday shield is shown in Ref.[3].) As a result, the heating efficiency has increased by a factor of 2.3. The central temperature of bulk ions increased from 160 eV to 430 eV in application of  $P_{Net} = 115$  kW with the heating efficiency of 80 %.

##### 3.1.1 Majority and minority heatings

Figure II.3.1-1 compares charge-exchange neutral spectra for the cases of (a)  $\epsilon_p \lesssim 5\%$  and (b)  $\epsilon_p = 5 \sim 10\%$ . The other parameters and the RF net powers were almost same in these cases, i.e. the average electron density  $\bar{n}_e \approx 3.5 \times 10^{13} \text{ cm}^{-3}$ , the base ion temperature  $T_{i0} \approx 160$  eV, the base electron temperature  $T_{e0} \sim 330$  eV, the plasma current  $I_p = 33$  kA and  $B_T = 18$  kG. The Faraday shield was not used in this experiment. These spectra were measured by the analyser which was not capable of mass-discrimination. So they contain both contributions from deuterium and hydrogen.

It is shown that a remarkable high-energy tail was built up for  $\epsilon_p \lesssim 5\%$ . It is quite natural that we assume the origin of the high-energy tail as the minority protons. On the other hand, for  $\epsilon_p = 5 \sim 10\%$ , a high-energy tail became very small, but the slope of the bulk component in the range of 0.5 - 1.5 keV was rather larger than that of the case of  $\epsilon_p \lesssim 5\%$ . The results indicates that majority heating is dominant for  $\epsilon_p = 5 \sim 10\%$ , while minority heating for  $\epsilon_p \lesssim 5\%$ . Increases of the electron temperature were within 10 % in both cases.

The critical values of  $\epsilon_p$  for the mode conversion and for the maximum proton damping are given in Ref.[5].

$$\epsilon_p = \left( \frac{\beta_e T_H}{2T_e} \right)^{\frac{1}{2}} S \left( \frac{4}{3} + S_z^2 \right) \quad \text{for the mode conversion} \quad (1)$$

$$\epsilon_p = [\beta_d S_Z^2 (4 + S_Z^2) (\frac{4}{3} + S_Z^2) / 4\pi]^{\frac{1}{2}} \quad (2)$$

for the maximum proton damping

where  $S \equiv kc/\omega_p D$ , with  $\omega_p D$  the plasma frequency in deuterium, and  $k_z$  and  $k$  are wave numbers along the toroidal and total magnetic field, respectively. These critical values are calculated to be  $4 \sim 7\%$  for the mode conversion and  $\sim 2\%$  for the maximum proton damping, using the measured value of  $k_z \sim 0.15 \text{ cm}^{-1}$  [2]. These provide theoretical evidence for our experimental results. It has been confirmed that the majority heating occurs when the condition of the mode conversion is fulfilled.

It was shown that the majority heating was sensitive to  $\epsilon_p$  and  $B_T$  in Ref.[1]. These parameter dependence was well explained by the mode conversion theory [2].

The excited fast wave is converted to the ion Bernstein wave near the two-ion hybrid resonance layer. The ion Bernstein wave is strongly damped by the plasma particles via ion cyclotron resonance and electron Landau damping. Therefore, we can estimate the power absorbed by the plasma as that transferred from the fast wave to the ion Bernstein wave, using the Budden tunneling parameter  $\eta$  [6].

When the proton-to-electron density ratio  $n_H/n_e$  is much smaller than unity,  $\eta$  is given as follows.

$$\eta \approx \sqrt{6} \pi \frac{R}{c} \frac{\epsilon_p \omega_p D}{8 + 6S_Z^2} \quad (3)$$

where  $R$  and  $c$  are respectively a major radius and speed of light. Figure II.3.1-2(a) shows the power flow schematically for the fast wave incident from the lower field side. Some of the wave power is absorbed and the rest of the power is tunneled through or reflected near the two-ion hybrid resonance layer, and goes to the plasma periphery where the power is again reflected back to the plasma center with the effective power reflection coefficient  $\xi$ .

Figure II.3.1-2(b) is an example of the comparison between experiment and theory. The increases of the bulk ion temperature  $\Delta T_i$  divided by the RF net power are plotted as a function of the proton-to-electron density ratio. The solid lines are the total absorption coefficient calculated on the basis of the above model with the parameter  $\xi$ .

These curves are normalized at their maxima. Experimental results and calculated ones are in agreement with each other when  $\xi = 0.8 \sim 0.95$ , which is consistent with the one derived from the measured wave power evolutions in the toroidal direction [2]. The  $B_T$ -dependence of the heating and the wave amplitude is also well explained by the above model.

We can conclude that the optimum heating conditions for the lower field excitation are to select  $\eta$  to be  $\sim 0.5$ , for which the total power absorption coefficient takes the maximum value, and to adjust  $B_T$  so as to locate the two-ion hybrid resonance layer near the plasma center. In our case,  $\epsilon_p = 5 \sim 10\%$  and  $B_T = 17.5 \sim 18$  kG corresponding to the optimum heating conditions.

### 3.1.2 Increase of the heating efficiency

The equivalent antenna loading impedance  $R_S$  is divided into three components.

$$R_S = R_1 + R_2 + R_C$$

$R_1$ ,  $R_2$  and  $R_C$  are impedances related to a core heating, a surface heating and a circuit loss, respectively. The surface heating is due to the acceleration of plasma particles by the potential gap between the antenna and the wall as well as due to the direct wave heating if the wave has a large damping decrement in the surface. We can write the heating efficiency  $\eta_1$  as  $R_1/(R_1 + R_2)$ . Therefore, reduction of  $R_2$  is necessary to improve the heating efficiency. The Faraday shield played an important role for this purpose. The loading impedance was reduced from  $6 \sim 7 \Omega$  to  $2 \sim 3 \Omega$  by using the Faraday shield.

Figure II.3.1-3(a) and (b) show increase of the central ion temperature  $\Delta T_1$  and that of the boundary electron temperature  $\Delta T_{eb}$ , versus  $P_{Net}$  for the cases with and without the Faraday shield.

The proportional coefficients are written as

$$\begin{aligned} \Delta T_1 &\propto R_1 I_C^2 = \frac{R_1}{R_S - R_C} P_{Net} \\ \Delta T_{eb} &\propto R_2 I_C^2 = \frac{R_2}{R_S - R_C} P_{Net} \end{aligned} \quad (4)$$

where  $I_C$  is the antenna current.

From the ratio of the proportional coefficients between the cases with and without the Faraday shield, one can evaluate the heating efficiency.

$$\eta_i = \frac{u(1-v)}{u-v} \quad (5)$$

$$\eta_i' = \frac{1-v}{u-v}$$

where  $u$  and  $v$  are respectively the ratio of the proportional coefficients of  $\Delta T_i$  and  $\Delta T_{eb}$ , and the prime denotes the quantity without the Faraday shield.

We obtain  $\eta_i = 61 \sim 85 \%$  and  $\eta_i' = 27 \sim 33 \%$  for  $B_T = 17.5 \sim 18$  kG and  $\epsilon_p = 5 \sim 10 \%$ . Thus, the Faraday shield increased the heating efficiency by a factor of 2.3. In spite of the limited data with large error bars for the case without the Faraday shield, the result  $\eta_i' = 27 \sim 33 \%$  is reasonable in comparison with the one derived from the decay of the ion temperature [1]. It will be shown that  $\eta_i$  agrees well with that evaluated with a 1-D tokamak simulation code in the next section.

### 3.1.3 Power balance in the optimum heating conditions

Figure II.3.1-4 shows the charge-exchange neutral spectra for the optimum conditions, i.e.  $\epsilon_p \sim 9 \%$ ,  $B_T = 17.5$  kG and with the Faraday shield. Although this is the majority heating case as is shown in Fig. II.3.1-1(b), a significant high-energy tail appeared since the effective RF power increased by a factor of three from that in Fig. II.3.1-1. The spectrum is well separated into the deuteron and proton components as is shown in the figure, using a one-component Maxwell distribution for deuterium and the steady-state solution of the Fokker-Planck equation derived by Stix [4], for hydrogen. We obtain  $T_D \sim 430$  eV and the average proton temperature  $\langle T_H \rangle \sim 740$  eV from the spectrum.

Heating power densities to each species are determined from point-model power balance equations including the collisional power transfer between each species and the neoclassical thermal conduction in the plateau regime. The thermal conduction is an order of magnitude larger than the other loss channels such as the ion-electron power transfer and the charge-exchange loss in the present conditions. The results are  $p_{rf}^D \sim 7.5$ ,  $p_{rf}^H \sim 3.5$ ,  $p_{He} \sim 0.4$ ,  $p_{HD} \sim 1.1$  W/cm<sup>3</sup> where  $p_{He}$  and  $p_{HD}$

are power densities transferred from protons to electrons and deuterons, respectively. The ratio  $p_{\text{rf}}^{\text{D}} / (p_{\text{rf}}^{\text{D}} + p_{\text{rf}}^{\text{H}})$  is about 0.7. The increase of the electron temperature was within 20 %, which is fully explained by the ion-electron power transfer.

Figure II.3.1-5(a) and (b) shows the radial profiles and time evolutions of the ion temperature, respectively. The solid lines are results of the computer simulation. The ion heat conduction coefficient is taken to be neoclassical in the plateau regime with an anomaly factor of three. The electron heat conduction and the particle diffusion are assumed to follow the Alcator scaling. We further assume a rectangular power deposition profile with a radius of 3 cm for the majority deuterons. Presence of the proton component is ignored for simplicity. The contribution of protons to the deuteron power balance (about 10 %) is included in the RF heating power to deuterons. The radius of 3 cm is easily deduced from the consideration of the RF power density required to be balanced with the thermal conduction loss. The heating efficiency is taken to be 83 %.

The simulation results agree well with the experiment. The combination of the above assumptions is unique choice to match the simulation with the experiment.

In summary, in the optimum conditions, the majority deuterons are heated mainly by the RF power ( $\sim 90$  %) and partly by the minority protons ( $\sim 10$  %) with the heating efficiency of 80 %. The RF power is concentrated in the central regions ( $r \sim 3$  cm). The transport of the RF-heated ions is well explained by the neoclassical theory with the anomaly factor of three even when the input power density is 10 times larger than that in the Ohmic heating.

#### References

- [1] KIMURA, H., ODAJIMA, K., SENGOKU, S., OHASA, K., SUGIE, T., et al., Nucl. Fusion 19 (1979) 1499.
- [2] IIZUKA, S., ODAJIMA, K., KIMURA, H., SENGOKU, S., SUGIE, T., Propagation and Absorption of the Fast Magnetosonic Wave Near a Two-ion Hybrid Resonance Layer., Japan Atomic Energy Research Institute Report JAERI-M 8595 (1979), to be published in Phys. Rev. Lett.

- [3] KIMURA, H., ODAJIMA, K., SENGOKU, S., IIZUKA, S., SUGIE, T., ICRF Heating in DIVA: Parameter Survey and Very High Efficiency Ion Heating Experiment, Japan Atomic Energy Research Institute Report JAERI-M 8429 (1979).
- [4] STIX, T., Nucl. Fusion 15 (1975) 737.
- [5] JACQUINOT, J., in Heating in Toroidal Plasmas (Proc. Joint Varenna-Grenoble Int. Symp. Grenoble, 1978) 1. (1979) 127.
- [6] NGAN, Y.C., SWANSON, D.G., Phy. Fluids 20 (1977) 1920.

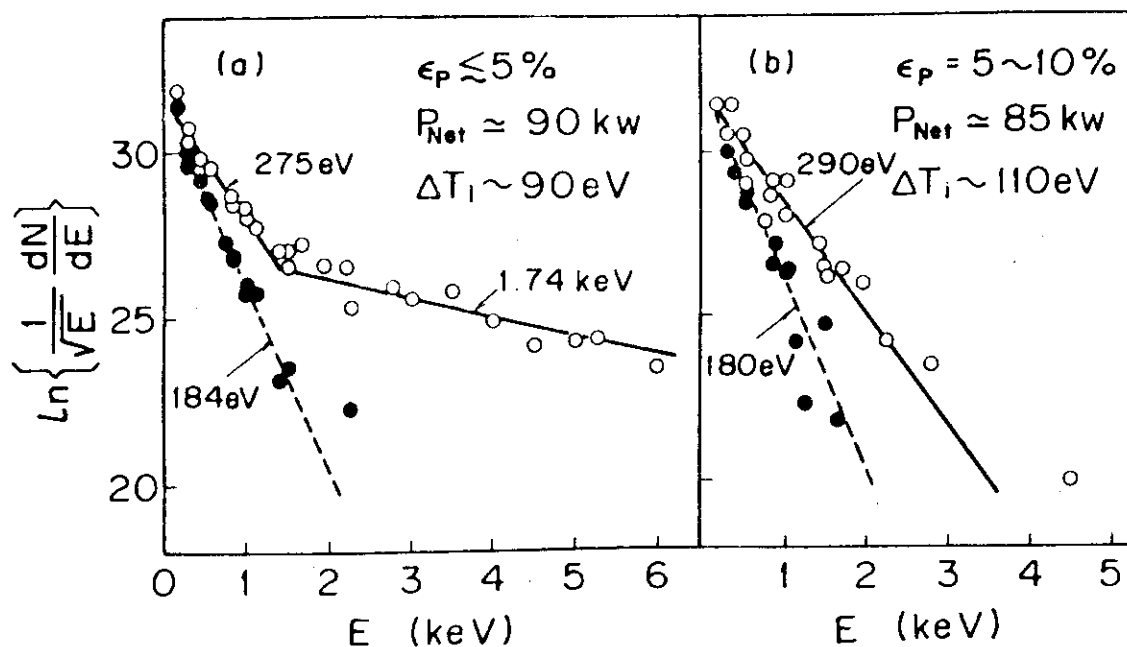


Fig. II.3.1-1 Charge-exchange neutral spectra indicating (a) minority heating and (b) majority heating; O with RF, ● without RF.

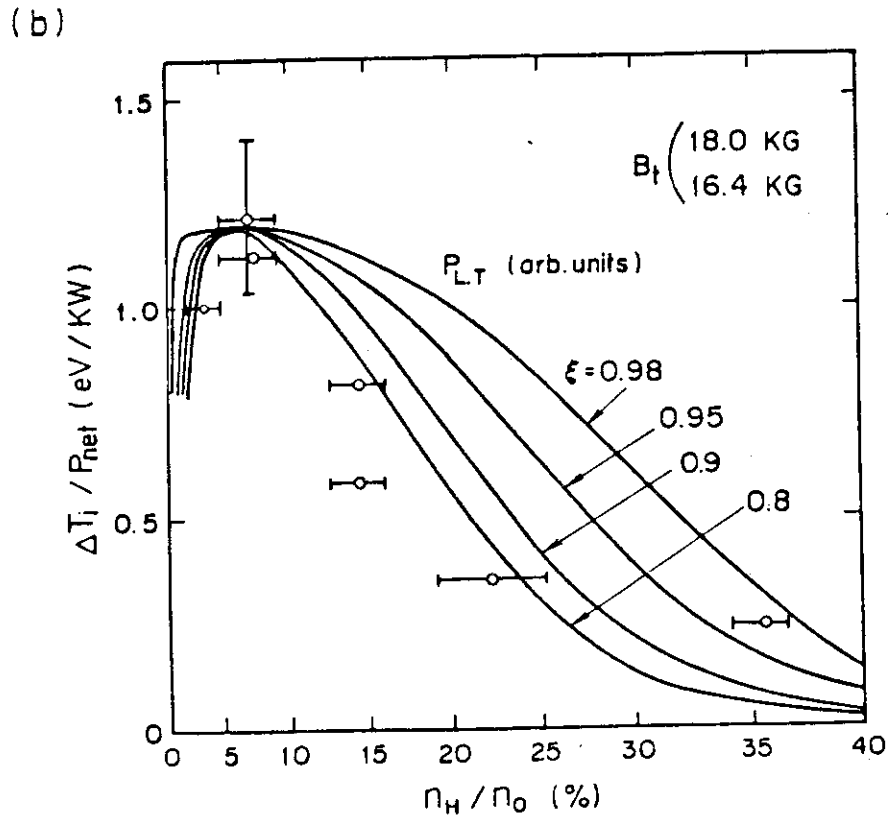
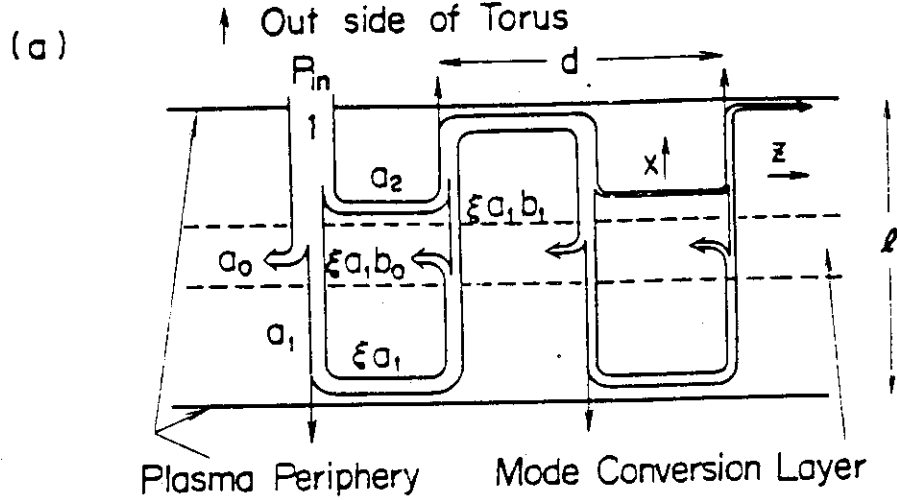


Fig. II.3.1-2(a) Model of the wave power flow.  $a_0 = e^{-2\eta}(1 - e^{-2\eta})$ ,  $a_1 = e^{-2\eta}$  and  $a_2 = (1 - e^{-2\eta})^2$  are coefficients of absorption, tunneling and reflection, respectively, for the wave incident from the lower field side.  $b_0 = 1 - e^{-2\eta}$  and  $b_1 = a_1$  are respectively those of absorption and tunneling for the wave from the higher field side.  $\xi$  is the effective power reflection coefficient at the plasma periphery.

(b) Increase of the bulk ion temperature divided by the RF net power,  $\Delta T_i / P_{net}$ , versus the proton-to-electron density ratio,  $n_H / n_0$ . The solid lines are total power absorption coefficients  $P_{L,T} = (a_0 + a_1 b_0 \xi) / (1 - a_2 \xi - a_1 b_1 \xi^2)$  derived from the above model. These are normalized at their maxima.



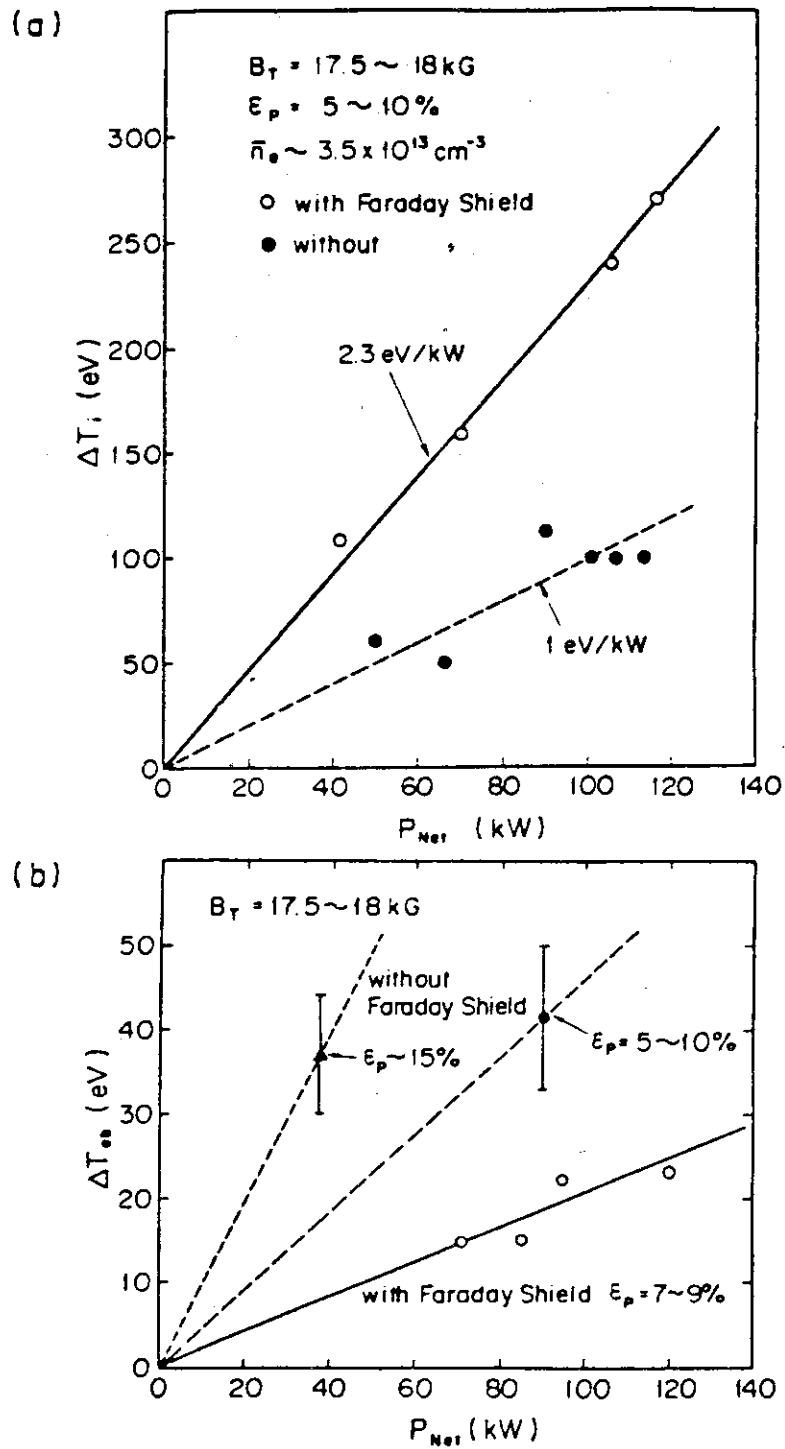


Fig. II.3.1-3 (a) Bulk ion temperature increase,  $\Delta T_i$ , versus RF net power,  $P_{Net}$ , for the cases with and without the Faraday shield.  
 (b) Boundary electron temperature increase,  $\Delta T_{eb}$ , versus  $P_{Net}$ , for the cases with and without the Faraday shield.

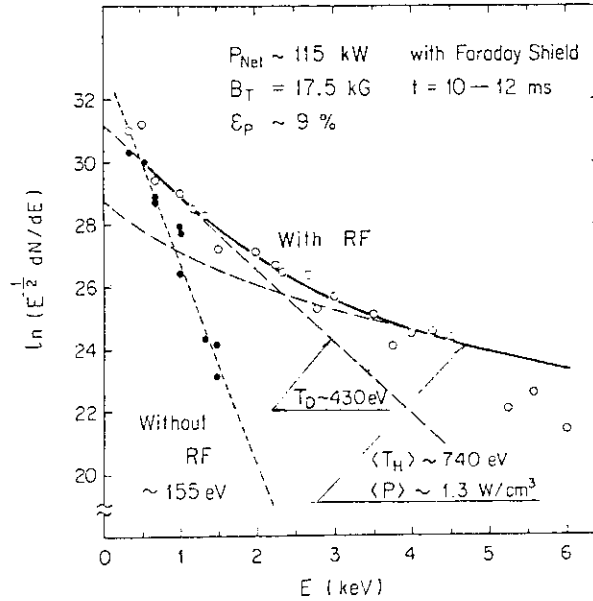


Fig. II.3.1-4 Charge-exchange neutral spectra for the majority heating averaged over the latter 2 ms of the RF pulse shown in Fig.5(b). The deuteron temperature was determined in the energy range of up to 1.5 keV where the contribution from the proton component was negligibly small. The theoretical curve for hydrogens are for  $T_e = 330$  eV,  $n_e = 7 \times 10^{13} \text{ cm}^{-3}$ ,  $Z_{\text{eff}} = 1$  and the local heating power density  $\langle P \rangle = 1.3 \text{ W/cm}^3$ .

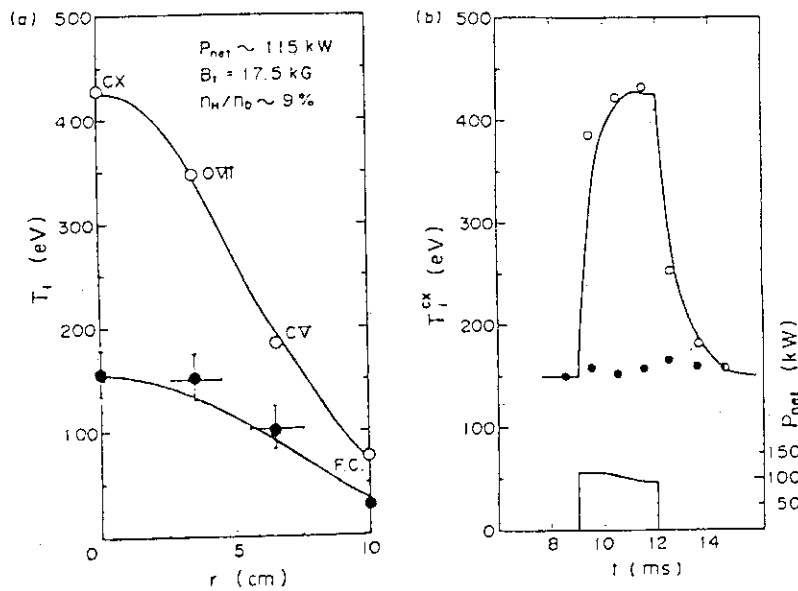


Fig. II.3.1-5 (a) Radial profiles of the ion temperature obtained by combining data of the charge-exchange neutral, the impurity Doppler broadening and the multigrid energy analyser (Faraday cup) at 11-12 ms;  $\circ$  with RF,  $\bullet$  without RF.

The solid lines are the results of the numerical simulation.

(b) Time evolutions of the perpendicular ion temperature measured by the charge-exchange analyser;  $\circ$  with RF,  $\bullet$  without RF.

The solid line is the result of the numerical simulation.

### 3.2 Carbon limiter and wall experiment

The following three kinds of carbons were tested as the limiter surface in DIVA.

- 1) Pyrolytic graphite (P.G.) (ideal carbon surface),
- 2) Precoated carbon film<sup>8)</sup> (pulverized carbon surface),
- 3) Carbon film produced in-situ by methane discharges.

Next, the carbon surface produced by the rf sputtering method and P.G. were applied to the DIVA tokamak as a first wall and poloidal rail limiters respectively. Confinement characteristics and impurity concentration are studied there.

#### 3.2.1 Sputtering characteristics of carbon surfaces

Figure II.3.2-1(a), (b), (c) are SEM pictures of three kinds of carbon. Precoated carbon has the form similar to powder. The carbon produced by methane discharges has smooth surface similar to the P.G. surface. In the methane discharges, the carbon ions which flow onto the surface have energy of about 100 eV because they are accelerated by the sheath potential. This mechanism is same as ion plating. Thickness of a few Å on the limiter surface is obtained by one discharge. The discharge current is 20 kA, the duration is 30 ms and the filling methane pressure is  $1 \times 10^{-4}$  Torr.

To study the sputtering characteristics of three types of carbon surfaces, a retractable target mounting which can be biased up to -1200 V and heated up to 750 °C is prepared. Each carbon surfaces are degassed and exposed as a limiter in the scrape-off plasma, whose electron temperature,  $T_{es}$ , and electron density,  $n_{es}$ , are  $T_e = 50$  eV and  $n_{es} = 3 \times 10^{12} \text{ cm}^{-3}$ , respectively.

The target limiter is negatively biased in the room temperature. The limiter current and the intensity of CII line radiation near the limiter are observed. The emitted carbon is ionized within 100 μsec. Therefore the intensity of CII line is proportional to the efflux from the limiter surface. Figure II.3.2-2 shows the results. Arcing is frequently observed on the pulverized carbon surface even in a stable phase, e.g. the probability of arcing is 17 % with -400 V of applied voltage. This situation simulates the surface which contacts to the plasma with  $T_e \approx 200$  eV. Arcing is observed only in a disruptive phase of discharge on the P.G. surface and the carbon film produced by methane discharges.

This result is very similar to those of metal surfaces<sup>(1)</sup>. Relation between  $\Delta I_{CII}$  and  $V$  is also investigated and ion sputtering is shown to be the dominant process of the carbon efflux from the normal surface.

The next problem is a chemical sputtering at a high temperature regime. The target limiter is heated up to 750 °C and the above method is employed to measure the relative sputtering yield. Figure II.3.2-3 shows that sputtering yield is enhanced at a high temperature, probably due to the chemical sputtering. However, the temperature dependance disappears after the first heat cycle. Therefore, the chemical reaction is easily suppressed. A similar result was also obtained by T. Abe et al.<sup>(3)</sup>.

### 3.2.2 Properties of obtained C-wall

The titanium coated shell surface of DIVA is coated with carbon by rf sputtering method. Coated area is about 70 % of the shell surface. The obtained surface differs from precoated carbon surface used above as a pulverlized limiter but is rather similar to the P.G. surface with the observation of SEM pictures. The AES spectrum of the carbon surface is compared with the titanium surface as shown in Fig. II.3.2-4. The surface of carbon is very pure, i.e., contaminated oxygen level is less than 0.2 %. Implanted argon used as working gas of rf sputtering and the oxygen contamination by air leakage can be easilly eliminated from the surface to the negligible level by several tens of discharge cleaning shots as shown in Fig. II.3.2-5. The surface is still clean after 500 discharges or more. This life time is ten times longer than that of the  $T_i$ -wall surface. Residual gas analysis shows that the methane formation arises in the first several discharges and the partial pressure decreases within a hundred discharges.

### 3.2.3 Low-q discharges in C-wall

Low-q plasmas are studied with the P.G. limiters and the carbon wall. Exchanging the first wall from titanium to carbon, the effective ionic charge,  $Z_{eff}$ , rises from 1.2 to about 2.0. It is estimated that an carbon density is equal to about 2.4 % of the electron density and is reasonable with the content estimated from the sputtering yield. A typical profile of radiation and charge exchange power loss ( $P_R + P_{CX}$ ),  $T_e$  and  $n_e$  of the case of C-wall is shown in Fig. II.3.2-6. This profile is similar to that of the case of  $T_i$ -wall except the boundary temperature

and  $P_R + P_{cx}$ . The radiation loss is dominated by oxygen impurities in the case of Ti-wall but is dominated by carbon impurities with the carbon wall. The total line radiation of carbon impurities is concentrated in outer layer than that of oxygen. In addition to these facts, the line radiation of the partially stripped metal impurity ions decreases three to four times when metal surface is coated. In the case of C-wall, the boundary temperature is rather low due to peripheral peaked radiative cooling. These situations are analogous to self boundary cooling.

Therefore, we can obtain fat plasmas such as scaled by previous experiments with Ti-wall<sup>(2)</sup>. Consequently, good confinement characteristics such as the factor-improved Alcator scaling are obtained as shown in Fig. II.3.2-7.

#### References

- 1) K. Ohasa et al., Nuclear Fusion 18 (1978) 872, J. Nuclear Material 76 & 77 (1978) 487, J. Phys. Soc. Japan 46 (1979) 1635, JAERI-M 7935.
- 2) DIVA Group, Nuclear Fusion 20 (1980) 271.
- 3) T. Abe et al., "Interaction of Atomic Hydrogen with Carbon" J. Nucl. Mat. 91 (1980) 223.

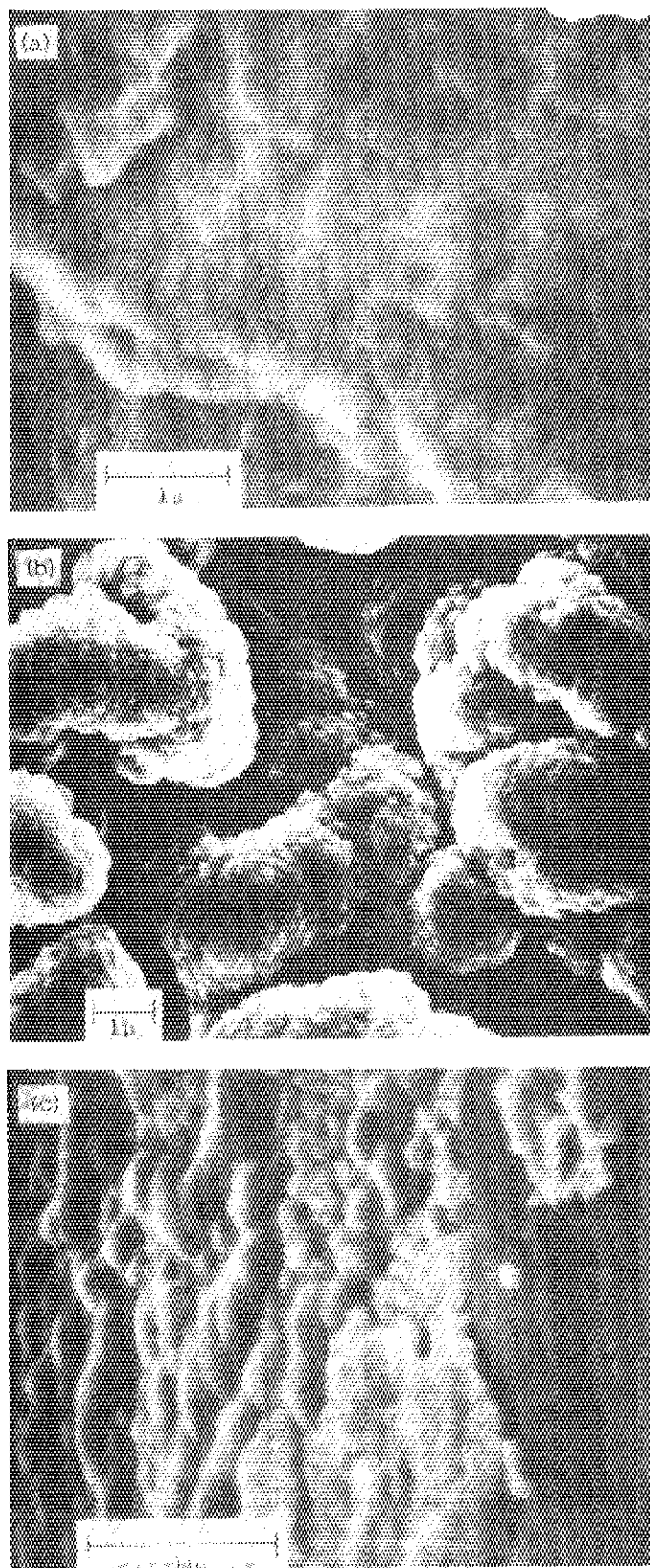


Fig. II.3.2-1 Scanning electron microscopic (SEM) picture of (a) pyrolytic graphite surface, (b) precoated carbon surface (pulverized surface), and (c) carbon surface produced by methane discharges.

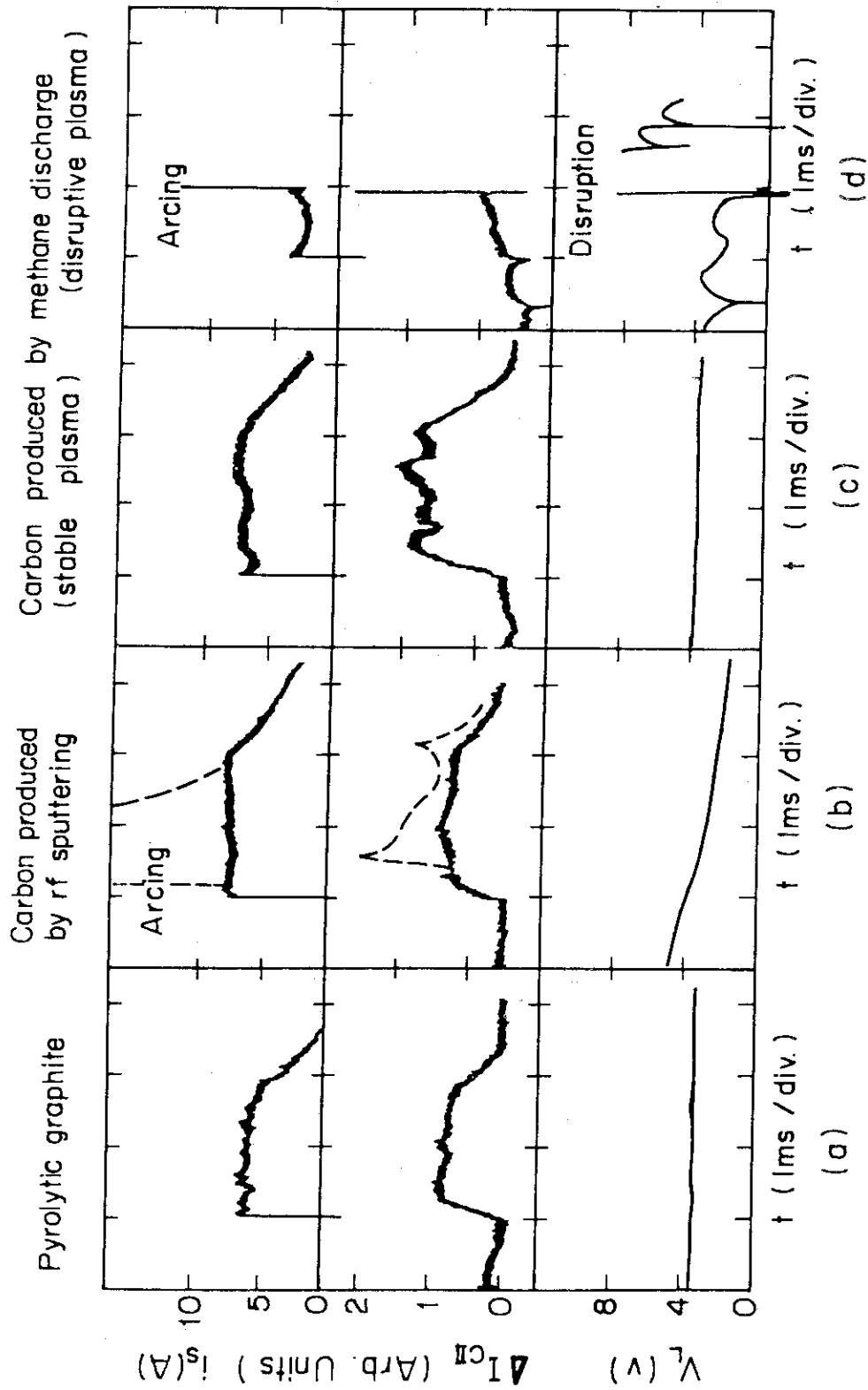


Fig. II.3.2-2 Typical wave forms of ion saturation currents  $i_s$  of a target limiter, increment of CII line intensity  $\Delta I_{CII}$  and loop voltage  $V_L$

(a) Pyrolytic graphite.  
 (b) Precoated carbon surface (pulverized surface). Arcing is observed.  
 (c) Carbon surface produced by methane discharges.  
 (d) Carbon surface produced by methane discharges in a disruptive phase of discharge. Arcing is observed.

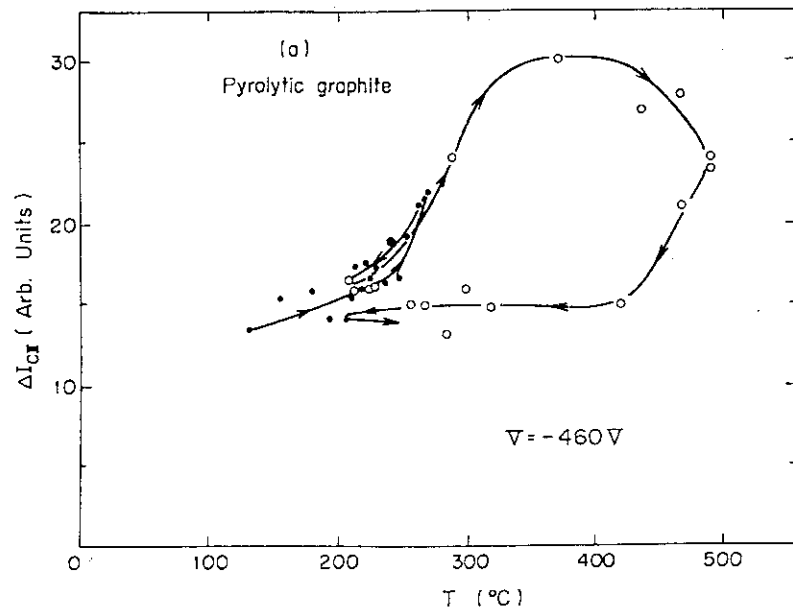


Fig. II.3.2-3  $\Delta I_{CII}$  v.s.  $T$ . Suppression of chemical reaction is observed after one heat cycle.

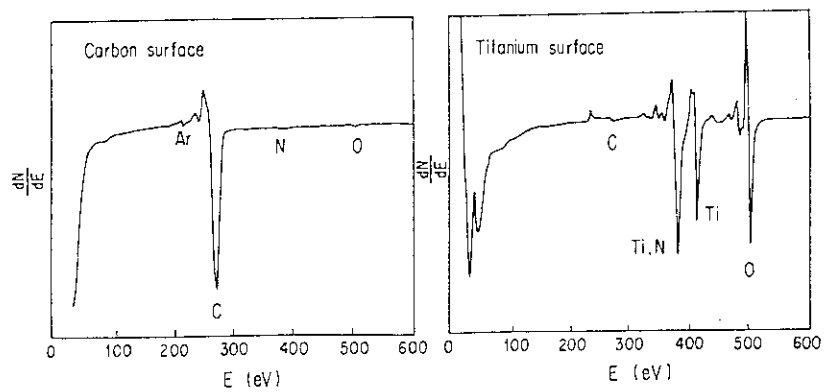


Fig. II.3.2-4 Auger spectra of titanium and carbon surface obtained by in-situ coating. Both are analysed in situ immediately after coating.

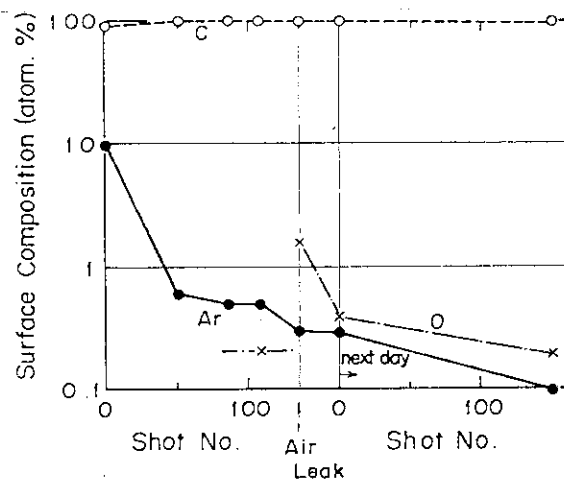


Fig. II.3.2-5 Time history of surface composition of coated carbon wall.



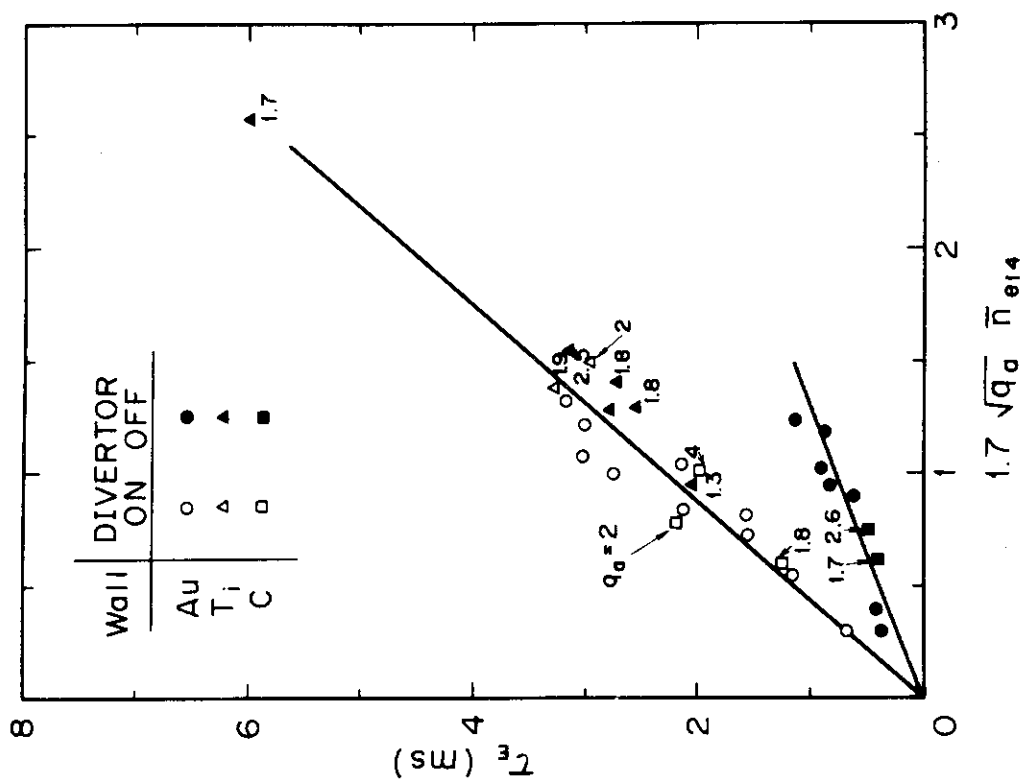


Fig. II.3.2-7  $T_e$  v.s.  $1.7\sqrt{q_a} \bar{n}_{e14}$  where  $\bar{n}_e$  is line-averaged density in  $10^{14} \text{ cm}^{-3}$  and  $\tau_E$  in ms. Au wall (○, ●), Ti wall (△, ▲) and C wall (□, ■) are investigated with divertor (○, △, □) and without divertor (●, ▲, ■).

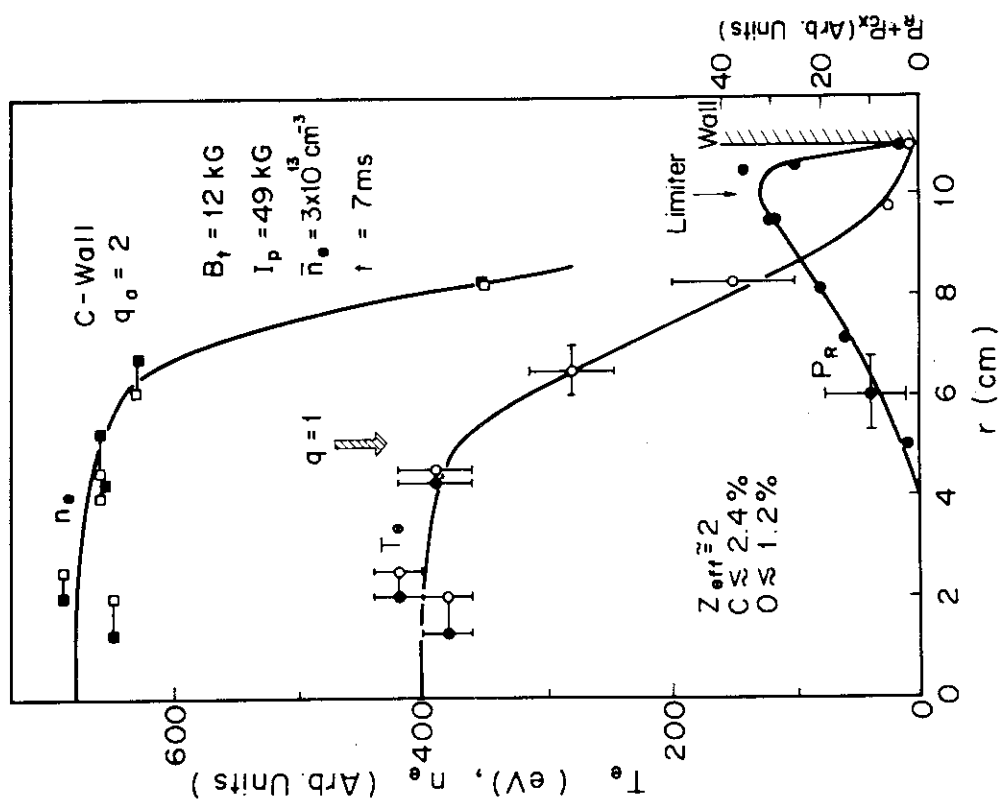


Fig. II.3.2-6 Typical profiles of  $E_e$ ,  $n_e$  and  $P_R + P_{CX}$  in case of low- $q$ , C-wall experiments.

### 3.3 Role of runaway electrons in the formation of arcing on the electrically isolated target in tokamak

In this section, we discuss the role of runaway electrons in the formation of arcing. Figure II.3.3-1 shows the cross-sectional view of DIVA and experimental set-up. Divertor region is distinguished as the electron side and the ion side of the divertor with respect to the median plane<sup>1)</sup>. Runaway electrons appear in the main plasma are well guided to the electron side along the diverted magnetic field lines, and disappear after colliding with the divertor plate<sup>2)</sup>. We use two kind of test aluminum targets located normal to the toroidal magnetic field. The target (a) of 16 cm<sup>2</sup> in area is in the ion-side and the target (b) of 40 cm<sup>2</sup> in area covers the both side (i.e. the ion side and the electron side), across the median plane. The target (b) well simulates the poloidal limiter in the normal tokamak. Plasma parameters of the scrape-off layer are as follows;  $T_e = 50 - 60$  eV,  $T_i = 60 - 80$  eV and  $n_e = 2 \times 10^{12}$  cm<sup>-3</sup>. Figure II.3.3-2 shows the distribution of arc tracks and melted area on the target (b), which was exposed to the plasma in only one shot of a normal discharge. Each of those is made on the surface faced to the main plasma. The arc track is found along the separatrix magnetic surface in the ion side and the melted area is found in the electron side on the same target. Figure II.3.3-3-a and 3-b show the scanning electron micrograph pictures of target (b) shown in Fig. II.3.3-2. While, we can seldom find the arc tracks on the electrically isolated target (a) in one shot of normal discharge. Even if there appear arc tracks on the target (a), they are shallower compared to those on the target (b).

In the following we discuss the reason why the arc track is found in the ion side and the melted area is found in the electron side on the target (b).

Figure II.3.3-4 shows the profiles at  $R = 40$  cm of floating potential  $\psi_f$  and space potential  $\psi_s$  measured with the Langmuir probe in the quiet phase. We find that the most negative peak of  $\psi_f$  always appears along the separatrix magnetic surface in the electron side<sup>3)</sup> and the most positive peak of  $\psi_s$  always appears along the separatrix magnetic surface in the ion side. If the target (b) covers the both side across the median plane, the target (b) has a common floating potential  $\psi_f$  and the effective sheath potential  $\psi_s - \psi_f$  along the separatrix magnetic surface is slightly increased in the ion side and slightly decreased in the

electron side. Thus, the ion sputtering is enhanced in the ion side and the ion sputtering is mitigated in the electron side. The large amount of runaway electrons produce the same effect as the large negative biased potential used in the previous experiment<sup>4)</sup>. That is, the runaway electrons offer the sufficient sheath potential to the target (b) along the separatrix in the ion side to produce an arc spot and supply the circulating current to sustain an arc. The melted area is produced by the heat flux due to runaway electrons. These model well explain the arcing phenomena observed in the normal tokamak. That is, in the normal tokamak, arcing is observed in the current rising phase and in the disruptive phase<sup>5,6)</sup>. In the current rising phase, the production rate of runaway is large because of large loop voltage and low plasma densities. In the disruptive phase, large amount of runaways are extracted from the main plasma because of poor confinements due to m.h.d. instabilities.

#### References

- 1) S. Yamamoto: Japan Atomic Energy Research Institute Report JAERI-M 8151 "Experimental Studies on an Axisymmetric Divertor in DIVA (JFT-2a)" (1979) (in Japanese).
- 2) S. Yamamoto, et al.: Nucl. Fusion 18 (1978) 205.
- 3) H. Ohtsuka, et al.: Plasma Physics 20 (1978) 749.
- 4) K. Ohasa, et al.: J. Phys. Soc. Jpn. 46 (1979) 1635.
- 5) D.H.J. Goodall et al.: Nucl. Fusion 19 (1979) 1396.
- 6) P. Mioduszewski et al., to be published in J. Nucl. Mater.

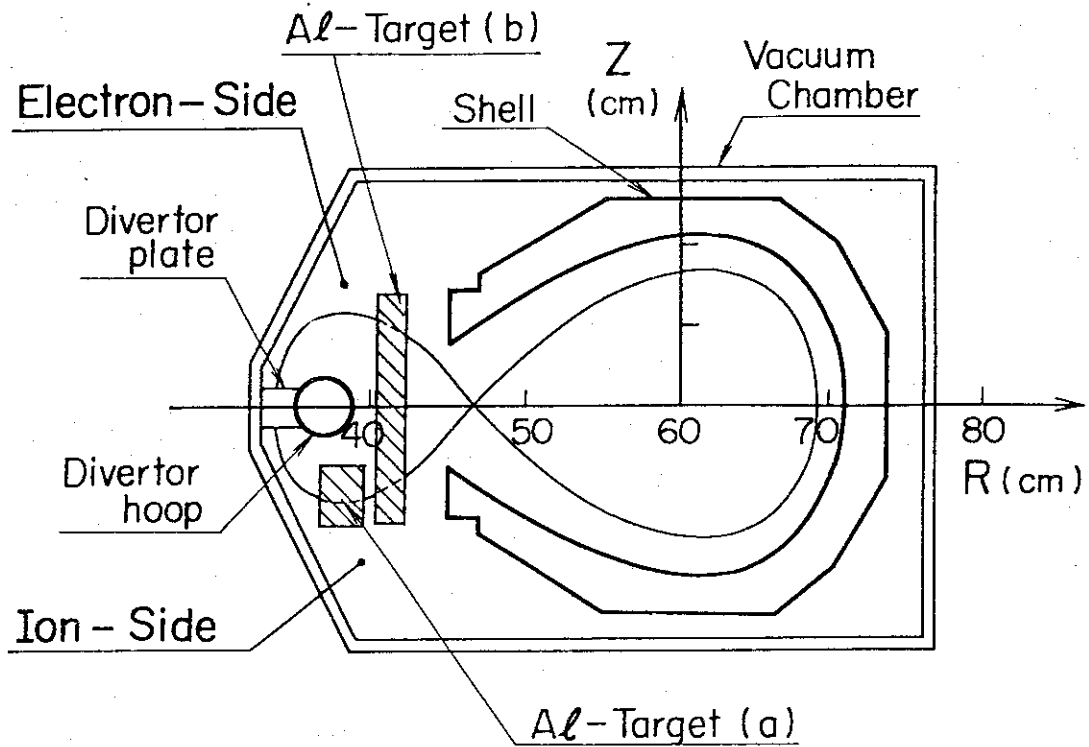


Fig. II.3.3-1 Cross-sectional view of DIVA and experimental set-up. The target (a) is in the ion-side of the divertor and the target (b) covers the both side, i.e., the ion-side and electron-side of the divertor.

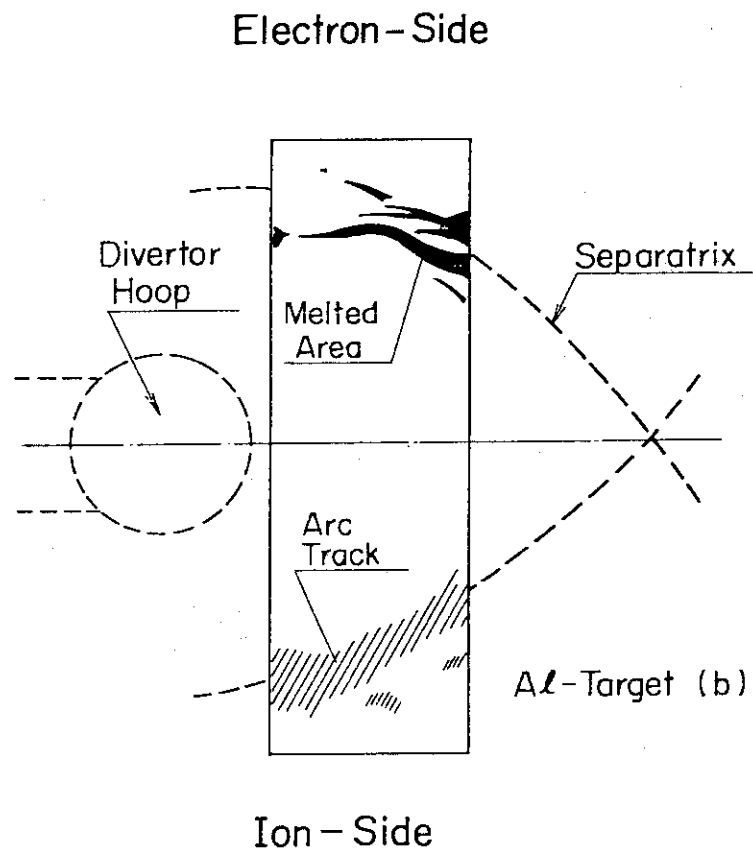


Fig. II.3.3-2 The distribution of arc tracks and melted area.

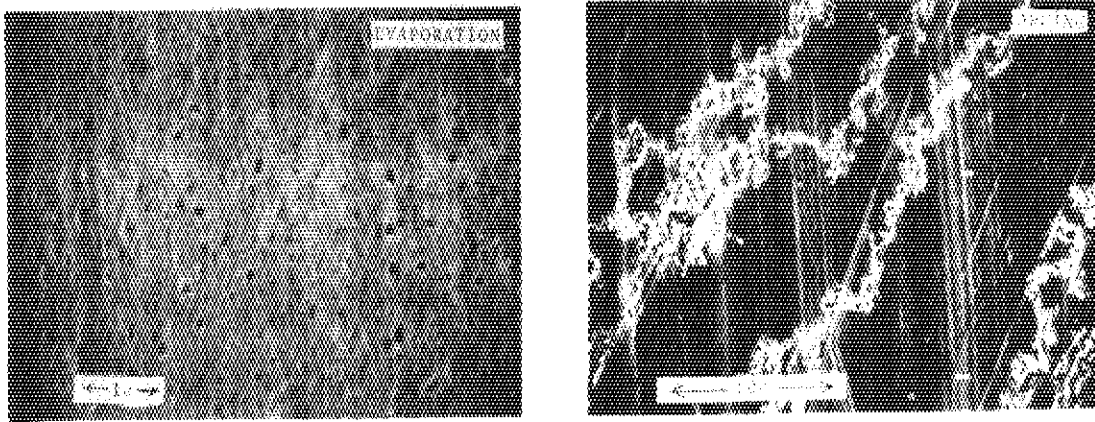


Fig. II.3.3-3 (a) Melted area; melted area is produced by the heat flux due to runaway electrons.  
 (b) Arc tracks; the tracks run orthogonal to the magnetic field in a direction opposite to the expected  $\mathbf{J} \times \mathbf{B}_T$  force, where  $\mathbf{J}$  is the arc current and  $\mathbf{B}_T$  is the magnetic field.

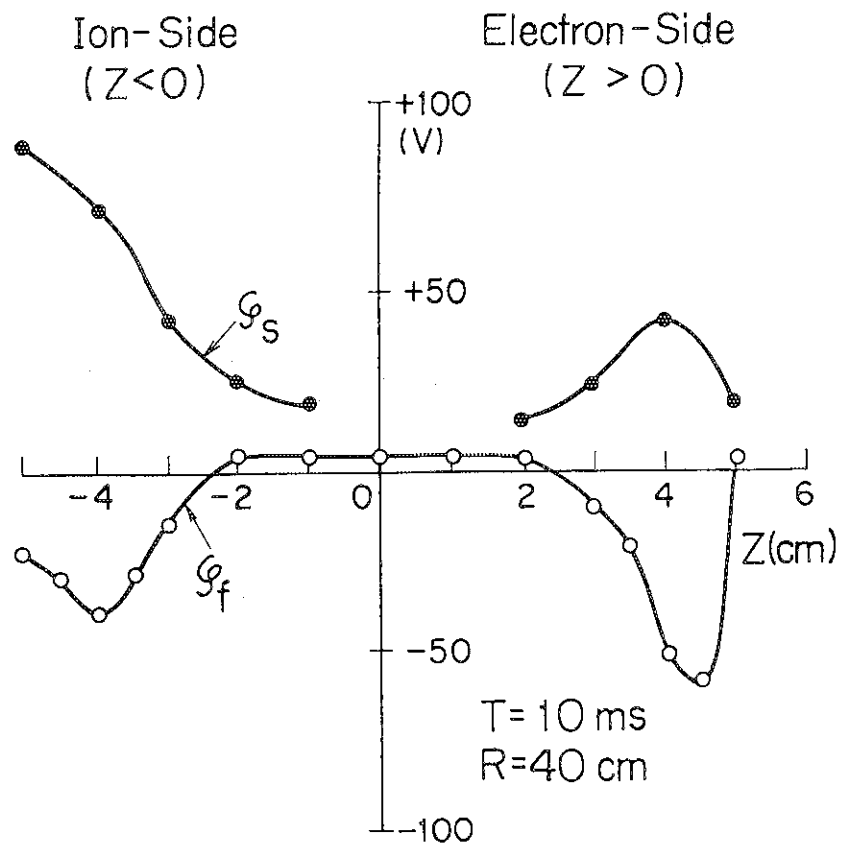


Fig. II.3.3-4 Typical profiles of floating potential  $\psi_f$  and space potential  $\psi_s$  at  $R = 40$  cm in the divertor region.

## 4. JFT-2M

The JFT-2M is now scheduled to be operational at JAERI in later 1982. It has a plasma major radius 1.3 m, and minor radius  $0.35 \times 0.5$  m with D shaped cross section; a maximum plasma current of 0.5 MA; a toroidal field at major radius of up to 15 kG and capable of 45 kG with the upgraded power supply system.

The main purpose of JFT-2M is research on the improved high performance tokamak reactor. The following issues are included.

## 1) Improvement of the additional heating system

Ion cyclotron range of frequency heating is very attractive to heat a reactor level plasma because of its clear understanding of physical mechanisms and the high heating efficiency demonstrated. In order that ICRF heating be employed as a main additional heating, it is necessary to get a high ion temperature up to several keV. For this purpose, the following research and development are necessary, i.e., I) quantitative understanding of heating mechanisms and optimization of heating condition in a reactor like plasma; II) optimization of launching structure to get a high coupling efficiency and high power feeding.

## 2) High beta, non circular plasma

The JFT-2 has demonstrated stable plasma with beta about 3 %. This value is higher than the critical values predicted from the ballooning analysis. Therefore, it is very interesting to know the critical value of beta by optimizing the heating condition and plasma cross section.

## 3) Steady state current drive

Preliminary results in JFT-2 show that a plasma current is driven by the excitation of lower hybrid wave. This result should be extended in more powerful MW level experiments with optimized high power system.

## 4) Impurity control and ash exhaust

Diverter experiments in JFT-2a/DIVA indicate the reduction of impurities levels and the possibility of Helium pumping out. Divertor should be tested in a reactor like plasma with the more simple configuration.

## 5) Control of plasma with simple, high reliability technique

Very low  $q$  ( $q_a < 2$ ) discharge is attractive with respect to the control of the plasma disruption and to obtain the high beta plasma as demonstrated in JFT-2a/DIVA. The accessibility to the low  $q$  discharge should be established in the larger machine in order to suppress the plasma disruption and to obtain the high beta plasma. The hybrid control

of toroidal coil system is also necessary technique in the future reactor.

The research objectives mentioned above have been preliminary demonstrated in JAERI tokamak experiments, and should be developed under reactor level conditions of heating power density. The JFT-2M also provide flexible, easily modified facility for studies relevant to the improved advanced concepts of the tokamak reactors in mid 1980s.

### III. OPERATION AND MAINTENANCE

#### 1. Introduction

Facility Operation and Engineering section has been engaged in Operation and maintenance of JFT-2 and JFT-2a (DIVA) Tokamaks and a flywheel motor-generator, and development of auxiliary equipments and instruments.

Modification of JFT-2 started in December 1978 and finished in July 1979.

Operation of JFT-2a was terminated on September 27, 1979 after 5 years Operation. A high power neutral beam injection system was installed on JFT-2 in April 1980.

#### 2. Operation and Maintenance

The JFT-2 and JFT-2a Tokamaks and flywheel motor-generator (M-G) were operated on schedule as shown in table III-1.

Modification of JFT-2 was completed at the end of July, 1979. Table III-2 shows specifications of the modified JFT-2 Tokamak. A cross-sectional view of the device is shown in Figs. III-1,2.

Operation of JFT-2a was brought to the end in September 27, 1979. Cumulative shot number of JFT-2a amounted to 131, 122 without no major troubles.

The MW-class neutral beam injector system was installed on JFT-2 in April 1980. Table III-3 shows the specifications of the system.

#### 3. Development of Equipment and Instrument

During the period under the review the following developmental works have been performed.

A diagnostic instrument for malfunction of tokamak devices was completed, and installed on JFT-2.

The control system for plasma positioning in JFT-2 was completed. The power supply of the system is controlled by the direct digital control using a digital process computer and a micro-processor-controlled regulator for the 0.8 MW thyristor of double 3-phase bridge connection.



The new vacuum pumping system of JFT-2 consists of two systems, turbomolecular pumps with Liq-N<sub>2</sub> traps and with 20°K cryo-traps. The total pumping speed at the port of the vacuum pumping has been upgraded to 1,800 l/s (N<sub>2</sub>). Metal seals are employed for the vacuum seal. These improvements have resulted in that the final base pressure decreases down to  $6 \times 10^{-9}$  Torr without installing diagnostics devices into the vacuum chamber.

In the modified JFT-2, RF sputter technique has been successfully applied to generate fresh titanium surfaces. The chamber wall was kept clean through a whole day with five minutes operation of the RF sputter instrument.

Table III-1

## Operation of JFT-2, JFT-2a and motor-generator (M-G)

| ( month ) | 1979                      |   |   |   |   |   |                           |    |    |    |   |   | 1980 |   |   |  |  |
|-----------|---------------------------|---|---|---|---|---|---------------------------|----|----|----|---|---|------|---|---|--|--|
|           | 3                         | 4 | 5 | 6 | 7 | 8 | 9                         | 10 | 11 | 12 | 1 | 2 | 3    | 4 | 5 |  |  |
| JFT - 2   | Under Modification        |   |   |   |   |   | Operation and Maintenance |    |    |    |   |   |      |   |   |  |  |
| JFT - 2a  | Operation and Maintenance |   |   |   |   |   | (Shut down)               |    |    |    |   |   |      |   |   |  |  |
| M - G     | Operation and Maintenance |   |   |   |   |   |                           |    |    |    |   |   |      |   |   |  |  |

## Detail of the operation (JFT-2, JFT-2a and M-G)

| ( fisical year ) |   | 1978      | 1979    |              |              |             |               |
|------------------|---|-----------|---------|--------------|--------------|-------------|---------------|
|                  |   |           | APR-JUN | JUL-SEP      | OCT-DEC      | JAN-MAR     | Total         |
| 1)<br>JFT-2      | Number of discharges ( Shots )                                  | 15,179    |         | 1,644        | 3,359        | 2,106       | 7,109         |
|                  | Total days of operation ( days )                                | 106       |         | 28           | 30           | 27          | 85            |
|                  | Baking ( times )  | 8         |         | 2            | 1            | 3           | 6             |
|                  | Discharge cleaning ( Shots or hours )                           | 107 Shots |         | 85 ( hours ) | 25 ( hours ) | 7 ( hours ) | 117 ( hours ) |
|                  | Tayler - type discharge cleaning                                |           |         |              |              |             |               |
|                  | Vent of vacuum chamber ( Times )                                | 24        |         | 2            | 2            | 4           | 8             |
| 2)<br>JFT-2a     | Number of discharges ( Shots )                                  | 23,627    | 7,049   | 9,134        |              |             | 16,184        |
|                  | Total days of operation ( days )                                | 111       | 44      | 43           |              |             | 87            |
|                  | Baking ( times )  |           |         |              |              |             |               |
|                  | (Note: times in a parenthesis are on the vacuum pumping system) | 24+(38)   | 12+(15) | 11+(12)      |              |             | 23+(27)       |
|                  | Titanium gettering ( hours )                                    |           | 20      | 5            |              |             | 25            |
|                  | Vent of vacuum chamber ( times )                                | 31        | 12      | 8            |              |             | 20            |
| 3)<br>M-G        | M-G (#1) ( hours )  | 969       | 330     | 440          | 307          | 194         | 1,271         |
|                  | M-G (#2) ( hours )  | 967       | 330     | 439          | 307          | 195         | 1,271         |

Table III-2  
Specification of the modified JFT-2

|   |                        |  |
|---|------------------------|--|
| 1. Vacuum Vessel  |                        |  |
|   | Major radius           | 900mm  |
|   | Minor radius           | 320mm  |
|   | Material               | SUS 304, SUS 304L  |
|   | Electric resistance    | 2.63m $\Omega$ (for 20°)                                 |
|   | Baking temperature     | 350°C  |
|   | He leak rate           | $<5 \times 10^{-10}$ Torr l/s                            |
|   | Number of ports        | 14   |
| 2. Limiter  |                        |  |
|   | Fixed limiter          | 550 <sup><math>\phi</math></sup> mm, SUS 304             |
|   | Movable limiters       | Mo   |
| 3. Vacuum pumping   |                        |  |
|   | Pumping speed          | 1,800 l/s (H <sub>2</sub> ), 2,150 l/s (H <sub>2</sub> ) |
|   | Final base pressure    | $\sim 6 \times 10^{-9}$ Torr                             |
| 4. Surface coating system                                 |                        |  |
|   | RF spatter system (Ti) | two sets   |
|   | Ti ball                | one set  |
|   |                        | [gettered between individual discharge shots]            |
| 5. Toroidal field coil                                    |                        |  |
|   | Number of coil         | 14   |
|   | Maximum field          | 16KG   |
| 6. Primary winding coil                                   |                        |  |
|   | Number of turns        | 52/116/180   |
|   | Maximum current        | 5KG (0.2s/2.5min)  |
| 7. DC vertical field                                      |                        |  |
|   | Number of turns        | 96turnsx2x2  |
|   | Maximum current        | 520A (0.2s/2.5min)                                       |
| 8. Control and pulse vertical field coil                  |                        |  |
|   | Number of turns        | 4turnsx4   |
|   | Maximum current        | 2,500A (0.2s/2.5min)                                     |
| 9. Horizontal field coil                                  |                        |  |
|   | Number of turns        | 100turnsx2   |
|   | Maximum current        | 150A (5s/2.5min)   |
| 10. Toroidal field power supply (M-G)                     |                        |  |
|   | Maximum current        | 12.1KA (2.5s/2.5min)                                     |
| 11. Primary winding power supply (condenser banks)        |                        |  |
|   | Stored energy          | 530KJ  |
| 12. DC Vertical field power supply (Thyrister rectifiers) |                        |  |
|   | Output                 | 196KW (377V, 520A)                                       |
| 13. Pulse vertical field power supply (condenser banks)   |                        |  |
|   | Stored energy          | 140KJ  |

Table III-2 (continued)

|   |                                   |
|---|-----------------------------------|
| 14. Control vertical field power supply (Thyrister rectifiers controlled by a digital computer HIDIC-80 system) |                                   |
| Output  | 3.6MW (480V, 7500A)               |
| 15. Horizontal field power supply (Thyrister rectifiers)  |                                   |
| Output  | 50KW (413V, 120A)                 |
| 16. System of position control of plasma  |                                   |
| Method  | direct digital control            |
| Response time   | 3.6ms, 7500A/5ms (375G/5ms)       |
| Computer system   | HIDIC-80 (48KW), HIDIC-08E (16KW) |

Table III-3

## Specifications of the NBI systems for JFT-2

|   |  |
|---|--|
| 1. Acceleration power supply                |  |
| Output                                      | DC 40KV, 65A, 300ms<br>Duty 1/30, two sets   |
| 2. Deceleration power supply                |  |
| Output                                      | DC 5KV, 10A, 300ms<br>Duty 1/30, two sets    |
| 3. Arc power supply                         |  |
| Output                                      | DC 100V, 800A, 300ms<br>Duty 1/30, four sets |
| 4. Filament power supply                    |  |
| Output                                      | DC 10V, 1200A, 5s<br>Duty 1/10, four sets    |
| 5. Ion source                               |  |
| Output                                      | 40KV, 30A, four sets                         |
| 6. Vacuum pumping system (TMP, two systems) |  |
| Pumping speed                               | 3,700 l/s                                    |
| Expansion chamber                           | 20m <sup>3</sup>                             |
| 7. Cooling system                           |  |
| Water                                       | 800 l/min                                    |
| 8. Beam line                                |  |
| Number of lines                             | 2  |

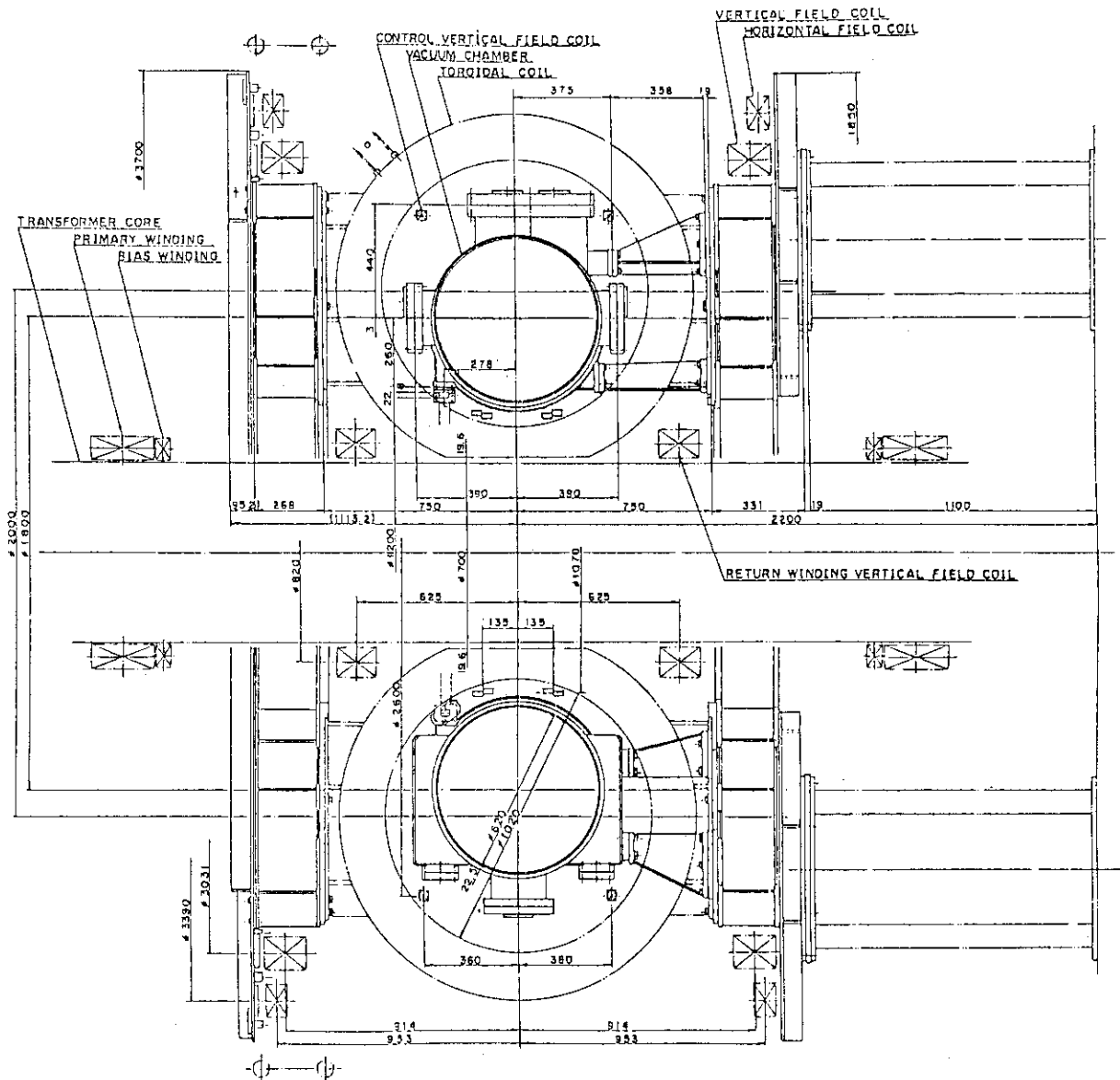


Fig. III-1 Cross-sectional view of the JFT-2 device modified in 1979.

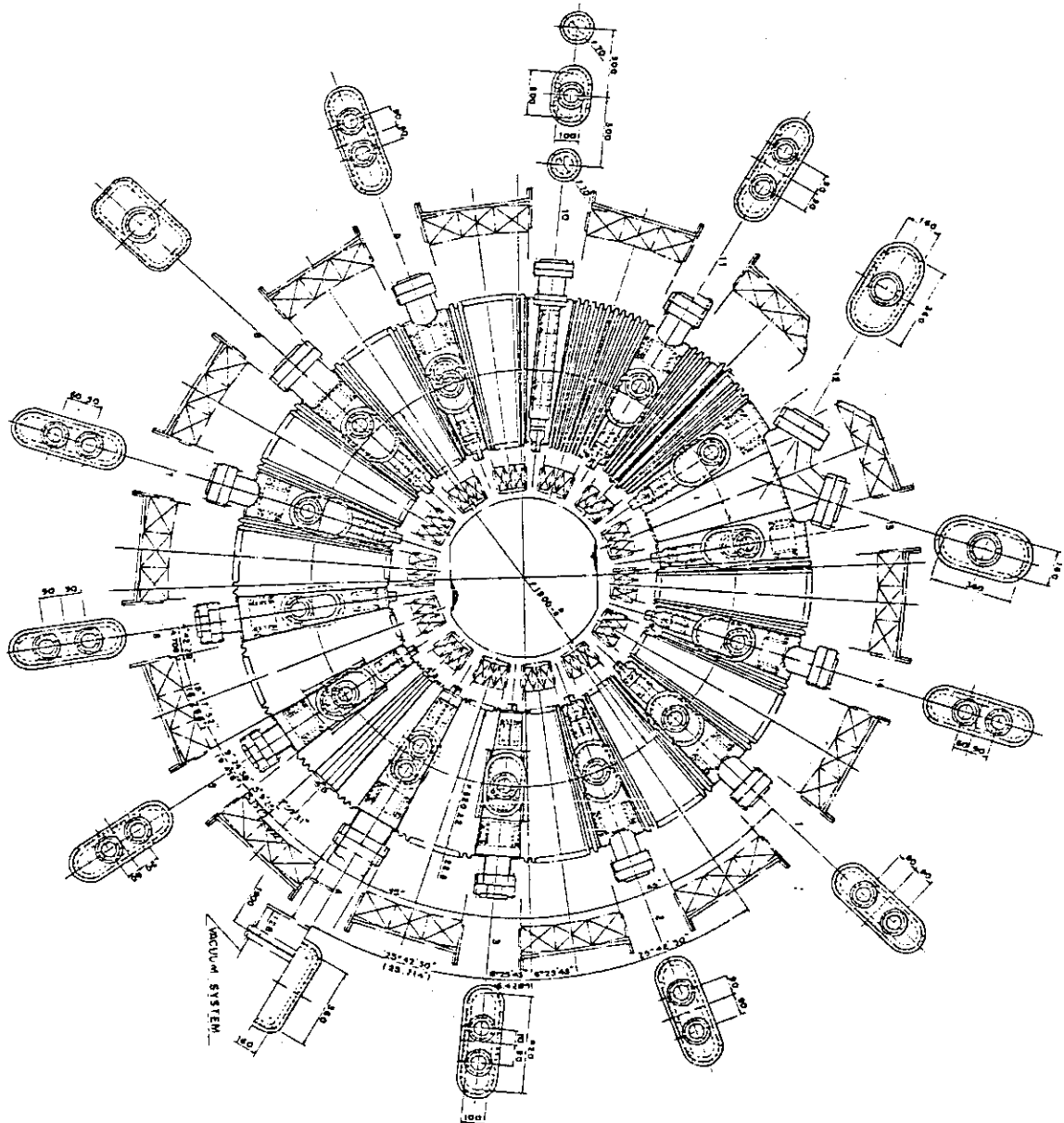


Fig. III-2 Plane view of the JFT-2 device modified in 1979.

## IV. US-JAPAN RESEARCH COOPERATION IN DOUBLET III

### 1. US-Japan Joint Program

Cooperative research between the United States and Japan using Doublet III started in August 1979 under an agreement between the United States Department of Energy and JAERI. This cooperation at the Doublet III facility is the first project implemented under the US-Japan Fusion Research Cooperation Agreement. The focus of activities on the part of the Japanese experimental team is to carry out experimental research on higher beta tokamak plasmas with dee-shaped cross-sections. The Doublet III research program is discussed and decided upon at the US-Japan Doublet III Steering Committee which meets twice a year. Each side is represented by two official members, and all decisions are made unanimously. The first Steering Committee Meeting was held in November 1979.

Doublet III is a tokamak device with elongated plasma cross-sections located at the General Atomic Company, San Diego, California. This is the largest tokamak device in the world presently operating. The machine is almost spherical in appearance with a diameter of approximately 6 m, as shown in Fig. IV.1-1. It has a large vacuum vessel of inconel with a cross-section 3 m high and 1 m wide which was originally designed for plasmas with doublet-shaped cross-sections. There are 24 poloidal field-shaping coils surrounding the immediate exterior of the vessel. The dee-shaped toroidal field coils have demountable joints providing the machine with operational flexibility. The major parameters of Doublet III are shown in Table IV.1-1. Each shaping coil is connected to a terminal board and can be connected with any combination of coils and power supplies. By choosing a proper connection of coils and power supplies, either a circular or dee-shaped plasma can be produced in the upper half of the vessel.

A group of Japanese physicists called the JAERI team are working at General Atomic Company as an independent group under their own leadership and carrying out experimental research using one-half the machine time. The JAERI team is working on dee-shaped plasmas, while the General Atomic physics team is primarily working on doublet-shaped plasmas.

## 2. Experimental Results

The objective of the JAERI dee experiments in the present Joule heating phase was to prepare for the forthcoming neutral beam injection heating experiments. In this context the first priority was to obtain high plasma density, and then to achieve highly elongated dee-shaped plasmas. In order to have a less than 10 percent shine-through by the neutral beam, a line-averaged plasma density of more than  $6 \times 10^{13} \text{ cm}^{-3}$  is required for the nearly perpendicular neutral beam injection at 80 keV. The rated pulse length of the beam is 0.5 sec.

The dee-shaped plasmas in the upper half of Doublet III were obtained with various connections of shaping coils and power supplies devised by the JAERI team. However, the elongation (height-to-width ratio) of the cross-section was initially held at approximately 1.2 until the density requirement was to be met. The density requirement was achieved in December, after the machine was cleaned up and the plasma position control and waveforms of plasma current and gas puffing were optimized. Almost two months were required after a major summer vent to raise the plasma density to more than  $6 \times 10^{13} \text{ cm}^{-3}$ . A titanium gettering system was installed in February 1980 to improve the plasma characteristics. Immediately after the start of gettering, a plasma density of  $10^{14} \text{ cm}^{-3}$  was attained, which surpasses considerably the minimum requirement mentioned above. The density corresponds to the Murakami coefficient  $N/(B_T/R)$  of 6.

The elongation of the dee-shaped plasmas was then gradually increased with the highest value of 1.5 obtained by March 1980, as shown in Fig. IV.2-1. As a result of the effect of the elongated cross-section, the plasma current could be increased and the highest plasma current with flat-top of 1 MA was obtained with a toroidal field of 24 kG. Typical waveforms are shown in Fig. IV.2-2. This current is the world's highest record for circular and dee-shaped plasmas and is twice the value of PLT with 35 kG and FT tokamak with 70 kG.

A sawtooth oscillation was found in the signals of the PIN diode array and the radiometer of the fundamental electron cyclotron frequency. The sawtooth oscillation signal was used to find the position of the  $q = 1$  magnetic surface, and the results by both diagnostics are in agreement. The JAERI-made five detector bolometer array was installed in the machine and worked as one of the most effective diagnostics.



The bolometer data shows that the radiation power profile becomes flatter as the vacuum vessel wall becomes cleaner, and plasma contamination by metal impurity is suggested. For more conclusive evidence, it will be necessary to use a bolometer with more detectors and other impurity diagnostics.

A single null poloidal divertor configuration was conceived and realized by the JAERI team. The shape of the cross-section is shown in Fig. IV.2-3(a). It has unique features in that the shape is controlled solely by coils outside the vessel, and the divertor action such as impurity reduction has been experimentally demonstrated even though there is no particular divertor chamber or throat. Several typical properties of this configuration are shown in Fig. IV.2-3(b). Two of the inside shaping coils shown by black squares are used as divertor coils. When the ratio of the sum of the currents through those two coils to the plasma current exceeds 0.35, this divertor configuration is produced. In the case of the configuration shown in Fig. IV.2-3(a), the divertor coil current is increased during a discharge and the divertor action appears at approximately 0.3 sec. TV observation also shows that when this divertor configuration is produced, the plasma no longer touch the limiters but only touches the lower inner walls of the vessel where the separatrix magnetic surface intersects with the wall (Fig. IV.2-4). The plasma density is half that of the non-diverted discharge for the same gas puffing pulse. Radiation loss from the central part of the main plasma decreases to about 50 percent, which shows that the deleterious effect of impurities in the central plasma is decreased. Spectrometer observations of NiXI and OV lines which indicate influx of those impurities show a decrease by more than a factor of 5. Future research plans are to obtain higher elongations as well as higher plasma densities with lower toroidal magnetic fields in order to make higher beta experiments easier.

Table IV.1-1 Doublet III parameters

|                              |                                 |
|------------------------------|---------------------------------|
| Major radius $R$             | 1.43 m                          |
| Height of cross-section $2b$ | 1.4 m<br>for dee-shaped plasmas |
| Width of cross-section $2a$  | 0.9 m                           |
| Toroidal field $B_T$         | 24 kG                           |
| Ohmic heating flux           | 5 V·S (7.5)                     |
| Flattop                      | 1 sec                           |
| NBI power                    | 7 MW (14)                       |
| Plasma current               | 1 MA (1.5)                      |

( ): Upgrade

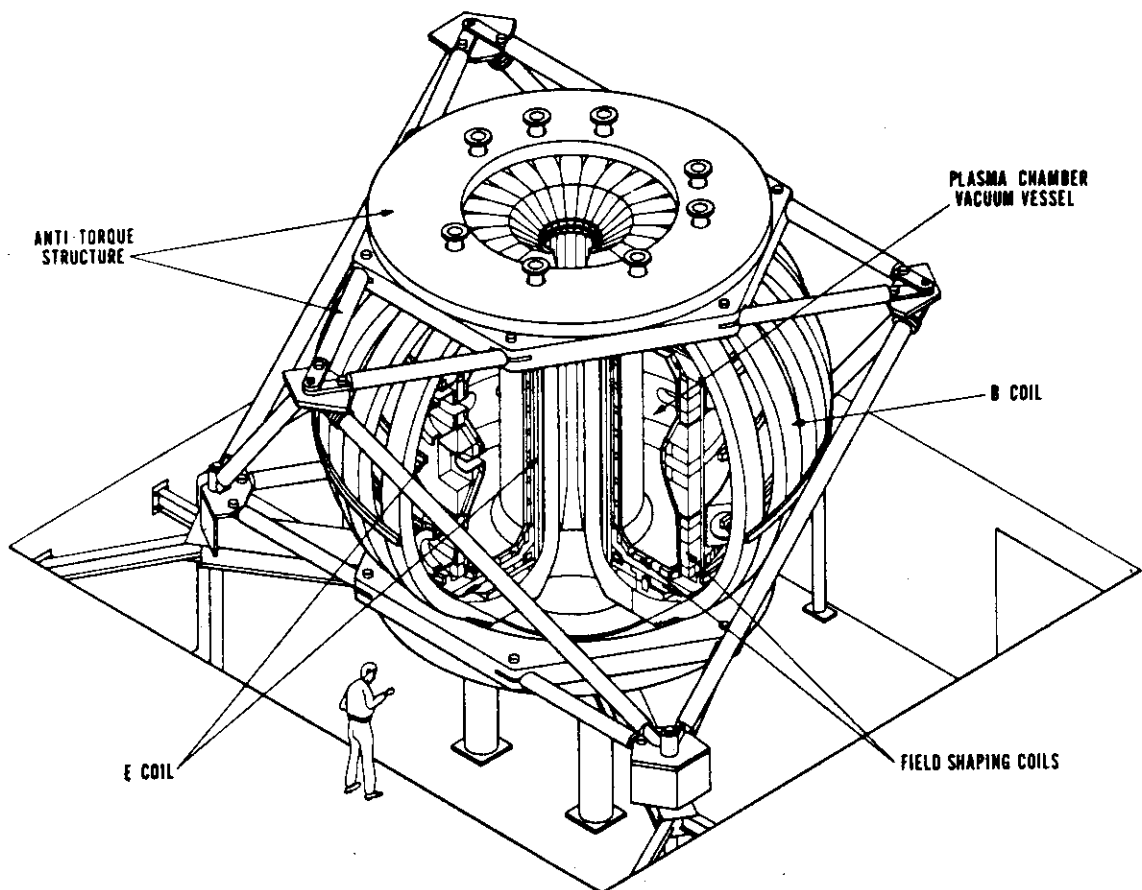
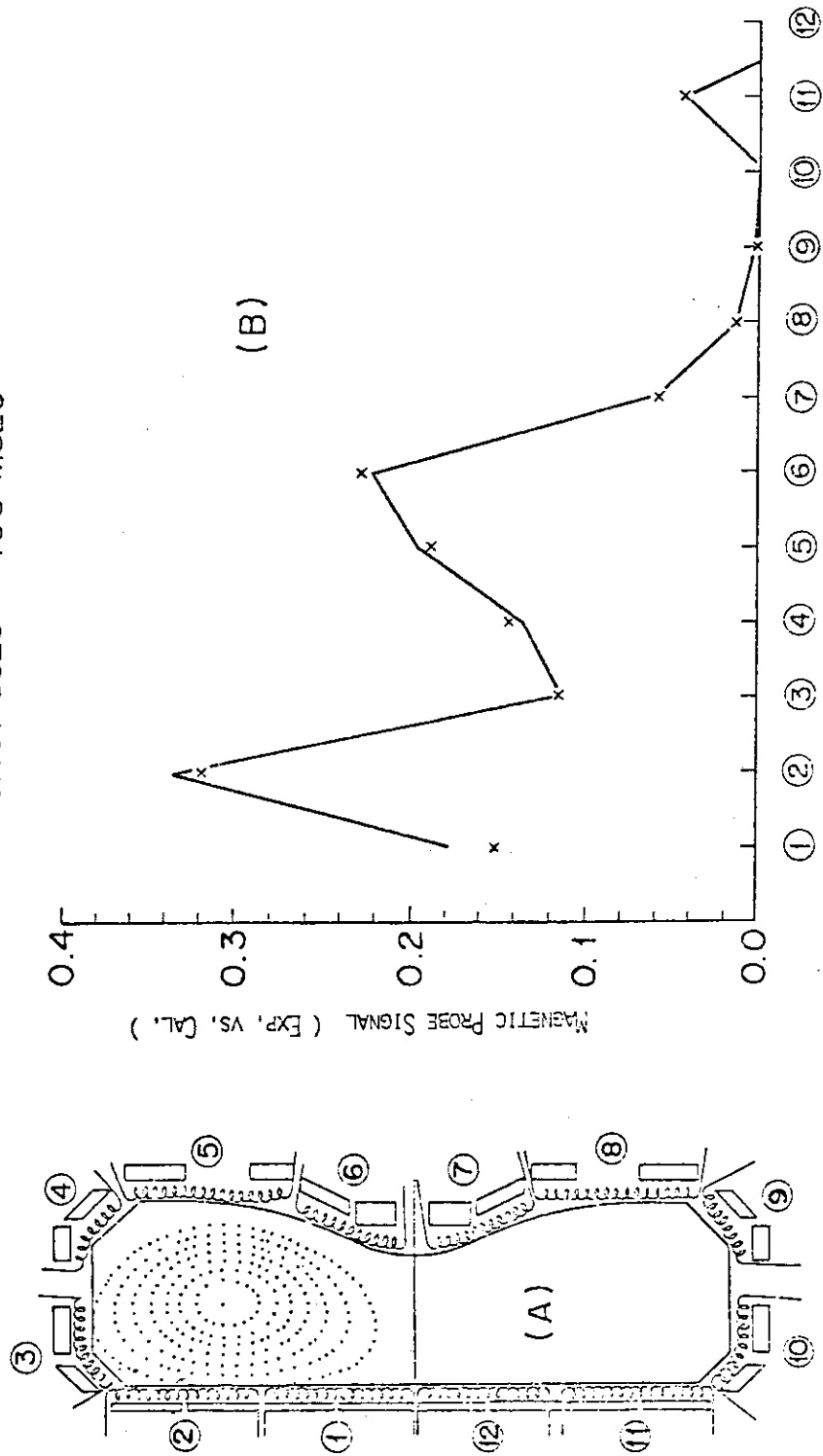


Fig. IV.1-1 Schematic of Doublet III

JAERI-002013

SHOT 8329 400 MSEC



Magnetic probe NO.

Fig. IV.2-1  
 (A): Dee-shaped plasma (flux contours) of  $\kappa \sim 1.5$  from MHD equilibrium calculation for the experimentally obtained flux value. (B): Fitting accuracy with calculation (solid line) and experimental value (crosses) by comparing magnetic field at positions indicated schematically in (A).  $I_p = 1$  MA.

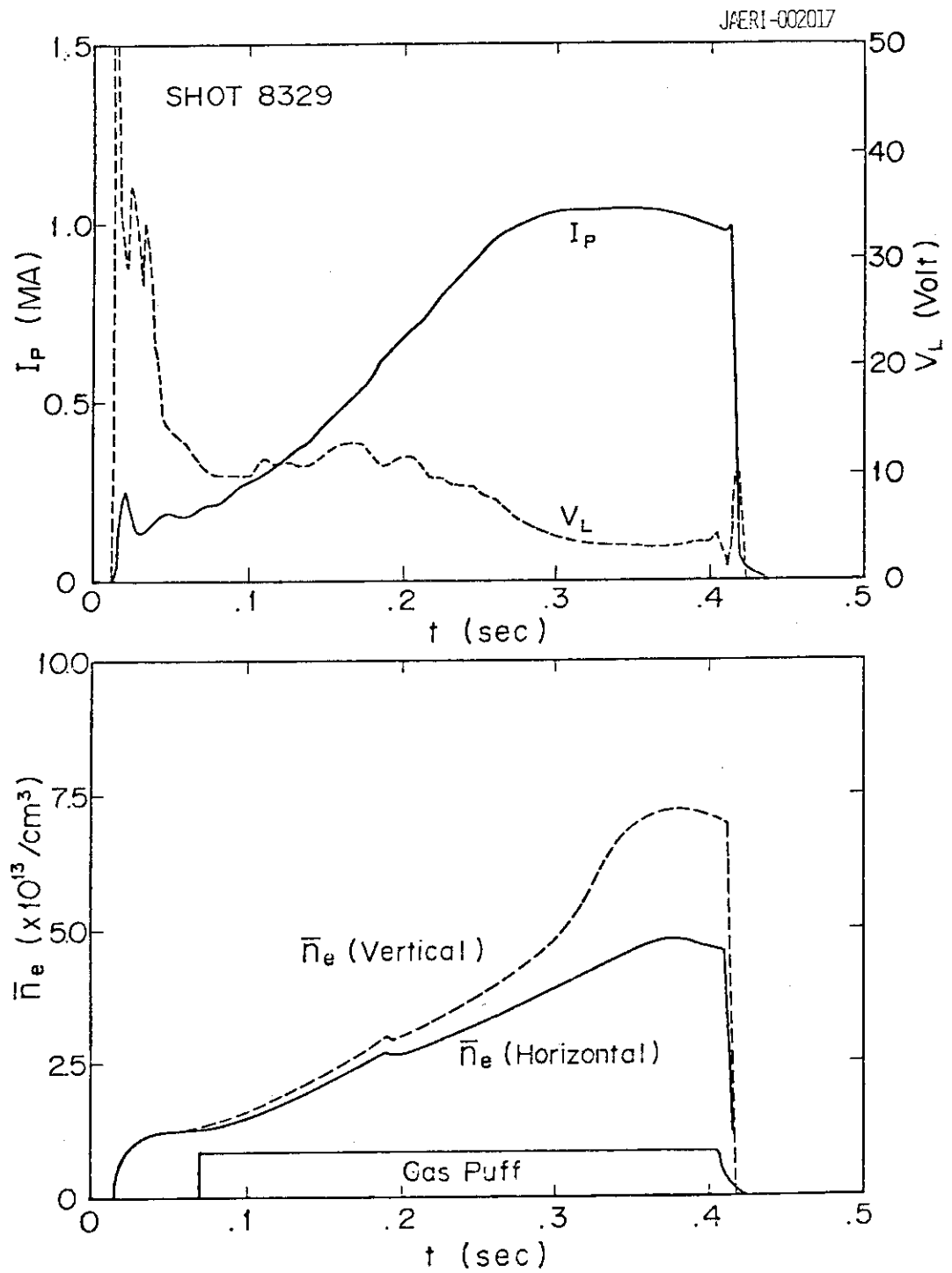


Fig. IV.2-2 Highest current discharge of  $\kappa \sim 1.5$  dee-shaped plasma.  
 $B_t = 2.4$  T.

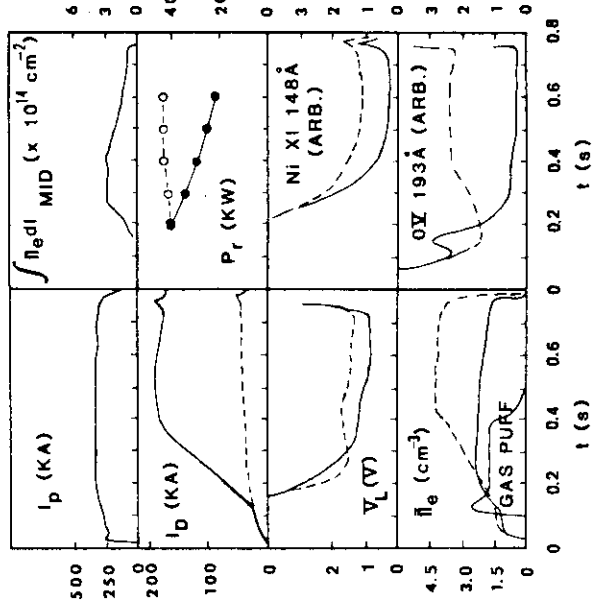


Fig. IV.2-3(b) Comparisons of discharges with  $I_D/I_p = 0.58$ , solid lines) and without (dotted lines) divertor:  $I_p$ : plasma current,  $I_D$ : divertor current,  $V_L$ : plasma loop voltage,  $\bar{n}_e$ : line-averaged electron density of the main plasma,  $f_{n_{eI}dl}$ : line-integrated electron density of the scrape-off plasma measured at the mid-plane of the vacuum chamber,  $P_r$ : total radiation loss power, intensities of Ni XI 148 Å and O V 193 Å line emission from the main plasma.

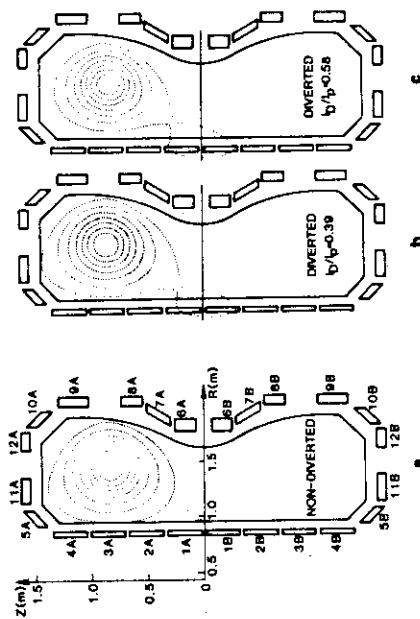


Fig. IV.2-3(a) Arrangement of 24 plasma shaping coils and limiter positions. Three typical plasma equilibria are shown: (a) non-diverted, (b) diverted,  $I_D/I_p = 0.39$ , (c) diverted,  $I_D/I_p = 0.58$ . In the diverted discharge of  $I_D/I_p = 0.58$ , the separatrix magnetic surface around the main plasma is separated from the limiter by more than 7 cm.

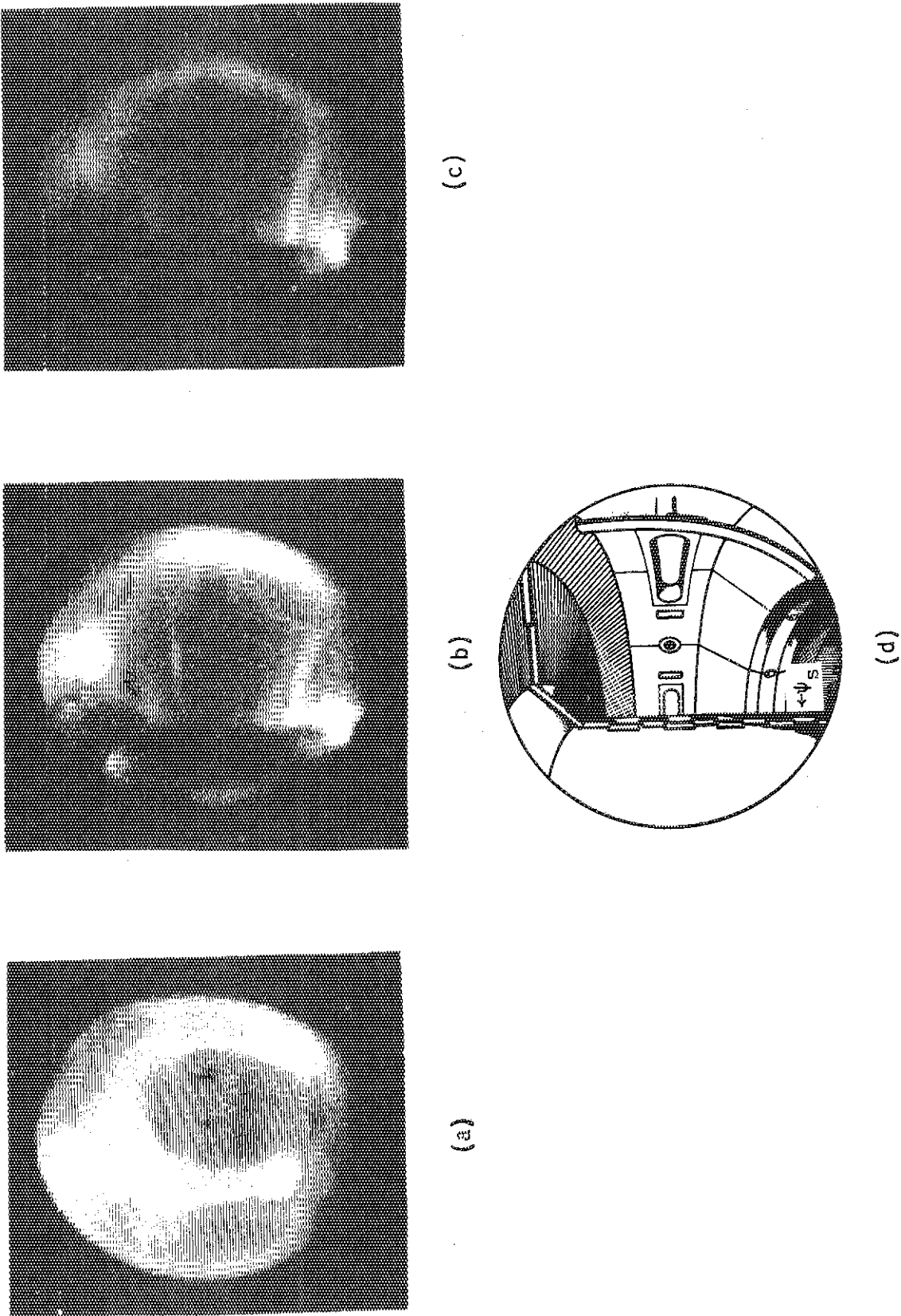


Fig. IV.2-4 Tangential TV observations of plasma cross-sections in the wavelength range between 4000 to 8000 Å for the discharges present in Fig. 1: (a) non-diverted, (b) diverted with  $I_D/I_p = 0.39$ , (c) diverted with  $I_D/I_p = 0.58$ , (d) inside view of vacuum chamber by TV observation; the figure also shows the location of the intersection of separatrix magnetic surface and the inside wall presented in Fig. 1c.

## V. DEVELOPMENT OF PLASMA HEATING SYSTEM

### 1. Introduction

Neutral beam injection and radiofrequency (RF) heating systems are under development.

In the neutral beam injection system, ion source development and beam line studies for JT-60 injectors have been made using test stands ITS-1, ITS-2 and ITS-3. Especially, progress has been made in the development of a long pulse ion source. Hydrogen beams of 65 - 75 keV, 4 - 6 A, 6 - 30 sec were extracted in a two-stage ion source of 10 cm in diameter. A new type ion source with backstream electron beam dump (Lambdatron) has been developed. A 1.5 MW, 35 keV neutral beam injector for JFT-2 was completed and is now in operation. Design work of the prototype unit of neutral beam injectors for JT-60 was finished, and the construction of the prototype unit was ordered to two firms in March 1980.

In the RF heating, the phase II lower hybrid experiment on JFT-2 has been made up to 300 kW, and the ion heating efficiency was doubled as compared with that in the phase I experiment. An improved waveguide coupler can transmit RF power density up to 2 kW/cm<sup>2</sup>. Design work of the lower hybrid heating system for JT-60 has continued.

### 2. Neutral Beam Injection System

#### 2.1 Ion source development<sup>1)</sup>

##### 2.1.1 Long pulse beam extraction<sup>2)</sup>

To study problems associated with long pulse beam extraction at high energy, we fabricated and tested a quasi-dc ion source. This source is a modified duoPIGatron with a two stage accelerator, as shown in Fig. V.2.1-1, which can produce ion beams of 5 A at 70 keV for 10 sec. The extraction grid of the source is made of a oxygen free copper disk in which 191 apertures with 4 mm diam are drilled over the central 10 cm diam. area, and is provided with copper cooling tubes of 1.8 mm diam. alternately along rows of apertures. The cooling water was circulated at a flow rate of 10 l/min per each grid.

Figure V.2.1-2 shows the ratio of the heat loading on the grids to

the total beam power  $I_{acc} \times V_b$  as functions of ion beam current  $I_{acc}$ , where beam energy  $V_b$  is 75 keV and the gas pressure at the entrance of the neutralizer cell  $P_n$  is 1 mTorr. The heat loading shows minimum at a beam current of 5 to 6 A, where the beam divergence also becomes minimum. These heat loadings increase almost linearly with  $P_n$ . The heat loading at the minimum point amounts to 125 W/cm<sup>2</sup> at grid surface and 143 W/cm<sup>2</sup> at cooling surface of pipes. This heat flux is sufficiently lower than our design value for quasidc operation as indicated in Ref. 3.

The heat loading due to the backstream electrons on the back plate of the plasma generator is shown in Fig. V.2.1-3, where the beam energy and the beam current are fixed at 75 keV and 5 A, respectively. The heat loading increases linearly with the pressure.

To avoid damage to the back plate we had to keep the heat loading below 2.5 % of the beam power by limiting the pressure in the accel gap below several mTorr. Under such condition ion beams of 5 A at 70 keV for 10 sec was obtained repeatedly without any deleterious problems. We have also operated the source at 75 keV, 6 A for 6 sec, where the pulse length was limited by the cooling of the beam target.

#### 2.1.2 Impurity measurement<sup>4)</sup>

Impurity concentration in the beam is an important problem. We measured the impurity level of the ion beam extracted from the quasi-dc ion source with a magnetic deflection mass analyzer. The line density of the drift space of the beam was fixed to 0.39 Torr·cm, which gives 90 % neutralization for 75 keV proton beam.

Table V.2.1-1 shows a typical beam composition at 75 keV, 6.2 A. These data were measured at 0.5 sec after the beam initiation. The pressure in the arc chamber was 8 mTorr. The ion beams produced by the duoPIGatron contains light impurities of 1 to 2 % ( $C^+$ ,  $O^+$ ,  $H_2O^+$ ) and heavy impurities of up to 0.02 % ( $Cu^+$ ,  $Zn^+$ ,  $Ag^+$ ). From these results the neutral beam is estimated to contain light impurities of 3 to 6 % and heavy impurities of up to 0.04 %. However, the ion beams generated by the magnetic multipole line cusp source contains higher level of impurities, typically heavy impurities of 0.15 %. The impurities associated with oxygen decreased with time during a 10 sec pulse, while those related to carbon, copper and tungsten increase slightly with time. The time dependence of  $H_2O^+$  impurity level is shown in Fig. V.2.1-4.



### 2.1.3 Beam focusing by aperture displacement<sup>5)</sup>

The injection power into the JT-60 is estimated to be increased by about 13 % of the total beam power by focusing the individual beamlets to the injection port. As one of the most promising methods, we have studied experimentally the focusing by aperture displacement. In the experiment with 4.0 mm diam aperture the deflection angle increased linearly with the displacement of the aperture. Figure V.2.1-5 shows the dependence of each deflection characteristic on the field intensity ratio. Here, the triangular, rectangular and circular points indicate the displacement of apertures in the plasma, gradient and suppressor grid, respectively. The lines indicate the analytical results obtained by thin lens approximation for each case. From this figure, it is seen that the displacement of aperture in the suppressor grid is most adequate, since the deflection characteristic is insensitive to the field intensity ratio, that is, the focal point does not change over a wide range of the source operating condition.

### 2.1.4 Lambdatron ion source

Numerical calculation showed that the back plate of the arc chamber is exposed to a high heat flux of the backstream electrons of up to 1 kw/cm<sup>2</sup>, which will be more increased due to focusing of the beam by the source magnetic field.<sup>6)</sup> This is the case for the plasma generator such as duoPIGatron and bucket source (magnetic multipole line cusp source) where a spatially inhomogeneous magnetic field is applied for efficient production of the source plasma. In the quasi-dc source operation, it is quite difficult to remove such a high heat flux without any significant modification of the source structure. The major deficiency of the conventional ion sources such as the duoPIGatron and bucket is that they may not be able to handle such a high heat flux. To overcome this problem, a new source with a electron beam dump in the arc chamber is devised, which is named Lambdatron.<sup>7)</sup>

In this source the back plate is modified with A-shaped beam dump to reduce the surface heat flux due to the backstream electrons. This beam dump increases ion loss area approximately two times than that of a bucket source of comparable size, resulting in a reduction of arc efficiency and in an increase of operable gas pressure in the arc chamber. The characteristics of this new source were compared experimentally with those of the conventional bucket source, using a circular

grid system with 18.5 cm diam as shown in Fig. V.2.1-6, and a rectangular grid system with  $12 \times 27 \text{ cm}^2$  as shown in Figs. V.2.1-7 and 8.<sup>8)</sup>

In the circular case, the line cusp field arrangement is composed of 18 columns of Co-Sm magnets of 20 cm long which produce the maximum magnetic field of 1.2 KG on the wall surface. The cathode is 9 pieces of hairpin tungsten filaments. The plasma densities obtained are uniform within  $\pm 5 \%$  over the grid area. Table V.2.1-2 shows typical operating parameters of these sources for ion beam currents of 30 A at 30 kV. Here the gas pressures in the arc chamber are 3.5 and 6.0 mTorr for the bucket and Lambdatron ion source, respectively, which give the maximum arc efficiencies. We had to permit 40 % decrease of the arc efficiency when we used the Lambdatron instead of the conventional bucket source, while no significant change in atomic fraction was observed.

In the rectangular case, the line cusp of 24 columns of 25 cm long was attached on the chamber with  $21 \times 33 \times 28 \text{ cm}^3$ . The cathode is made of 16 pieces of hairpin tungsten filaments. Ion beams of 27.5 and 20 A were extracted from the bucket and the Lambdatron source, respectively, which were limited by the capacity of the arc power supply. The arc efficiency of the Lambdatron also showed 40 % decrease from that of the bucket source. Consequently, it is envisaged that this source is a candidate for the source plasma generator of the JT-60 ion source.

#### 2.1.5 Coaxial DuoPIGatron ion source<sup>9)</sup>

We have developed a new modified duoPIGatron ion source. Figure V.2.1-9 shows a coaxial duoPIGatron ion source originally designed and developed at JAERI. The characteristic of this source is expressed as follows. A magnetic center pole located at the center of the nozzle actualizes hollow feeding of primary ionizing electrons to the arc chamber. Then it widens the plasma production area by diverting the arc column from on-axis to off-axis, thereby contributes to the uniform plasma distribution. The shapes and structures of both the magnetic center pole and nozzle were optimized by numerical calculations of the magnetic field pattern. The density profiles of the source plasma is uniform to  $\pm 10 \%$  over the 18.5 cm grid area with the ion saturation current density of up to  $0.27 \text{ A/cm}^2$  at an arc current of 370 A. The source has been operated reliably producing hydrogen beams of 30 A at 30 kV.

2.1.6 Hollow cathode<sup>1)</sup>

Long pulse operation of ion sources with high current arc requires a high degree of reliability and durability to cathodes. A hollow cathode such as designed and developed at UCLA seems to be most adequate for a long pulse ion source. And we have fabricated and tested hollow cathode with the bucket source as shown in Fig. V.2.1-10. A cylindrical impregnated tungsten was used as an electron emitter, which is heated from the inside by a noninductively wound tungsten coil. While a considerable gas flow rate (more than 20 Torr l/sec) are required to start a hollow cathode discharge, we found that the gas flow rate can be reduced below 5 Torr l/sec if once arc discharge is turned on. Therefore the gas feed line was modified so that the flow rate can be reduced stepwise as shown in Fig. V.2.1-11. Using this hollow cathode with a 10 mm diameter aperture stable arc discharges were obtained for 1 sec with arc current up to 380 A. Consequently this hollow cathode will be used as the cathode of the JT-60 ion source.

References

- 1) Y. Arakawa et al.: JAERI-M 8869 (1980).
- 2) Y. Okumura, S. Matsuda, Y. Mizutani, Y. Ohara and T. Ohga: Rev. Sci. Instrum. 51 (1980) 728.
- 3) H. Horiike et al.: JAERI-M 9004 (1980).
- 4) Y. Okumura, Y. Mizutani, Y. Ohara and T. Shibata: Rev. Sci. Instrum. 52 (1981) 1.
- 5) Y. Okumura, Y. Mizutani and Y. Ohara: Rev. Sci. Instrum. 51 (1980) 471.
- 6) Y. Ohara, M. Akiba, Y. Arakawa, Y. Okumura and J. Sakuraba: J. Appl. Phys. 51 (1980) 3614.
- 7) Y. Ohara et al.: Proc. 8th Sympo. on Engineering Problems of Fusion Research, San Francisco, Calif., (1979).
- 8) M. Akiba et al.: Proc. 4th Sympo. on Ion Sources and Ion Application Technology, Tokyo, (1980).
- 9) H. Horiike, M. Akiba, Y. Arakawa, S. Matsuda and J. Sakuraba: Rev. Sci. Instrum. 50 (1980) 1463.

Table V.2.1-1 Ion beam fraction after passage of  
90 % equilibrium cell  
( $1.38 \times 10^{16}$  molecules/cm<sup>2</sup>).

## BEAM FRACTION AT 75kV, 62A

| M      | %      |  | M       | %      |  |
|--------|--------|--|---------|--------|--|
| 1/3    | 10.7   | H <sup>+</sup> (1/3 E)   | 63      | 0.008  | <sup>63</sup> Cu <sup>+</sup>  |
| 1/2    | 17.9   | H <sup>+</sup> (1/2 E)   | 64      | 0.003  | <sup>64</sup> Zr <sup>+</sup>  |
| 1      | 60.3   | H <sup>+</sup> (E)   | 65      | 0.004  | <sup>65</sup> Cu <sup>+</sup>  |
| 4/3    | 0.6    | H <sub>2</sub> <sup>+</sup> (2/3 E)  | 66      | 0.0015 | <sup>66</sup> Zn <sup>+</sup>  |
| 2      | 1.2    | H <sub>2</sub> <sup>+</sup> (E)  | 68      | 0.001  | <sup>68</sup> Zn <sup>+</sup>  |
| 3      | 0.24   | H <sub>3</sub> <sup>+</sup> (E)  | 107     | 0.0006 | <sup>107</sup> Ag <sup>+</sup>   |
| 0~3    | 90.94  |  | 109     | 0.0005 | <sup>109</sup> Ag <sup>+</sup>   |
| 8.5    | 0.015  | CH <sub>n</sub> <sup>+</sup> → C <sup>+</sup> , CH <sub>m</sub> <sup>+</sup>   | 63~60   | 0.019  |  |
| 9      | 0.039  |  | -1/3    | 3.28   | H <sup>-</sup> (1/3 E)   |
| 10.0   | 0.024  |  | -1/2    | 2.09   | H <sup>-</sup> (1/2 E)   |
| 10.8   | 0.024  |  | -1      | 0.48   | H <sup>-</sup> (E)   |
| 11.2   | 0.030  | C <sup>+</sup><br>CH <sup>+</sup><br>H <sub>3</sub> O <sup>+</sup> → O <sup>+</sup><br>CH <sub>2</sub> <sup>+</sup> , H <sub>2</sub> O <sup>+</sup> → O <sup>+</sup><br>CH <sub>3</sub> <sup>+</sup> , OH <sup>+</sup> → O <sup>+</sup><br>O <sup>+</sup><br>OH <sup>+</sup><br>H <sub>2</sub> O <sup>+</sup><br>H <sub>3</sub> O <sup>+</sup> | 0~-1    | 5.85   |  |
| 12     | 0.011  |  | -8.5    | 0.01   | CH <sub>n</sub> <sup>-</sup> → C <sup>-</sup> , CH <sub>m</sub> <sup>-</sup>   |
| 13     | 0.015  |  | -9      | 0.01   |  |
| 13.5   | 0.24   |  | -10.0   | 0.005  |  |
| 14,142 | 0.55   |  | -10.8   | 0.005  |  |
| 15     | 0.17   |  | -11.2   | 0.005  | C <sup>-</sup><br>H <sub>3</sub> O <sup>+</sup> → O <sup>-</sup><br>H <sub>2</sub> O <sup>+</sup> → O <sup>-</sup><br>OH <sup>+</sup> → O <sup>-</sup><br>O <sup>-</sup> |
| 16     | 0.095  |  | -12     | 0.030  |  |
| 17     | 0.015  |  | -13.5   | 0.43   |  |
| 18     | 0.015  |  | -14.2   | 0.85   |  |
| 19     | 0.010  |  | -15     | 0.24   |  |
| 8~19   | 1.35   | Na <sup>+</sup><br>Mg <sup>+</sup><br><br>N <sub>2</sub> <sup>+</sup><br>O <sub>2</sub> <sup>+</sup><br><br>Ca <sup>+</sup>  | -16     | 0.09   |  |
| 23     | 0.001  |  | -8~-16  | 1.67   |  |
| 24     | 0.002  |  | -24     | 0.0005 | O <sub>2</sub> <sup>-</sup>  |
| 27     | 0.0001 |  | -32     | 0.0002 |  |
| 28     | 0.0003 |  | -24~-32 | 0.0007 |  |
| 32     | 0.001  |  |         |        |  |
| 34     | 0.0003 |  |         |        |  |
| 35     | 0.0003 |  |         |        |  |
| 39     | 0.0005 |  |         |        |  |
| 40     | 0.0006 |  |         |        |  |
| 44     | 0.0003 |  |         |        |  |
| 23~44  | 0.006  |  |         |        |  |

TABLE V.2.1-2 TYPICAL PERFORMANCE CHARACTERISTICS OF THE  
BUCKET SOURCE AND LAMBDATRON FOR ION BEAM  
CURRENT OF 30 A AT 30 kV.

|  | BUCKET       | LAMBDATRON   |
|--|--------------|--------------|
| FILAMENT CURRENT   | 720 A        | 1080 A       |
| ARC CURRENT  | 260 A        | 460 A        |
| ARC VOLTAGE  | 100 V        | 95 V         |
| PRESSURE   | 3.5 mTorr    | 6 mTorr      |
| H <sup>+</sup> : H <sub>2</sub> <sup>+</sup> : H <sub>3</sub> <sup>+</sup> | 70 : 20 : 10 | 70 : 20 : 10 |
| ARC EFFICIENCY   | 1.1 A/kW     | 0.7 A/kW     |

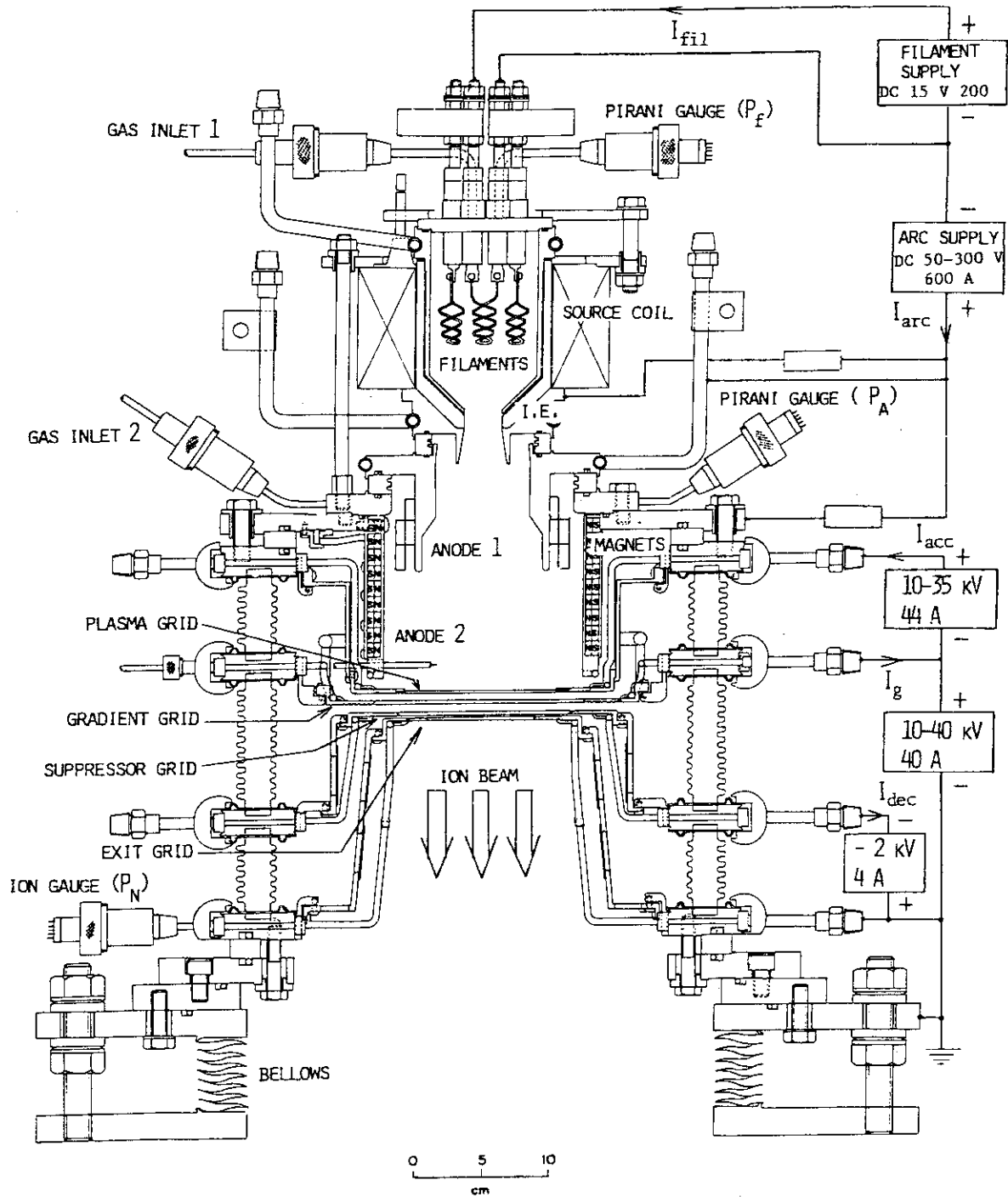


Fig. V.2.1-1 Modified duoPIGatron ion source with two-stage accelerator.

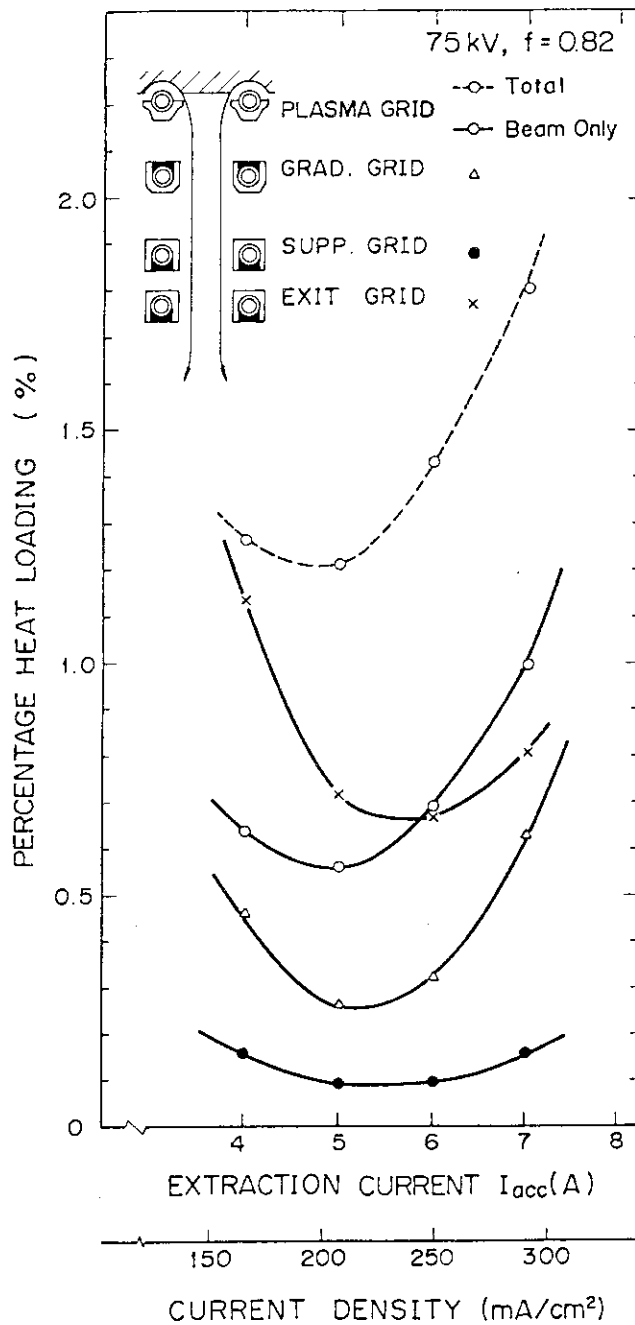


Fig. V.2.1-2 Percentage heat loading of each grid as a function of extraction current at constant pressure ( $P_A = 6$  mTorr,  $P_N = 1$  mTorr). The loading of plasma grid is composed of loading from source plasma and loading due to the presence of the beam.

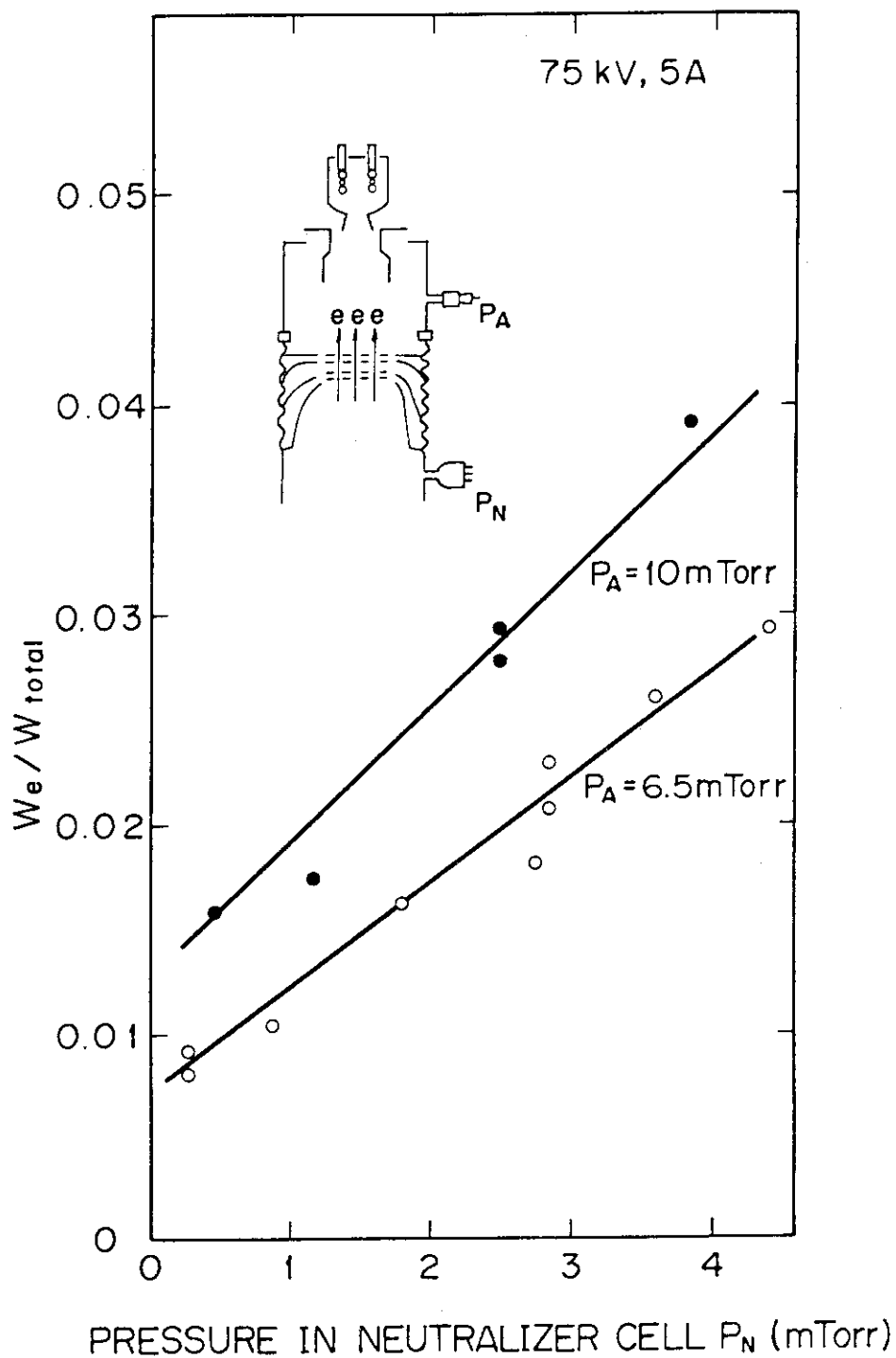


Fig. V.2.1-3 Power of backstream electrons as a function of pressure in neutralizer cell  $P_N$  for various pressures in arc chamber  $P_A$ .

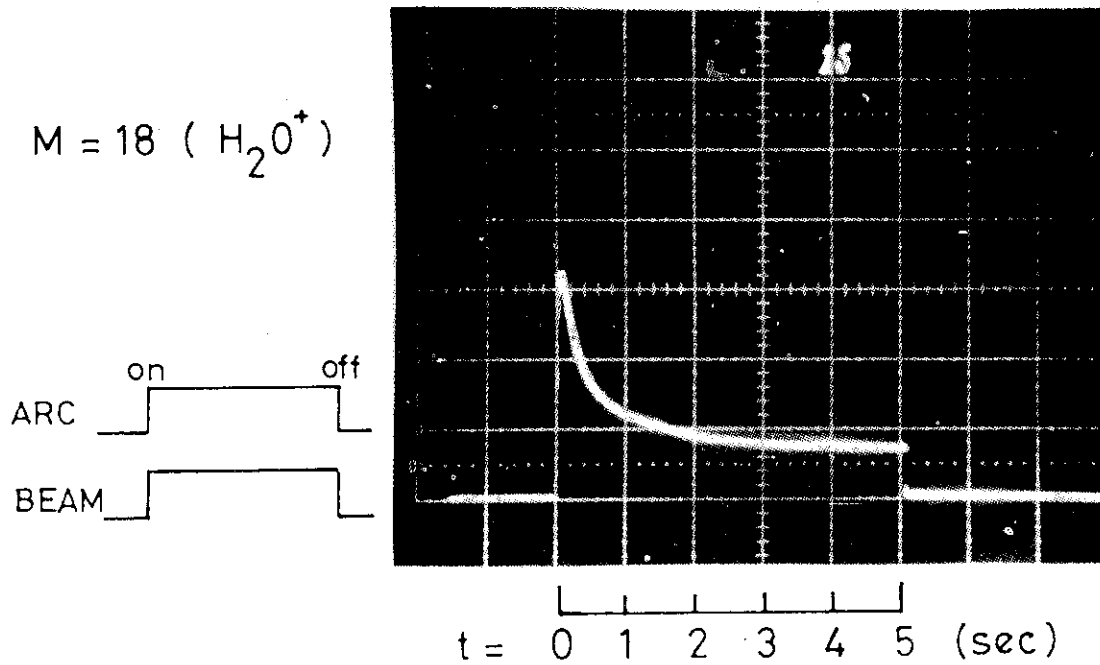


Fig. V.2.1-4 Time dependence of  $\text{H}_2\text{O}^+$  ion level measured by ion beam mass analyzer.

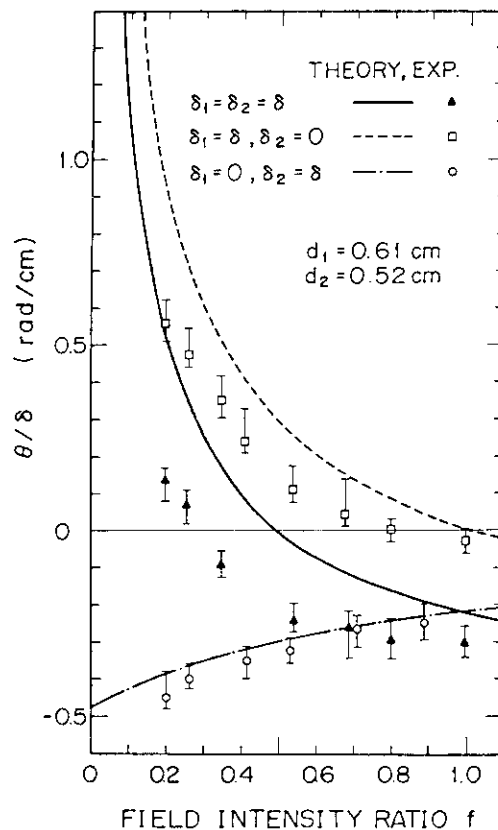


Fig. V.2.1-5 Comparison of measured steering angle per unit displacement distance ( $\theta/\delta$ ) with the value predicted by a linear theory for three cases of displacement; displacement of (1) plasma grid ( $\delta_1 = \delta_2 = \delta$ ), (2) gradient grid ( $\delta_1 = \delta, \delta_2 = 0$ ), or (3) suppressor grid ( $\delta_1 = 0, \delta_2 = \delta$ ) with respect to the other three grids.



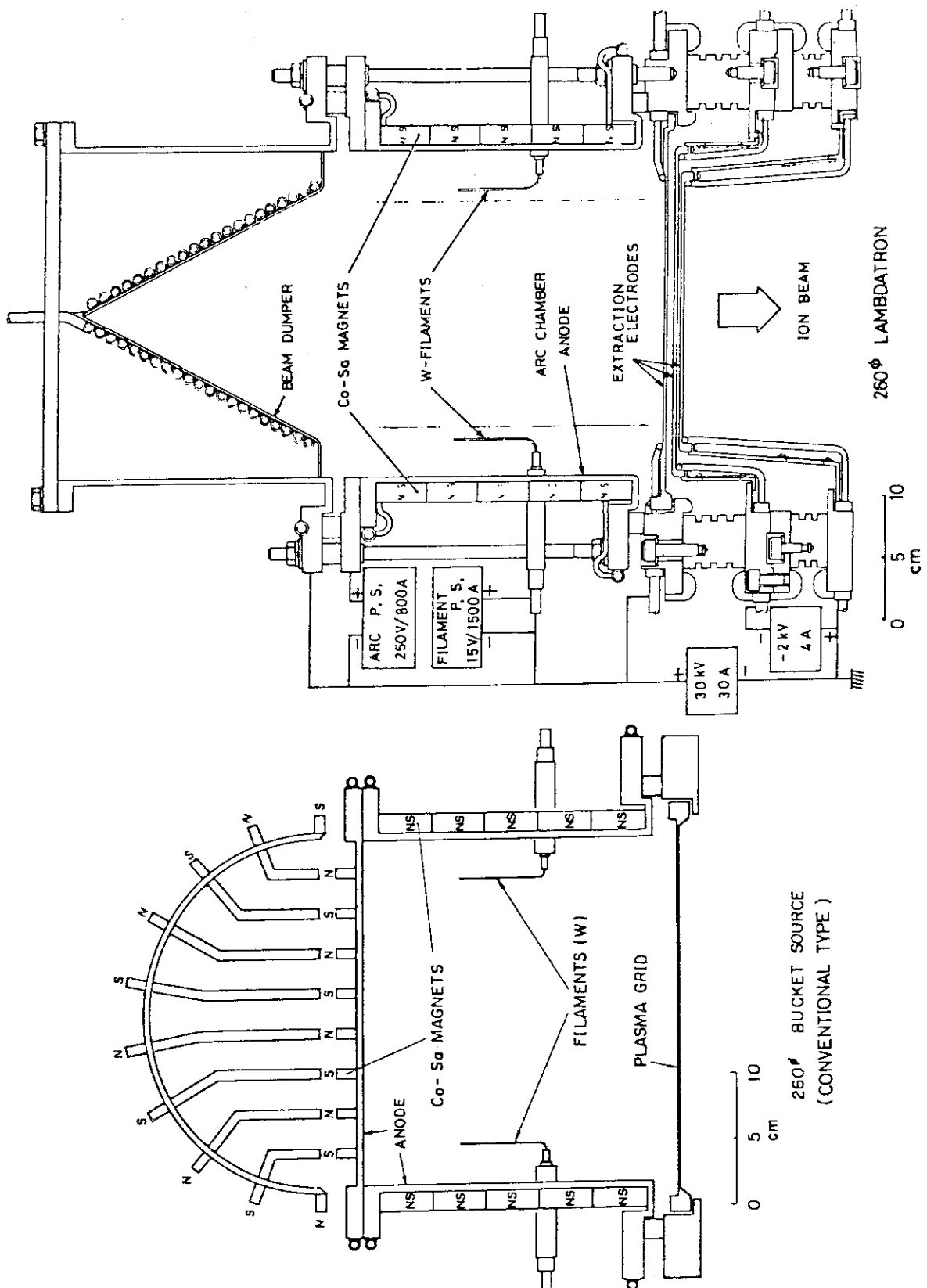


Fig. V.2.1.1-6 Schematic of the circular bucket source (a) and the circular Lambdatron ion source (b).

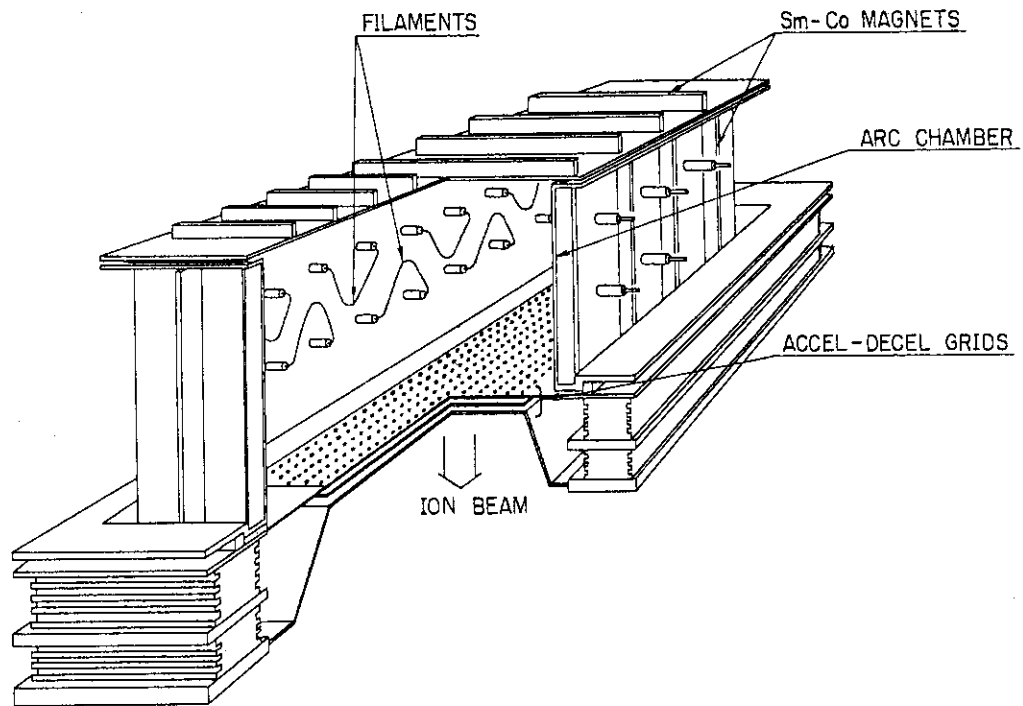


Fig. V.2.1-7 Schematic of rectangular bucket ion source

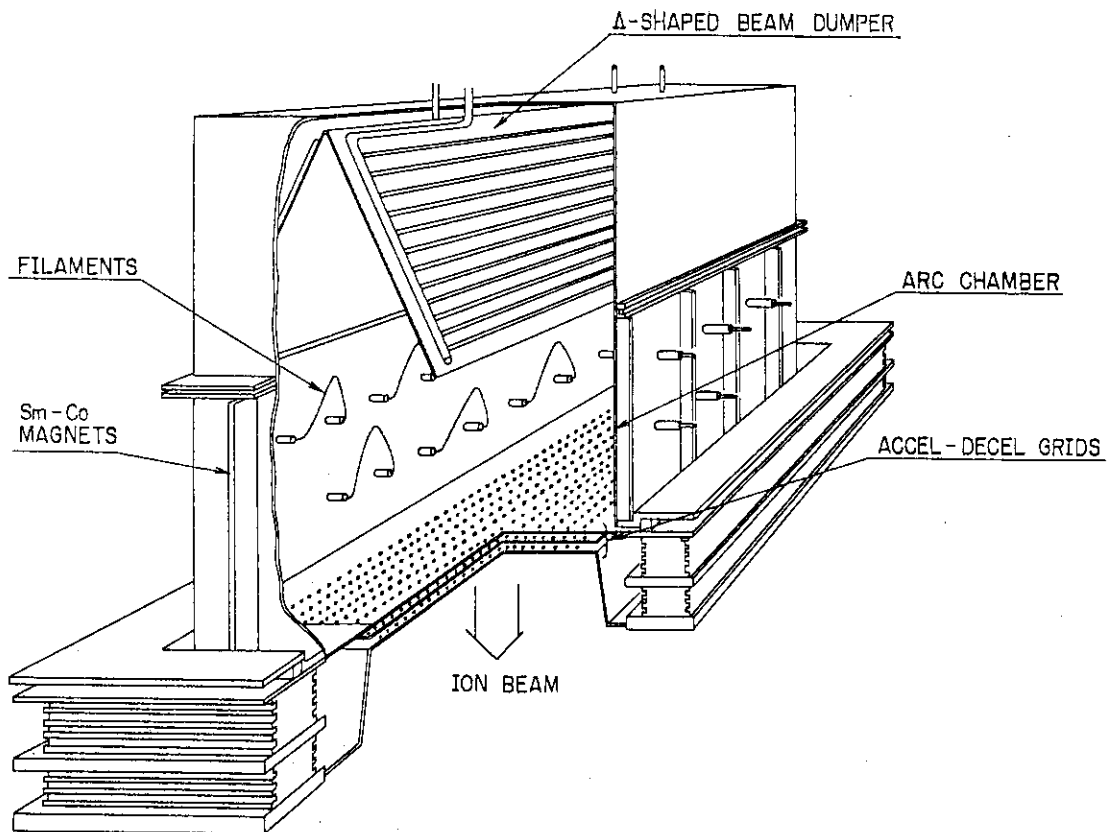


Fig. V.2.1-8 Schematic of rectangular Lambdatron ion source

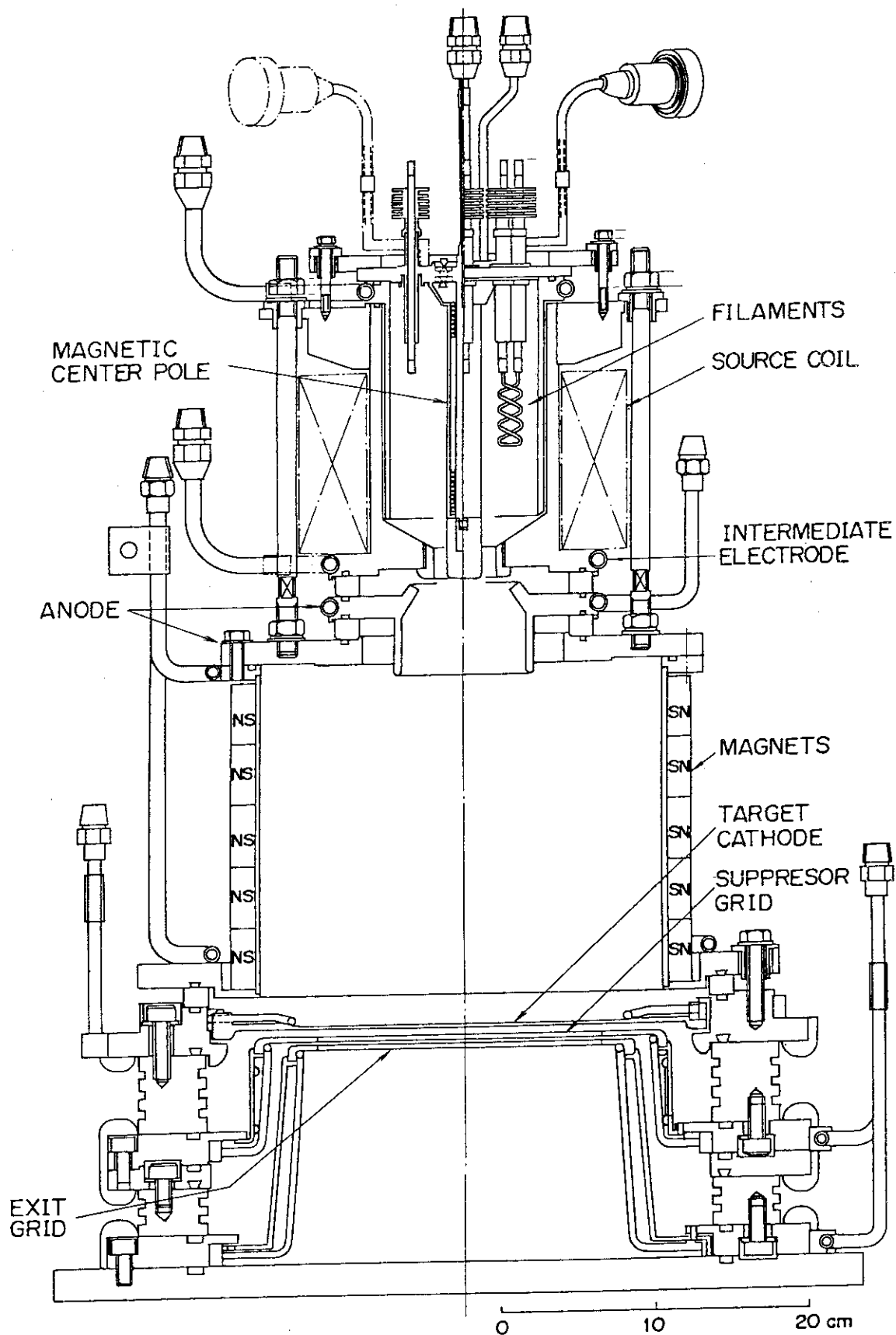


Fig. V.2.1-9 Sketch of coaxial duoPIGatron ion source

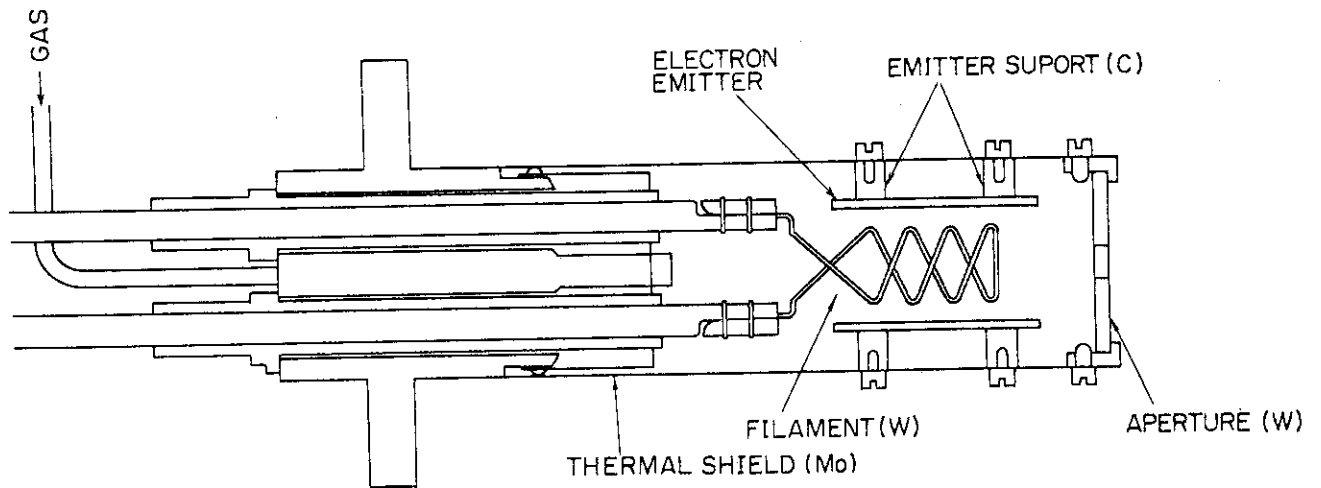


Fig. V.2.1-10 Detail of the hollow cathode used and tested at JAERI.

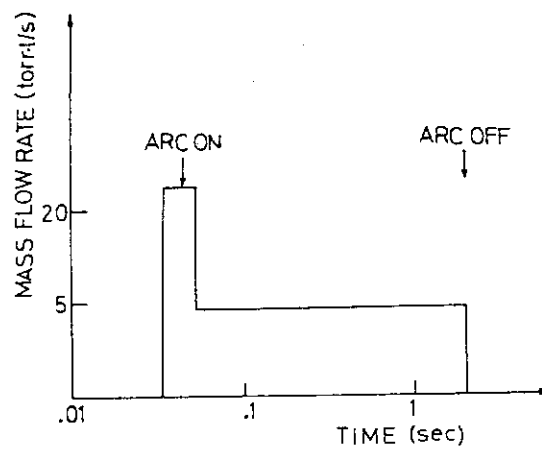


Fig. V.2.1-11 Time dependence of gas flow through the hollow cathode.

## 2.2 Development of the JT-60 neutral beam injection system

Neutral beam injection is expected to play an important role in the stage of additional heating of JT-60 plasma beyond 5 keV. Performances of the injector are specified as follows.

- (1) Beam energy: 30 - 100 keV
- (2) Total neutral beam power: 20 MW
- (3) Pulse width of injection: 10 seconds
- (4) Number of injector unit: 14 units
- (5) Permissible cold gas influx into the torus: a value corresponding to 15 % of the fast neutral atoms.

Prior to fabrication of the fourteen units, a prototype unit will be constructed to test and demonstrate a single unit performance. The prototype injector unit consists of a beam line unit, a power supply unit, a target chamber and auxiliary systems. A scheme of the beam line and the target chamber is shown in Fig. V.2.2-1. A cylindrical main vacuum chamber made of stainless steel contains all the necessary components. Two ion sources are installed to the chamber and the ion beam extracted from the source is introduced to the subsequent neutralizer cell. A reflecting magnet is placed behind the neutralizer cell to separate and guide unneutralized ions to a forced water cooled beam dump. Cryopumps are used to pump out almost 98 % of the cold and dumped hydrogen gases. A retractable calorimeter is mounted behind the reflecting magnet and is used as a neutral beam target during source conditioning. To prevent excessive backward cold gas from entering into the main vacuum chamber, a fast shutter (valve) is considered and is housed in a drift pumping room.

The remained design work of this unit has been done during the period under review, especially, R & D work about a few components in the beam line which relate with the reflecting magnet, with the stray magnetic field from the JT-60 tokamak and with cryopumps. The construction of this unit has been ordered to two manufactures in March 1980, then this unit will be fabricated and installed by the summer of 1981.

### (1) Reflecting magnet and beam dump design

Compared with a bending type magnet, a reflecting type magnet effectively reduces a heat flux to the beam dump. But because of its diverging effect on ion orbits, a part of ions hit the water jacket which is placed near the surface of the pole piece and the heat flux

there becomes over a permissible level. To solve this problem, a shape of the magnet has been designed by trial and error method using a computer code<sup>1)</sup> which traces every ion trajectories in a magnetic field starting from the multi aperture extracting grids and calculates the heat flux at every position where any ion impinges.

After extensive calculations, magnetic field intensity at the gap was altered from 1.2 KG to 1.32 KG for a 75 keV beam, and the gap distance was changed from 38 cm to 40 cm, and then two pole pieces were shifted by 5.5 cm towards the neutralizer. By shifting the pole pieces, the center of the magnetic field is also shifted, then ions are reflected without deeply penetrating into the gap region of the magnet, which leads to the reduction of the heat flux at the warer jacket surface.

Since the ions are diverged when passing through the magnetic field, the beam dump has a top view shape like a winner's cup. By using the computer code, the shape was designed to suppress surface heat flux in a level of less than  $500 \text{ w/cm}^2$  at every position and to keep the thermal stress below a permissible level. The dump is composed of many finned tubes which are made of oxygen free copper with 0.2 % silver added. The fin plays a role of reducing temperature gradient across the tube by absorbing heat on its surface.

## (2) Canceling magnetic field coil<sup>2)</sup>

In the absence of magnetic materials along the beam line, strength of the stray magnetic field from the JT-60 tokamak is expected to be at most 210 G around the position of the reflecting magnet. In the presence of magnetic materials such as the reflecting magnet and the magnetic shields for neutralizer and for ion sources, the stray field is absorbed by them and the field in the space between the neutralizer and the reflecting magnet is strengthened by a factor of 2 to 3. This field strongly influences the orbits of unneutralized ions and shifts the beam axes to one side, then heat flux at some places easily overcome the permissible level.

To reduce the influence of the stray magnetic field, we decided to employ the canceling magnetic field whose vector is almost antiparallel to that of the stray field and almost the same in strength. This canceling field is generated by the current passing through the coil wound around the reflecting magnet. Using 1/10 models of the magnetic materials, we carried out the experiment and confirmed the effectiveness of

the canceling field. Since the distribution of canceling magnetic field is not perfectly the same as that of stray field in the presence of magnetic materials, still remains a definite field distribution even after the canceling. The absolute value of the canceled field is much smaller than that of stray field itself.

### (3) Cryopumps

The compatibility of cryopumps with the high energy beam in neutral beam line is one of the important problems. To investigate this problem, hydrogen ion beams of 5 A at 75 keV were introduced for 10 sec into the  $6 \times 10^4$  l/s cryopump<sup>3)</sup> in which a beam dump was installed. From this experiment, it was found that beam injection did not affect the pumping performance essentially. However, a little decrease of the pumping speed was observed during the beam injection as shown in Fig. V.2.2-2. This decrease of pumping speed was attributed to the temperature rise of spot welded area of quilted liquid helium panel.

### References

- 1) T. Itoh et al.: to be published in JAERI-M.
- 2) M. Matsuoka et al.: to be published in JAERI-M.
- 3) J. Sakuraba, T. Ohga and T. Shibata: JAERI-M 8013 (1978).

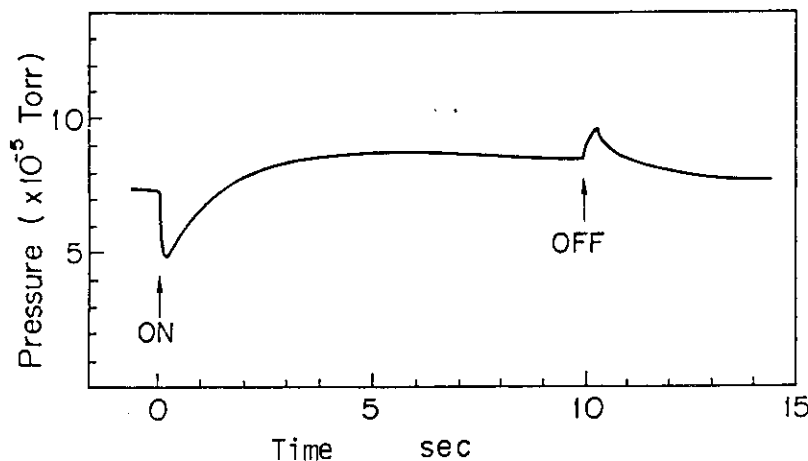


Fig. V.2.2-2 Temporal behavior of gas pressure in the cryopump during beam injection

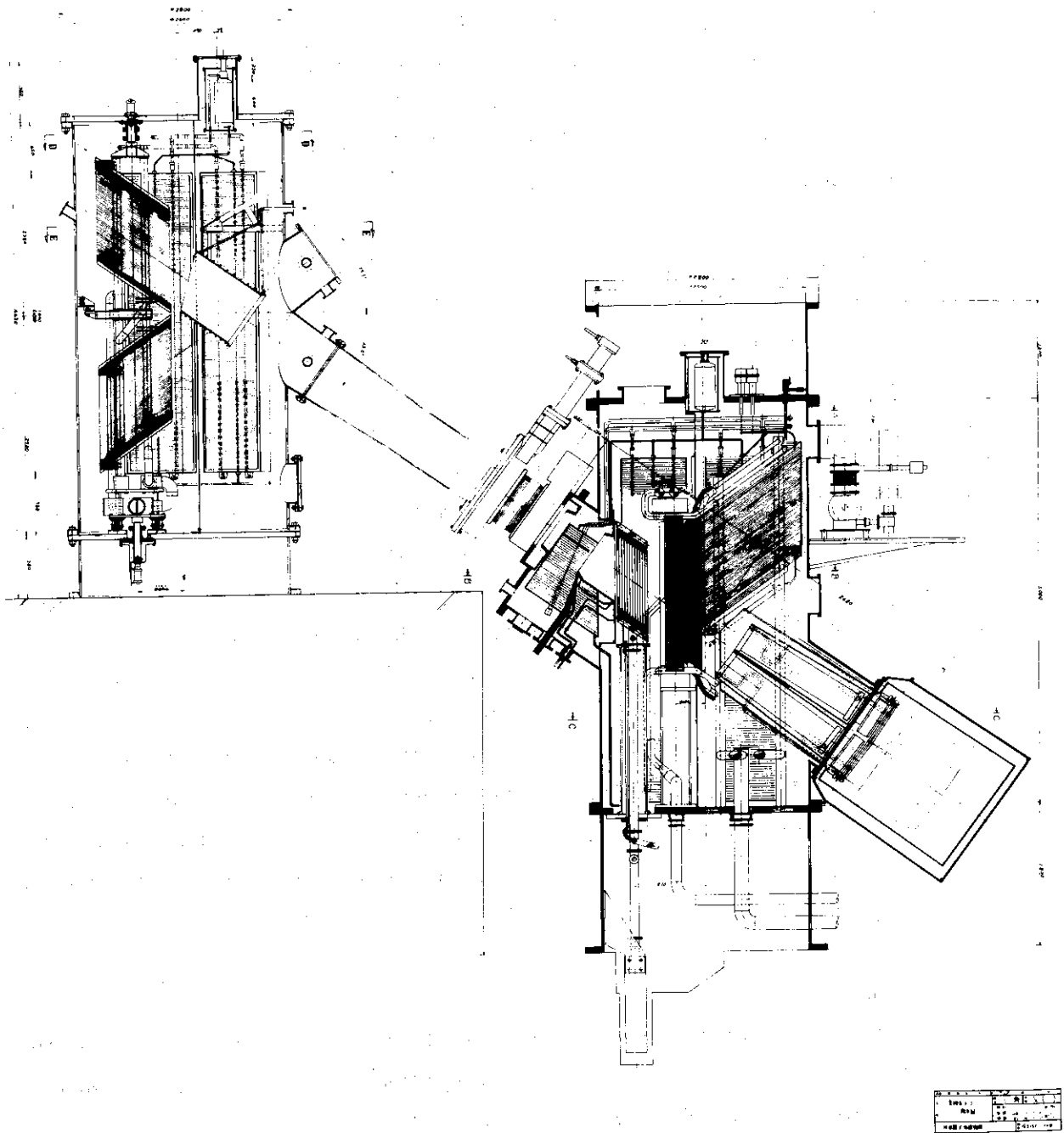


Fig. V.2.2-1 A cross-sectional view of the prototype unit of the JT-60 NBI



### 2.3 The neutral beam injection system for the JFT-2

The neutral beam injector for JFT-2 was developed and is now in operation. This injector was designed, fabricated, assembled and tested within about one year. Main efforts to develop this system were made to achieve high reliability and high availability of operation and effective experiments of plasma heating.

The NBI system was designed and constructed by members of plasma Heating Laboratory, Facility Operation and Engineering Section and Experimental Plasma Physics Laboratory. In this section, outline of the NBI system is described.

#### 2.3.1 DuoPIGatron ion source for JFT-2 neutral beam injector

The neutral beam injector consists of four ion sources each of which can deliver a hydrogen ion beam of more than 20 A at 40 kV for 0.1 sec. To satisfy these specifications, we have developed an axisymmetric 18.5 cm diam. duoPIGatron ion source with a water-cooled button located in the neighborhood of the intermediate electrode and a set of line cusp confinement magnets around the arc chamber wall (See Fig. V.2.3-1).

Each beamlet is focused to a point 2.5 m apart from the source by the aperture displacement technique. The source performance is shown in Table V.2.3-1. The calorimetrically measured power fraction to the target which simulates the injection port of the JFT-2 tokamak is up to 80 %. Consequently, we expect the total neutral beam power to the torus will be up to 1.7 MW with the neutralization efficiency of 0.6.

#### 2.3.2 Beam line

In order to obtain higher beam transmission efficiency, the beamline was designed as short as possible. The fundamental specifications and design features are as follows (Fig. V.2.3-2).

- 1) Injection power. This injector is specified to inject 1.5 MW of 30 kV neutral hydrogen atoms for 50 msec. through two beamlines connected to a single port. Two sets of duoPIGatron ion source<sup>1)</sup> are mounted in each beamline. The efficiency of injected neutral/extracted ion is about 45 %.
- 2) Beamline components. The beamline consists of an expansion chamber, beamline steering mechanisms, neutralizer, a deflection magnet, a beam dump, a calorimeter, a high speed shutter, beam limiters, a drift tube and so on. These components are arranged within 2.5 meter

along the beamline.

- 3) Vacuum system. The vacuum system consists of a large expansion chamber and two sets of turbo-molecular pump. This expansion chamber is about 20 m<sup>3</sup> in volume and is connected to two drift chambers through metal bellows. Thirty sets of Ti flasher are provided in the expansion chamber, drift chambers and drift tubes to clean the vacuum surface.
- 4) Magnetic Shields. Ion sources and the neutralizer were enclosed by large magnetic shields made of soft magnetic iron and high permeability material to reduce the effect of external magnetic field.

### 2.3.3 Power supply system

To supply power to four ion sources, the system consists of two sets of accel and decel power supplies and four sets of PIG power supplies. The fundamental specifications and design features of each power supply are as follows.

- 1) Accel power supply (10 ~ 40kV 65A 300msec duty 1/30)

Main components of the accel power supply are an ac-thyristor switch, a converter transformer, a diode rectifier, dc-filter capacitors, a thyristor crowbar switch, a series regulator tube and a surge blocking core.

- 2) PIG power supply. A set of PIG power supply consists of an arc, a filament, a source coil and an auxiliary power supply. The rating of the arc power supply is 180V 800A 300msec duty 1/30. This power supply has an arc snubber circuit using GTOs, which reduces an arc current to 1/10 of the rated value for a short time and return it to the rated value in accordance with the turn on of the accel voltage. This is to decrease the possibility of break downs in the beam initiation phase.
- 3) Grounding system. The grounding system of the power supply is separated into two sections: an ac-grounding system and a dc-grounding system. Main components in the dc circuit such as a thyristor crowbar switch, a series regulator tube of accel power supply, PIG insulating transformers are put on a common dc-grounding conducting plate which is insulated from the floor of the building. This system is effective to reduce malfunctions of the control circuits in the case of breakdowns of the ion source.
- 4) Control system. The control system has functions for control,

monitor and protection of power supply system and beam line system. The power supply system is controlled by a sequential controller consists of IC timer and IC logic circuits.

#### Reference

- 1) Y. Arakawa et al. "The Present Status of Ion Source Development at JAERI." JAERI-M 8869, (May 1980)

Table V.2.3-1 Performance characteristics of a modified duoPIGatron ion source with 185 mm diameter accelerator

|  |           |
|--|-----------|
| FILAMENT CURRENT   | 60 A x 12 |
| ARC VOLTAGE  | 80 V      |
| ARC CURRENT  | 250 A     |
| ACCEL VOLTAGE  | 30 kV     |
| ACCEL CURRENT  | 25 A      |
| DECEL VOLTAGE  | -1.6 kV   |
| DECEL CURRENT  | 2.8 A     |
| DURATION TIME  | 0.1 sec   |
| POWER FRACTION<br>TO TARGET  | 80 %      |
| H <sup>+</sup> : H <sub>2</sub> <sup>+</sup> : H <sub>3</sub> <sup>+</sup> | 59:28:13  |
| IMPURITY (C,O)   | 1 %       |
| ARC EFFICIENCY   | 1.25      |

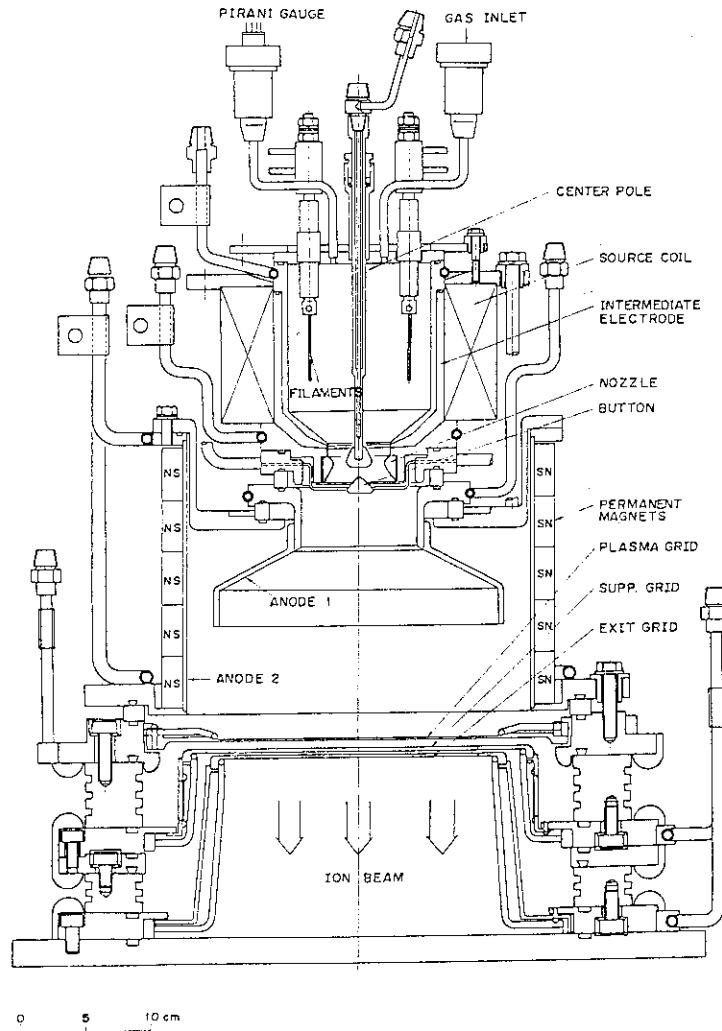


Fig. V.2.3-1 DuoPIGatron ion source for JFT-2 NBI

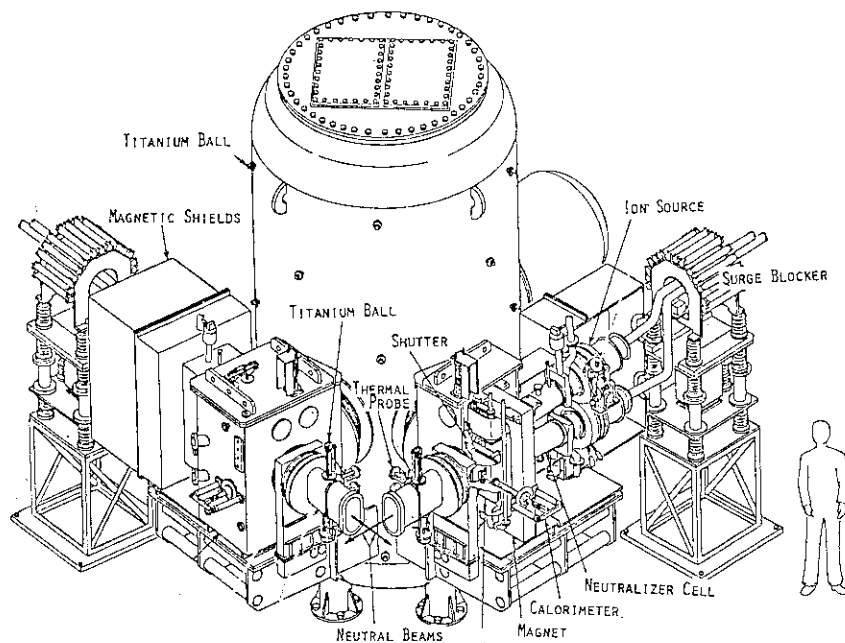


Fig. V.2.3-2 Schematic view of NBI system for JFT-2

### 3. Radiofrequency Heating System

#### 3.1 Development of waveguide coupler

A phased array of waveguides can be used as a wave launcher for lower hybrid RF heating.<sup>1)</sup> The launcher is one of the most important components of RF heating system because it faces directly at a plasma and heating efficiency of plasma depends on its design. We have been studying characteristic of it and improving its design to obtain good coupling and good plasma heating. A phased array of multi-waveguides will be used as the launcher of RF system for JT-60.

A phased array of four waveguides has been used in lower hybrid range of frequencies heating experiment on JFT-2.<sup>2),3),4)</sup> In the first phase of the experiment (1977-78), the narrow launcher (14mm  $\times$  290mm) made of aluminium was used. In the early experiment, the power was not well transmitted to the plasma due to the breakdown near the ceramic window. Improvement of the ceramic window brought the transmitted power of  $\sim 100$  kW. Power reflection coefficient depends on phase difference  $\Delta\phi$  between the adjacent waveguides. This dependence is an important property of the launcher. The experimental results were shown in Fig. V.3.1-1. At low power ( $\sim 5$  kW), power reflection coefficient agrees with that from linear theory.<sup>1),3)</sup> At high power ( $\sim 100$  kW), the discharge, presumably multipactoring discharge, had been likely to limit the transmitted power since the traces of discharge were found at the front tip of the launcher. Power reflection coefficient became very small and did not agree with calculated value from linear theory. But the discrepancy is explained well by taking the resistive loss part due to the discharge into consideration as shown with the dotted line in Fig. V.3.1-1.<sup>5)</sup>

In the second phase of the experiment (1979), the wide launcher (33mm  $\times$  290mm) optimized for ion heating was used. It was made of stainless steel plated with copper and further coated with titanium so as to suppress the secondary electron emission. Heating efficiency of ion was doubled as compared with that in the first phase of the experiment. The dependence of power reflection coefficient on phase difference  $\Delta\phi$  is shown in Fig. V.3.1-2. Power reflection coefficient varies with  $\Delta\phi$ , which means the reduction of the discharge loss. Its dependence, however, is different from that expected from linear theory. But the difference is explained well by nonlinear effect such as the modification of density gradient due to the ponderomotive force.<sup>5)</sup> Power

reflection coefficient versus transmitted power is shown with circles in Fig. V.3.1-3. It was possible to couple stably up to the transmitted power of 200 kW.

Furthermore the similar dependence shown with x in Fig. V.3.1-3 was obtained up to more than 280 kW with the narrow launcher (15mm  $\times$  290mm) made of titanium. It corresponds to the transmitted power density of 2 kW/cm<sup>2</sup>. Since this limitation is due to the capability of the present power source, it is expected that transmitted power density more than 2 kW/cm<sup>2</sup> will be obtained with increasing the maximum output of power source.

We are planning to input a RF power of 10 MW to the plasma core in JT-60. It requires RF power density of 3.5 - 4 kW/cm<sup>2</sup>. Test of the material and design of the optimum geometrical structure for the launching system of wave are now being conducted to achieve the above requirement.

#### References

- 1) Brambilla, M.: Nuclear Fusion 16 (1976) 47.
- 2) Imai, T., Nagashima, T., Azumi, M.: Numerical Studies of Lower Hybrid Wave Propagation in JFT-2, JAERI-M 6902 (February 1977).
- 3) Nagashima, T. and Fujisawa, N.: In Proceedings of the Joint Varenna-Grenoble Int. Symp. on Heating in Toroidal Plasma, Grenoble (1978).
- 4) Fujii, T., et al.: In Proceedings of the 7th Int. Conf. Plasma Physics and Controlled Nuclear Fusion Research, Innsbruck (1978) IAEA-CN-37/A-4-2.
- 5) Fujii, T., et al.: to be published.
- 6) Imai, T., et al.: In Proceedings of the 2nd Joint Grenoble-Varenna Int. Symp. on Heating in Toroidal Plasma, Como (1980).

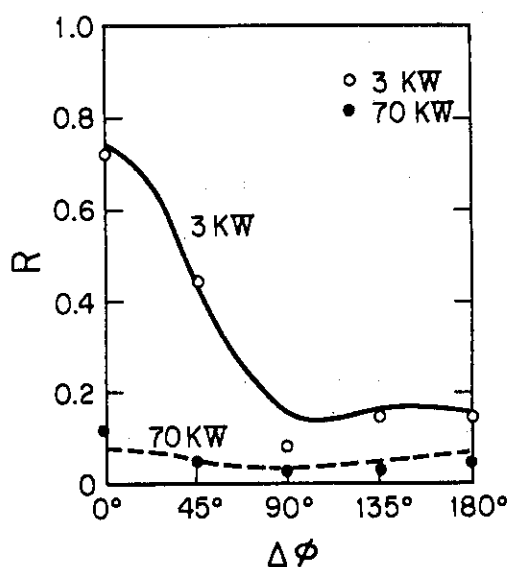


Fig. V.3.1-1 Reflection coefficient  $R$  versus phase difference  $\Delta\phi$ . Circles show experimental results of aluminium launcher in the first phase (1977-78). The solid and dotted lines indicate those calculated from linear and modified linear theory, respectively.

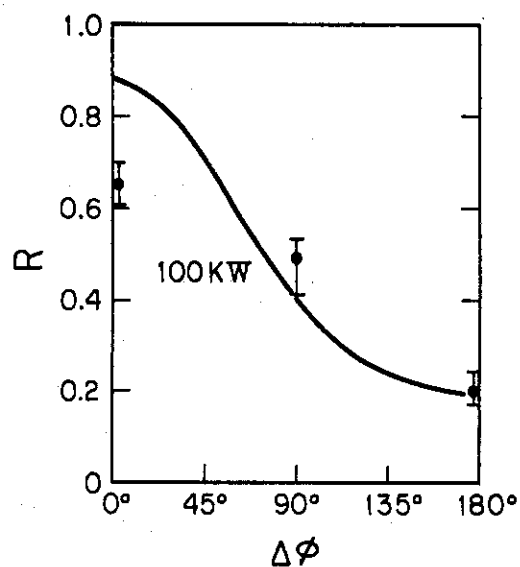


Fig. V.3.1-2 Reflection coefficient  $R$  versus phase difference  $\Delta\phi$ . Circles show experimental results of stainless steel launcher coated with titanium in the second phase (1979). The solid line indicates calculation value from linear theory.

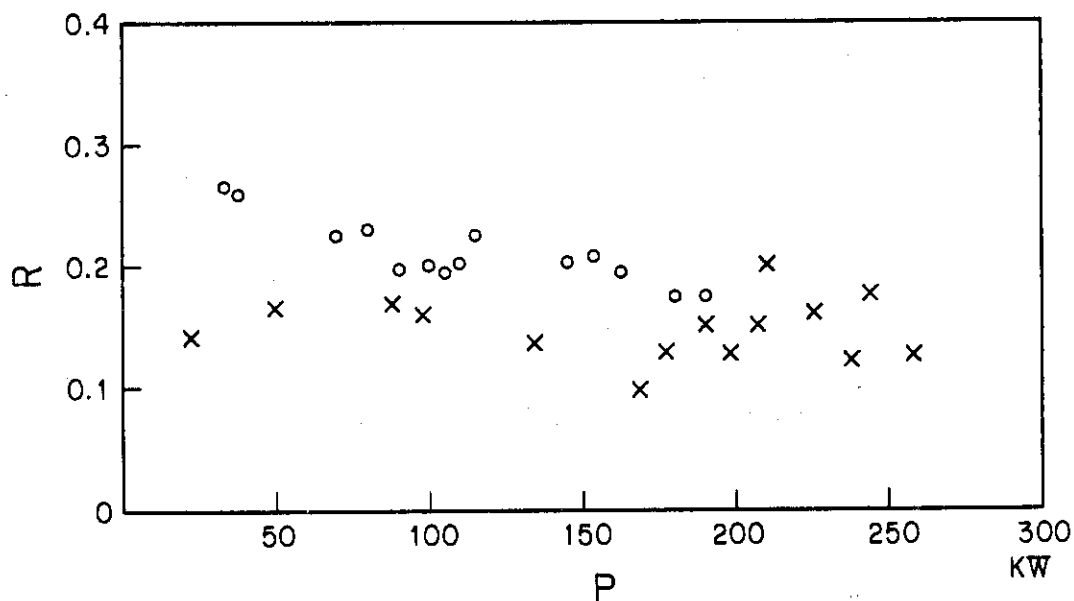


Fig. V.3.1-3 Power dependence of reflection coefficient  $R$  in the second phase of the experiment (1979).

○; experimental results of stainless steel launcher coated with titanium.  
 ×; experimental results of titanium launcher.

### 3.2 Radio-frequency heating system in JT-60<sup>1)</sup>

#### 3.2.1 Introduction

Design study of radio-frequency heating system in JT-60 has been further advanced during the period under review. In the JT-60 project, the energy deposition in the plasma of 10 MW - 10 sec is planned for RF heating experiment. This requires 40 MW RF power as total out put of amplifiers. The projected frequency range is of lower hybrid waves. Thirty-two klystrons will be employed as the amplifier having 1.25 MW out put power per one unit. The design studies summarized here have been made with the cooperation of Nippon Electric Co. Ltd., and Tokyo Shibaura Electric Co. Ltd..

In §3.2.2 the low power drive train for the high power klystron is presented and in §3.2.3 the high power klystron. The control system of the JT-60 RF heating apparatus is presented in §3.2.4.

#### 3.2.2 Low power drive train

The low power drive train consists of the signal source and low power amplifiers.

##### (1) Signal source

The signal source produces the initial RF pulse, and regulates the level of final RF power, phase relation and operation mode. The signal source has also a function to compensate the linearity of the amplifier and the distortion due to the AM-PM transformation. The block diagram of the signal source is shown in Fig. V.3.2-1. The standard signal generator drives carrier wave which is sent to the excitation modulator. The modulational signal generator produces the modulation wave which modulates the carrier wave in the excitation modulator.

Then the drive signal thus generated is divided into eight by the RF distributor and is sent to the RF exciter, which consists of the RF phaser, amplitude compensator and phase compensator, to be amplified up to 100 mW by pre-power amplifier. This is the input to the low power amplifier. The excitation processor controls the whole processes described above.

The level diagram of the signal source is shown in Fig. V.3.2-2. The out put power from the standard signal generator is 5 mW and the peak power of the modulated signal about 20 mW (CW). This is divided by the RF distributor to be 1.6 mW in each channel. After amplified to 4 mW by the RF phasers, the pre-amplifiers amplify each signal to 100 mW,



which is the output power of the signal source.

In each RF exciter, amplifiers and attenuators are employed to provide prescribed RF power stably in each channel.

## (2) Low power amplifier

In the low power amplifier, the RF signal from the signal source is amplified to necessary power level (200 W) before it enters into high power klystrons. Klystron, travelling wave tube (TWT), and transistor amplifier are candidates of the low power amplifier. The transistor amplifier above 200 W power per one unit exceeds the present technological level. The distortion due to AM-PM transformation is larger in TWT than in klystron. There is much heat generation both in the klystron and in the TWT because of large back-off power. The design study described here assumes klystrons as the low power amplifiers.

The system of the low power amplifier is shown in Fig. V.3.2-3 and the level diagram in Fig. V.3.2-4. The RF signal from the signal source is first sent to the isolator which optimizes VSWR viewing from the signal source side. Then the phase shifter determines the phase of the RF signal as prescribed. Finally, the power of the RF signal is arranged by the variable attenuator.

Then the RF power is amplified by the power klystron up to 200 W. The gain of the klystron is 40 dB and the saturation level of the output power is 1 kW. Hence there may be no distortion of the signal in power amplification and the AM-PM transformation. The output power from the klystron is finally led to the circulator to improve the output VSWR. When, large back-off power is reflected during vary short time, the reflected power is completely absorbed in the circulator dummy load.

## 3.2.3 High power klystrons

The RF wave preamplified in the low power amplifier is sent to high power klystrons and amplified up to 1.35 MW per one unit. The design study of the high power klystron was described in detail in the previous annual report.

The klystron is about 2.7 m in length and is about 1.5 ton in weight. The drift chamber must be fabricated using non-magnetic metal. The inner part of the drift chamber is exhausted by ion pumps below  $10^{-7}$  Torr. The collector must be cooled by evaporating water to avoid large heat damage due to high power electron beam from the cathode. The cathode is immersed in an oil tank for cooling and electrical insulation.

The efficiency of the klystron is about 50 % in the present design. The specifications of the klystron are summarized in Table V.3.2-1. Fabrication and tests of the proto-type klystrons will be initiated from 1980.

The power supply consists of high voltage power supply for anodes and cathodes of the klystrons and low voltage power supply for filaments, ion pumps etc. The collector and anode circuits equip the protecting circuits preventing the damage of the klystron from accidents.

#### 3.2.4 Control system

The control system of the JT-60 RF heating system consists of the control and display section, monitoring section and data processing section. The control and display section performs the operation of the RF heating apparatus and the surveillance of the operating condition. The monitoring section supervises each apparatus during experiment and maintenance. The data processing section performs the processing of control and diagnostic data.

##### (1) control and display section

The RF heating apparatus is one of the block equipments of JT-60, and basically governed by ZENKEI, a top hierarchy control system in JT-60.

In usual experiments (denoted by ZENKEI mode) the control system of the RF heating system obeys the setting command from the central console of ZENKEI on the operating conditions, and controls the RF heating apparatus. The RF control system can also independently operate without interference of ZENKEI when necessary. Namely the RF heating apparatus can be controlled from the central control panel of the RF control system even during the ZENKEI mode. The CAMAC system is adopted except in the protection interlock, in which hard-wired circuits are used. Optical cables are employed for signal transmission between building.

The operating conditions of the RF heating apparatus are set by the RF control system. The feed back control provides the power setting with an accuracy below  $\pm 3$  %. The range of RF power is more than 26 dB and the response time is below 10 msec with feed back and below 1 msec without feed back.

There are three setting modes, i.e., preset mode, program mode and dynamic control mode. In the preset mode, phase difference of injected

RF waves from grill is fixed during discharge. The time variation of the phase difference is prescribed in the program mode. In this case the pluse shape is generated by using N rectangular pulses ( $N \leq 100$ ) as shown in Fig. V.3.2-5(a). In the dynamic control mode, the pulses are controlled with the time constant below 100 msec following the variation of the plasma parameters as shown by B loop of Fig. V.3.2-5(b).

The block diagram of the control system in the RF heating apparatus is shown in Fig. V.3.2-6. The control system has the central control panel and the RF mini-computer placed in the control building, and the local panel and the apparatus control unit for klystrons placed in the JT-60 building.

#### (2) Monitoring section

The diagnostic data necessary for the control, experiment and maintenance are sent to the central control panel or the RF mini-computer in the controlling building through the optical fiber after A/D conversion. The subjects of the diagnostics amount to 1500 items, e.g. input and reflection powers, phase relations at the top of the launcher, frequency, modulational wave form etc.

#### (3) Data processing section

As shown in Fig. V.3.2-6, the computer for the RF heating apparatus intermediates with ZENKEI control system and processes the control and diagnostic data from the central panel. All informations are displayed on CRT and recorded in printer.

#### References

- 1) T. Nagashima, T. Imai, K. Uehara, H. Shirakata and T. Fujii : unpublished.

Table V.3.2-1 The specification of the high power klystron.

## ELECTRICAL

|                                |     |           |
|--------------------------------|-----|-----------|
| Heater Power                   | w   | 450       |
| Output Power (Saturation)      | Mw  | 1.35      |
| Bandwidth (Instantaneous 1 dB) | MHz | 6         |
| Efficiency                     | %   | $\geq 50$ |
| Power Gain                     | dB  | 43.6      |

## MECHANICAL

|                    |    |        |
|--------------------|----|--------|
| Input rf Coupling  |    | Type-N |
| Output rf Coupling |    | WR-650 |
| Dimension Length   | mm | 2700   |
| Weights            |    |        |
| Klystron           | kg | 1500   |
| Magnet             | kg | 400    |

## OPERATION

|                                |     |      |
|--------------------------------|-----|------|
| Frequency                      | GHz | 1.7  |
| RF Pulse Length Maximum        | sec | 10   |
| Repetition Period              | min | 10   |
| Output Power                   | Mw  | 1.25 |
| Driving Power                  | w   | 160  |
| Beam Voltage                   | kV  | 87   |
| Beam Current                   | A   | 30   |
| Body, Collector, Anode Voltage | kV  | 87   |
| Body Current                   | A   | 1    |

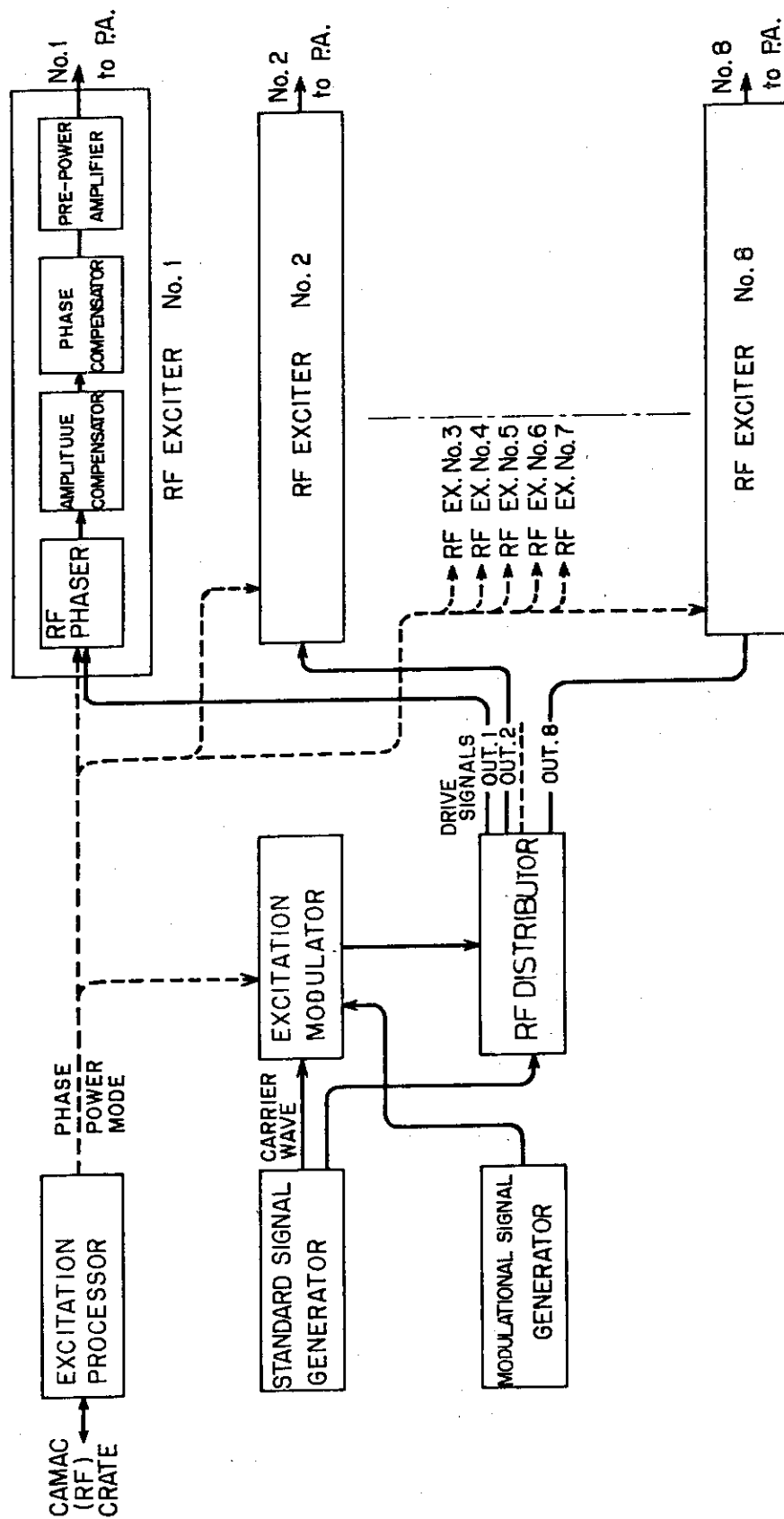


Fig. V.3.2-1 Block diagram of the signal source.

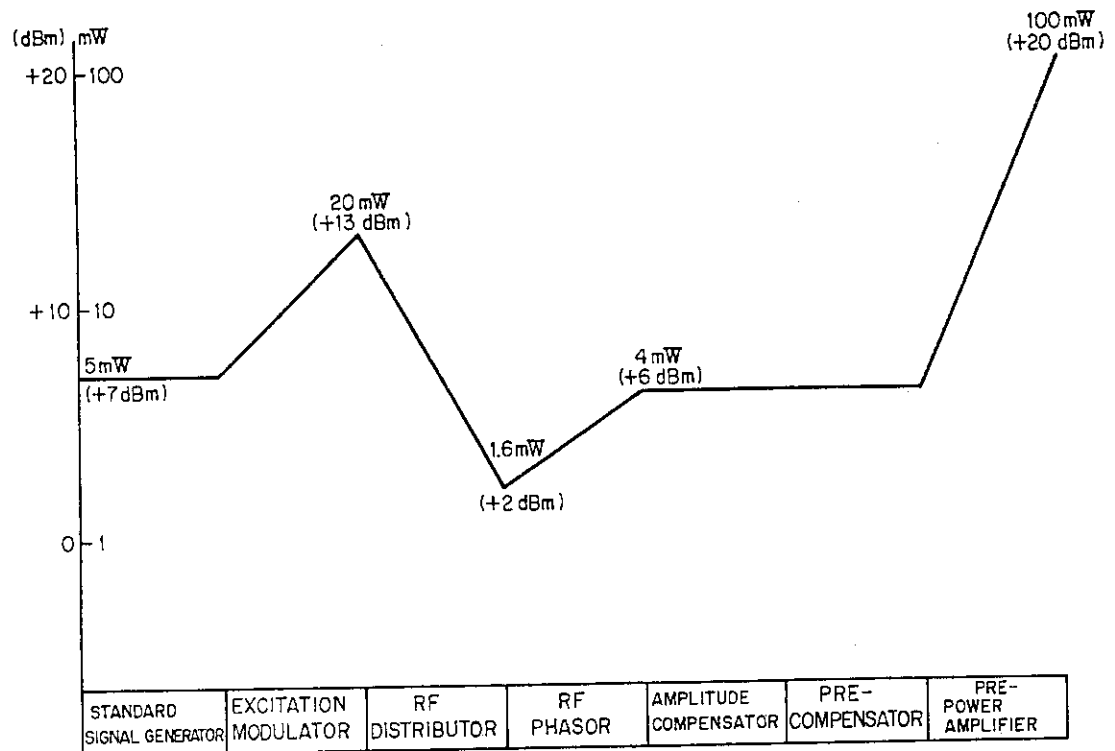


Fig. V.3.2-2 The level diagram of the signal source.

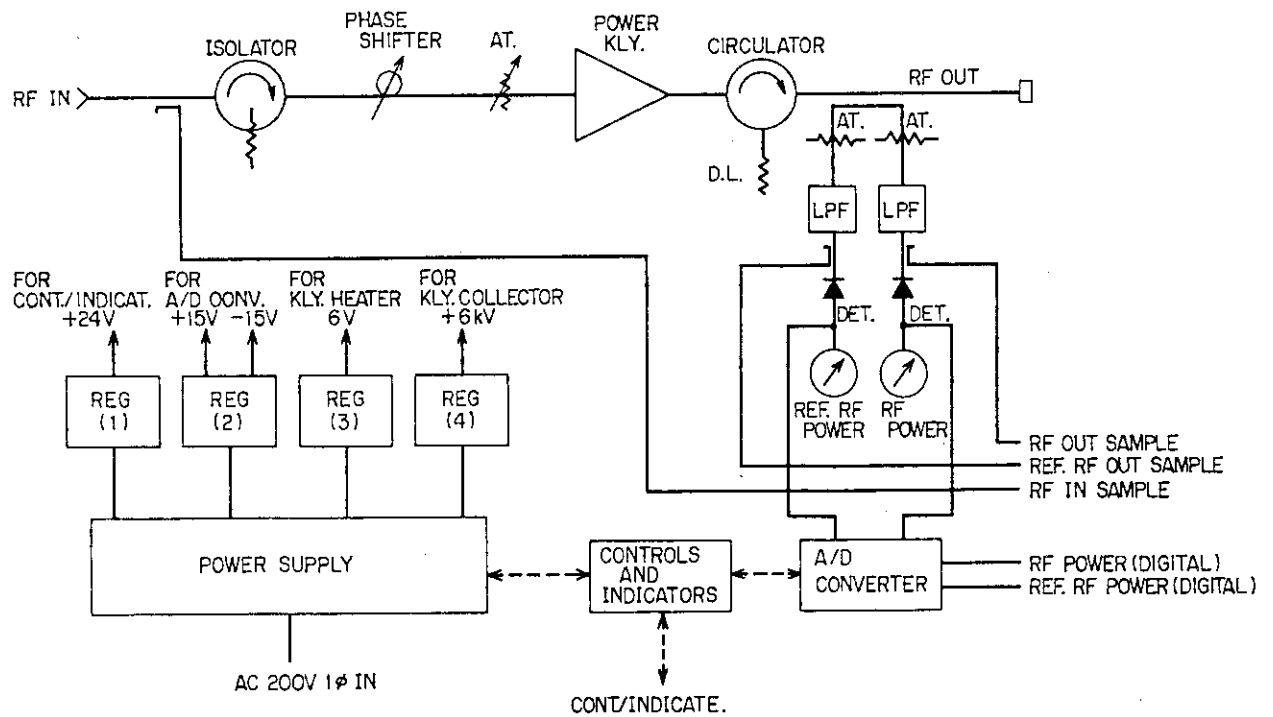


Fig. V.3.2-3 The system of the low power amplifier.

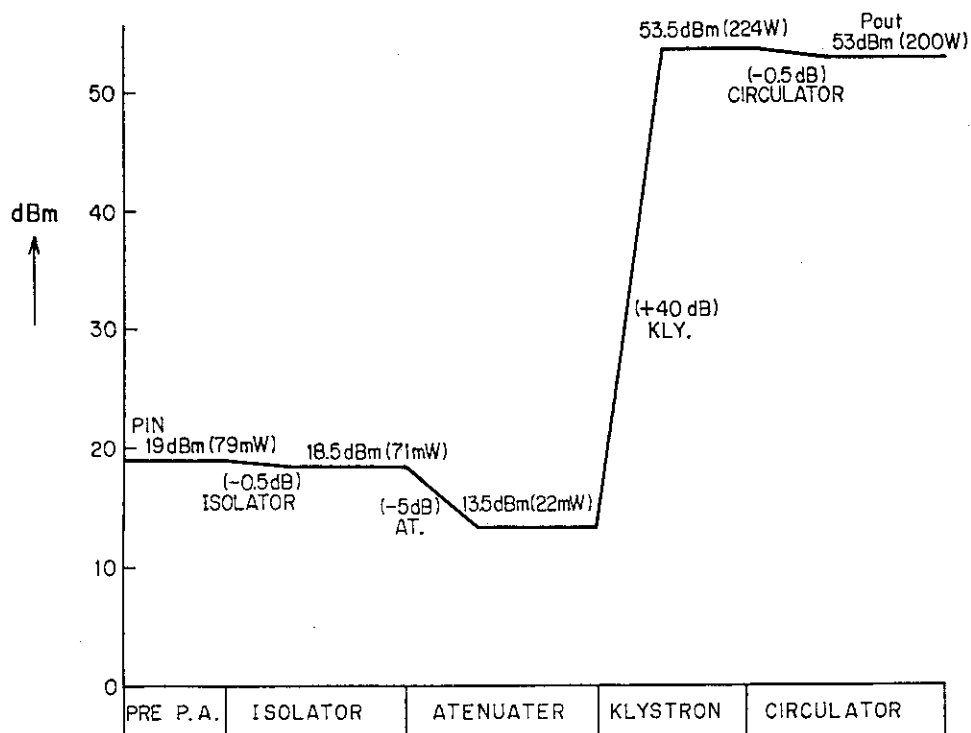


Fig. V.3.2-4 The level diagram of the low power amplifier.

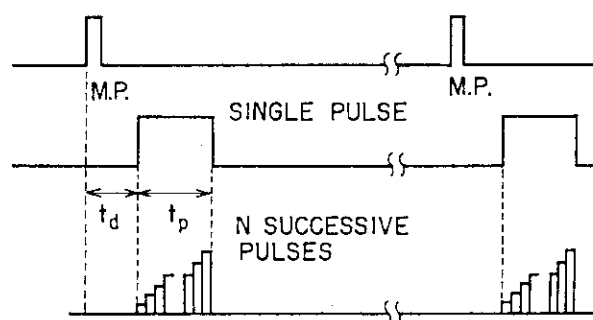
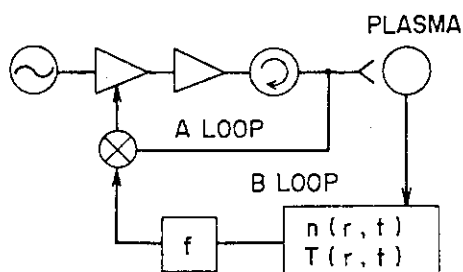


Fig. V.3.2-5 (a) The wave form of the RF pulses, single rectangular pulse and N successive rectangular pulses ( $1 < N < 100$ )



(b) The dynamic control mode (A loop) and the feed back control mode (B loop).

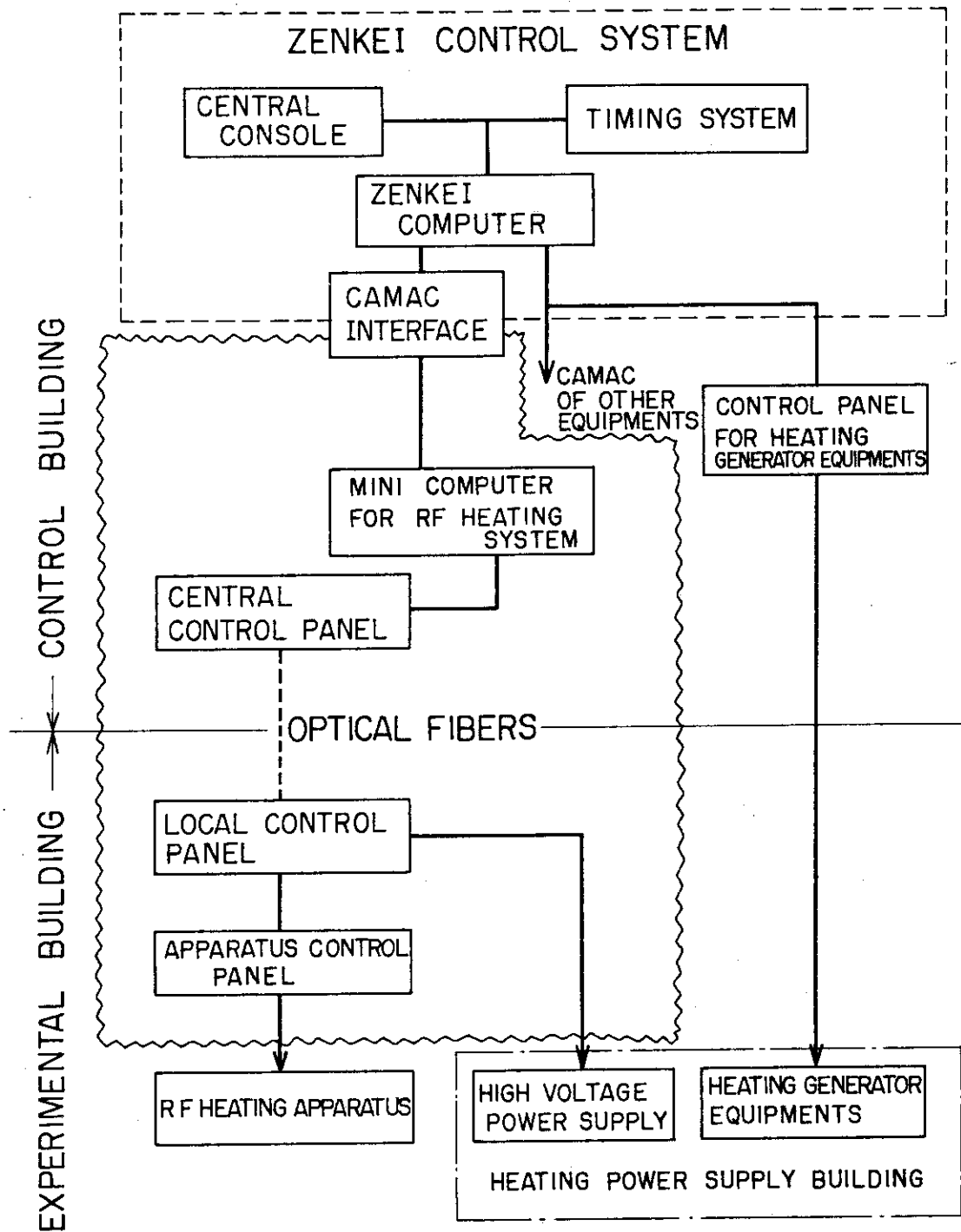


Fig. V.3.2-6 The block diagram of the control system in the RF heating system.



## VI. SURFACE SCIENCE AND VACUUM TECHNOLOGY

### 1. Introduction

The particle-surface interaction research program in the Division of Thermonuclear Fusion Research was started in April 1975, and has been continued in close connection with the JT-60 project and with the JFT-2 and DIVA experiments. The main objectives of this program are to investigate the individual phenomena in plasma-wall interaction which can occur in present and near-term tokamaks and to develop related vacuum techniques.

In this fiscal year of 1979, an emphasis was laid on low-Z materials and low-Z surface coatings for the first wall because results from recent plasma experiments with additional heatings raised serious questions about the use of conventional, high-Z liners and limiters in forth-coming experiments. Chemical sputtering yield of various types of carbon was intently measured with hydrogen ions in the energy range of 0.1 - 6 keV. Total sputtering yield of silicon carbide coatings with different atomic fraction of silicon was also determined with a 3.0 keV  $\text{H}_3^+$  (equivalent to 1.0 keV  $\text{H}^+$ ) beam at temperatures around 500°C by using a newly constructed high-current, duoPIGatron ion source. Reactive ion plating of silicon carbide on molybdenum was done in National Research Institute for Metals.

The mechanism of blistering is still a controversial topic. Practically, it is important to find out how to reduce the surface erosion by blistering and flaking in actual and possible conditions. From this point of view, experiments were made on the helium ion bombardment with multiple energies from 60 to 200 keV.

Unipolar arcs in a tokamak plasma was studied in JFT-2. Measurements were made by using a limiter and a test piece mounted on a surface station. A possible cause of the arc initiation has been proposed.

Particle induced desorption from molybdenum was also studied with low energy hydrogen/deuterium ions. It has been concluded that the hydrogen concentration in the tokamak first wall increases with increasing time of operation because of the radiation damage increase.

As to vacuum technological studies, vacuum systems data base assessment and evaluation of the principal vacuum parameters for INTOR-J concepts were made after the First Session of IAEA INTOR Workshop. Since the INTOR concept tries to sustain 100 - 200 second burning, impurity control, especially pumping helium is one of major issues of the vacuum systems.

Therefore, emphasis was laid on helium pumping by cryopumps. Regeneration cycle and tritium inventory of the cryopumps were evaluated from the published data.

## 2. Instrumental Development

### 2.1 Construction of medium energy sputtering testing accelerator with high current, light ion source

The construction of a Medium energy SPuttering testing accelerator (MSP) with high current, light ion source was completed in September 1979. Special intention was directed to the following points:

- (1) MSP should cover the energy range lacked in LSP and HSP.
- (2) MSP should produce two orders of magnitude larger current than LSP so that the absolute values of erosion rate of materials could be obtained by measuring the weight change of the materials induced by ion bombardment.

From these requirements a duoPIGatron type ion source was employed and the available accelerating voltage ranged from 0.1 to 30 kV.

A schematic diagram of MSP was shown in Fig. VI.2-1. Ions in the duoPIGatron ion source were extracted through three grids, each of which had 37 holes of 2 mm in diameter. Ion beams were analyzed with a sector magnet (radius 30 cm, deflection angle  $45^\circ$ ) and introduced into the target chamber after being focussed with two sets of einzel lens.

A 1800  $\ell$ /sec oil diffusion pump and two 1400  $\ell$ /sec oil diffusion pumps with two liquid nitrogen traps serve to evacuate the system differentially. A base pressure of  $1 \times 10^{-8}$  Torr and an operating pressure of  $2 \times 10^{-6}$  Torr were recorded in the target chamber, respectively.

A dominant composition of the hydrogen ion beam was  $H_3^+$  ion, typically of 80 %, so that an analyzed  $H_3^+$  ion beam was used for the experiment. Beam current of  $H_3^+$  ion with 1 keV was 1 mA at the target.

Some experimental results obtained with MSP will be reviewed in Section 3.2.

## 3. Sputtering Experiments with Low Energy Hydrogen Ions

### 3.1 Chemical sputtering of various types of carbon<sup>1)</sup>

The energy and temperature dependences of methane production rates

of various types of carbon, i.e., pyrolytic graphites, isotropic graphite and glassy carbon, were measured at the bombardments with low energetic hydrogen ions whose energies ranged from 0.1 to 6 keV. In Fig. VI.3-1. are shown the results of pyrolytic graphite purchased from Nippon Carbon Co., Ltd. The features of dependences are almost the same among the various types of carbon, even though there are large differences in the properties, such as structure, thermal and electrical conductivities and strength between them. The reason of it should be attributed to the surface damage by bombardment with energetic ions which leads various types of carbon to have the same surface condition for methane production. As there are no difference in the chemical sputtering between them, the types of carbon for limiters and liners can be selected by another properties such as thermal conductivity, strength, etc. The dose dependence of methane production rate was very influenced by hydrogen concentration in a target prior to bombardment, but the steady rate was obtained after the target was bombarded with protons at the dose more than  $1 \times 10^{18} \text{ H}^+/\text{cm}^2$  in the energy range used (see Fig. VI.3-2).

The maximum rate at the steady state is  $0.07 \pm 0.01$  atoms/ion at which the target temperature is about  $525^\circ\text{C}$  and incident energy is about 1 keV. Not only the temperature dependence of chemical sputtering but also yields themselves become smaller for bombardment with lower incident energy. If small chemical sputtering is necessary, the incident energy of hydrogen ions should be lessen in the same manner for physical sputtering.

### 3.2 Total erosion of SiC coatings on molybdenum<sup>2)</sup>

Total sputtering yield of various types of silicon carbide coatings was measured with a 3.0 keV  $\text{H}_3^+$  (equivalent to 1.0 keV  $\text{H}^+$ ) beam at temperatures around  $500^\circ\text{C}$  by using MSP. Reactive ion plating of silicon carbide on molybdenum was done by glow discharging a mixture of silicon vapor and acetylene with an RF coil in National Research Institute for Metals<sup>3)</sup>. Figure VI.3-3 shows the experimental results, in which the total sputtering yield is plotted as a function of atomic fraction of silicon. As the extreme cases, we also measured the yield for pyrolytic graphite and pure silicon. It should be noted in Fig. VI.3-3 that the sputtering yield has the lowest value of  $1.2 \times 10^{-2}$  atoms/ $\text{H}^+$  at the stoichiometric SiC. As the stoichiometry deviates from this point, the sputtering yield shows larger values. The temperature dependence of the sputtering yield in stoichiometric samples is almost negligible below

600°C. No surface topography change occurs in stoichiometric samples even at a high fluence of  $2 \times 10^{20} \text{ H}^+/\text{cm}^2$ , while severe erosion takes place in non-stoichiometric silicon carbide and graphite. By Auger electron spectroscopy, carbon exists on the surface in the form of carbide in stoichiometric SiC before and after bombardment, while it exists in the form of graphite in carbon rich samples, which suggests that the bound state of carbon in the form of carbide should correspond to the low sputtering yield in stoichiometric SiC coatings.

#### 4. Surface Erosion Experiments with High Energy Helium Ions<sup>4)</sup>

The study on the surface erosion due to helium blistering, so far, has been made by employing monoenergetic helium ion in a certain energy range. From the practical point it is necessary to know whether the bombardment of helium ions with a continuous and broad energy distribution can induce the surface deformation such as blister and exfoliation or not.

We have already shown<sup>5)</sup> that the pre-treatments of the samples including irradiation and annealing influence the surface deformation mode of the successively bombarded molybdenum. In the previous experiment we have used the special scanning electron microscope<sup>6)</sup> which enables us to observe the sample surface continuously under ion bombardment.

In April 1979 a video recording system for a continuous recording was constructed so that we could examine the development processes of the surface deformation of the sample repeatedly after bombardment. Here we observed the detailed development processes of the surface deformation in molybdenum as a function of irradiation dose under bombardment of helium ions with different energies using the special scanning electron microscope with the video recording system. In order to know the effect of multiple energy implantation, three types of irradiation modes were employed. The first was simple monoenergetic irradiation with 100 keV and 200 keV helium ions. The second consisted of the single sequential irradiation of samples to different pre-implantation helium concentrations, and then observing the effects of these pre-implantations on subsequent 200 keV bombardment. The third consisted of multiple sequential irradiation of the sample with 60 keV, 100 keV, 140 keV and 200 keV helium ions, implantation ratio of which was 3.0:1.4:2.7:6.0. Two different annealing temperatures (800°C and 1300°C) of the samples were employed.

The main results were as follows:

- (1) Blister formation and exfoliation of surface layer take place at a rate faster than the video scan rate (16.6 msec).
- (2) The peak helium concentration at the critical fluence for blistering agrees well between 100 keV and 200 keV implantations for single energy implantation, whereas those obtained from sequential irradiation are distributed around that from single implantation.
- (3) Surface deformation mode depends strongly on the annealing temperature and irradiation mode as shown in Figs.VI.4-1 and VI.4-2.  
Annealing of the sample at 1300°C, which causes the recrystallization of the sample, enhances the exfoliation. Multiple sequential irradiation, in which a relatively broad implanted helium profile is attained, reduces the occurrence of exfoliation but still induces the formation of blister.
- (4) The average thickness of the exfoliated layer lies nearly at the peak in the depth profile of implanted helium and this is independent of irradiation mode and annealing temperature.

## 5. Unipolar Arcs in JFT-2 Tokamak

Unipolar arcs in a tokamak plasma have been studied in JFT-2. Measurements were made by using a limiter and a test piece which were mounted on a surface station. An in-situ SEM on the station was used to observe arc traces and other surface damages. Frequency of arcing and the timing of the occurrence were determined by electrical and optical methods. A schematic diagram of the surface station and an experimental set up for electrical/optical measurements are illustrated in Fig. VI.5-1.

A detailed study has been made on the problem of the real time observation and a method how to identify unipolar arcs has been presented<sup>7)</sup>. It has been also shown that the occurrence of unipolar arcs in the tokamak is closely related to runaway electrons and high flux plasma flow to the first wall. A possible cause of the arc initiation has been proposed<sup>8),9)</sup>.

## 6. Particle Induced Desorption from Molybdenum by Low Energy Hydrogen Ions<sup>10)</sup>

The ion induced desorption of deuterium trapped in molybdenum at room temperature was investigated by subsequent bombardment with protons using the incident energies ranged from 0.5 to 6 keV for deuterons and protons. The decay of release rate of deuterium pre-implanted at 1 keV due to proton bombardment at energies from 1 to 6 keV consisted of two exponential decay curves, but only one exponential decay curve was observed at 0.5 keV  $H^+$ .

The two decay constants, i.e., desorption cross sections, decreased with the increase of the dose of implanted deuterium (see Fig. VI.6-1). The two distinct peaks were observed in the release spectra of deuterium pre-implanted at energies from 3 to 6 keV due to proton bombardments at the corresponding energies (see Fig. VI.6-2). From the results of the thermal desorption of deuterium implanted at energies from 1 to 6 keV and the ion induced desorption it seems clear that there are two different kinds of trapping sites.

The desorption cross section decreased with increasing deuteron dose, i.e., the implanted deuterium became difficult to be emitted from the surface according to the increase of dose of implanted deuterons. The result can be explained by the increase of trapping sites and the expansion of saturated region into the target with the increasing deuteron dose, which lead deuterium atoms to take a long path to reach the surface with random jumping among trapping sites. Some of them are also unable to reach the surface, only wandering among the trapping sites, if the deep trapping sites are highly produced by radiation damage. It can be concluded from our results that the hydrogen concentration in first wall of torus increases with increasing time of operation because of the increase of radiation damage due to energetic ions and neutrals from the plasma.

## 7. Some Considerations on Helium Pumping by Cryopumps<sup>11)</sup>

Since the INTOR concept tries to sustain 100 - 200 second burning, helium exhaust from a tokamak plasma is one of major issues of the INTOR vacuum system.

Helium is considered to be the most difficult gas to pump of all gases in fusion reactors because of its physicochemical nature. The

difficulty in helium pumping by cryopumps arises from the small heat of condensation and adsorption of helium. Only cryosorption panels (using porous materials such as molecular sieves, charcoals and frozen gases) at 4.2 K are capable of pumping helium at a reasonable rate.

At the beginning of the D-T burn, the torus vacuum pumps will remove a mixture of deuterium and tritium, and during the burn and the dwell time, the pumps must remove a mixture containing as much as 10 % helium. If the mixture directly arrives the sorption panel, the pores of the adsorbent may be blocked with hydrogen isotopes. Thus, the cryosorption panels for helium will be surrounded by two chevrons, one at 77 K and the other at 4.2 K. In this case the expected maximum speeds per unit projected area are about  $30 \text{ m}^3/\text{sec}\cdot\text{m}^2$  for helium and about  $78 \text{ m}^3/\text{sec}\cdot\text{m}^2$  for deuterium (at 300 K) assuming the unity sticking (or condensation) coefficient and the chevron baffle transmission coefficient being 0.25. The ratio of helium speed to deuterium speed will be smaller than 0.4.

A preliminary design of the torus vacuum system for INTOR-J has been made under following conditions:

|  |  |
|--|--|
| ◦ burn time  | 100 sec  |
| ◦ dwell time   | 30 sec   |
| ◦ duty   | 0.77   |
| ◦ He production rate<br>(during burn)  | $1.6 \times 10^{20} \text{ sec}^{-1} = 0.6 \text{ Pa}\cdot\text{m}^3/\text{sec}$<br>at 300 K |
| ◦ pumping rate of hydrogen<br>isotopes (during burn)   | $1.6 \times 10^{21} \text{ sec}^{-1} = 3.0 \text{ Pa}\cdot\text{m}^3/\text{sec}$<br>at 300 K |
| ◦ average ion density  | $1.2 \times 10^{20} \text{ m}^{-3}$  |
| ◦ plasma volume  | $200 \text{ m}^3$  |
| $\left. \begin{array}{l} 45 \text{ Pa}\cdot\text{m}^3 \text{ per one} \\ \text{dwell time} \end{array} \right\}$ |  |

The torus pumping system is composed of 12 cryopumping units, 4 roughing units, and 4 regeneration and fuel recovery units. Six cryopumping units are alternately operated at an interval of 6 hours. The cryosorption panels for helium pumping are surrounded by two chevrons, one at 77 K and the other at 4.2 K. Hydrogen isotopes are accumulated mainly on the 4.2 K chevron. Table VI.7-1 summarizes a preliminary design of the torus pumping system.

References

- 1) Yamada, R., Nakamura, K., Sone, K. and Saidoh, M., J. Nucl. Mater. 95 (1980) 278
- 2) Sone, K., et al., to be published in J. Nucl. Mater.
- 3) Fukutomi, M., et al., J. Electrochem. Soc. 124 (1977) 1420.
- 4) Saidoh, M., Sone, K., Yamada, R. and Nakamura, K., J. Nucl. Mater. 96 (1981) 358
- 5) Saidoh, M., Sone, K., Yamada, R., and Ohtsuka, H., JAERI-M 7997 (1978).
- 6) Obara, K., Abe, T. and Sone, K., JAERI-M 7797 (1978).
- 7) Ohtsuka, H., Ogiwara, N. and Maeno, M., J. Nucl. Mater. 94 & 95 (1980).
- 8) Maeno, M., Ohtsuka, H., et al., J. Phys. Soc. Japan 48 (1980) 2177.
- 9) Maeno, M., et al., to be published in Nuclear Fusion.
- 10) Yamada, R., Nakamura, K., Sone, K. and Saidoh, M., submitted to J. Nucl. Mater.
- 11) Murakami, Y., Nakamura, K., Abe, T. and Obara, K., JAERI-M 8513 (1979).



Table VI.7-1 A preliminary design of a torus cryopumping system

|   |   |
|---|---|
| Duct conductance (total)                              |   |
| He & D <sub>2</sub> (T <sub>2</sub> )                 | ~1,000 m <sup>3</sup> /sec  |
| Pumping speed per unit projected area                 |   |
| He  | 30 m <sup>3</sup> /sec·m <sup>2</sup>   |
| D <sub>2</sub> (T <sub>2</sub> )                      | 73 m <sup>3</sup> /sec·m <sup>2</sup>   |
| Projected area of cryopanel (total in operation mode) | ~36 m <sup>2</sup>  |
| Number of pumping units                               |   |
| in operation mode                                     | 6   |
| in regeneration mode                                  | 6   |
| Pumping speed at 77 K chevrons (total)                |   |
| He  | ~1,080 m <sup>3</sup> /sec  |
| D <sub>2</sub> (T <sub>2</sub> )                      | ~2,800 m <sup>3</sup> /sec  |
| Effective pumping speed (total)                       |   |
| He  | ~500 m <sup>3</sup> /sec  |
| D <sub>2</sub> (T <sub>2</sub> )                      | ~700 m <sup>3</sup> /sec  |
| Regeneration cycle                                    | 12 hr   |
| Operating time  | 6 hr  |
| Regeneration time                                     | < 6 hr  |
| Pumped amount after 6-hour operation (total)          |   |
| He  | ~1.0 × 10 <sup>4</sup> Pa·m <sup>3</sup><br>(~2.8 × 10 <sup>2</sup> Pa·m <sup>3</sup> /m <sup>2</sup> ) |
| hydrogen isotopes                                     | ~5.8 × 10 <sup>4</sup> Pa·m <sup>3</sup><br>(~1.6 × 10 <sup>3</sup> Pa·m <sup>3</sup> /m <sup>2</sup> ) |
| Tritium inventory in cryopumping system               | ~5.8 × 10 <sup>4</sup> Pa·m <sup>3</sup><br>(~0.15 kg)  |

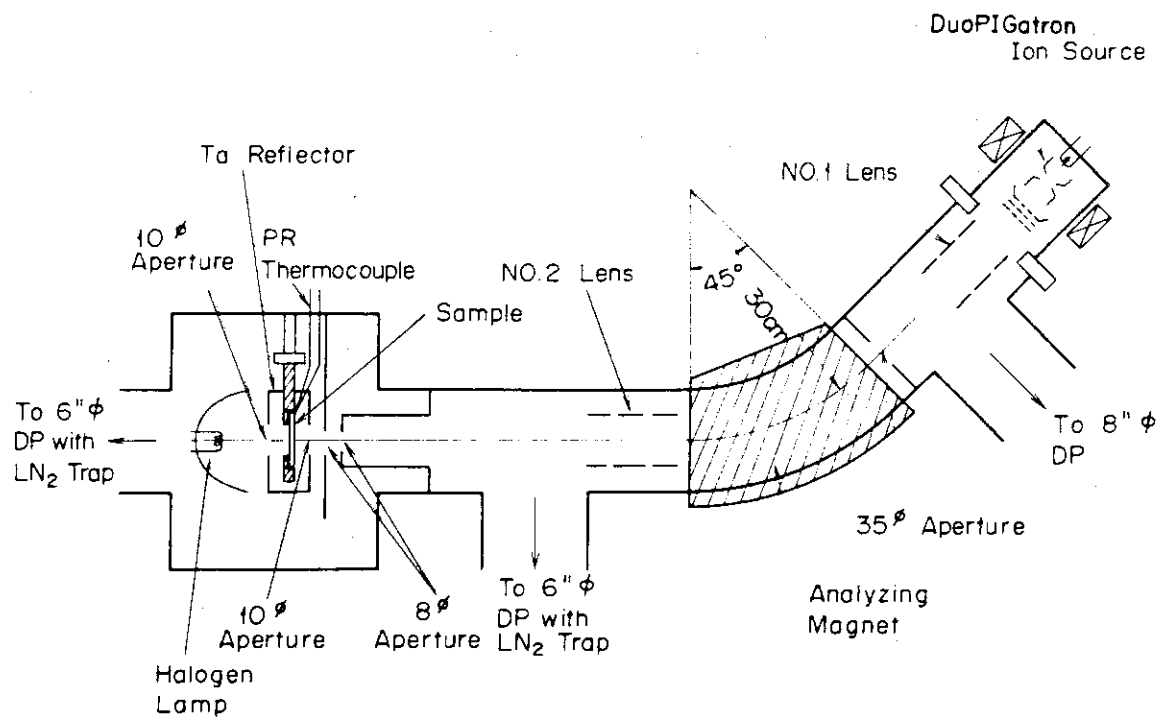


Fig. VI.2-1 A schematic diagram of MSP.

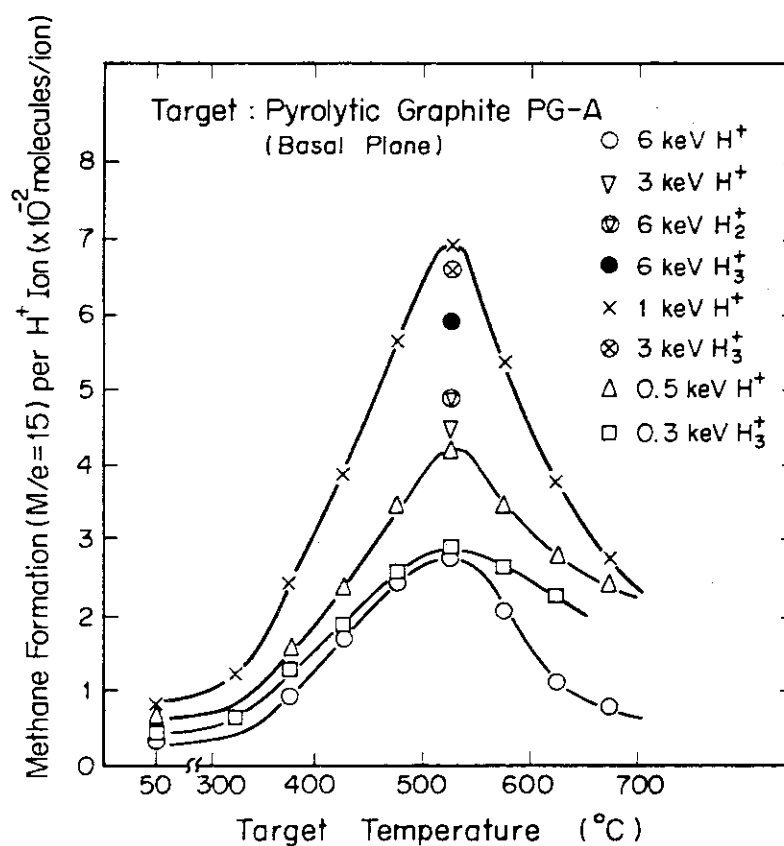


Fig. VI.3-1 Methane formation rate from the basal plane of pyrolytic graphite as a function of temperature.

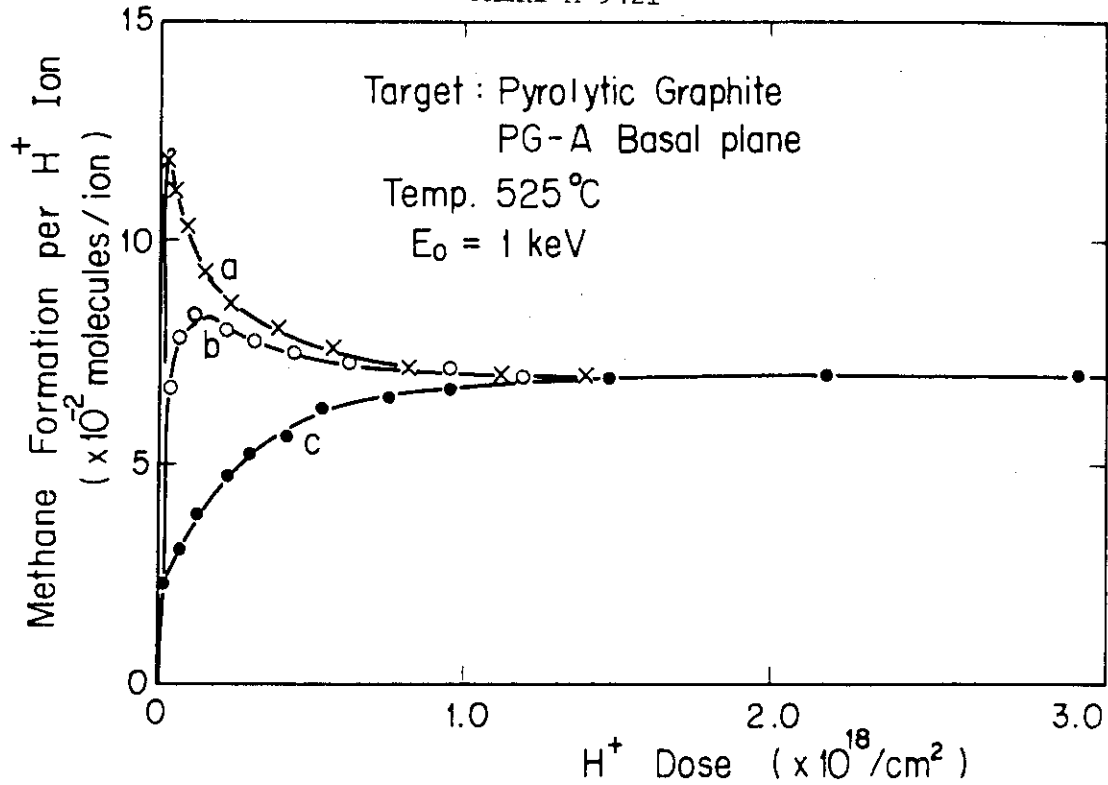


Fig. VI.3-2 Dose dependence of methane formation of pre-bombarded samples. The individual treatments of targets before the bombardment with 1 keV  $\text{H}^+$  at 525 °C were as follows.  
a) Pre-bombardment of  $9 \times 10^{17} \text{ H}^+/\text{cm}^2$  with 1 keV at room temperature.  
b) Pre-bombardment condition was the same as a). The target once heated up to 700 °C and cooled down to 525 °C after the pre-bombardment.  
c) Pre-bombardment at room temperature was not done.

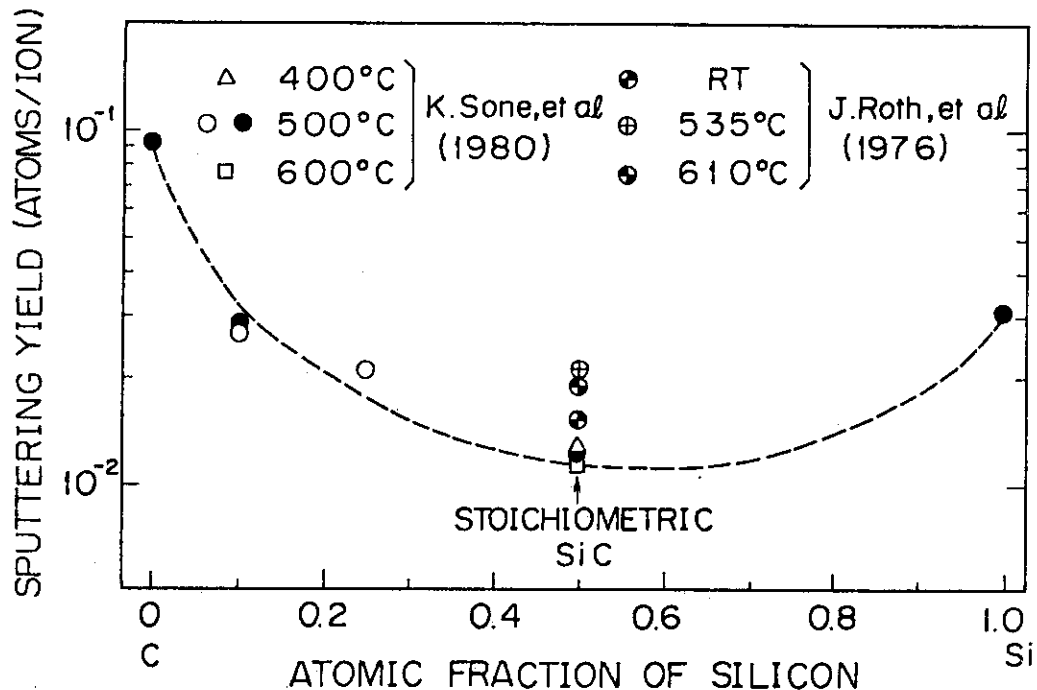
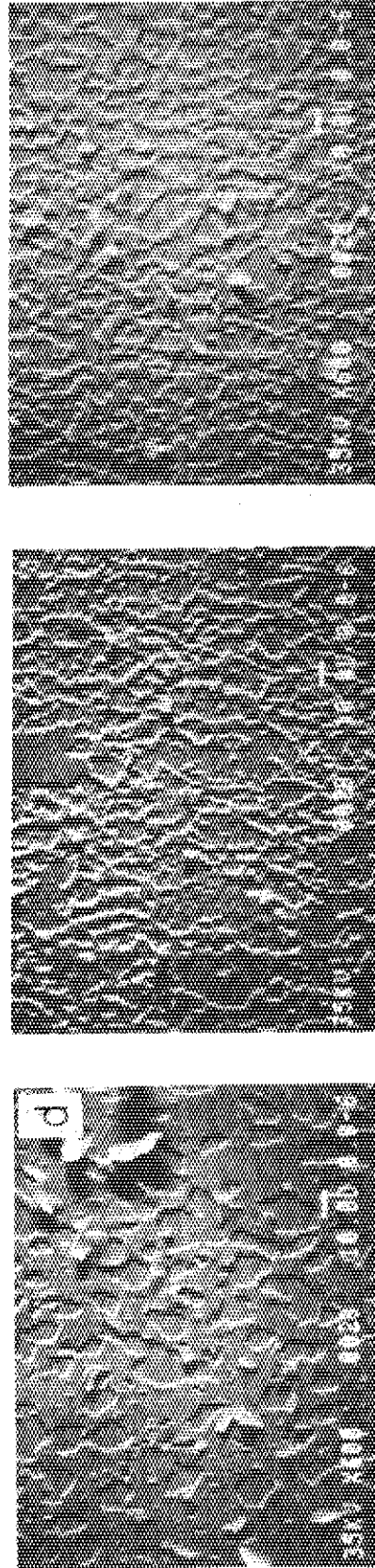
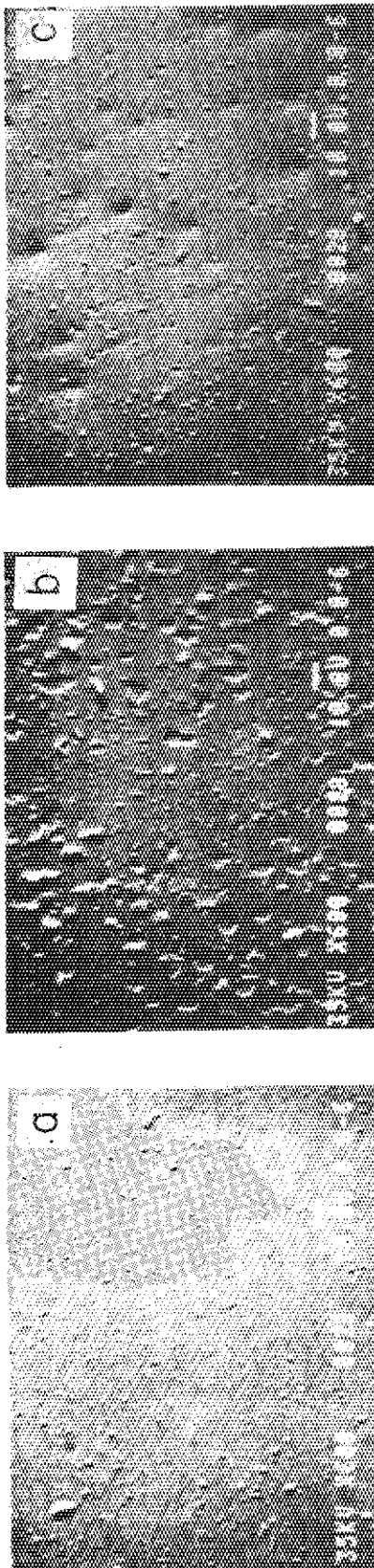


Fig. VI.3-3 Sputtering yield  $S \text{ atoms/H}^+$  for a 3.0 keV  $\text{H}_3^+$  beam as a function of atomic fraction of silicon. R.T. denotes room temperature.

## 800 °C Annealed Molybdenum



## 1300 °C Annealed Molybdenum

20μm

|         |  |         |  |         |  |
|---------|--|---------|--|---------|--|
| 200 keV | $12.3 \times 10^{17} \text{ He}^+/\text{cm}^2$ | 100 keV | $4.4 \times 10^{17} \text{ He}^+/\text{cm}^2$  | 80 keV  | $2.2 \times 10^{17} \text{ He}^+/\text{cm}^2$  |
|         |  | 200 keV | $12.3 \times 10^{17} \text{ He}^+/\text{cm}^2$ | 100 keV | $2.2 \times 10^{17} \text{ He}^+/\text{cm}^2$  |
|         |  |         |  | 120 keV | $2.2 \times 10^{17} \text{ He}^+/\text{cm}^2$  |
|         |  |         |  | 200 keV | $12.3 \times 10^{17} \text{ He}^+/\text{cm}^2$ |

Fig. VI.4-1 SEM micrographs after 200 keV helium ion irradiation to a fluence of  $12.3 \times 10^{17} \text{ He}^+/\text{cm}^2$  of molybdenum. (a), (b), (c) and (d), (e), (f) show for 800 °C and 1300 °C annealed targets, respectively. Prior to the 200 keV bombardment the pre-irradiation was carried out; (b) and (e) - 100 keV,  $4.4 \times 10^{17} \text{ He}^+/\text{cm}^2$ , (c) and (f) - 80 keV, 100 keV and 120 keV, respective fluences to  $2.2 \times 10^{17} \text{ He}^+/\text{cm}^2$ .

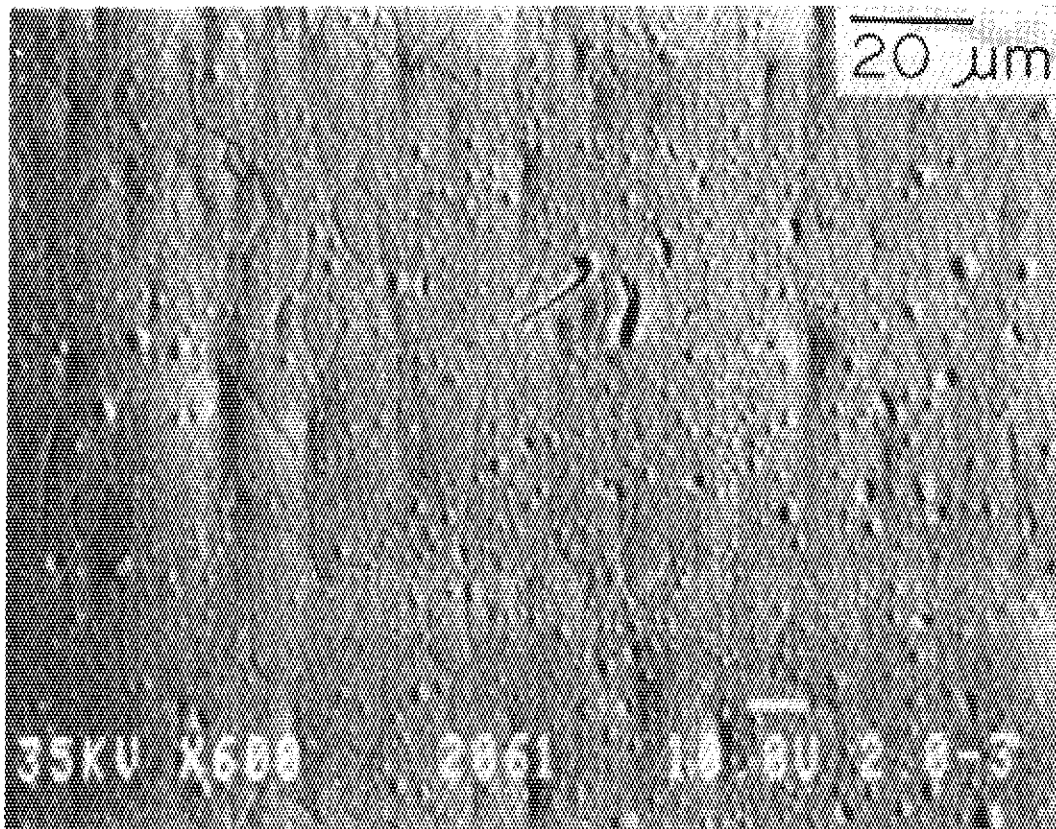


Fig. VI.4-2 SEM micrograph after six times repeated sequential irradiation with 60 keV, 100 keV, 140 keV and 200 keV incident energies of molybdenum. Total fluence was  $11.6 \times 10^{17} \text{ He}^+/\text{cm}^2$ . The target was annealed at 1300 °C for 1 hour.

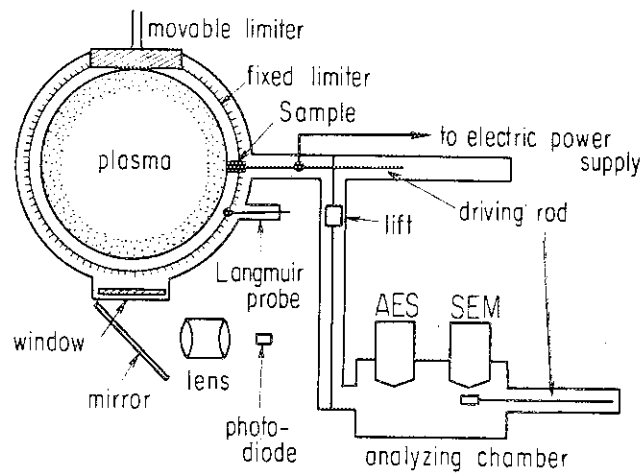


Fig. VI.5-1 A schematic diagram of the experimental set up for the study of unipolar arcs.

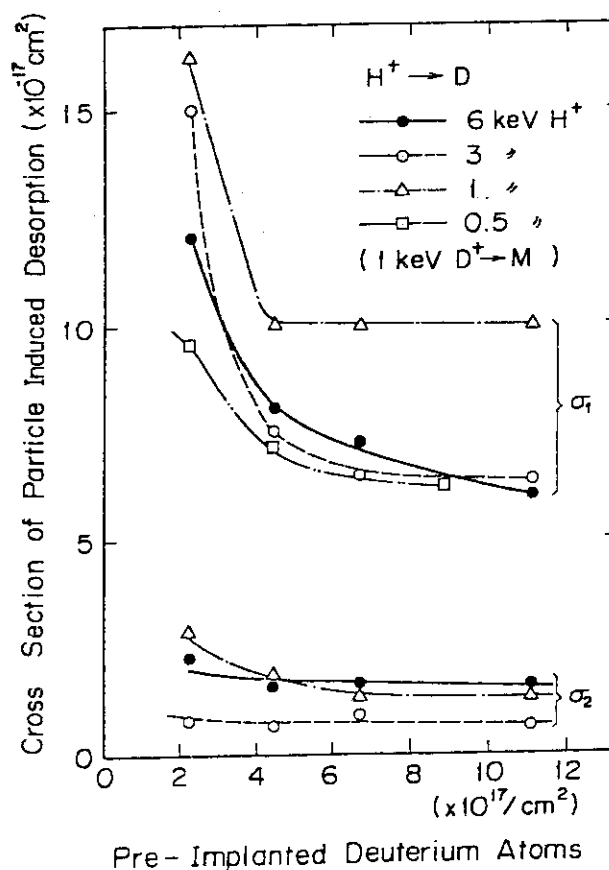


Fig. VI.6-1 Cross section for release of deuterium from molybdenum due to proton bombardment as a function of proton energy and the deuteron dose. Deuterons were pre-implanted at 1 keV and the target temperature was room temperature.

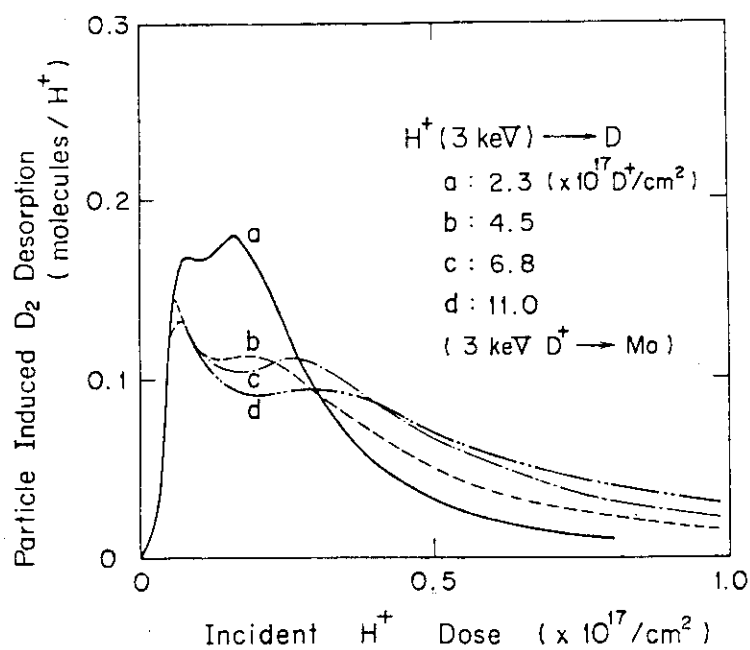


Fig. VI.6-2 Release rate of  $D_2$  during bombardment with protons at 3 keV after pre-implantation with deuterons at 3 keV as a function of deuteron dose.

## VII. SUPERCONDUCTING MAGNET DEVELOPMENT

### 1. Introduction

The main objective of research and development of superconducting magnet and its system for fusion research is the construction of a superconducting Tokamak machine, for example, Plasma Engineering Test Facility (PETF) after JT-60.

For this purpose, JAERI has been engaged specially in toroidal coil development since 1976. The following works have mainly been done in FY 79;

1. stability study of LCT 1/4 model conductor,
2. realization of 10T - 15cm bore Nb<sub>3</sub>Sn solenoid,
3. realization of 1T/sec - 13cm bore pulse solenoid in 8T,
4. final stage of fabrication and construction of the cluster test facility, including helium liquefier / refrigerator and data acquisition computer system,
5. fabrication of the Japanese LCT (Large Coil Task) coil including verification test,
6. fabrication of the domestic test facility for the Japanese LCT coil,
7. construction of the building for the domestic test facility.

### 2. Cluster Test Program

#### 2.1 Construction of the cluster test facility

The construction of the cluster test facility<sup>1)</sup>, in which a model toroidal coil can be tested for fusion research, was started in 1979. (Fig. VII.2-1) The cluster test facility consists of five systems described below.

##### (1) The cluster test coils (CTC)

Inner diameter and outer diameter of CTC are 1m and 2m respectively. Maximum field is 7T and operational current density is 30 A/mm<sup>2</sup>.

##### (2) Cryogenic system

Liquefire/refrigerator is designed for helium liquefaction and cooldown and steady state refrigeration. The refrigerator system has a closed turbine cycle, which is separated from liquefaction/refrigeration circuit in order to avoid contaminations and damage of turbine

expanders.(Fig. VI.2-2) Its capacity is 100 liter/hour or 220W at 4.4K refrigeration.

(3) Vacuum system

The vacuum vessel is 5m in height and 3.4m in diameter. The specification value of the base pressure is less than  $1 \times 10^{-4}$  torr.

(4) Electric and electronic system

The capacity of DC current supply for CTC is 10V-3,000A. A circuit breaker of 1kV-3,000A and a pair of 0.233 ohm resistance are provided for coil protection.

(5) Data acquisition system

Two computers and CAMAC system are used for the coil current and voltage, magnetic field, strain, pressure, vacuum condition and helium level.(Fig. VI.2-3)

After some initial checkouts on dimension, insulation, coil resistivity, vacuum tightness and sensor connection, the cluster test coils were carried into JAERI and were assembled in the vacuum vessel in March 1980. Helium leakage check, proof pressure check and magnetic field check were carried out after jointing work of current leads, cryogenic pipes and sensor lead. Cryogenic system, electric and electronic system and data acquisition system are now being construction and the test of whole systems will be started from May 1980.

## 2.2 Test module coil

The first test module coil (TMC-1)<sup>2)</sup>, which will be tested in the cluster test facility, has been designed by taking account of recent trend in design studies of engineering test tokamaks in which the maximum magnetic field on the toroidal field coil is higher than 10T with cryo-stability. Therefore Nb<sub>3</sub>Sn has been selected as superconducting material and the conductor has a roughened surface to provide a high heat flux to liquid helium in the pool boiling method. The operating current is 6,000A with the current density of 30 A/mm<sup>2</sup> to generate 10T on the background field of CTC. Figure IV.2-4 shows the field distribution. Double pancake and edge wise winding method is employed using multifilamentary Nb<sub>3</sub>Sn conductor reacted before winding. Main parameters of TMC-1 are shown in table VI.2-1.

In the beginning of 1980, the work on hardware of the TMC-1 was started and the test will be done in the end of 1981.



Table VII.2-1 Main Parameters of TMC

|                               |                                       |
|-------------------------------|---------------------------------------|
| Maximum Magnetic Field        | 10 T                                  |
| Rated Current                 | 6 KA                                  |
| Coil Shape                    | Circular                              |
| Winding Bore                  | 0.6 m                                 |
| Winding Cross Section         | $0.5 \times 0.3 \text{ m}^2$          |
| Average Current Density       | $30 \text{ A/mm}^2$                   |
| Stored Energy (including CTC) | 32 MJ                                 |
| Superconductor                | $\text{Nb}_3\text{Sn} + \text{Nb-Ti}$ |
| Wire Length                   | 2.6 km                                |
| Cooling Method                | Pool Boiling                          |

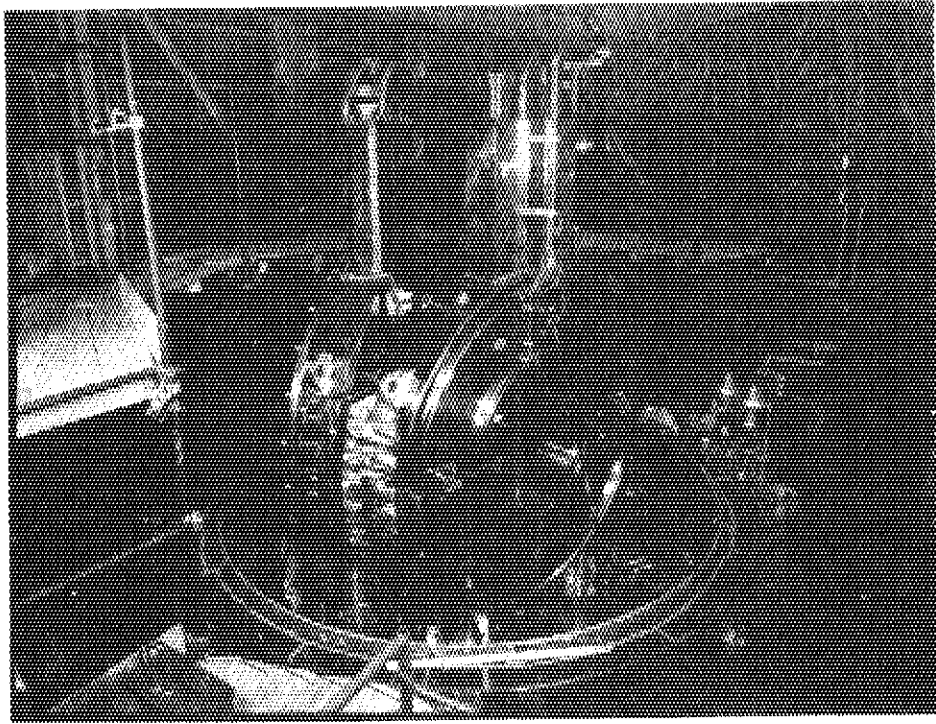


Fig. VI.2-1 Two cluster test coils assembled in vacuum vessel

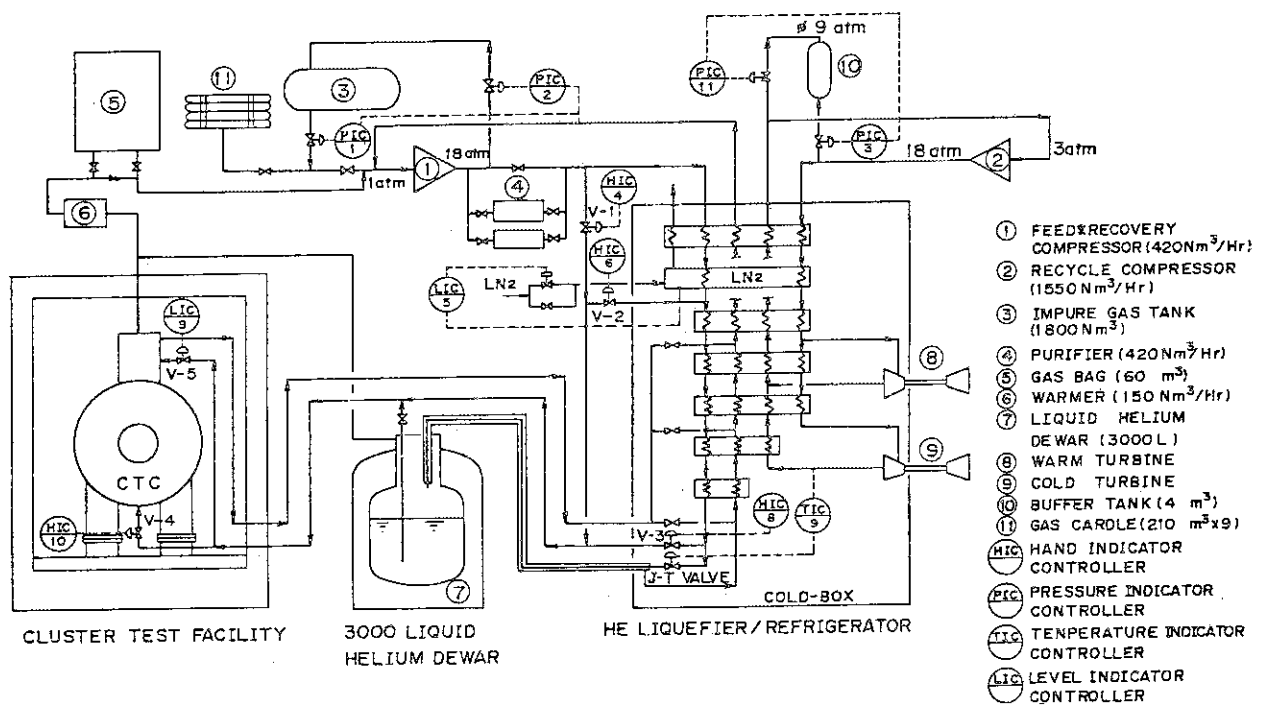


Fig. VI.2-2 Helium Liquefier/refrigerator Flow Diagram

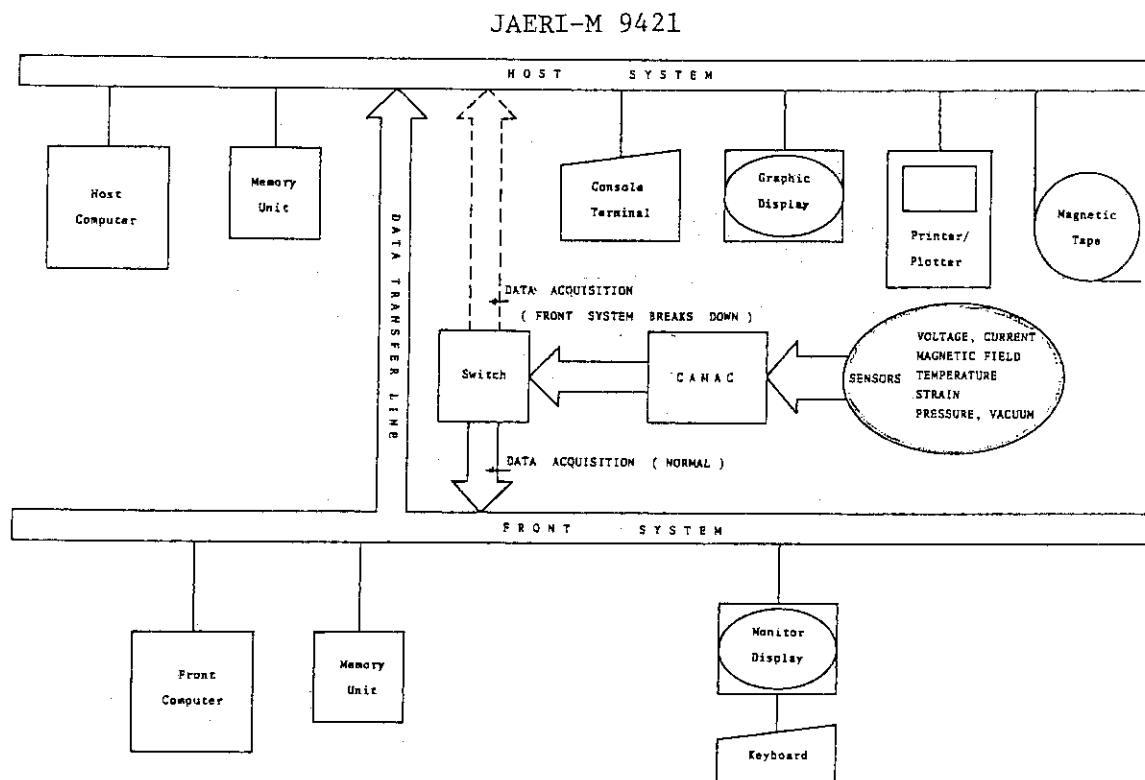


Fig. VII.2-3 Data Acquisition and Analysis System of the Cluster Test Facility

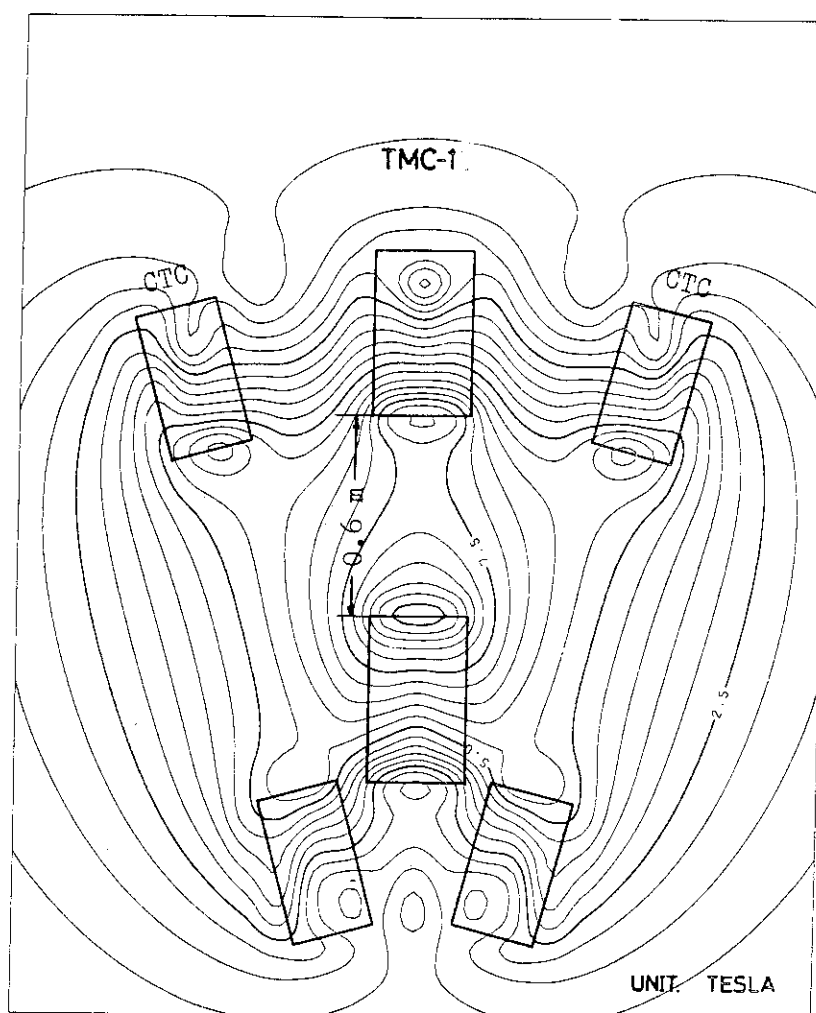


Fig. VII.2-4 Dimension and field distribution of TMC-1

### 3. Large Coil Task of IEA

#### 3.1 LCT coil

##### 3.1.1 Design concepts

Detailed design of LCT coil was finished in March 1979 and review works from the view point of actual construction has been carried out. According to the final design thus compiled, major characteristics of the Japanese LCT coil are shown in Table VII.3-1.

In this design, NbTi is selected as superconducting material and one of the most important design goals is to make a coil which has as much stability margin as possible based on the practical reliability and industrial experiences of NbTi. The conductor current is 10,220A and the total number of turns is 658 to get the maximum field of 8T. The surface of the conductor is both mechanically and chemically treated so as to get high heat flux to liquid helium. Thus the conductor is effectively cooled by pool cooling method. The conductor is wound "edge-wise" and "double pancake". A cross sectional view of this winding is shown in Fig. VII.3-1.

Between pancake is a glass epoxy flat bar spacer whose thickness is 2.9mm. This spacer is stuck on pancakes and covers 30 % surface of the conductor flat side as is shown in Fig. VII.3-2.

As is described in later, the maximum stress intensity reaches almost  $70 \text{ kg/mm}^2$  at the corner part of the winding cavity, 304LN stainless steel, which is nitrogen strengthened, is employed based on the mechanical property test at 4K.

##### 3.1.2 Conductor design and development

One of the objectives of the Japanese LCT coil is to pursue as much stability margin as possible using Nb-Ti superconductor and pool cooling method. Based on this principal, the conductors were designed as shown in Table VII.3-2.

The degree of conductor stability depends upon the relation between the heat generated in the conductor and the capacity of the conductor to dissipate by heat transfer. After a lot of measurements on boiling helium heat transfer characteristics<sup>3)</sup>, three types of conductor surface structures were chosen for these high cooling capacities. As the next step, three test solenoids with 1/4 size model conductors. Each of which had cooling surface chosen above, were made and tested.<sup>4)</sup> It was found that these solenoids are all enough stable against heat disturbance

of almost  $1 \text{ J/cm}^3$  at nominal current of 2.55 kA at 8.0 T field and that these solenoids can be stable against disturbances of a certain spatial extent in the condition exceeding the maximum nucleate boiling heat flux. As the result of this experiment, chemically treated Thermoexcel surface was selected for the cooling surface structure of the Japanese LCT coil's conductors, because of its high cooling capacity and its weak azimuth angle dependency. Equal area heat flux of this surface with narrow cooling channel was measured to reach  $1.05 \text{ W/cm}^2$ .

The critical current density of the strands were measured and both strand for 8T and that for 5T showed the critical current density around  $1 \times 10^5 \text{ A/cm}^2$  at 8T. Degradation by stranding was also measured and no particular signs of degradation was measured.

1/2 hard copper was selected for the conductor stabilizer because the maximum stress value calculated under condition of the normal test was  $12.5 \text{ kg/mm}^2$ .

Conductor stability was analyzed with one dimensional model<sup>5)</sup>. Fig. VII.3-3 shows the calculated propagation velocity of normal zone. Both 8T conductor and 5T conductor are expected to be stable up to the current of 12 kA. It was also calculated that within 140 msec superconductivity recovers after  $100 \text{ mJ/cm}^3$  energy input over half turn of coil on the condition of maximum 8T field and of nominal current.

### 3.1.3 Stress analysis and verification

The review of the stress analysis which were performed in the detailed design of the Japanese LCT coil have been carried out for several test conditions. In order to evaluate the peak stress of the helium vessel in the most critical test condition "ALT-B", 1/4 size model experiment of the helium vessel have been carried out.<sup>6)</sup> The force applied to the test piece was controlled to simulate ALT-B test condition and measured values of the stress distribution have been compared with two dimensional FEM calculations. Both were in good agreement under the uniform electromagnetic force distribution as is shown in Fig. VII.3-4 and the peak stress on the corner of the vessel was  $67 \text{ kg/mm}^2$ . With the practical electromagnetic distribution, two dimensional calculation showed that the peak stress is  $63.5 \text{ kg/mm}^2$ . On the basis of these results version of the Japanese helium vessel have been carried out on material and structural geometry, stainless steel 304LN (nitrogen enriched) was selected for the structural material. The mechanical

properties of stainless steel 304LN have been critically studied at room temperature, liquid nitrogen temperature and liquid helium temperature. Table VII.3-3 shows experimental results of the tensile test of stainless steel 304LN at liquid helium temperature.

On the other hand, in order to investigate the effect of conductor composition on the mechanical properties of the whole conductor which consists of OFHC housing and the composite material of stranded cable and solder, the tensile test of 1/4 size model conductor and full size conductor of the Japanese LCT coil have been performed at liquid nitrogen and room temperatures. Test results show that the contribution of the composite material to its strength at plastic strain of 0.2 % is 24.0 % of the whole conductor at each test temperature. According to these results it is considered that the composite material which consists of stranded cable and solder can be considered to be the supporting member of the electromagnetic forces.

#### 3.1.4 Coil protection

When one of the LCT coils quenches, the others are rapidly dumped. In that case electric losses are caused by the transient magnetic field B.

Estimated electric loss in the conductor in Japanese LCT coil are as follows, where the dumping time constant is assumed to 24 sec..

Energy loss in 8T region :  $q = 316 \text{ J/m per conductor length}$

Energy loss in the coil :  $q = 689 \text{ kJ}$

Power loss in 8T region :  $W_{t=0} = 26.3 \text{ w/m}$

The power loss in 8T region corresponds to the heat flux

$$\frac{0.2633 \text{ w/cm}}{2.68 \text{ cm}} = 0.0491 \text{ w/cm}^2$$

It leads to a temperature difference between the conductor and Liq. He of 0.02 K, which would be negligible.

Secondly, the final temperature and pressure rise are calculated in the condition of He inventory of 1,200 l Liq. He and 500 l gaseous He, and are 1.0 K and 1.0 kg/cm<sup>2</sup>, respectively. The Liq. He level remains almost constant or slightly increased. On the other hand, the dumped current and the magnetic field decrease, so that the critical current of the conductor increases. (Fig. VII.3-5) Since the critical current

exceeds the transport current, the transition to normal state would not take place.

### 3.2 Domestic test facility

The domestic test facility for the LCT coil consists of a helium liquefier/refrigerator system, a vacuum system, a power supply with protection system, and a data acquisition system. Detailed design of these systems has been finished and manufacturing of the systems has already started. The new building for domestic testing of the LCT coil is now under construction at JAERI. The surface area of the building is around 3,000 m<sup>2</sup>. The design and specification of each system is described below.

The capacity of the liquefier/refrigerator system is specified as 300 l of liquefaction per hour, or 1 kw of refrigeration at 4.5 K, to accomplish cool-down of the LCT coil from 300 K to 4 K in 120 hrs. A gas flow diagram incorporating the main components is shown in Fig. VII.3-6. The system is composed of two separated circuits; turbine circuit and liquefaction circuit (LCT circuit). The purpose of this scheme is to promote long term operation of the turbo-expanders by decoupling them from contaminated He gas recovered from the LCT coil and also from thermal disturbances in the LCT coil. In addition, the flow rate and temperature of He gas, which is supplied from cold-box to the LCT coil, can be controlled to avoid excessive thermal stress within the LCT coil during cool-down and warm-up.

The vacuum chamber, with Liq. N<sub>2</sub> shield, is 8 m in height and 5 m in diameter. The LCT coil, which is set into the vacuum chamber, is supported by four thermal insulated legs and four earthquake-proof stays on the bottom of the vacuum chamber as shown in Fig. VII.3-7. The capacity of the rotary pump and diffusion pump are designed to be 7,500 l/min and 20,000 l/s respectively, in order to evacuate the vacuum chamber to  $1 \times 10^{-4}$  torr in 40 hours.

The capacity of the DC current supply for the LCT coil is 12V-30KA. A circuit breaker of 1KV-30KA and 0.1 ohm resistance are provided for coil protection.

A data acquisition system has been designed to measure the LCT coil performance during several operational modes. The main CPU, which is specified as a PDP 11/70, can record several signal from Hall probes, Pt resistance thermometers, strain gauges, Liq. He indicators, pressure

gauges and voltage tapes. In addition, the system is designed to control the temperature and flow rates of He gas.

Table VII.3-1 Characteristics of the Japanese LCT coil

|                          |  |
|--------------------------|--|
| SC Material              | Nb-Ti  |
| Coil Bore                | 2.5m × 3.5m  |
| Maximum Field            | 8.0 T  |
| Operational Current      | 10,220 A   |
| Number of Turns          | 658  |
| Ampere Turns             | 6.725×10 <sup>6</sup> AT   |
| Winding Cross Section    | 0.253 m <sup>2</sup>   |
| Averaged Current Density | 25.56 A/cm <sup>2</sup>  |
| Self Inductance          | 2.11 H   |
| Conductor Type           | Roughened Surface<br>Copper Stabilizer<br>Soldered Cable<br>Superconductor |
| Cooling                  | Pool Cooling   |
| Winding Concept          | Edge Wise, 2 Gradings<br>20 Double Pancakes                                |
| Structural Material      | 304LN Stainless Steel  |
| Assembly                 | Welded Case with Bolos   |
| Weight                   | 39 - 40 ton  |



Table VII.3-2 Parameters of the Japanese LCT conductor

|                             | 8T Conductor   | 5T conductor   |                                   |
|-----------------------------|----------------|----------------|-----------------------------------|
| Conductor Width             | 12.6           | 12.6           | mm                                |
| Conductor Thickness         | 26.8           | 21.3           | mm                                |
| Aspect Ratio                | 2.13           | 1.69           |                                   |
| Cross Section               | 337.7          | 268.4          | mm <sup>2</sup>                   |
| Operational Current         | 10,220         | 10,220         | A                                 |
| Current Density             | 30.26          | 38.08          | A/mm <sup>2</sup>                 |
| Strand Diameter             | 2.3            | 1.73           | mm                                |
| Number of Strands           | 15             | 11             |                                   |
| Copper Ratio<br>(Strand)    | 1.0            | 1.0            |                                   |
| Filament Diameter           | 50             | 38             | um                                |
| Number of Filaments         | 1,060          | 1,060          |                                   |
| Twist Pitch                 | 30             | 25             | mm                                |
| Critical Current<br>Density | 6.3<br>(8T)    | 14.9<br>(5T)   | 10 <sup>4</sup> A/cm <sup>2</sup> |
| Critical Current            | 19,700<br>(8T) | 19,700<br>(5T) | A                                 |
| Yield Strength              | 27             | 27             | kg/mm <sup>2</sup>                |
| Effective Heat Flux         | 0.8            | 0.8            | W/cm <sup>2</sup>                 |
| Strand Pitch                | 150            | 90             | mm                                |

Table VII.3-3    Tensile Characteristics of Stainless Steel  
304L (N : 0.10 %) at 4.2K

measured at JAERI

|   | Sample I | Sample II | Sample III |
|---|----------|-----------|------------|
| Cross Section<br>(mm <sup>2</sup> )                     | 50.0     | 50.0      | 50.0       |
| Length of Straight<br>Part (mm)                         | 100.0    | 100.0     | 100.0      |
| Ultimate Strength<br>(Kg/mm <sup>2</sup> )              | 154.0    | 154.0     | 154.0      |
| Yield Strength<br>0.2 % (Kg/mm <sup>2</sup> )           | 67.6     | 67.2      | 62.8       |
| Elongation (%)  | 38.0     | 38.0      | 38.0       |
| Contraction<br>of Area (%)                              | 58.0     | 51.0      | 51.0       |
| Young's Modulus<br>( $\times 10^4$ Kg/mm <sup>2</sup> ) | 2.11     | 2.21      | 2.09       |

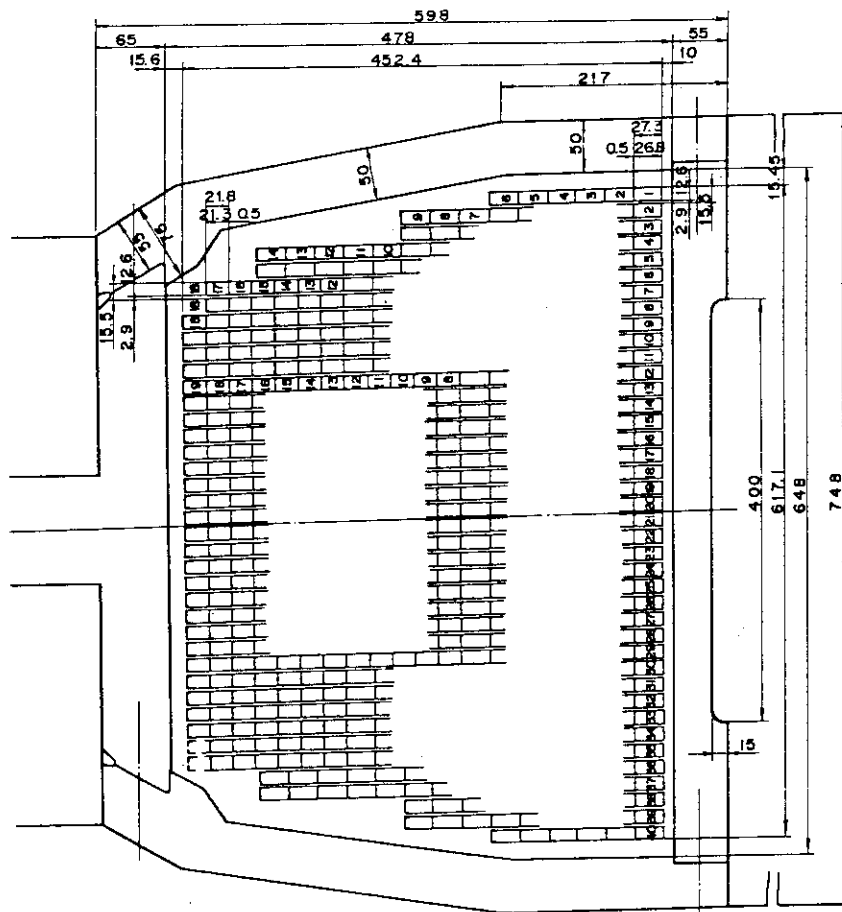


Fig. VII.3-1 Cross sectional View of Winding

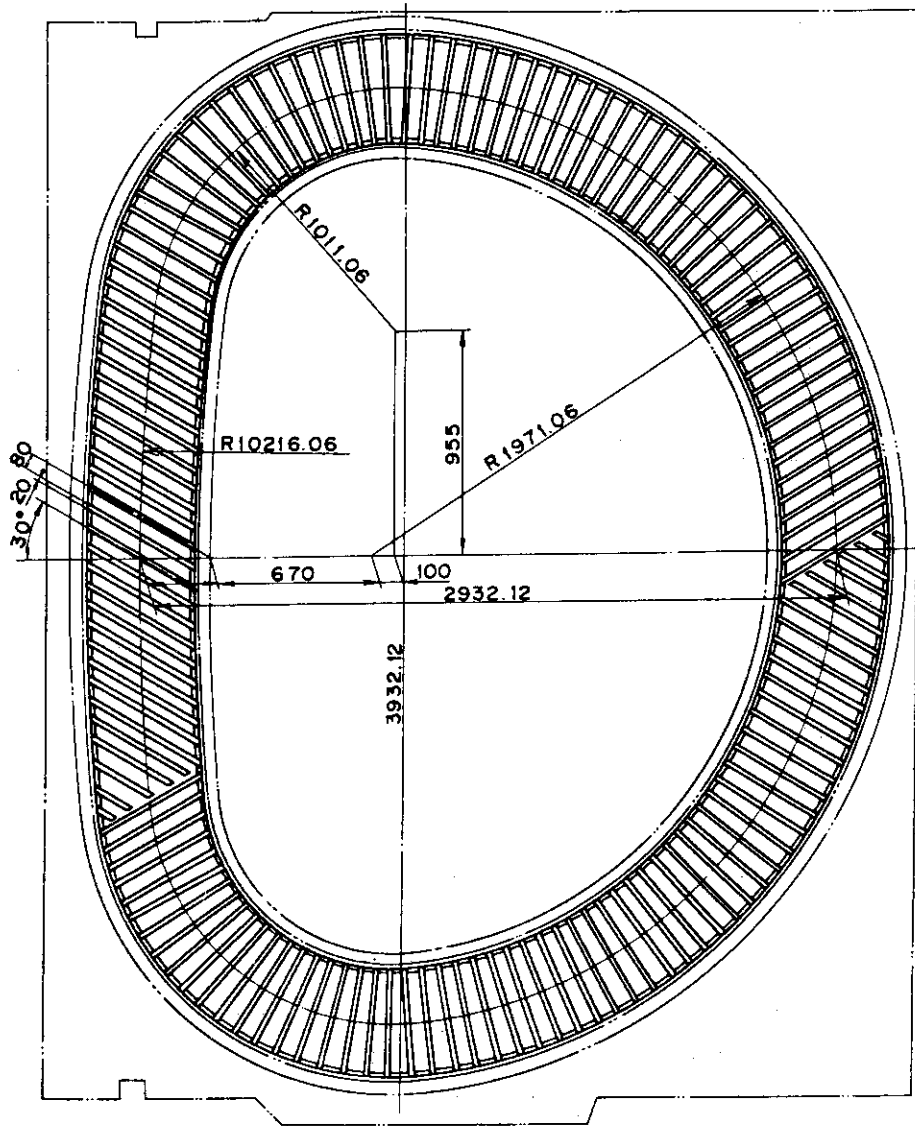


Fig. VII.3-2 Vertical Cross Section of LCT Coil and Spacers between Pancakes

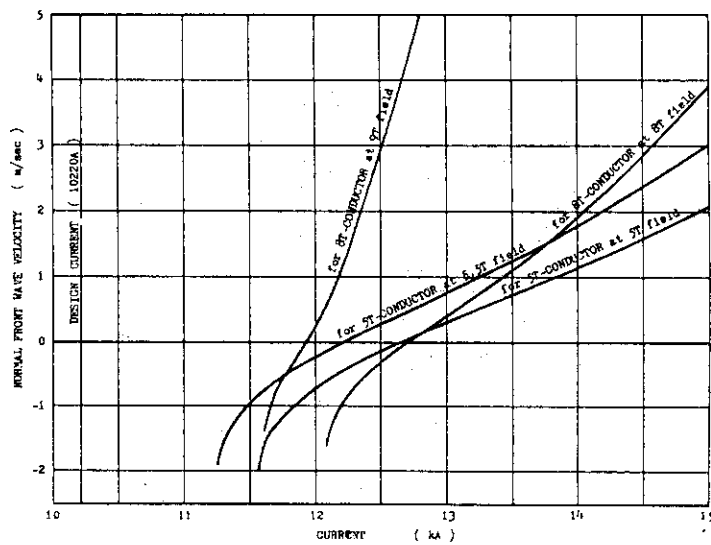


Fig. VII.3-3 Propagation velocity of normal zone

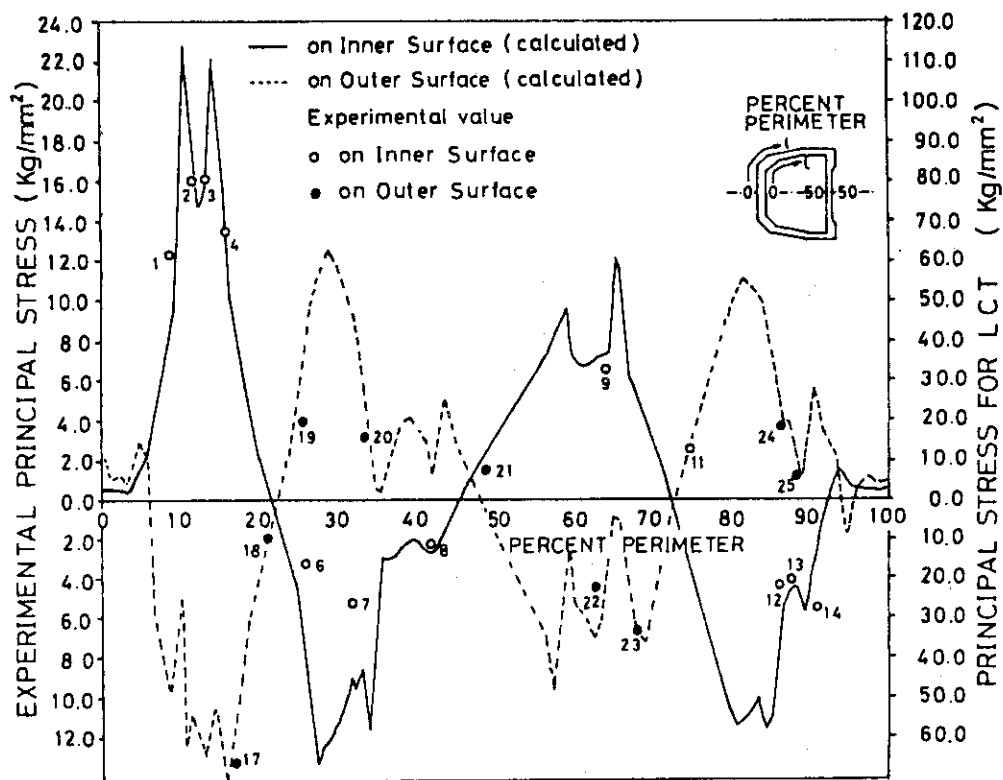


Fig. VII.3-4 Comparison of calculated principal stresses with experimental values

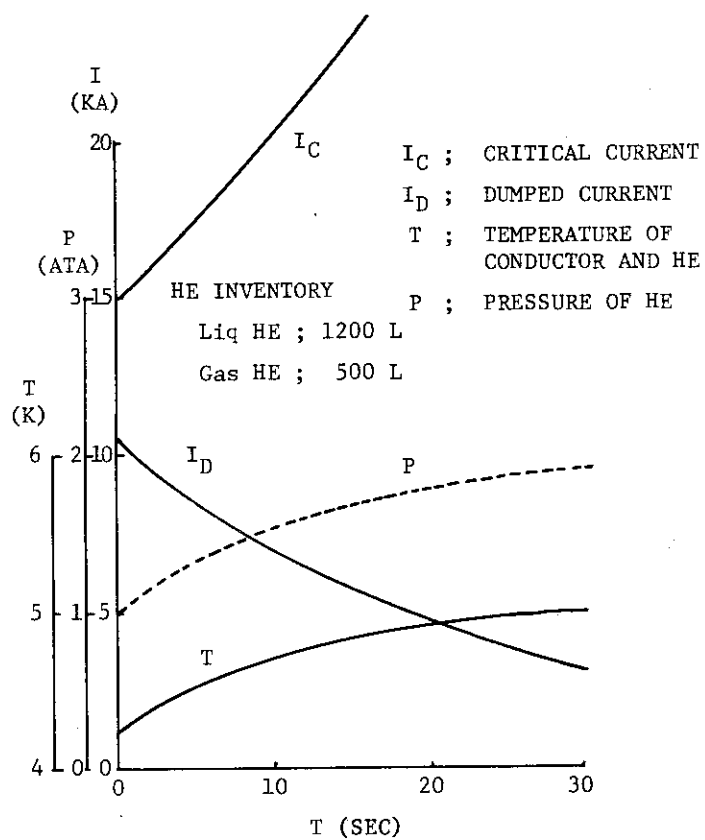


Fig. VII.3-5 Characteristics in Energy Dump

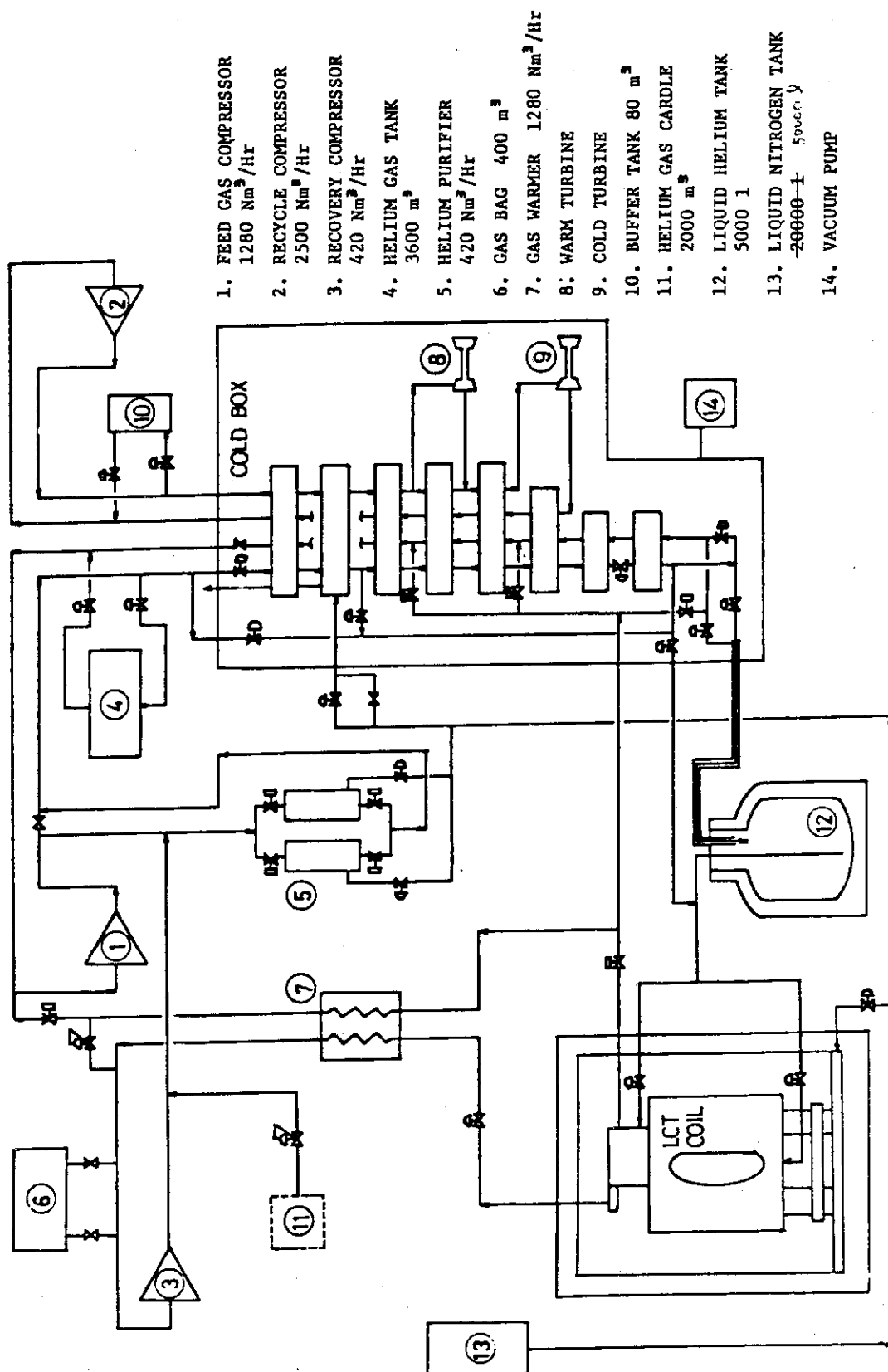


Fig. VII.3-6 300 L/Hr Helium liquefier/refrigerator system

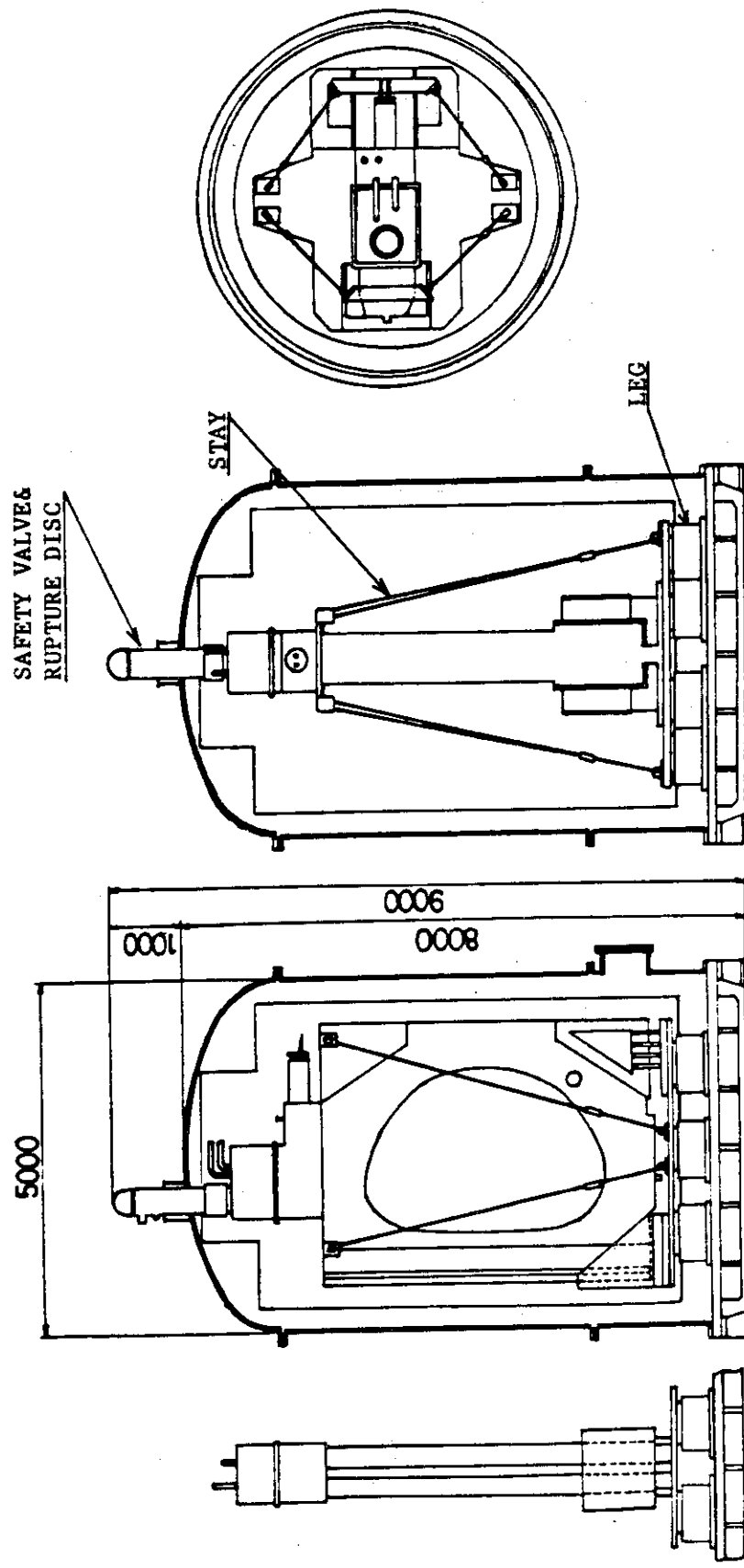


Fig. VI.3-7 Vacuum chamber

#### 4. High Field Superconducting Magnet Development

As the first step on the development of high field magnet,<sup>7)</sup> a 15cm-winding diameter coil has been constructed under the following conditions

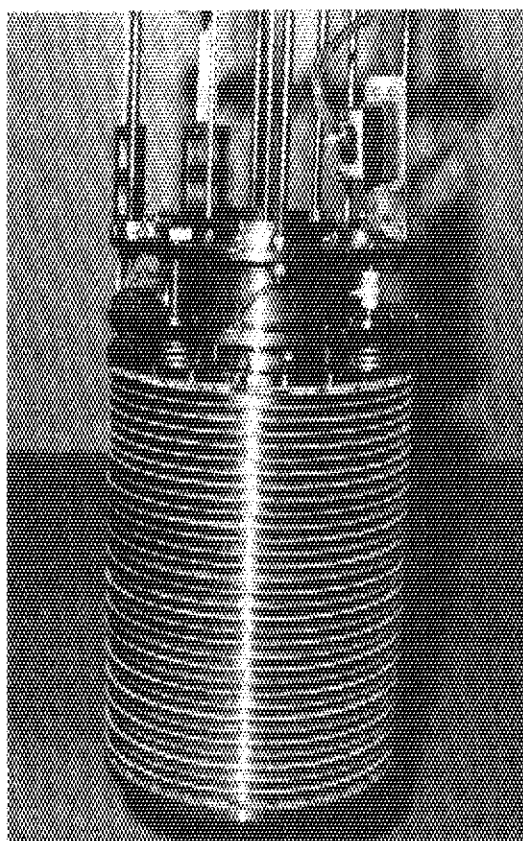
- a. use of multifilamentary Nb<sub>3</sub>Sn
- b. field more than 10T
- c. winding after reaction
- d. cryostable state

A monolithic conductor fabricated by the bronze method was used. The conductor  $1.3 \times 8.5 \text{ mm}^2$  in cross section contained 42,037 filaments, each approximately  $3\mu\text{m}$  in diameter. OFHC copper for stabilization occupies 77 % of the conductor cross-section. Because of high aspect ratio of conductor, cooling channel between turns is indispensable for cryogenic stabilization. The spacer of 0.4 mm thickness is put on the surface of conductor with 50 % covering. Fig. VII.4-1 shows the multifilamentary Nb<sub>3</sub>Sn coil and main parameters are shown in Table VII.4-1. The experiment on the coil was carried out with an external Nb-Ti coil in series connection with a power supply and a field slightly above 10T was successfully obtained with 817 A.

The successful test demonstrates the potential feasibility of multifilamentary Nb<sub>3</sub>Sn conductors in the construction of large high field magnet.

Table VII.4-1 Cryostable MF Nb<sub>3</sub>Sn coil parameters

|                       |                               |
|-----------------------|-------------------------------|
| Conductor size        | 8.5 x 1.3 mm <sup>2</sup>     |
| Winding inner dia.    | 150 mm                        |
| Winding outer dia.    | 221.4 mm                      |
| Winding length        | 304 mm                        |
| No of double pancakes | 16                            |
| No of turns           | 672                           |
| Geometrical factor    | 24.45 gauss/Amp               |
| Inductance            | 32.4 mH                       |
| Cooling channel       |                               |
| turn to turn          | 0.4 mm (50 % cooling surface) |
| pai to pai            | 1.0 mm                        |

Fig. VII.4-1 10T-15cm cryostable multifilamentary Nb<sub>3</sub>Sn coil



## 5. Pulsed Field Magnet Development

Using the conductor test facility installed in 1978, JAERI has been developing many kinds of superconducting cables to fit the requirements of tokamak coil systems.

A pulsed coil, called "Pulser-A", was fabricated as an additional equipment to the conductor test facility and succeeded in pulsed operation in 1979. The conductor for Pulser-A was also selected according to the results obtained by the existing test facility.

Major parameters and winding cross section of Pulser-A are shown in Table VII.5-1 and Fig. VII.5-1 respectively. A resistive CuNi shielding layer is placed around NbTi superconducting filaments. This shielding layer is employed to reduce the coupling eddy current between filaments and was effective as shown in Fig. VII.5-2. In this figure, the ratio of the measured loss energy to the magnetic energy of pulsed field is shown as a function of the characteristic time of pulsed field in a half cycle. The resulting coupling time constant without this shielding layer is estimated to be 67ms. The total loss of Pulser-A in its 22.7 T/s operation from 1T has been measured to be 7J. If a CuNi layer is not employed the loss energy should have been about 50J.

Pulser-A is now being operated under conditions of 1 T/s from 7T, and 25 T/s from 1T, for pulsed field loss measurements of many cables under development in JAERI.

## References

- 1) Shimamoto, S. et al.; Proc. of 8th Symp. on Eng. Problems of Fusion Research, San Francisco, Nov. 1979 p269-272.
- 2) Shimamoto, S. et al.; Workshop of High Field Superconductor, Tokyo, March 1980.
- 3) Nishi, M. et al.; JAERI-M 8771 (1980).
- 4) Ando, T. et al.; Proc. of 8th Symp. on Eng. Problems of Fusion Research, San Francisco, Nov. 1979 p1436-1439.
- 5) Shimamoto, S. et al.; Proc. of 8th Symp. on Eng. Problems of Fusion Research, San Francisco, Nov. 1979 p1174-1178.
- 6) Yoshida, K. et al.; JAERI-M 8784 (1980).
- 7) Tada, E. et al.; Workshop of High Field Superconductor, Tokyo, March 1980.

Table VII.5-1 Major Parameters of Pulser-A

| #.Coil         |        | #.Conductor       |                   |
|----------------|--------|-------------------|-------------------|
| Maximum Field  | 9 T    | Material          | NbTi : CuNi : Cu  |
| Original Field | 1 T    |                   | 1.0 : 0.52 : 1.73 |
| Pulsed Field   | 25 T/s | Filament Dia.     | 11 $\mu$ m        |
| Winding ID     | 170 mm | Num. of Filaments | 10,920            |
| Winding OD     | 215 mm | Operating Curr.   | 300 A             |
| Winding Length | 350 mm | Coupling Const.   | 4 ms              |

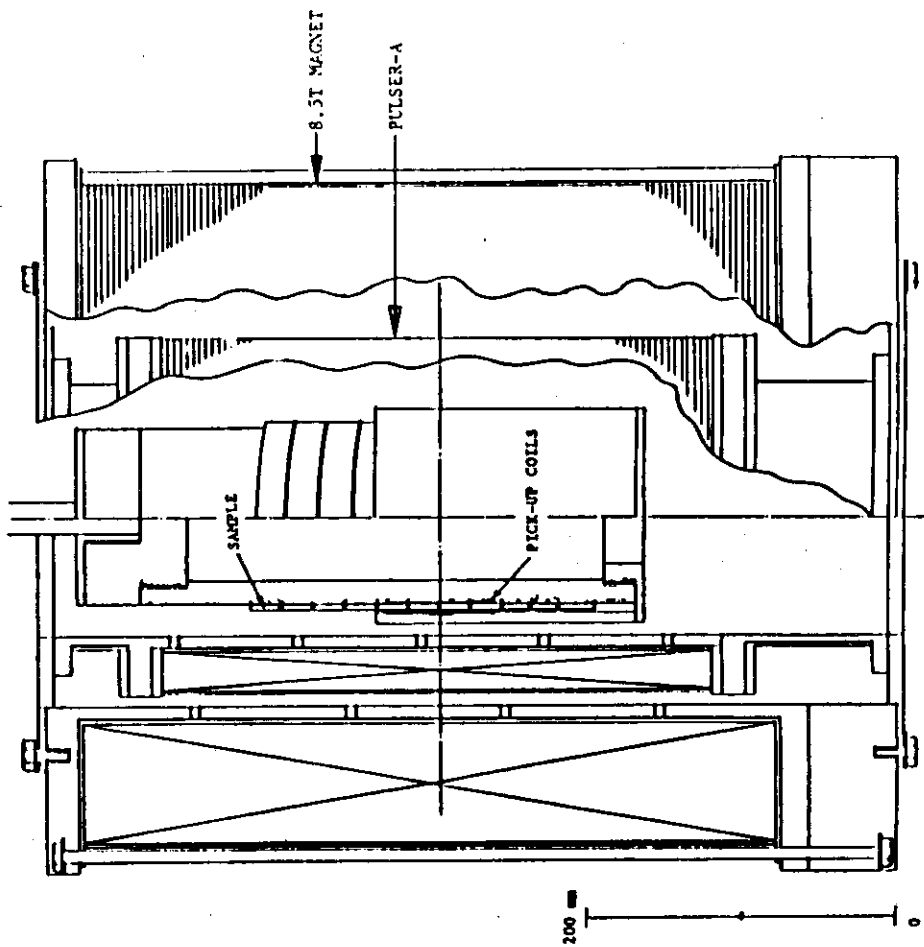


Fig. VII.5-1 Arrangement of a Pulsed Field Loss Measurement using 8.5 T magnet and Pulser-A

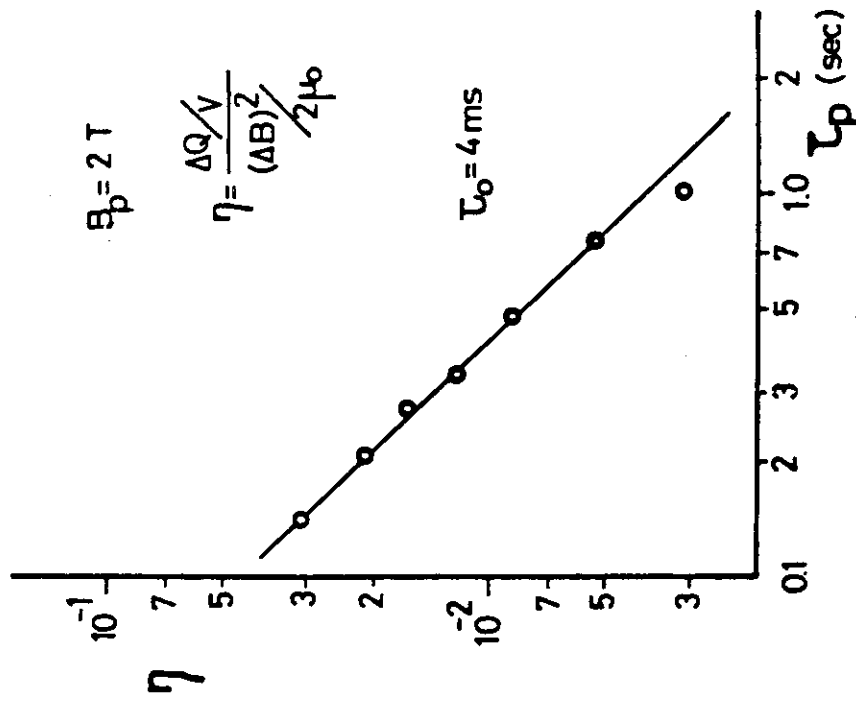


Fig. VII.5-2 Pulsed Field Loss Characteristics of the Conductor for Pulser-A

## VIII. TRITIUM

Tritium engineering technology includes a number of subjects relevant to fuel cycle in fusion reactor. The development of tritium process technology and the design of tritium process laboratory are being performed as a first stage of R & D.

### 1. Development of Tritium Process Technology

#### 1.1 Gas chromatographic measurement of hydrogen isotopes

In order to develop hydrogen isotope separation technology, the establishment of quantitative analysis of hydrogen isotopes, i.e., the separation and the measurement of  $H_2$ , HD,  $D_2$ , HT, DT, and  $T_2$  mixture, are required. As analytical methods, gas chromatography and mass-spectrometry are used for this purpose. The gas chromatographic analysis is firstly chosen to study. For the analysis by gas chromatography, the selection of proper columns and the application of a new device for detector were made.

The chromatographic apparatus consists of Moore type column and catalytic combustion type detector. A chromatographic condition is; column temperature  $-196^\circ\text{C}$ , carrier gas helium, reactant gas dry air and measurement tube volume 20 ml. A typical chromatogram is shown in Fig. VIII.1-1. Calibration curves obtained by using  $H_2$ , HD and  $D_2$  mixture are shown in Fig. VIII.1-2. The good linearity is obviously found in the concentration range between a few microlitre and 500 microlitre(STP) in each component of hydrogen isotopes. The lowest detection limit 0.4 - 1 microlitre is 100 times lower than the ordinary value obtained with a conventional thermal conductivity detector(TCD) using helium as carrier gas.

#### 1.2 Hydrogen recovery experiment

In the facility for handling a large amount of tritium, excellent tritium recovery system is required to protect radiation exposure of operators and to prevent tritium release to the environment. For the recovery system the selected process consists of catalytic oxidation of tritium gas following adsorption of tritiated water. As shown in Fig.

VIII.1-3, the equipment consists of a tank of 300 l which simulates the glovebox, a gas circulation pump whose maximum flow rate is  $4 \text{ m}^3/\text{hr}$ , a catalytic oxidizer of 53.3 mm I.D., 388 mm L. filled with 0.8 kg of the catalyst, and a water adsorber of 83.1 mm I.D., 920 mm L. filled with molecular sieve type 5A. The highest changing rate of the atmosphere of experimental system is 13 times per hour. The temperature of the catalytic oxidizer is elevated up to  $600^\circ\text{C}$  to study the decomposition of organic vapor.

A typical example of the experimental results is shown in Fig. VIII.1-4, where a fixed amount of  $\text{D}_2$  gas is put into the tank and gas in the system is circulated by pump. This experiment simulates abrupt release of tritium gas from the experimental apparatus to the glovebox. Initial gas component is  $\text{D}_2$  : 1 %,  $\text{O}_2$  : 5 %, and  $\text{N}_2$  : 94 %. The oxidizer temperature is maintained at  $100^\circ\text{C}$  and the changing rate is varied as variables.

The results show that the conversion factor reached 99.99 % at the catalytic oxidizer,  $\text{D}_2$  concentration in the tank decreased exponentially with the operating time in the concentration range from  $10^4$  to  $10^1$  ppm, and the recovery rate increases with the increase of changing rate. If the changing rate is 12 times per hour,  $\text{D}_2$  concentration decreased to  $1/10^4$  within 50 min.

### 1.3 System analysis

Fuel cycle of fusion reactors is made up of (i) fuel gas circulation system, (ii) blanket cooling and tritium recovery system, (iii) tritium production system, (iv) tritium containment system and (v) waste treatment system. In order to establish the design and operation method of the fusion fuel cycle systems, it is necessary to make both experimental studies and computer simulation studies. Computer simulation studies include development of model system components for mathematical simulations, derivations of model equations, application of various numerical analysis techniques and optimization techniques, development of computer codes, investigations of fundamental data, detailed analyses on characteristics in both steady state and unsteady state, etc. These computer simulation studies were initiated for such components as cryogenic distillation systems for hydrogen isotope separation in the fuel circulation system and in the blanket cooling system, a falling liquid film condenser for separation of helium from hydrogen isotopes in the fuel

circulation system, a catalytic oxidizer and a tritiated water adsorber in the containment system.

As an example of these studies, a steady state computer simulation for the cryogenic distillation system is briefly summarized. A simulation was performed on the assembly of four distillation columns and two isotopic equilibrators as shown in Fig. VIII.1-5 (this model is a candidate process in the fuel circulation system). The equilibrators are located to decrease the percentage of HT. The survey calculations were made on separation performance of each column to optimize the system. The principal parameters were reflux ratio, number of total theoretical stages, feed location, top product flow rate, decay heat of tritium, pressure drop of the column, etc. The design conditions established by the survey calculations and the predicted composition distribution in liquid phase of the lead column (Column (1)) are shown in Fig. VIII.1-6. And the calculated material balances in the system are shown in Fig. VIII.1-7.

One of the significant results of our study is that effect of decay heat. If the tritium concentration in the column is considerably high as in the case of Column (3), both vapor and liquid flows decrease especially in the stripping section due to tritium decay heat effect, which results in significant lowering of the column performance. The design margin (overestimation of reflux ratio or number of total theoretical stages) or adequate improvement such as refrigeration of the stripping section of the column are required in this case.

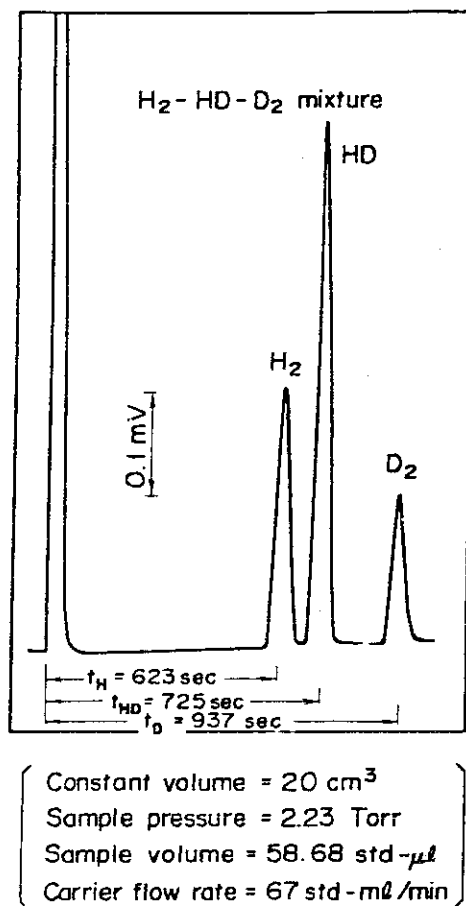


Fig. VIII.1-1 Typical Separation Chromatograms for H<sub>2</sub>-HD-D<sub>2</sub> Gas Mixture

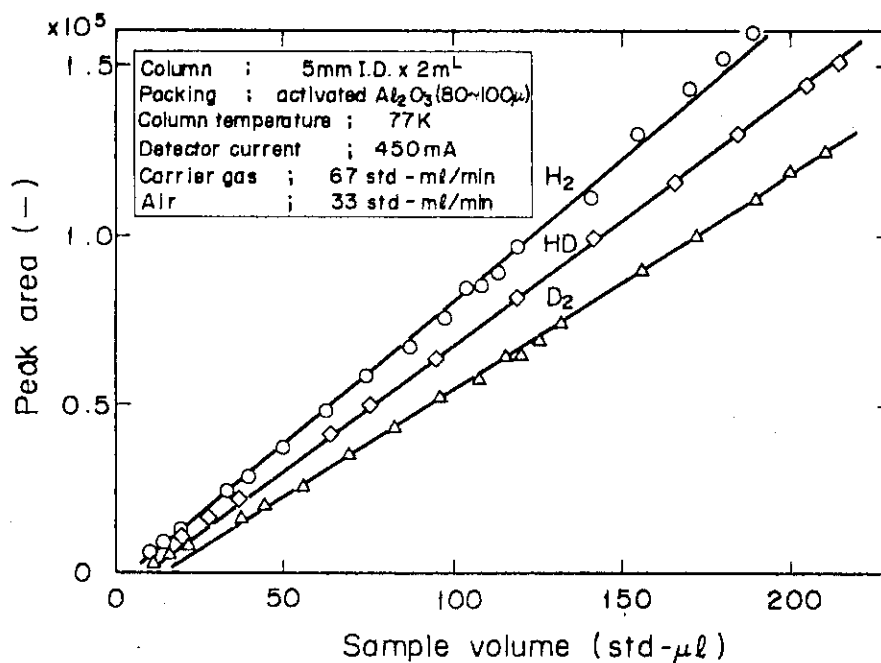
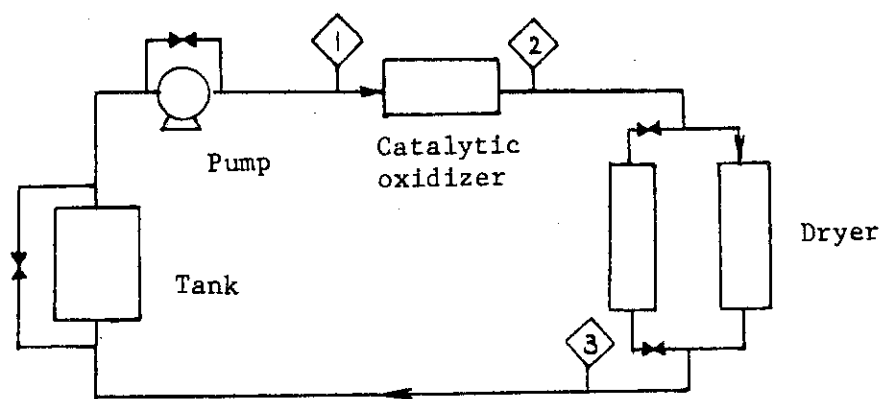


Fig. VIII.1-2 Calibration Curves for H<sub>2</sub>-HD-D<sub>2</sub>  
 (Sample Gas Composition; 24.91% H<sub>2</sub>,  
 47.1% HD, 27.68% D<sub>2</sub>)



1 ~ 3 Sampling point

Fig. VIII.1-3 Block Diagram of Experimental Equipment

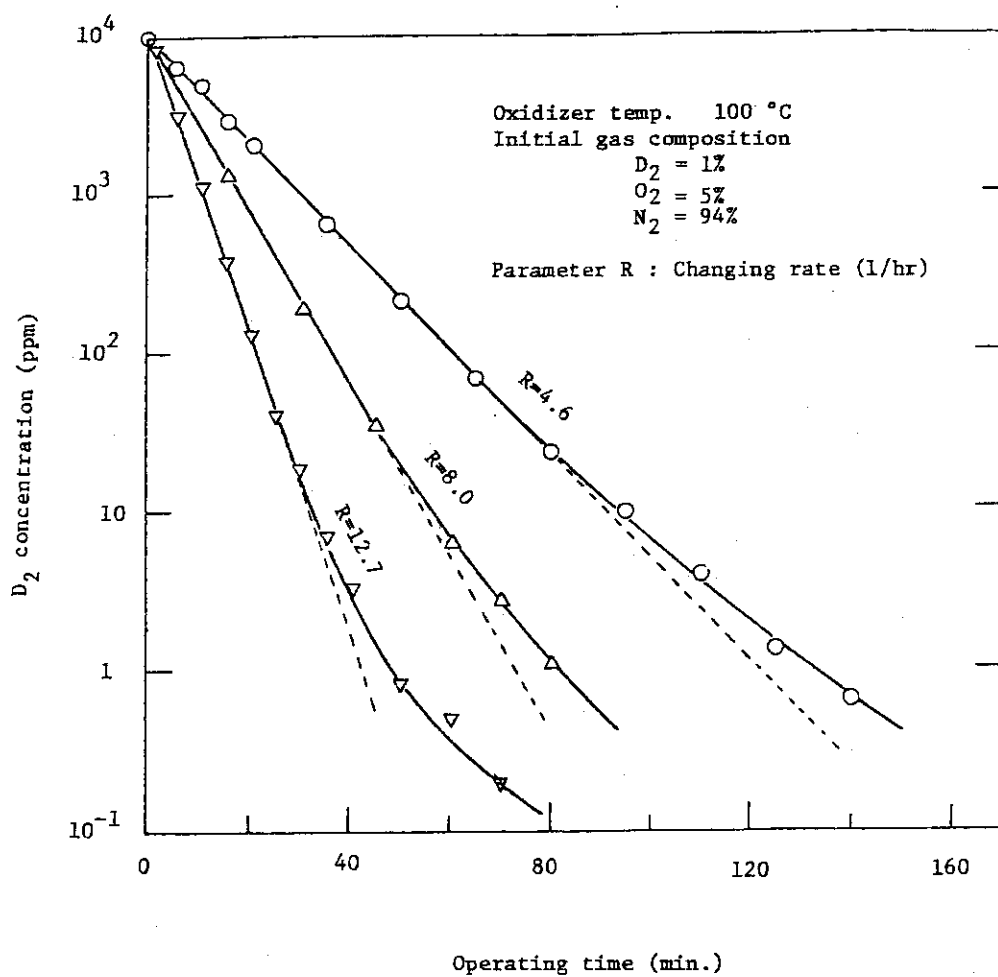


Fig. VIII.1-4 Effect of Changing Rate on Recovery Characteristics



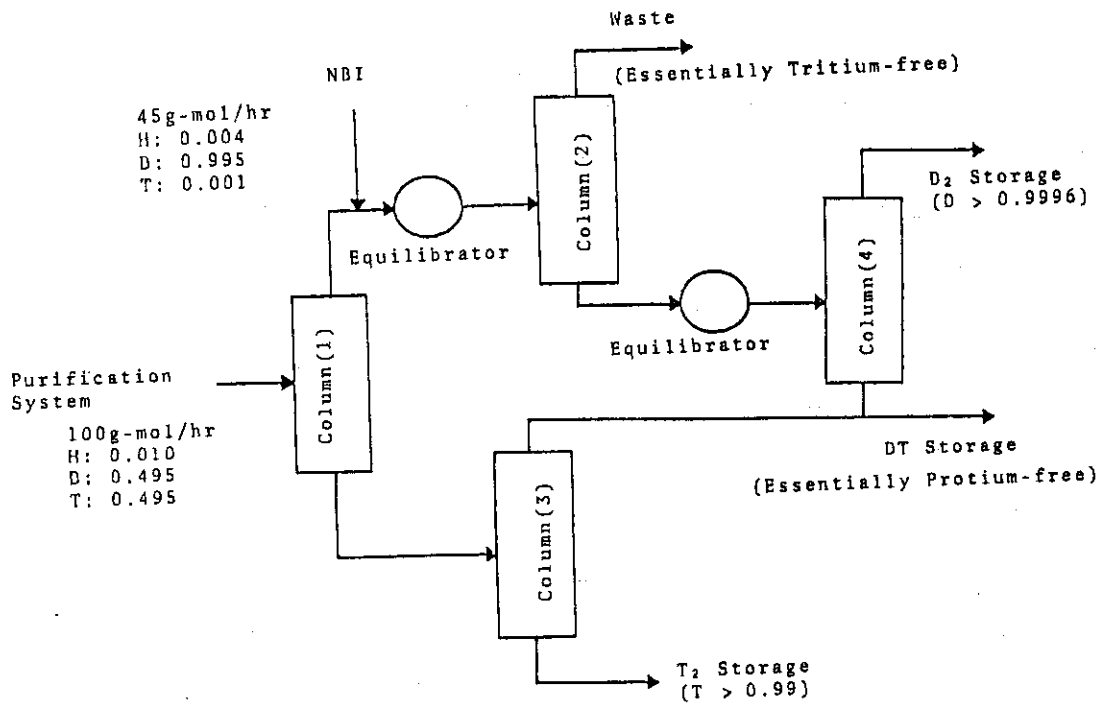


Fig. VIII.1-5 Conceptual Flow Sheet of Cryogenic Distillation System in the Fuel Circulation System

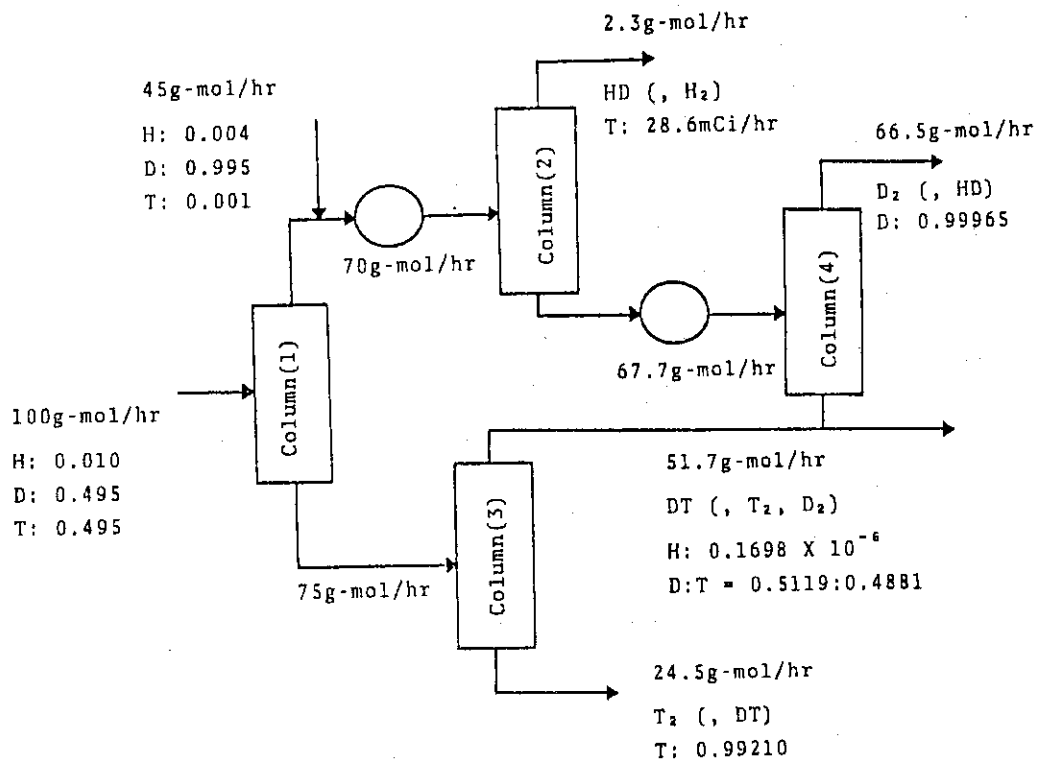


Fig. VIII.1-7 Material Balances in Cryogenic Distillation System

Top Product Flow Rate / Feed Flow Rate = 0.25

Reflux Ratio = 25

Number of Total Theoretical Stages = 70

Feed Location (Feed Stage Number) = 35

Operating Pressure = 1 atm

Condenser = Total Condenser

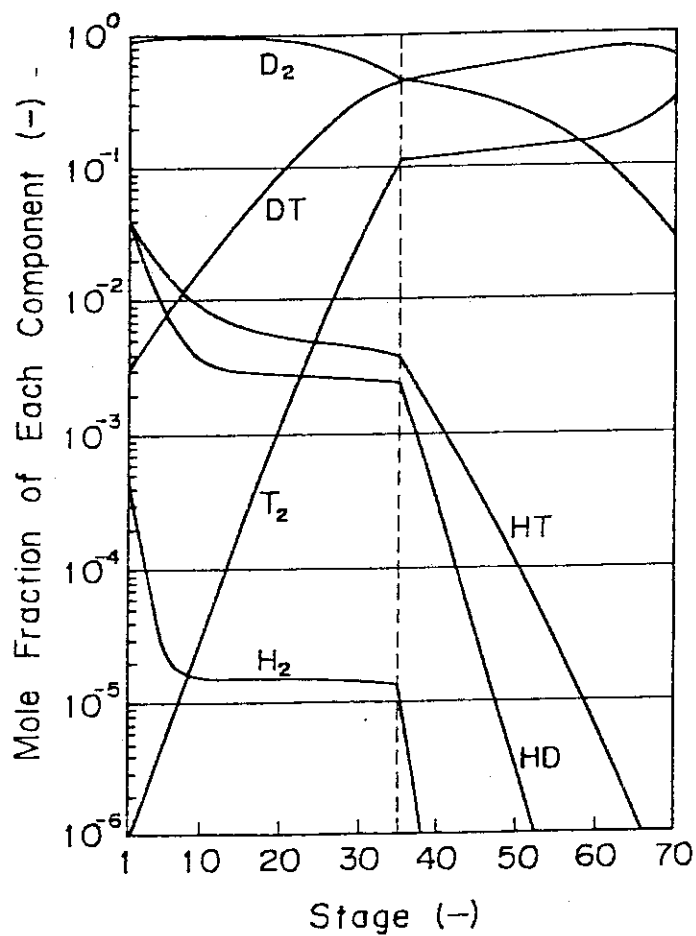


Fig. VIII.1-6 Design Conditions and Predicted Composition Distribution in Column (1) (Liquid Phase)

## 2. A Conceptual Design of Tritium Handling Facility

### 2.1 Introduction

A design study was carried out to construct the facility where grams of tritium is to be used. In the Tritium Process Laboratory (TPL), basic engineering experiment is programmed to study following subjects;

- (1) hydrogen isotope separation by cryogenic distillation and thermal diffusion,
- (2) purification, recovery and storage of tritium gas with metal getters and Pd-Ag membranes,
- (3) safe handling of tritium, e.g. containment and removal, waste treatment, monitoring and accountability

In the design of TPL, the concept of "as low as reasonably achievable" is applied to prevent radiation exposure from tritium activity.

Main characteristics of the design are;

- (1) to apply multiple barrier containment system equipped with tritium removal system,
- (2) to make zoning division clear and install proper ventillation system,
- (3) to select materials and components compatible with tritium,

The basic design conditions for radiation protection are as follows;

- (1) average tritium concentration at the outlet of the stack is less than  $2 \times 10^{-7}$   $\mu\text{Ci/cc}$ ,
- (2) Permissible level of controlled area is less than  $0.01(\text{MPC})_{\text{air}}^{48}$  in year's average, and less than  $0.1(\text{MPC})_{\text{air}}^{48}$  in week's average,
- (3) permissible level in uncontrolled area is less than 30 mrem/w.

The design of TPL is in the final stage and the detailed design of the multiple barrier containment systems and the safety analysis are being made.

The building is made of reinforced concrete to withstand the seismic forces. The building is 48m  $\times$  26m. There is a large experimental room, basement and second floor. The controlled area of this building is about 1080 m<sup>2</sup>. In the experimental room, which is 15m high, there is a glove-box room in which tritium handling gloveboxes are arranged, and an equipment room where various types of tritium removal systems are furnished. The both rooms are of airtight structure with air lock systems. All ventillation systems in the controlled area are designed to be operated in once through mode and the exhaust is released from the stack of 30m high.

## 2.2 Multiple barrier containment systems

The concept of the multiple barrier containment system is shown in Fig. VII.2-1. Glovebox Purification System (GPS) and Air Detritiation System (ADS) are furnished to maintain tritium concentration in the controlled area less than the permissible level. Effluent Removal System (ERS) is equipped for the detritiation of various effluents from the experimental apparatus. By the application of multiple barrier containment system, tritium release from the building is fully decreased to safety level in the populational area, even though the accidental tritium emission from the experimental apparatus is taken into account. Another characteristics of this design is an alternative use of each tritium removal system; in other words, each tritium removal system can be used for multi-purpose operation. Those systems are provided for the case of deterioration of the performance or some troubles of each system.

As an example of the containment system, the outline of glovebox and GPS are described.

### (1) Gloveboxes

In TPL, ten gloveboxes are disposed as shown in Fig. VII.2-2 and classified by 5 blocks according to the purpose of the experiments and the convenience of the experimental operation.

To satisfy the operational and maintenance requirements, each block of gloveboxes has a function of individual ventillation and pressure control. Therefore, each block is independently operated in prescribed pressure and ventillation rate. To transfer samples between two blocks, a leak-proof tunnel mechanism is established. At the sides of all blocks except block 1, there are pass boxes for loading and unloading the samples. In the block 1, evacuable boxes are arranged at the both sides for loading and unloading big samples or components and for decontaminating the parts of the experimental apparatus. Under each glovebox, there are airtight boxes which accomodate vacuum pumps. The atmosphere in the airtight box is cooled with heat exchanger, because the temperature of the atmosphere is elevated by heat generation of vacuum pumps. Inleak air to this box is treated by the ERS. In order to decrease the leakage of tritiated water through gloves of the gloveboxes to the operation area, the glove ports are covered with port covers. If the glove is used, the stagnant gas between the port cover and the glove is previously substituted with fresh air and the exhaust is introduced into the ERS for tritium removal.

## (2) GPS (Glovebox Purification System)

The GPS is installed to satisfy the following two functions. One is to remove tritium and air in eight helium atmosphere gloveboxes. The other is the pressure control of each block individually and/or simultaneously in order to prevent tritium leak from the gloveboxes and to avoid the deterioration of gloves during handling. The GPS reduces the radiation exposure of operators in the operation area, during normal and off-normal operation. The feed flow to the GPS is a mixture of glovebox atmosphere and sweep gas. The latter is used as a cover gas of jacket space in getter cartridges operated at high temperature. The design of the GPS is based on the consideration of safe handling of tritium in the following conditions;

- (1) tritium leak rate from the primary containment
  - leak rate of tritium from the experimental apparatus to the glovebox atmosphere 1 Ci/hr,
  - leak rate of tritium to sweep gas 4.9 Ci/hr,
- (2) the changing rate of the airtight room 3 times/hr,
- (3) tritium leak rate from helium atmosphere gloveboxes, 80 % of all the tritium leak rate to the airtight room.

A schematic flow diagram of the GPS is shown in Fig. VIII.2-3, and the designed performance criteria in Table VIII.2-1.

Helium gases from the gloveboxes pass through a filter to remove dusts and circulates by a low leakage rotary blower. The flow rate is controlled with a by-pass flow valve attached to the blower, because the flow rate changes according to the number of gloveboxes used in the experiment. If necessary, oxygen gas is added. The helium gas heated up to 473K is treated with a catalytic reactor filled with precious metal catalyser. The tritium gas concentration is reduced to 1/200 with the reactor. The gas is then water-cooled to 298K. The water vapor is added to become 200 ppm of water concentration at the inlet of the dryer. Two dryers are installed in parallel and if the water concentration of outlet of the operating dryer become higher than 5 ppm, the dryer is exchanged. After oxidation and adsorption processes, one half of the helium gas flow is sent to the cryogenic adsorber system. In the cryogenic adsorber system, helium is cooled in a gas-gas heat exchanger, and passes through the cold trap cooled with liquid nitrogen, removing impurities such as O<sub>2</sub>, N<sub>2</sub>, H<sub>2</sub>O, CO<sub>2</sub> and hydrocarbons. The helium gas is then heated successively in a gas-gas heat exchanger, and returned

to the main loop. In the case of regeneration of cryogenic adsorber, heated dry helium is supplied to the previously heated adsorber. The exhaust gas is treated by the ERS. In the main loop, the helium gas is monitored and returned to the gloveboxes after filtration with HEPA filter. If the deterioration of the GPS occurs, the experiment is paused, and the ADS or the ERS is used for treating the atmosphere of the gloveboxes in an once through mode. If the accidental high concentration is detected by the glovebox monitor, the ventilation of that block is changed from the GPS to the ADS or the ERS. In each block of the glovebox, there is a dry air supply system provided for these abnormal event. Each block of glovebox has a precise differential pressure control system which actuates two flow control valves for feeding and exhausting helium gas. There are on-off valves which are used for out of control of the flow control valves. In Fig. VIII.2-4, the principle of the pressure control system of the glovebox is illustrated. Each block of the glovebox has a bubbler system which is operated at +80 mm H<sub>2</sub>O to prevent the deterioration of gloves. The exhaust gas from the bubbler is treated by the ERS.

### 2.3 The other systems

The experimental apparatus are installed in each glovebox respectively. Projected experiments are cryogenic distillation of hydrogen isotopes, thermal diffusion of hydrogen isotopes, purification of impurities contained in hydrogen isotope gas, leakage test of tritium handling components, tritium removal test to develop containment technology, tritium recovery from used gas in TPL, analysis and measurement of tritium gas, measurement of low temperature properties of hydrogen isotope gas, etc.

The other supporting systems consist of monitoring system, tritium liquid waste storage tank system and utility supply systems such as cooling water, liquid nitrogen, helium gas, etc.

Table VIII.2-1 GPS Design Criteria

|                                     |                             |                              |
|-------------------------------------|-----------------------------|------------------------------|
| Processing capacity;                | Main loop                   | 150 m <sup>3</sup> /hr       |
|                                     | Bypass for cryogenic system | 75 m <sup>3</sup> /hr        |
| Catalytic reactor;                  |                             |                              |
| Operation temperature               |                             | 473 K                        |
| Catalyst                            |                             | Precious metal               |
| Tritium gas concentration reduction |                             | 200 per pass                 |
| Dryer;                              |                             |                              |
| Capacity                            |                             | 35 Kg water                  |
| Operation temperature               |                             | 298 K                        |
| Adsorbent                           |                             | Molecular sieve type 5A      |
| Regeneration cycle time             |                             | 1440 hr                      |
| Cryogenic adsorber;                 |                             |                              |
| Capacity                            |                             | 4.5 Kg nitrogen              |
| Operation temperature               |                             | 77 K                         |
| Adsorbent                           |                             | Molecular sieve type 5A      |
| Regeneration cycle time             |                             | 72 hr                        |
| System leak rate limit;             |                             | $2 \times 10^{-3}$ cc(STP)/s |

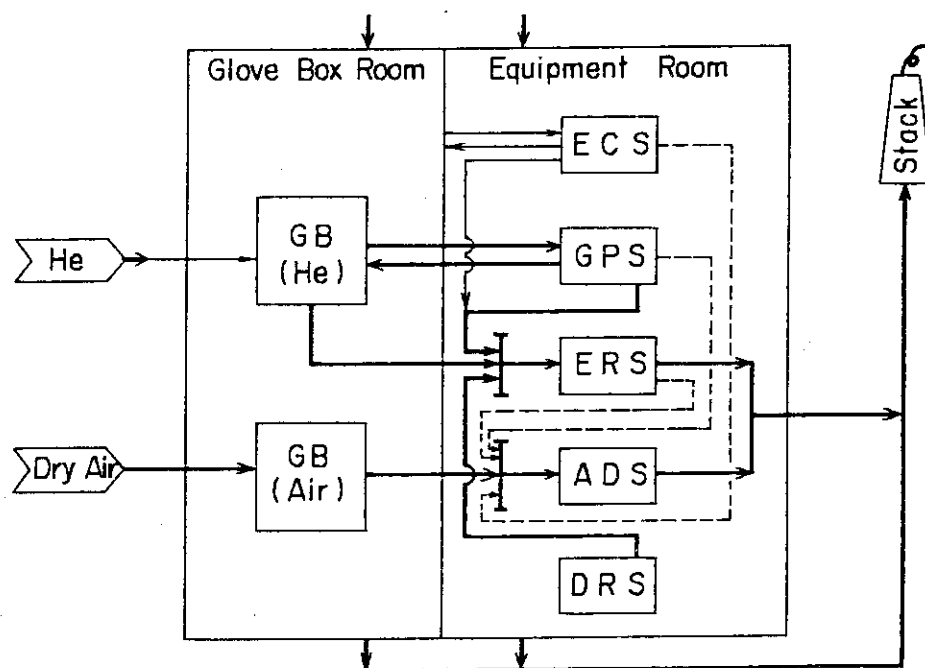


Fig. VIII.2-1 Multiple Barrier Containment System of TPL

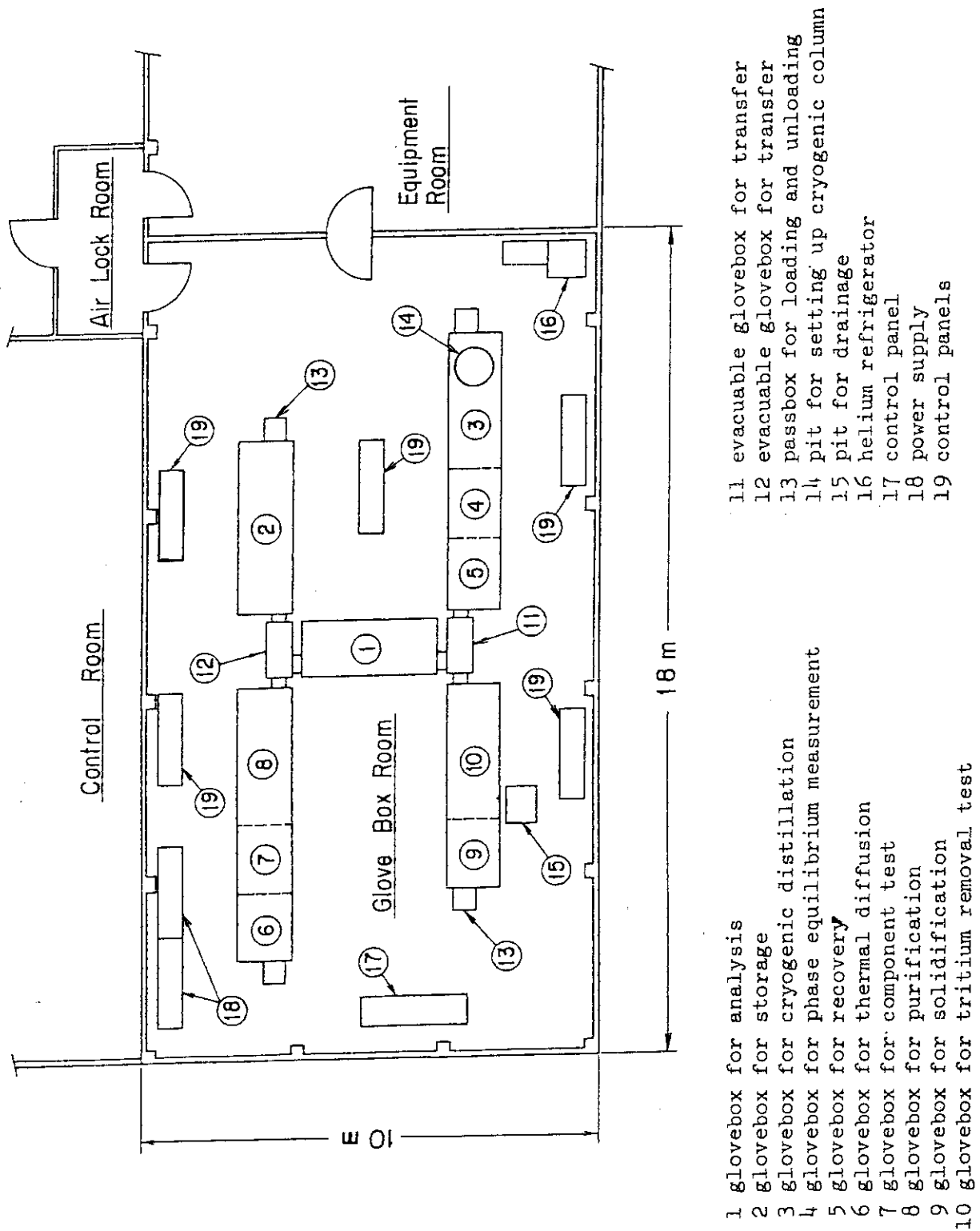


Fig. VIII.2-2 Layout of Gloveboxes



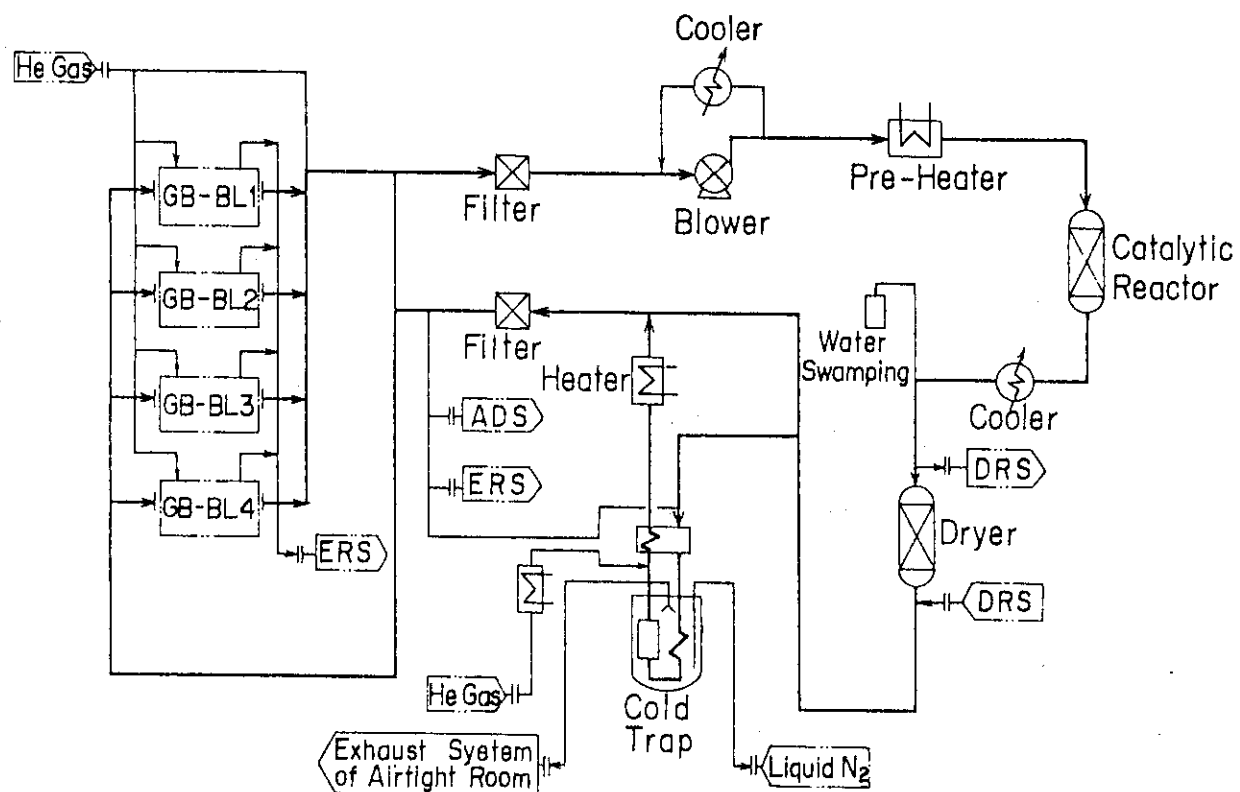


Fig. VIII.2-3 Schematic Flow Diagram of GPS

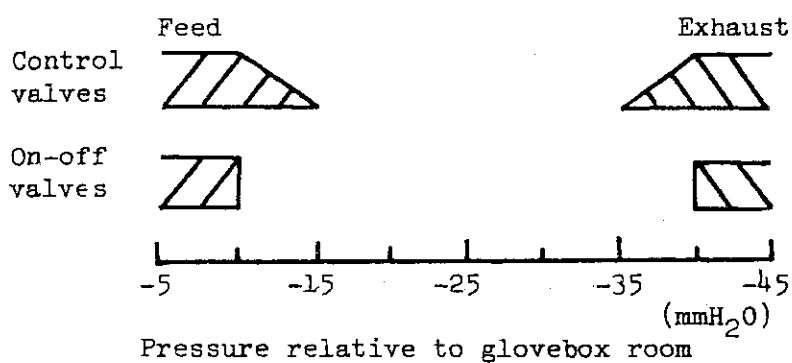


Fig. VIII.2-4 Principle of Pressure Control System for Gloveboxes

## IX. DESIGN STUDY OF FUSION REACTOR SYSTEM

### 1. Introduction

Preliminary design study of JAERI Experimental Fusion Reactor (JXFR) has been carried out for five years from 1975 to 1979 with basically unchanged design specifications. The design study progressed as planned at its beginning to elucidate the reactor concept, identify the problematic area, evaluate the overall design and establish plans on fusion reactor development. Design techniques of reactors were also established during this period.

In 1979 the design study of INTOR (International Tokamak Reactor), which is planned to be developed by IAEA, was carried out as one of the evaluation studies of experimental fusion reactor and the data base for selecting the INTOR design parameter was completed.

The study on fusion power reactors was also conducted. A new reactor concept was proposed to simplify repair and maintenance scheme, which is very important for realizing fusion reactors.

### 2. Preliminary Design of JXFR

The design was completed and evaluated, and the problematic area was identified. The key items of the related research and development were classified, and development schedule is examined projecting the construction of JXFR ten years later.

### 3. Design of Repair and Maintenance

In order to relieve the difficulties of repair and maintenance which are the most serious problem in a tokamak reactor, a concept of swimming pool type reactor has been proposed. A preliminary study on the feasibility of the concept has been carried out. Because blankets may be easily replaced in this reactor, this concept will have a wide applicability for an experimental reactor which seems still have many ambiguities remaining in plasma physics and reactor structure design.

The items covered are (1) reactor concept, (2) plasma vacuum boundary, (3) blanket structure, (4) tritium breeding, (5) shielding, (6) induced

radioactivity, (7) repair and maintenance and (8) overall evaluation.

Judging from the results obtained, this concept is promising and deserves a more detailed study.

#### 4. Design Study of a Fusion Power Reactor

Recent progress in tokamak confinement and heating allows us to presume higher  $\beta$  value which leads to larger fusion power with the same machine. On the other hand we had in anticipation studied the problems accompanying the increase of blanket power density in the preliminary design study of JXFR. In 1979 a proto-type reactor design was also carried out without changing major part of JXFR design employing a high power density blanket.

#### 5. Development of Design Techniques

A number of computer programs used for the reactor design have been developed and improved. Among them a brief description of those developed for plasma and neutronics designs is given below.

##### 5.1 Plasma design

Major issues in plasma design are power balance, impurity control, ash exhaust, fueling, alpha heating, additional heating, start-up, burn control, MHD equilibrium and configuration of poloidal coils. At the outset of the JXFR design the plasma parameters were determined on the basis of simple models. The detailed analysis of plasma characteristics has been made thereafter by developing and improving successively computer simulation codes. Major items for which the codes have been newly developed are as follows.

##### (1) Zero-dimensional power balance

The slowing down of high energy ions is analyzed on the basis of the Fokker-Planck model.

##### (2) Confinement of 3.5 MeV alpha particles

An orbit-following calculation code based on the drift kinetic equation has been developed.

(3) Gas blanket

Impurity control, ash exhaust and gas fueling by gas blanket are analysed based on a simple one-dimensional model

(4) Zero-dimensional start-up and shutdown analysis

This code is fit for an extensive survey of the characteristic of start-up and shutdown.

(5) Burn performance

The region and growth rate of thermal instability, burn dynamics and controllability are obtained by a zero-dimensional model.

(6) MHD equilibrium and poloidal coil configuration

Magnetic field configuration is calculated by a fixed-boundary model.

(7) Steady-state spatial distribution of plasma density

Steady-state density distribution for a given temperature distribution is obtained for various transport coefficients. This code is fit for a survey of the confinement time of full and alpha particles, recycling and particle fluxes.

(8) One-dimensional transport simulation

Simulation of energy and particle transport including start-up, burn control, fueling and heating is performed by one-dimensional model. A non-equilibrium transport model of impurities is incorporated.

## 5.2 Nuclear design

Nuclear design<sup>(1)</sup> of INTOR-J<sup>(2)</sup>, the JAERI proposal for the International Tokamak Reactor (INTOR)<sup>(3)</sup> has been carried out using one dimensional (1D)  $S_N$  code ANISN<sup>(4)</sup>, two dimensional (2D)  $S_N$  code DOT-3.5<sup>(5)</sup> and three dimensional (3D) Monte Carlo code MORSE-I<sup>(6)</sup>. A 42 group-neutron 21 group-gamma coupled cross-section library for 40 nuclides GICX40<sup>(7)</sup>, which is based on ENDF/B-III and IV<sup>(8)</sup> for neutron data and POPOP4 Library<sup>(9)</sup> for gamma-ray production data, was used.

The 1D calculations were used in preliminary calculations and parametric surveys on tritium breeding<sup>(10)</sup> and magnet shielding design. Neutron and gamma-ray fluxes, radiation damage rates and nuclear heating rate distributions were calculated with cylindrical models.

Gamma dose rates after reactor shutdown were also calculated using 1D model and THIDA code system<sup>(11)</sup>. THIDA is a code system which calculates Transmutation, Hazard potential, Induced activity, Dose rate and Afterheat. It consists of the following: induced activity calculation code; activation chain, activation cross section, radionuclide gamma-ray energy/intensity and gamma-ray group constant files; and gamma-ray flux to exposure dose rate conversion coefficients.

The 2D calculations were carried out to investigate the effect of neutron streaming through the divertor channel. As a result, the streaming effect is found to cause about two times as much nuclear heating rate in the magnet than the case without divertor channel.

Poloidal distributions of 14 MeV neutron flux, helium production, displacement damage and nuclear heating rates in the first wall system were calculated<sup>(12)</sup> using Monte Carlo transport code MORSE-I<sup>(6)</sup>. The peaking factors of 14 MeV neutron flux and helium production rate distributions were found to be about 1.3 and those of displacement damage and nuclear heating a little smaller. The peaks were always in the outboard side of the first wall.

An albedo Monte Carlo method was developed in order to evaluate the neutron streaming through neutral beam injector (NBI) ports<sup>(13)</sup>. Preliminary results of the evaluation suggest that nuclear heating and radiation damage in the NBI seems to be tolerable but the induced activation necessitates remote operation for the repair and maintenance of NBI components around the ion source.

The Monte Carlo Transport Code MORSE has been improved.

MORSE-I is a revision of the MORSE-GG code<sup>(14)</sup>. The following improvements are made.

- (1) MORSE-I can treat a torus geometry which is represented by using surface of fourth order while original MORSE-GG treats those which can be represented by surfaces of second order. The number of surfaces allowed in a block is increased from 17 to 35.<sup>(6)</sup>
- (2) Point-detector technique is improved
  - (2)-1 Computational time required is reduced significantly by the Score Point Selection technique.<sup>(15)</sup>
  - (2)-2 Specular reflection boundaries can be used as symmetric boundaries. Proper usage of this boundary also reduces computational time practically.<sup>(16)</sup>

- (2)-3 Infinite variance is eliminated by the Small Density Perturbation technique.<sup>(17)</sup>

### References

- (1) Seki, Y., Iida, H., Yamauchi, M., Kitamura, M. and Kawasaki, H.: Proc. 1980 Annual Meeting of the Atomic Energy Soc. of Japan, D29 (1980) (in Japanese)
- (2) Sako, K., Tone, T., Seki, Y., Iida, H., Yamato, H., et al.: Engineering Aspects of the JAERI Proposal for INTOR (I) and (II), JAERI-M 8503 and 8518 (1980)
- (3) INTOR (International Tokamak Reactor), Division of Research and Laboratories, IAEA, Vienna (1980)
- (4) Engle, W.W., Jr.: A User's Manual for ANISN, A One-Dimensional Discrete Ordinates Transport Code With Anisotropic Scattering, K-1693, Oak Ridge Gaseous Diffusion Plant (1967)
- (5) RSIC Computer Code Collection: DOT-3.5, Two Dimensional Discrete Ordinates Transport Code, CCC-276, Radiation Shielding Information Center, Oak Ridge National Laboratory (1976)
- (6) Iida, H. and Yamauchi, M.: Proc. 1978 Fall Meeting of the Atomic Energy Soc. of Japan, B35 (1978) (in Japanese)
- (7) Seki, Y. and Iida, H.: Coupled 42-Group Neutron and 21-Group Gamma Ray Cross Section Sets for Fusion Reactor Calculations, JAERI-M 8818 (1980)
- (8) Drake, M.K.: Data Formats and Procedures for the ENDF Neutron Cross Section Library, BNL-50274 (T-601, TID-4500) (1970) Rev. 1974
- (9) Ford, W.E., III.: The POPOP4 Library of Neutron-Induced Secondary Gamma-Ray Yield and Cross Section Data, CTC-42 (1970)
- (10) Iida, H. and Seki, Y.: Studies on Increasing Tritium Breeding Ratios of JXFR and INTOR-J Blankets, JAERI-M 8896 (1980) (in Japanese)
- (11) Iida, H. and Igarashi, M.: THIDA - Code System for Calculation of the Exposure Dose Rate Around a Fusion Device - , JAERI-M 8019 (1978) (in Japanese)
- (12) Iida, H., Seki, Y., Yamamoto, T. and Kawasaki, K.: Poloidal Distributions of Neutron Flux, Radiation Damage and Nuclear Heating Rate in a First Wall System of INTOR-J, JAERI-M 8517 (1979)

- (13) Yamauchi, M., Iida, H. and Murata, T.: Calculation of Neutron and Gamma-Ray Streaming Through the Neutral Beam Injector Port of INTOR-J, to be published in Proc. 11th Symposium on Fusion Technology, Oxford Sept. 15-19 (1980)
- (14) Straker, W.A., Stevens, P.N., Irving, D.C. and Cain, V.C. :  
The MORSE Code - A Multigroup Neutron and Gamma-Ray Monte Carlo Transport Code, ORNL-4585 (1970)
- (15) Iida, H. and Seki, Y.: Reduction of Computational Time for Point Detector Estimator in Monte Carlo Transport Code, Nucl. Sci. Eng., 74, 213 (1980)
- (16) Iida, H. and Seki, Y.: Simple Method of Eliminating Infinite Variance in Point Detector Problem of Monte Carlo Calculation, J. Nucl. Sci. Tech. 17, 315 (1980)
- (17) Iida, H. and Seki, Y.: A Point Detector Scoring Method Compatible with Monte Carlo Transport Calculations of Specularly Reflected Particles, to be published in Nucl. Sci. Eng.

## X. DEVELOPMENT OF LARGE TOKAMAK — JT-60

### 1. Introduction

A new site of Japan Atomic Energy Research Institute for fusion energy development was procured in October 1979, where JT-60 is to be located. The construction of JT-60 buildings was started; the experimental building in February 1980 and the power supplies building in March.

The construction of the JT-60 Tokamak machine and the poloidal field coil power supply is in progress at Hitachi, Ltd. and Toshiba Corporation, respectively. Contracts were concluded with Mitsubishi Electric Corporation for the construction of the toroidal field coil power supply and with Hitachi, Ltd. for the manufacture of the central control system. The construction of the secondary cooling and power distribution systems is expected in the next year. JT-60 completion is planned in 1984. Development works on the diagnostic system were continued vigorously. Construction was started for the prototype of JT-60 neutral beam injectors, which is described in more detail in V Development of Plasma Heating System.

With the JT-60 operation anticipated in the near future and the assessment of the next-generation devices being made here and elsewhere, emphasis was placed on the review of JT-60 experimental program and plasma physics and control analysis. Possible upgrade programs were explored in line with long-range development program towards tokamak reactors and also recent progress made here and abroad in tokamak research.

### 2. Outline of the Progress of JT-60

The fiscal year of 1979 is characterized for JT-60 as the initial year of the full scale construction.

The new site for JT-60 was formally determined and the ground-breaking ceremony was held on December 6, 1979. The new site is called Mukouyama Area in Naka-machi which is an westward adjacent town to Tokai-mura. It is flattend-T-shaped as shown in Fig. X.2-1 with the total area of about  $1.5 \text{ km}^2$  of which the central area of about  $0.6 \text{ km}^2$  was purchased and the site will be expanded in the following years. The lay-out plan of JT-60 site is shown in Fig. X.2-2. There are three major bouildings, Experimental Building, Power Supplies Building and Control Building. Flat and cross



sectional plans of Experimental Building are illustrated in Figs. X.2-3 to X.2-4.

Construction of Experimental Building and Underground Ducts connecting buildings were initiated from February, 1980 by Joint Venture of three construction companies, Kajima Corporation, Shimizu Construction Co. Ltd. and Takenaka Kokuten Co. Ltd.

Contracts for almost of major components of JT-60 have been concluded by the end of the fiscal year of 1979. Construction of tokamak machine and its auxiliary components have been on schedule. Six toroidal field coils were accomplished. The manufacture of the vacuum chamber, poloidal field coils, the primary coolant system and the vacuum system were initiated. The construction of the poloidal field coil power supplies was started from the final manufacturing of the thyristor convertor and other components. In March, 1980, contracts for the toroidal field coil power supplies and the central control system were concluded with Mitsubishi Electric Corporation and Hitachi, Ltd., respectively.

The organization related to JT-60 program is shown in Fig. X.2-5. Division of Large Tokamak Development (DLTD) is directly responsible to development and construction of JT-60. DLTD has one administrative section and three project offices and every project office has a few technical groups.

To cover systematically the whole JT-60 program, the engineering coordination was actively initiated since construction of major components were started. Planning and Coordination Group of JT-60 Program Office is directly responsible to coordination among various JT-60 activities. Hitachi, Ltd., as the coordinating company assists JAERI by coordination among manufacturers of JT-60 components. In Fig. X.2-6, the coordination mechanism are schematically illustrated.

The master schedule of JT-60 program is shown in Fig. X.2-7. The accomplishment of JT-60 is scheduled in September of 1984. The main reason for its delay was the prolonged negotiation on purchasing the land for JT-60 site. The major critical paths are the construction of the experimental building and the assemble and test of the tokamak machine.

Experimental program was reviewed in the light of recent progress in fusion research and from the perspective point of view for requirements from the next generation tokamak device. Reassessment of JT-60 objectives, improvement of JT-60 for higher beta value and acceleration of the schedule of secondary heating experiment have been executed.

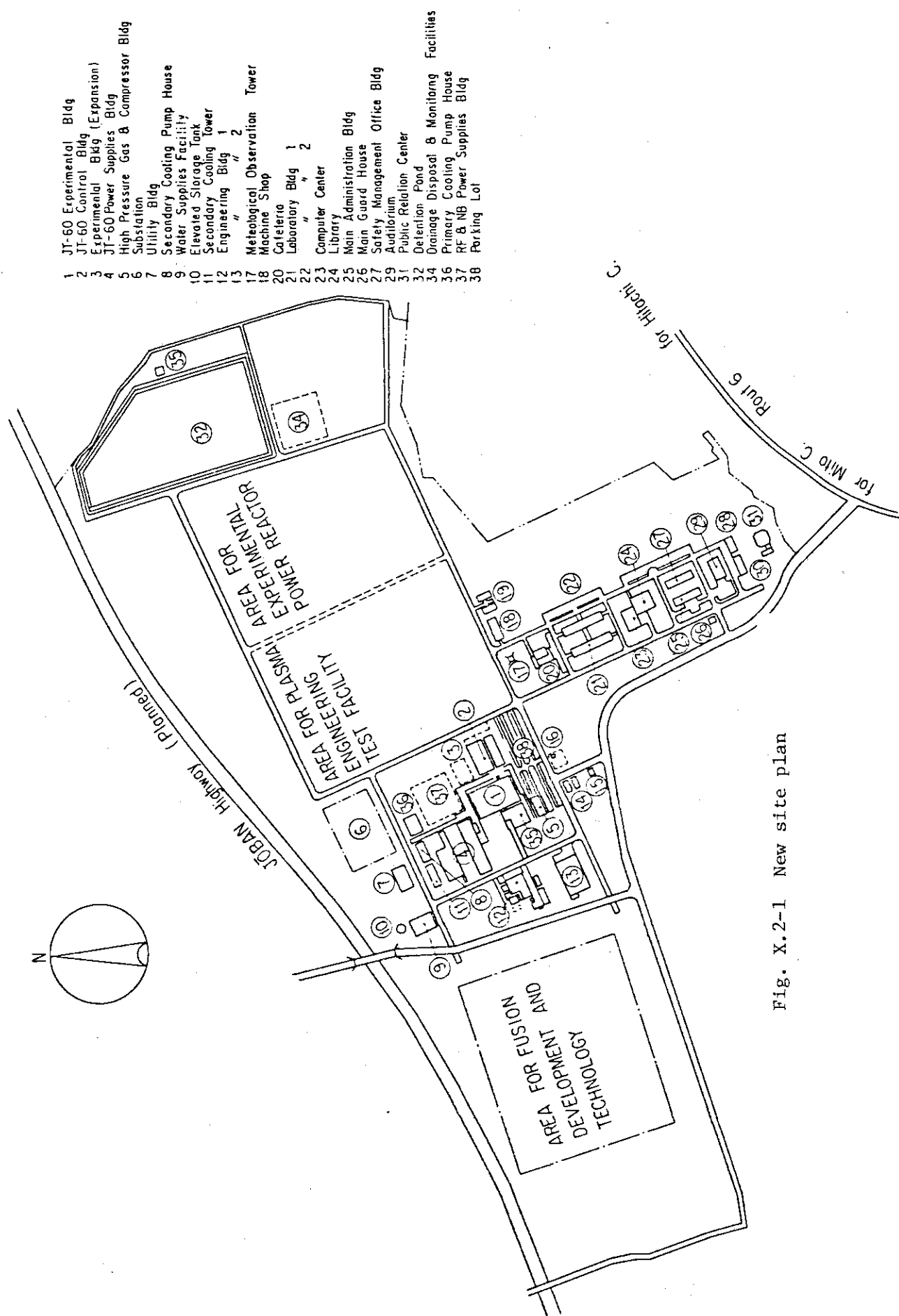
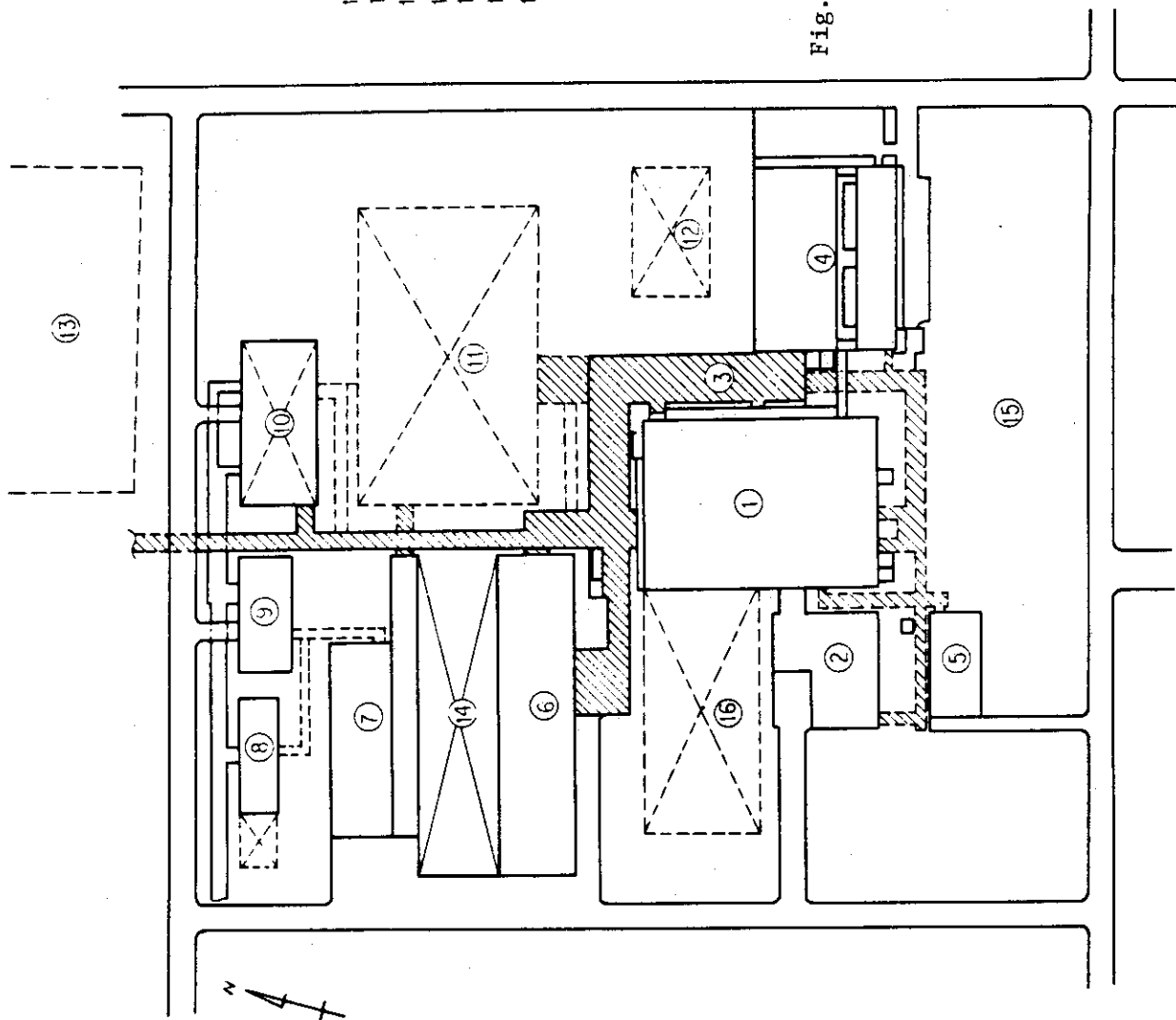


Fig. X.2-1 New site plan

- 1 JT-60 Experimental Bldg
- 2 " " (Equipment Test Area)
- 3 JT-60 Underground Ducts
- 4 JT-60 Control Bldg
- 5 High Pressure Gas & Compressor Bldg
- 6 Rectifier Bldg
- 7 Generator Bldg
- 8 Secondary Cooling Towers
- 9 Secondary Cooling Pump House
- 10 Primary Cooling Pump House
- 11 NB & RF Power supplies Bldg
- 12 Experimental Bldg (Future Device)
- 13 Substation
- 14 Transformer Yard
- 15 Parking Lot
- 16 Experimental Bldg (Expansion)

Fig. X.2-2 Layout of JT-60 underground ducts



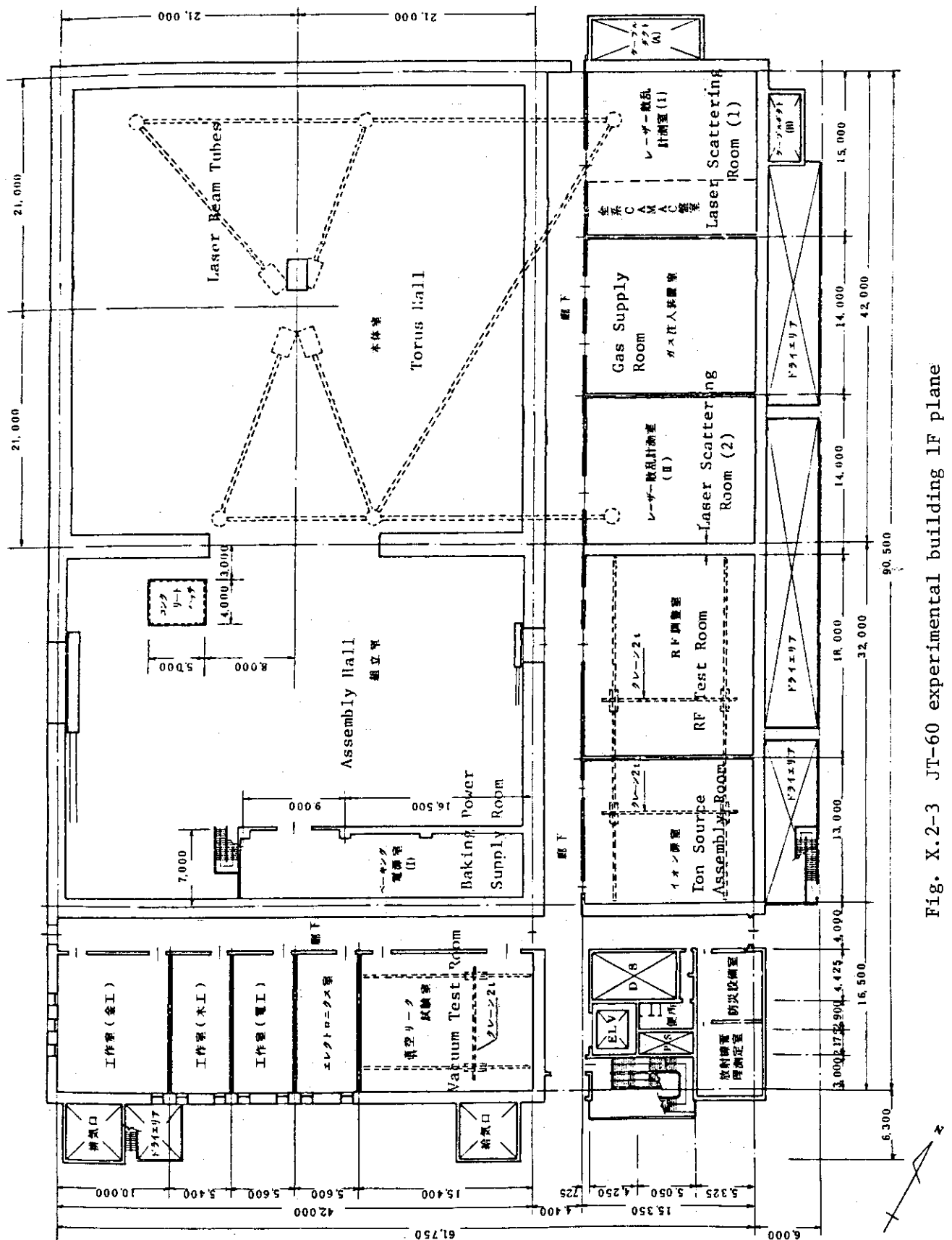
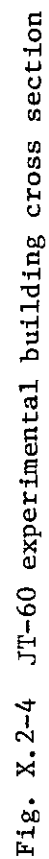


Fig. X.2-3 JT-60 experimental building 1F plane



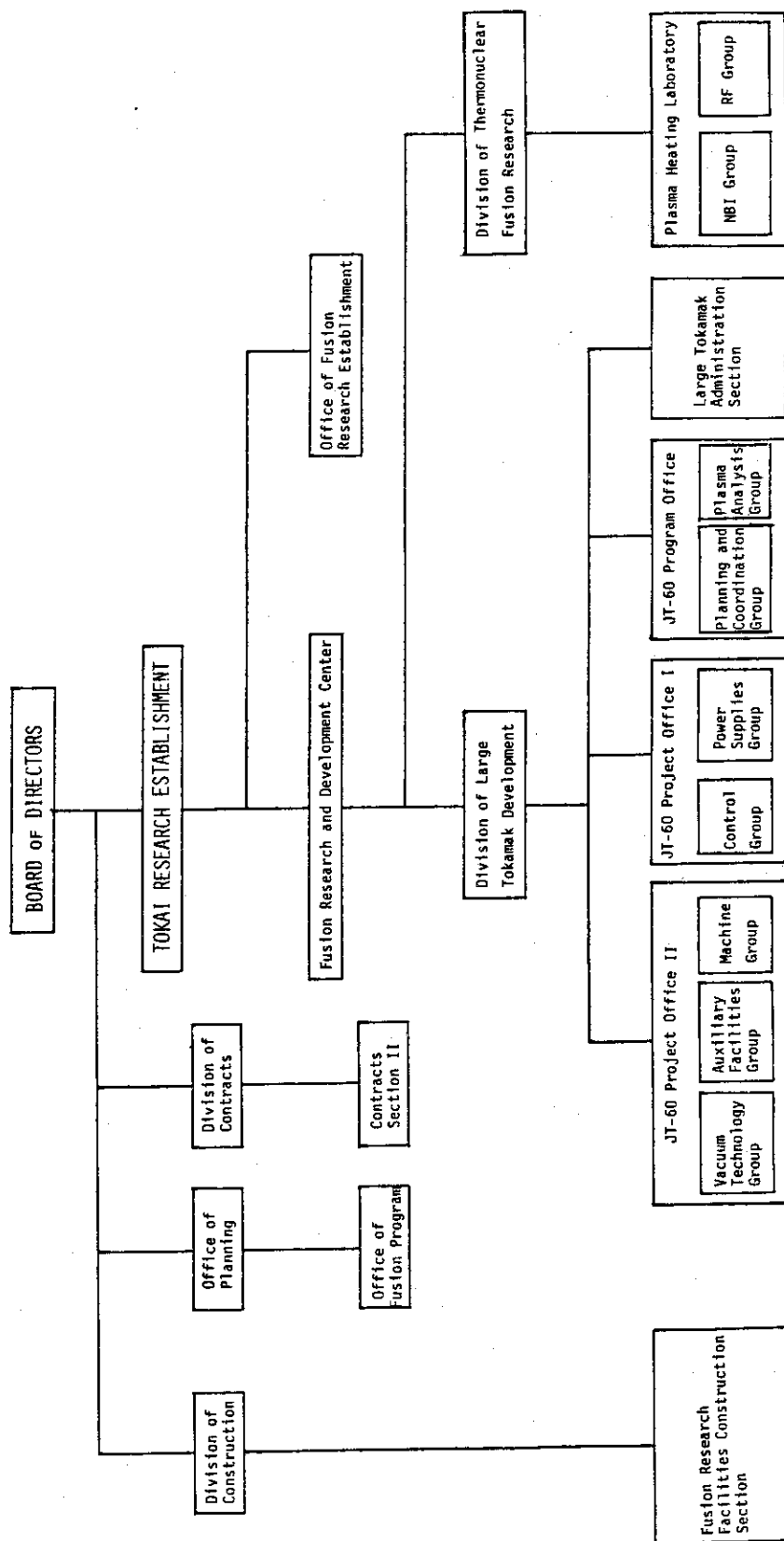


Fig. X.2-5 Organization related to JT-60 program

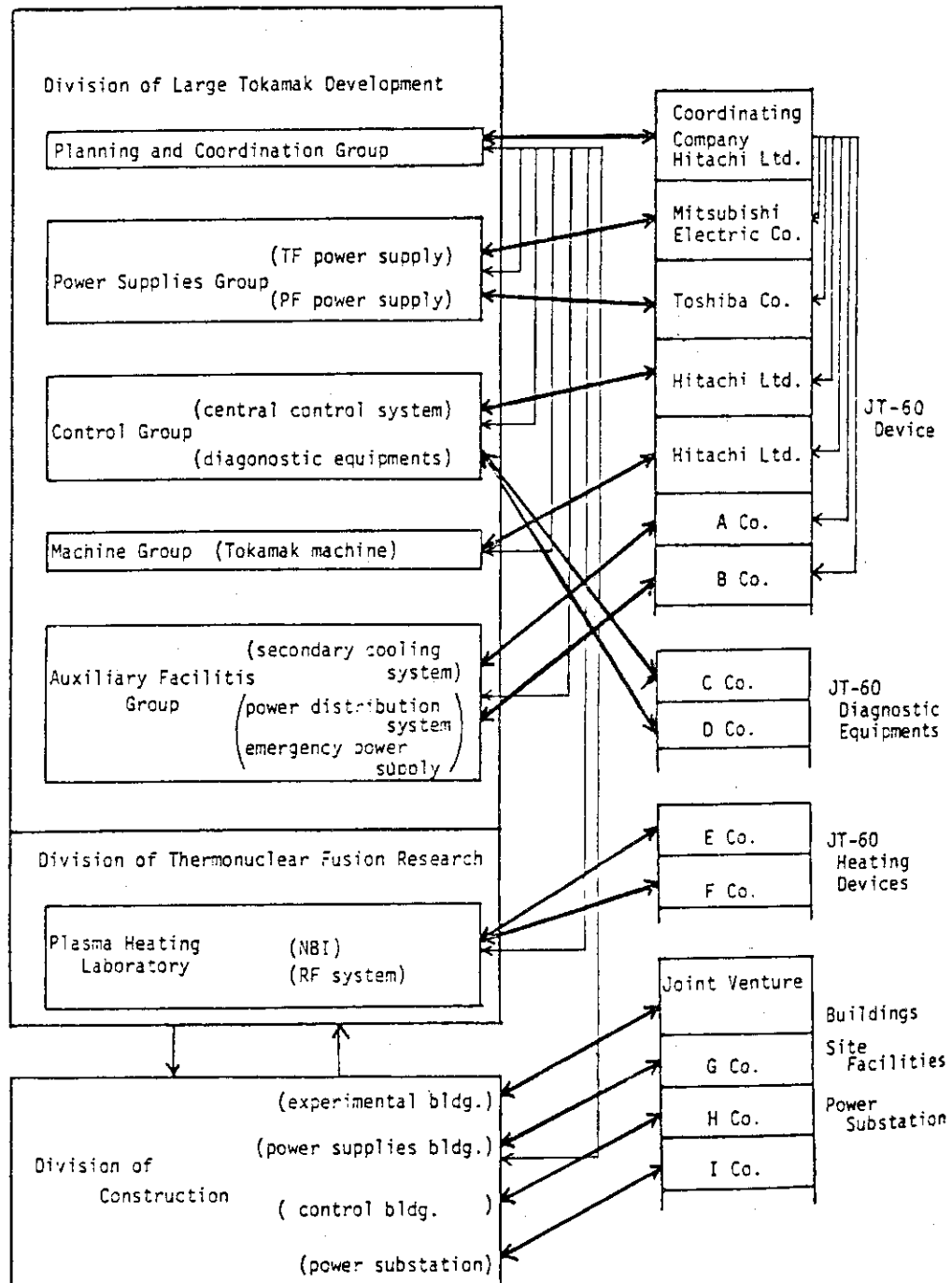


Fig. X.2-6 Organization structure

## JT-60 PROJECT SCHEDULE

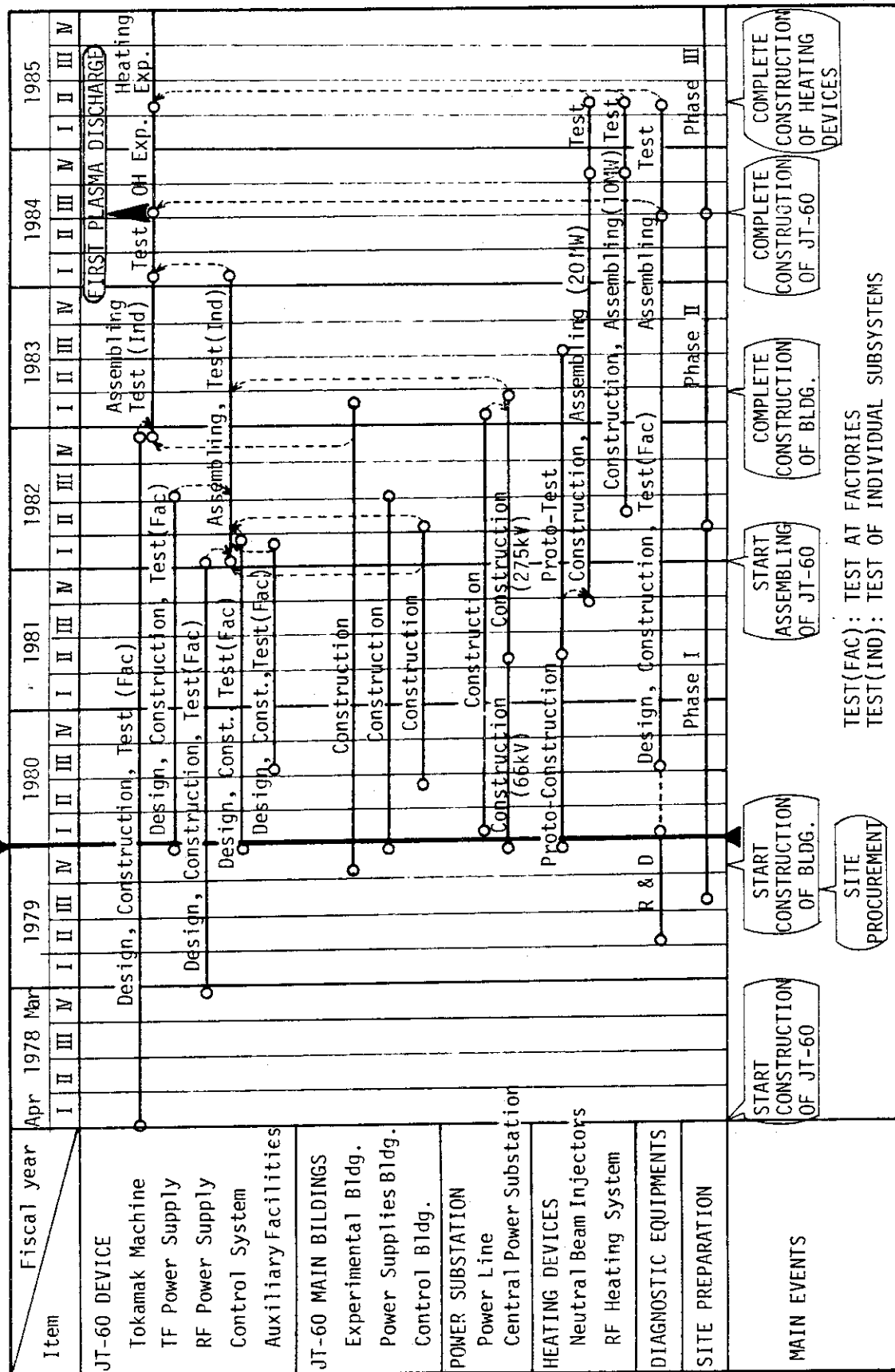


Fig. X.2-7 Master schedule of JT-60 program



### 3. Status of Tokamak Machine

Tokamak machine of JT-60 is composed of a vacuum vessel, toroidal field coils, poloidal field coils, support structures, a primary cooling system, a vacuum pumping system, fast movable limiters, a preionization system, a gas supply system, adjustable movable limiters and machine control system.

The design conditions for each operation mode are summarized in Table X.3-1. Main design conditions are as follows. (a) Total number of full power pulses does not exceed  $5 \times 10^4$ . In addition to the full power operation,  $1.5 \times 10^5$  shots of 50 % rated operation are taken into account in the design life time. (b) The number of such pulses that the plasma is of abnormal plasma disruption with time constant of at least 50 msec is not generated in the build-up phase is 5 % of total pulses. (c) The number 20 % of total pulses, and furthermore that with time constant shorter than 50 msec (at least 1 msec) is  $10^3$ . (d) The total exposure, the maximum exposure intensity per shot and the maximum energy of X-rays due to runaway electrons are  $2 \times 10^8$  R,  $10^5$  R and 10 MeV, respectively. (e) The negative spike of plasma induces the one-turn voltage of 3 kV with the pulse length of 100 - 400  $\mu$ sec. (f) The maximum acceleration of the earthquake does not exceed 0.2 G at the base of the machine.

#### 3.1 Time schedule and major activity

JT-60 will be in operation in October, 1984 as shown in Table X.3-2. The heavy lines in this Table mean the critical path.

After the contract completed on April 17, 1978 with Hitachi, Ltd., the construction design and the fabrication of the machine and its auxiliary systems have been carried on as planned in these two years.

Through reexaminations of the recent experimental results from other currently operating devices and the experimental program of JT-60, the necessity of design changes was recognized for ensuring the experimental and operational flexibility. Therefore, several changes of the design specifications were proposed and determined, especially in connection with the design of the vacuum vessel.<sup>1)</sup> The contract for the design changes above mentioned was completed in June, 1979.

Further, there are some unsolved problems concerning the heat load from plasma. These problems are under investigation. Most difficult one seems to be how the inner surface of vacuum vessel can be protected from the heat load caused by Ripple Loss.

18 TF coils are located around a torus axis at regular intervals. Therefore 18 ripple well regions are formed. Some of NBI particles are to be trapped in these wells. The trapped particles go up (or down) caused by B drift. Consequently these particles hit the inner surface of vacuum vessel — this is called Ripple Loss.

Computer simulation<sup>2)</sup> shows that total ripple loss is 0.4 MW and maximum heat flux at the plasma surface is  $60 \sim 80 \text{ W/cm}^2$  in the condition of 0.35 % ripple rate at the plasma surface and 75 keV NBI energy. It is difficult to design a heat removal structure because of the complicated inner surface of vacuum vessel. In order to protect the vacuum vessel, the protection plates made of 20 mm thick molybdenum plate are proposed. Thermal and stress analyses in detail are planned in the next fiscal year.

### 3.2 Status of machine components

#### 3.2.1 Vacuum vessel

The basic design of the vacuum vessel was almost complicated in the last fiscal year<sup>1)</sup> and in this fiscal year the fabrication design of the vacuum vessel, ports and support arms etc. were performed in details. The specifications are summarized at page 186 of Reference 1). And the cross sectional view of the vacuum vessel is shown in Fig. X.3-1.

The vacuum vessel consists of eight rigid rings and eight bellows. The thickness of the bellows was changed from 2.5 mm to 2.7 mm in order to decrease the primary stress.

The vacuum vessel is provided with a demountable section for assembly and disassembly of the machine. In the first design, the demountable section consisted of a welded seal with thin plate and clip joints. But, the clip joints were thought to become loose by cyclic thermal expansion. Hence the structure of the demountable section was changed from the clip joints to the welded joints. In addition to the seal method, the thickness of the section was reduced to an appropriate value for easy demountableness.

Ports have welded bellows in order to absorb the deflection of the rigid ring by thermal expansion and electro-magnetic force. The bellows structure is twisted around the port axis by the electro-magnetic force of the port. A test was planned to evaluate the bellows strength against the twisting moment. The result will be used for the final design of the ports.

The temperature of the vacuum vessel is controlled by electric heater for heating and by  $\text{N}_2$  gas and water for cooling. The control system

including monitoring sensors was almost decided in consideration of safety, reliability and efficiency etc. of the components. The cooling capacity of the magnetic limiter plate was upgraded from  $5 \text{ MW} \times 5 \text{ sec}$  to  $20 \text{ MW} \times 5 \text{ sec}$ .

The surface temperature of the vacuum vessel was designed to be less than  $200^\circ\text{C}$  in natural convection in order to protect the poloidal field coils closely located around the vacuum vessel. And in addition, fans are to be mounted at the lower support structure, in order to cool the coils in emergent condition.

Fabrication of the rigid rings was started. The rigid ring is fabricated from 65 mm thick Inconel 625 plates by hot press and electron beam welding.

### 3.2.2 First wall

In this F.Y., the design conditions of the first wall, mainly the heat loads, were reviewed in respect of the plasma-machine interaction and the design modifications were discussed. Main items are as follows, (a) the increase of the heat removal capacity of the magnetic limiter system, (b) the design modification of the liner around the magnetic limiter coil, (c) the estimation of heat load to the liner around the magnetic limiter coil in case of magnetic limiter operation, (d) the design modification of the toroidal fixed limiter, and (e) the provision for the localized deposition of the ripple loss.

Details are as follows.

- (a) The original design specification of the heat load to the magnetic limiter plate is  $5 \text{ MW} \times 5 \text{ sec}$  (guaranteed). This specification was modified to 5 MW (guaranteed value) and 20 MW (target value). According to thermal analysis, the maximum temperature of the magnetic limiter plate in the case of  $20 \text{ MW} \times 5 \text{ sec}$  is about  $900^\circ\text{C}$ . In this condition, the deterioration of Mo plate strength due to recrystallization is occurred. Further study as the thermo-mechanical analysis is necessary.
- (b) In case of the plasma disruption with the time constant of 1 msec, the induced electromagnetic force at the liner around the magnetic limiter coil is very large, which overhangs the magnetic limiter coil from the v.v.. Therefore, the design was modified for the liner to attach directly to the magnetic limiter coil can.

- (c) In case of the modified heat load to the magnetic limiter plate (20 MW), the heat load is estimated to be about  $80 \text{ W/cm}^2$ . Because this value exceeds the permissible heat flux of the liner, the provision to reduce the heat load is necessary. Therefore, the design of the poloidal fixed limiter is under investigation.
- (d) At the present design, seventeen toroidal fixed limiters are attached to the rigid ring by bolts from the plasma side. But, this attaching method is not desirable from the point of view of evaporation and arcing. Therefore, the toroidal fixed limiter is modified as shown in Fig. X.3-2.

In case of plasma disruption with the time constant of 1 msec, the mechanical stress of the toroidal fixed limiter overhanging the bellows is greater than the yield stress of Mo. At the positions of these limiters, the temperature differences between the surface and the back side of the vacuum vessel exceed  $200^\circ\text{C}$  after several shots due to the heat flow from the limiters and the thermal stress becomes serious problem. Therefore, the toroidal fixed limiters overhanging the bellows were removed.

- (e) According to the estimation of the ripple-loss by K. Tani<sup>2)</sup>, the loss particles localize in a specific area of  $20^\circ \sim 50^\circ$  poloidal angle. The average and peak heat deposition reach about  $20 \sim 30 \text{ W/cm}^2$  and  $60 \sim 80 \text{ W/cm}^2$ , respectively. Therefore, thick molybdenum plates are attached to protect the vacuum vessel.

### 3.2.3 Toroidal field coils

Fabrication techniques have been established through R & D<sup>3)</sup> carried out from 1975 to 1976. A flow chart of the fabrication process is roughly shown in Fig. X.3-3. And main fabrication processes are shown in Photo. X.3-1 - Photo. X.3-4.

At present day in March 1980, nine TF coils have been fabricated. Though the specified tensile strength of the conductor material containing 0.2 % silver is  $33 \text{ kg/mm}^2$ , the measured value have an average strength of  $35.3 \text{ kg/mm}^2$  and can be fitted by the normal distribution whose standard deviation is  $0.7 \text{ kg/mm}^2$ .

Mechanical strength of the brazed joints with initial defects was discussed on the basis of Fracture Mechanics theory and results of the fatigue crack growth test<sup>4)</sup>. According to the ultrasonic inspection

results for the brazed joints more than 1,300, only eighteen defects of  $\phi 6$  mm -  $\phi 10$  mm and only one defect of  $\phi 10$  mm -  $\phi 15$  mm were detected, and most of the brazed joints had no defect. An error in measurement in winding conductors is measured only 2 - 3 mm. This error is consistent with the assumption in error field.

The inspection and test results convinced us that TF coils satisfy sufficiently the requested performance.

And the reliability tests, which are the preload test of a pancake coil without ground insulation, and a simulation test using the first coil block composed of two pancake coils and a supporting case were performed. In this simulation test, four different modes of load were selected. Through the preload test and simulation test, the followings have been confirmed.

- (1) The preload test has a useful effect to the brazed parts.
- (2) It is possible to understand the soundness of the layer insulation by the strain distribution of the conductor at the preload test.
- (3) It was observed that the load on the ground insulation was transmitted to the supporting case.
- (4) The maximum temperature rise of the conductors at the wedge-shaped section was never false to the expected value.
- (5) The reliability of the TF coil system has been confirmed.

#### 3.2.4 Poloidal field coils

The poloidal field (PF) coils consist of five coil systems; ohmic heating coils (OH coils), vertical field coils (V coils), quadrupole field coils (Q coils), horizontal field coils (H coils), and magnetic limiter coils (M coils). The first four coils are placed between the toroidal field (TF) coils and the vacuum vessel (VV) to satisfy the required magnetic field conditions and provide access to the VV for the diagnostic ports. Each turn of the PF coils must have a welded joint on site caused by the geometrical relation with TF coils. The coils are attached to the frames in such a way that they can expand in the radial direction and the vertical force acting on the coils is transferred to the frames. The hoop force is supported by the conductors themselves.

The M coils are placed inside the VV and composed of 3 coils; one

8-turn main coil and two 4-turn subcoils. The coils are incased in the vacuum-tight Inc 625 case, consisting of bellows and 32 rigid rings with which the coils are supported in the vessel.

The construction design of the PF coils has been continued. The specifications and the arrangement of the coils are not changed from those reported in ref. 1) and shown in Table X.3-3 and Fig. X.3-4, respectively. The magnetic fields and the electromagnetic forces were estimated on the basis of the above arrangement. Stress analysis and thermal analysis were also performed not only for the regular part of the coils but also for the welded joint and the turn-to-turn connecting part of the coils. The design of the monitoring system, the grounding system, the electrical protection system and the feeders for the PF coils were started.

Together with these design works, the outline of the fabrication procedures and inspection methods were established. The arrangement and the cross-section of the conductors which are placed inner side of the torus were determined through these considerations. The specification documents for the purchase of the conductors and the cooling pipes were prepared. The orders of the conductors which are used for the coils less than 3 mm in diameter were finished. The fabrication of the conductors was started on July, 1979 at HITACHI Cable Co., Ltd. Following inspections, the completed conductors were transported to HITACHI Co., Ltd. The transportation of about 20 % of the conductors has been completed by the end of March 1980. The fabrication of the smallest diameter coil (F-13) was started.

The MIG welding technique of the copper conductors has almost been established and applied to the fabrication of the F-13 block. The development of the TIG welding technique for the connection of the joint on site are now underway.

Mecahnical and electrical tests of the coil insulations were performed for the samples which were irradiated up to  $10^9$  rads by  $^{60}\text{Co}$ -gamma rays. The results are shown in Fig. X.3-5, indicating that no significant change in tensile strength and breakdown voltage occurred, while elongations decrease as the increase in the irradiation dose. Preliminary fatigue test of the irradiated samples have also been performed and showed that the irradiated samples have almost the same properties as those of the non-irradiated ones.

The extensive examinations have been made on the magnetic limiter such

as the magnetic field configuration in the vicinity of the M coils, scrape-off layer width, heat flow to the liners attached to the cans, the effect of the fixed limiter position on the divertor efficiency, plasma control and monitoring system, and so on. As a result, the value of about 10 cm for the throat width was determined.

### 3.2.5 Support structures

Construction design of the support structures was almost completed. All of the components of the support structures are made from non-magnetic steel which has superior mechanical properties except the ball-jointed section of the support column of the vacuum vessel. The designed stress of each component is far below the allowable one except the central column.

Fabrication is now in progress without any trouble and will be completed by May in 1981.

### 3.2.6 Vacuum pumping system

#### (1) Functional requirements

Requirements for JT-60 vacuum pumping system are as follows;

- 1) to evacuate the torus in ultra high vacuum
- 2) to remove impurities liberated during bake-out, high temperature oxidation and hydrogen reduction, and discharge cleaning of vacuum vessel interior
- 3) to pump the past plasma constituents within the interval between plasma pulses — the interval is ten minutes
- 4) to operate continuously and reliably for long periods of time — at least two weeks
- 5) to minimize contamination of the torus by the vacuum pumps

#### (2) Configuration

In order to fulfill the above requirements, a turbomolecular pump system have been selected. Its configuration is schematically shown in Fig. X.3-6.

This system has four identical sets each connected to a pumping port of vacuum vessel. One set consists of a manifold, main pumping subsystem, rough pumping subsystem and maintenance pumping subsystem. Total pumping speed of each subsystem is required as shown in Table X.3-4.

The main pumping system has the pumping speed of 13,600 liters/sec

for nitrogen and 29,000 liters/sec for hydrogen. This system is used in the pressure range of less than  $10^{-2}$  Torr.

The rough pumping system evacuate the vacuum vessel from atmospheric pressure to  $10^{-2}$  Torr. Its pumping speed is from 120 liters/sec to 1,400 liters/sec. This subsystem is also used in oxidation and hydrogen reduction of vacuum vessel interior.

Maintenance pumping system keeps the vacuum vessel in high vacuum during suspension of operation. In addition, peripheral subsystems such as compressed air supply subsystem, cooling water supply subsystem, dry nitrogen supply subsystem, liquid nitrogen supply subsystem, pressure measurement subsystem and control subsystem are to be provided in order to support each pumping subsystem.

### (3) Problems related to the components

There are 2 main problems. One is related to large bakable gate valves. And the other is related to turbomolecular pumps.

#### 1) 40-cm ID all metal gate valve

40-cm ID all metal gate valves are needed to isolate the pumping system from the vacuum vessel. The specific requirements for valves are as follows;

- bake out over 250 °C
- helium leakage across the seat seal of less than  $1 \times 10^{-7}$  Torr-liters/sec
- operating life over 200

#### 2) Turbomolecular pump

We selected Leibold-Heraeus TurboVac 3500 TMPs as first stage ones and Leibold-Heraeus TurboVac 450 TMPs as second stage ones.

Possible disadvantages of the use of the pumps in JT-60 include the heating of the rotor caused by eddy current induced in high magnetic field and fear about endurance in rather high pressure (especially for second stage TMPs).

In JT-60, the magnetic field at the position of turbomolecular pumps in JT-60 is about 200 Gauss. And moreover tests in TFTR were examined. Therefore the turbomolecular pumps can be used safely.

Turbomolecular pumps evacuate the torus from the pressure of  $10^{-2}$  Torr. It is calculated to take 20 minutes to evacuate the torus



to the pressure of  $10^{-3}$  Torr.

The tests of turbomolecular pumps in high pressure of about  $10^{-2}$  Torr were carried out. From the results as shown in Table X.3-5, we can use the turbomolecular pump from the pressure of  $10^{-2}$  Torr in JT-60.

### 3.2.7 Primary cooling system<sup>1)</sup>

In this F.Y. the rationalization of the cooling system was advanced. Specifications of the primary cooling system are summarized in Table X.3-6, and flow diagram of the cooling system is shown in Fig. X.3-7.

Total flow rate for coil cooling subsystem was reduced from 200 m<sup>3</sup>/hr to 1480 m<sup>3</sup>/hr by separating the purification system and the maximum pressure was also reduced from 16 kg/cm<sup>2</sup> to 14 kg/cm<sup>2</sup>.

Fabrication of heat exchangers and other components was started.

### 3.2.8 Fast movable limiter

Fabrication design is now in progress to be completed in Oct. 1980. Because that the most of details on design and fabrication techniques were established in the engineering development, main efforts have been made for the geometrical interference with the diagnostic instruments and support structures. The analysis of vibration due to impulsive electromagnetic load exerted on support structures is now carried out. The design about the controller of movable limiter is little behind the schedule. But, fabrication will be expected to start without any delay.

### 3.2.9 Adjustable movable limiter

In accordance with the experimental and operational necessity a pair of adjustable movable limiter is to be installed in the vicinity of the sub-magnetic limiter coils. It provides the protection of the submagnetic limiter coils, the control of the plasma diameter and the research on the limiter materials.

The schematic view of the adjustable movable limiter is shown in Fig. X.3-8. The limiter head, which is to be made of the same material as the fixed limiter, is cooled by air forcedly and easily remountable with the vacuum vessel kept in ultra high vacuum circumstances.

Adjustable limiter contracted in June 1979 is now under the fabrication design to be completed in Oct. 1980.

### 3.2.10 Gas feed system

The gas feed system consists of four subsystems: a main feed system, an auxiliary feed system, and two impurity feed systems. The gases (H, He, Ne, O, and Ar) feed to the vacuum vessel are controlled by fast magnetic valves (FMV) and piezo-electric valves (PEV).

In order to examine the applicability of the PEV to JT-60, which was developed for use in TFTR (PPPL), one valve was loaned from PPPL and arrived at JAERI in June, 1979. However, its piezo element was broken during transportation. After the repair work was completed in February using repair parts received from TFTR, the performance test was carried out successfully.

### 3.2.11 Preionization system

Preionization system aims at producing a weekly-ionized plasma before discharge. Two types of preionization methods are adopted, i.e., electron gun type and  $\vec{J} \times \vec{B}$  plasma gun type.

### 3.2.12 Machine control system

In this F.Y., the design of control system was reexamined. Carrying out the work, micro-computerized CAMAC system was introduced for interface between Zenkei and machine control system, as shown in Fig. X.3-9. The main features of the machine control system are as follows:

- 1) The micro-computerized CAMAC system is constructed in a serial high-way configuration.
- 2) The STU (Serial Signal Transmission Unit) system is used as a back up to the CAMAC system.
- 3) The subconsole, man-machine interface of the machine control system, has cathode ray tube (CRT) to display the entire system informations.
- 4) Control system including CAMAC system has to work under severe electric surge and noise conditions.
- 5) The interlock system is made of hard-wired circuit aries.

## 3.3 Related Studies

### 3.3.1 Dynamic response analysis of the vacuum vessel

Eddy currents induced on the vacuum vessel have generally shorter time duration than the natural period of the vacuum vessel, so the dynamic

response of the vacuum vessel against the electromagnetic force is of great concern for machine design. Especially, saddle-like electromagnetic force — caused by the interaction between the poloidal component of the eddy current and the toroidal magnetic field — is predominant among all and is predicted to cause a high stress of the bellows.

Therefore, dynamic response analysis against the saddle-like electromagnetic force was carried out using three dimensional finite element method. The dynamic response of the bellows was computed by dividing it into three components; the first caused by the forced deflection due to the displacement of the adjacent rigid ring, the second caused by the saddle-like electromagnetic force acting on the bellows and the last caused by the inertia force acting on the bellows<sup>5)</sup>.

The results of the dynamic response analysis showed that the maximum deflection of the rigid ring, whose time behavior is shown in Fig. X.3-10, is about 3.2 mm in case of plasma disruption with time constant of 1 msec<sup>6)</sup> and computed stresses of the vacuum vessel are below the allowable one from the view point of fatigue fracture<sup>7)</sup>.

### 3.3.2 Studies of eddy currents induced on the vacuum vessel

Continuing efforts for the study of eddy current have been made in JT-60 design calculations with aid of numerical codes EDDYTORS and EDDYACT which were checked on the experimental results using a scale model<sup>8,9,10)</sup>. A suitable model for 1 msec current disruption provides the reasonable results of eddy currents on the vacuum vessel and the structural component installed inside within a desired accuracy.

The eddy currents due to 1 msec current disruption on the vacuum vessel were evaluated including the shielding effect of passive poloidal coils, i.e. the ohmic heating coil and the vertical field coil, and those are shown in Fig. X.3-11. Figure X.3-11 shows that the shielding effect of the vertical coil largely suppresses the saddle-like current on the rigid section of JT-60. Because that the vacuum vessel acts as a main shield against a rapid change of the magnetic field, structural components installed inside the vacuum vessel, such as a liner, the magnetic limiter plate and the magnetic limiter can, receive different electromotive forces from those without the current shield of the vacuum vessel. Figure X.3-12 shows the distribution of the magnetic field without the shielding effect of the vacuum vessel and Fig. X.3-13 shows that with the shielding effect.

One can easily find out from those figures that the larger electromotive force due to 1 msec current disruption loads on the component placed at outside of torus<sup>11)</sup>.

### 3.3.3 Wire type strain gauge under high temperatures and strong magnetic field

Development of resistance wire type strain gauges usable for JT-60 at high temperatures and strong magnetic field have been carried out. The developed gauges were tested at temperatures between room temperatures and 520 °C and the change rate of magnetic field between 216  $\mu\text{e}/\text{sec}$  and 1634  $\mu\text{e}/\text{sec}$ ; Zero drifts, linearities, change of gauge factors, insulation resistance, creep characteristics and effects of fatigue were examined. The following have been made clear.

- 1) Strain gauges with 6.25 mmR curvature and sensing element of nichrome U have been developed.
- 2) Induced apparent strains by the change of the magnetic field are dependent on the incline of the wire gauge to the magnetic field line.
- 3) Maximum induced apparent strain of 100  $\mu\text{e}$  was measured at the magnetic field change rate of 1600  $\mu\text{e}/\text{sec}$ .
- 4) Twisted lead wire is more desirable to compensate the induced apparent strain than the parallel ones.
- 5) Drift rate is less than 10  $\mu\text{e}/\text{hr}$  at 500 °C.

### References

- 1) Fusion Research and Development Center: JAERI-M 8661 (1980)
- 2) Tani, K., Azumi, M., Kishimoto, H., and Tamura, S.: To be published in Nucl. Fusion
- 3) Ohkubo, M., Kawasaki, K., Nishio, S., Ando, T., Ohta, M., Yoshikawa, M., Kazawa, Y., Saito, R., Matsui, A.: J. At. Energy Soc. Japan Vol.20 No.3 pp.195~206 (1978)
- 4) Nishio, S., Ohkubo, M., Sasajima, H.: JAERI-M 8822 (1980)
- 5) Udoguchi, T., Takatsu, H., Shimizu, M., Ohta, M., Minami, M., Uchino, K.: To be published in Proc. 11th SOFT (1980)
- 6) Takatsu, H., Shimizu, M., Ohta, M.: To be published

- 7) Takatsu, H., Shimizu, M., Ohta, M.: To be published
- 8) Kameari, A., Ninomiya, H., Suzuki, Y.: JAERI-M 6953 (1977)
- 9) Kameari, A., Suzuki, Y.: Proceeding of 7th Symposium on Engineering Problems of Fusion Research, P-1386 (Oct. 1977)
- 10) Ninomiya, H., Nakamura, Y., Ozeki, &., Kameari, A., Tsuzuki, N., Sometani, T.: Proceeding of 8th Symposium on Engineering Problems of Fusion Research, (Nov. 1979)
- 11) Ozeki, T., Nakamura, Y.: To be published in JAERI-M.

Table X.3-1 Operation modes and design conditions

| Operation mode          | Full power      | 50% rated         | Discharge cleaning<br>with longer duration | Discharge cleaning<br>with shorter duration |
|-------------------------|-----------------|-------------------|--|---|
| Plasma current          | 2.7 MA          | 1.35 MA           | $\sim 0.8$ MA                              | $\sim 80$ kA                                |
| Toroidal field          | 45 kG           | 22.5 kG           | $\sim 10$ kG                               | $\sim 10$ kG                                |
| Poloidal field coils    | 100 %           | 50 %              | $\sim 30$ %                                | $\sim 10$ %                                 |
| Plasma current duration | 5 sec           | -                 | $\sim 1$ sec                               | $\sim 25$ msec                              |
| Interval between shots  | 10 min          | -                 | $\sim 2$ min                               | $\sim 0.3$ sec                              |
| Total shots             | $5 \times 10^4$ | $1.5 \times 10^5$ | $10^5$                                     | -   |

Table X.3-3 Time schedule of tokamak system (JT-60)

| PARAMETER                                    | OH Coil | V Coil     | II Coil    | Q Coil    | M Coil      |
|--|---------|------------|------------|-----------|-------------|
| AMPERE TURNS (MAT)                           | 5.5     | $\pm 1.84$ | $\pm 0.12$ | $\pm 0.5$ | $\pm 0.755$ |
| TOTAL TURNS                                  | 60      | 64         | 12         | 40        | 16          |
| MAX. CURRENT (KA)                            | 91.7    | 57.5       | 20         | 25        | 94.4        |
| L (MH)                                       | 8.3     | 9.9        | 0.44       | 3.2       | 0.88        |
| R (M $\Omega$ )* (AT 75°C)                   | 4.6     | 12.1       | 5.0        | 17.4      | 3.2         |
| TIME CONSTANT (SEC)                          | 1.8     | 0.82       | 0.09       | 0.18      | 0.28        |
| R-I <sup>2</sup> (MW)                        | 38.7    | 40.0       | 2.0        | 10.9      | 28.5        |
| 1/2-LI <sup>2</sup> (MJ)                     | 34.9    | 16.4       | 0.09       | 1.0       | 3.9         |
| EQUIVALENT SQUARE<br>WAVE PULSE LENGTH (SEC) | 8       | 6          | 7          | 7         | 6           |

\* NOT INCLUDING FEEDERS

Table X.3-2 Poloidal field coil specifications

| F.Y.<br>(APR MAR) |                                       | 1978                      |   |   |   | 1979 |   |   |   | 1980 |   |   |   | 1981 |   |   |   | 1982 |   |   |   | 1983 |   |   |   | 1984 |  |  |  |
|-------------------|---------------------------------------|---------------------------|---|---|---|------|---|---|---|------|---|---|---|------|---|---|---|------|---|---|---|------|---|---|---|------|--|--|--|
| ITEMS             |                                       | 1                         | 2 | 3 | 4 | 1    | 2 | 3 | 4 | 1    | 2 | 3 | 4 | 1    | 2 | 3 | 4 | 1    | 2 | 3 | 4 | 1    | 2 | 3 | 4 | 1    |  |  |  |
| NO                | MAIN EVENTS                           | CONTRACT                  |   |   |   |      |   |   |   |      |   |   |   |      |   |   |   |      |   |   |   |      |   |   |   |      |  |  |  |
| 1                 | MAIN EVENTS                           | ▽                         |   |   |   |      |   |   |   |      |   |   |   |      |   |   |   |      |   |   |   |      |   |   |   |      |  |  |  |
| 2                 | VACUUM VESSEL                         | D M F AS TI TR INST FA BT |   |   |   |      |   |   |   |      |   |   |   |      |   |   |   |      |   |   |   |      |   |   |   |      |  |  |  |
| 3                 | TOROIDAL FIELD COILS                  | D M F AS TI TR INST FA BT |   |   |   |      |   |   |   |      |   |   |   |      |   |   |   |      |   |   |   |      |   |   |   |      |  |  |  |
| 4                 | POLOIDAL FIELD COILS                  | D M F AS TI TR INST FA BT |   |   |   |      |   |   |   |      |   |   |   |      |   |   |   |      |   |   |   |      |   |   |   |      |  |  |  |
| 5                 | SUPPORT STRUCTURE                     | D M F AS TI TR INST FA BT |   |   |   |      |   |   |   |      |   |   |   |      |   |   |   |      |   |   |   |      |   |   |   |      |  |  |  |
| 6                 | PRIMARY WATER COOLING SYSTEM          | D M F AS TI TR INST FA BT |   |   |   |      |   |   |   |      |   |   |   |      |   |   |   |      |   |   |   |      |   |   |   |      |  |  |  |
| 7                 | VACUUM PUMP -IMG SYSTEM               | D M F AS TI TR INST FA BT |   |   |   |      |   |   |   |      |   |   |   |      |   |   |   |      |   |   |   |      |   |   |   |      |  |  |  |
| 8                 | MACHINE CONTROL SYSTEM                | D M F AS TI TR INST FA BT |   |   |   |      |   |   |   |      |   |   |   |      |   |   |   |      |   |   |   |      |   |   |   |      |  |  |  |
| 9                 | GAS FEED SYSTEM, PREIONIZATION SYSTEM | D M F AS TI TR INST BT    |   |   |   |      |   |   |   |      |   |   |   |      |   |   |   |      |   |   |   |      |   |   |   |      |  |  |  |
| 10                | ELECTRO MAG -NETIC SENSORS            | D M F AS TI TR INST BT    |   |   |   |      |   |   |   |      |   |   |   |      |   |   |   |      |   |   |   |      |   |   |   |      |  |  |  |
| 11                | MOVABLE UNIT                          | D M F AS TI TR INST BT    |   |   |   |      |   |   |   |      |   |   |   |      |   |   |   |      |   |   |   |      |   |   |   |      |  |  |  |

D : DESIGN  
M : MATERIAL  
F : FABRICATION

AS : ASSEMBLING  
TI : TEST & INSPECTION  
TR : TRNSPORTATION

INST : INSTALLATION  
FA : FINAL ASSEMBLING  
BT : BLOCK CHECK & TEST

TT : TOKAMAK SYSTEM CHECK & TEST  
ITT : INTEGRATED TOKAMAK SYSTEM CHECK & TEST

Table X.3-4 Total pumping speed of each pumping system

| SYSTEM                        | PUMPING SPEED  | PRESSURE RANGE  |
|-------------------------------|--|---|
| MAIN PUMPING SYSTEM           | 13,600 l/sec ( N <sub>2</sub> )<br>29,000 l/sec ( H <sub>2</sub> ) | LESS THAN 1.33 PA<br>( 10 <sup>-2</sup> TORR )              |
| ROUGH PUMPING SYSTEM          | 120 ~ 1,400 l/sec  | ATMOSPHERIC PRESSURE<br>~ 1.33 PA ( 10 <sup>-2</sup> TORR ) |
| MAINTENANCE PUMPING<br>SYSTEM | 5,300 l/sec ( N <sub>2</sub> )<br>10,000 l/sec ( H <sub>2</sub> )  |   |

Table X.3-5 Test of TMP in the high pressure of 1.33 PA (10<sup>-2</sup> Torr)

| ITEM                | RESULT                 |
|---------------------|------------------------|
| 1) TEMPERATURE RISE |                        |
| • HOUSING           | 3 DEGREES              |
| • COOLING WATER     | 1 DEGREE               |
| • ROTOR             | LESS THAN 100°C        |
| 2) ROTATING SPEED   | CHANGE OF LESS THAN 1% |
| 3) PUMPING SPEED    | PLANNED VALUE IN JT-60 |

Table X.3-6 Specification of primary cooling system

|  |                      | Field coil system | Vacuum vessel system |
|--|----------------------|-------------------|----------------------|
| Total removal energy                           | MW                   | 18.4              | 0.9                  |
| Total water flow rate                          | m <sup>3</sup> /hr   | 1480              | 130                  |
| Maximum system pressure                        | kg/cm <sup>2</sup> G | 14                | 12                   |
| Number of pump                                 |                      | 4                 | 2                    |
| Number of heat exchanger                       |                      | 5                 | 1                    |
| Max. outlet temperature from<br>heat exchanger | °C                   |                   | 42                   |
| Resistivity of coolant                         | Ω-cm                 |                   | 10 <sup>5</sup>      |
| PH of coolant                                  |                      |                   | 5~9                  |



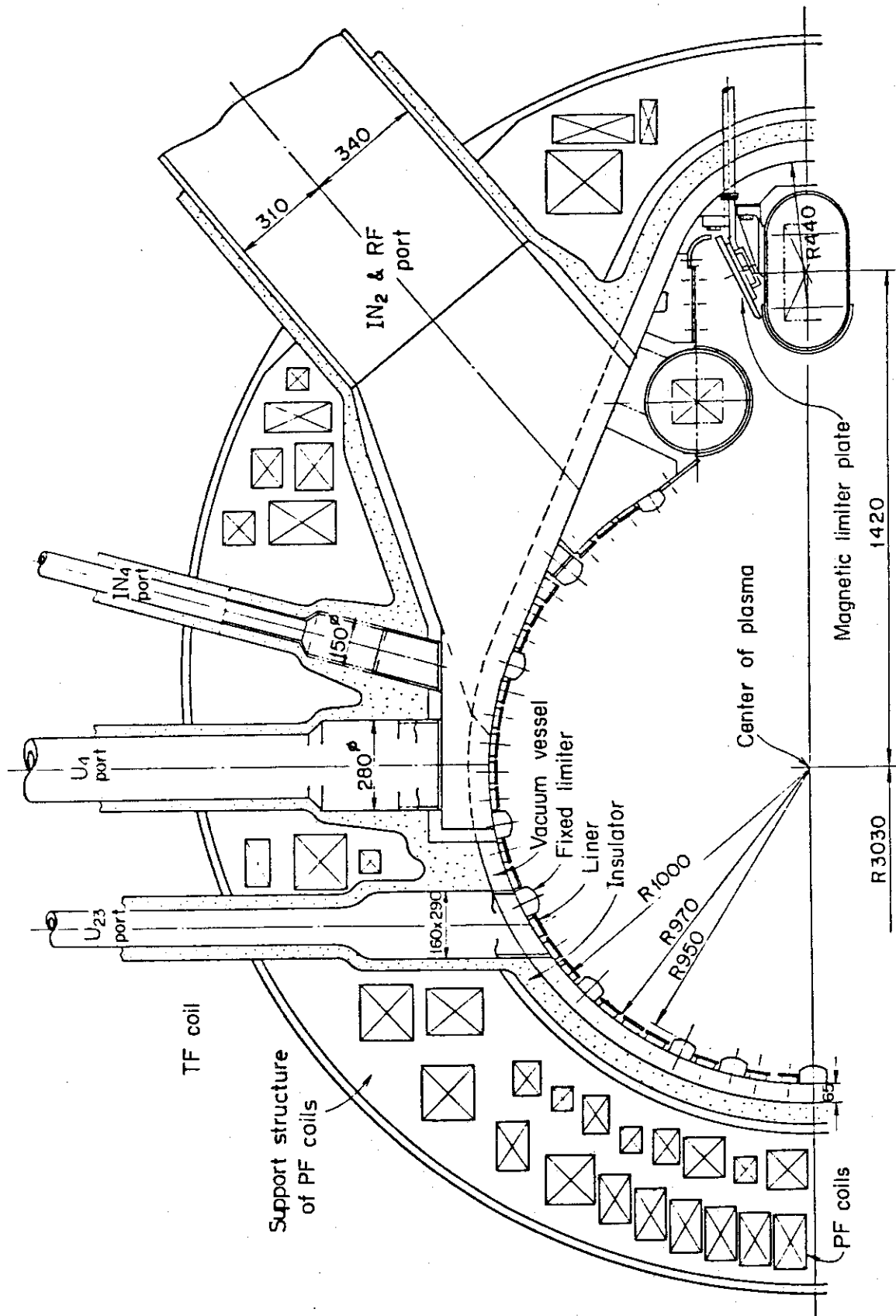


Fig. X.3-1 Crosssectional view of the vacuum vessel

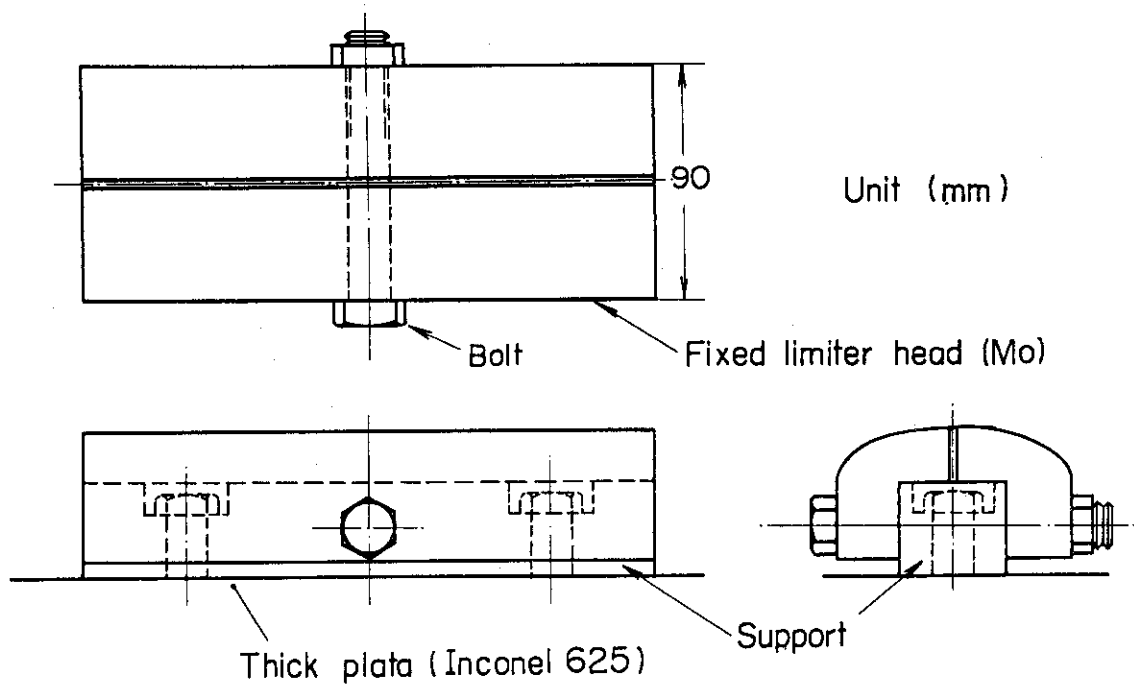


Fig. X.3-2 Toroidal fixed limiter

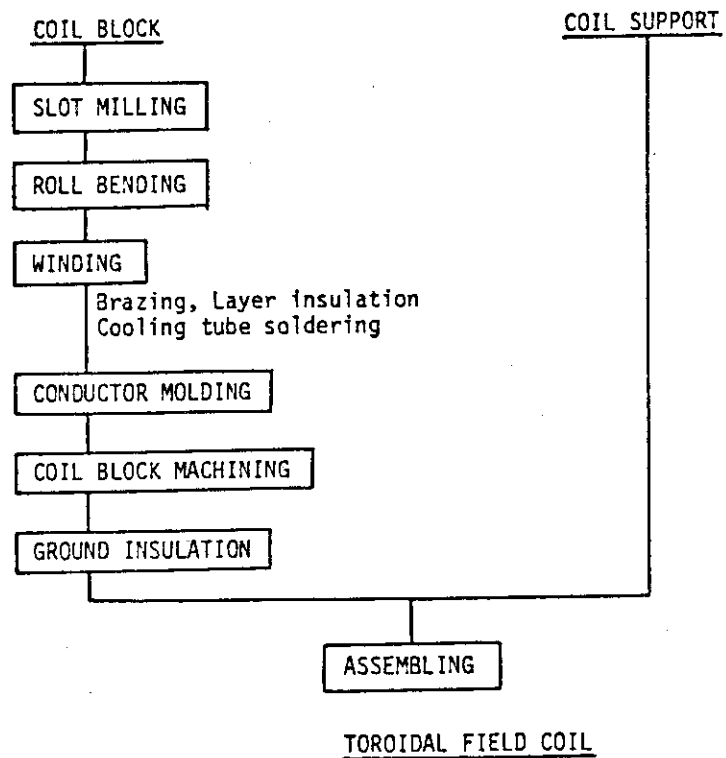


Fig. X.3-3 Fabrication procedure of TF coil

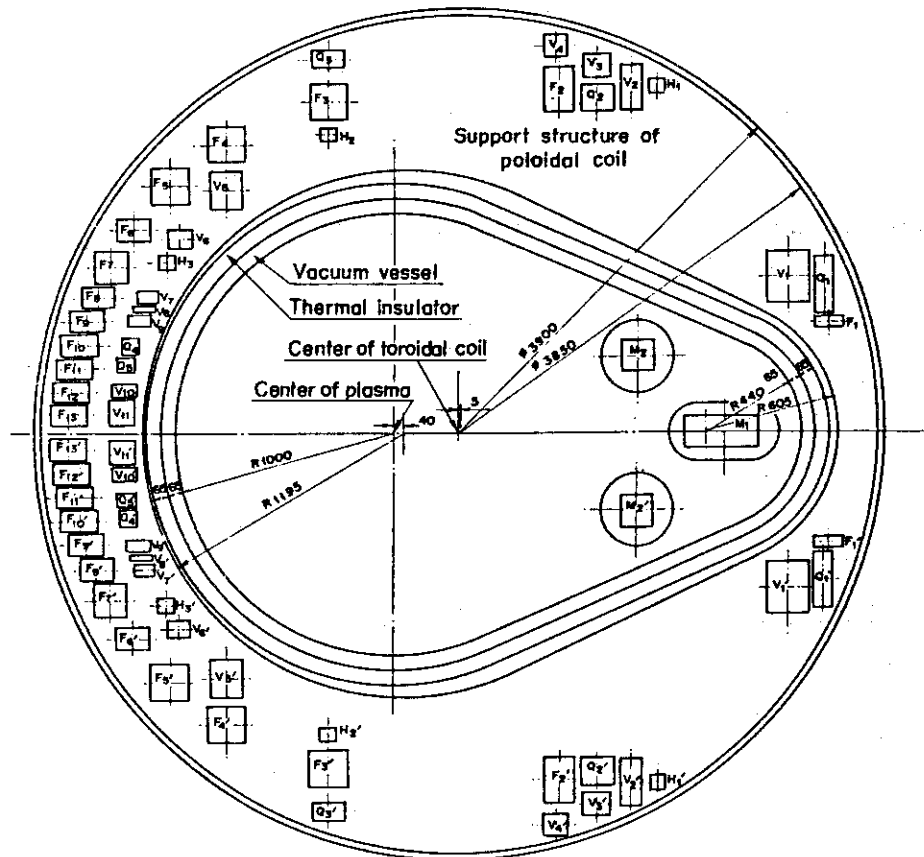
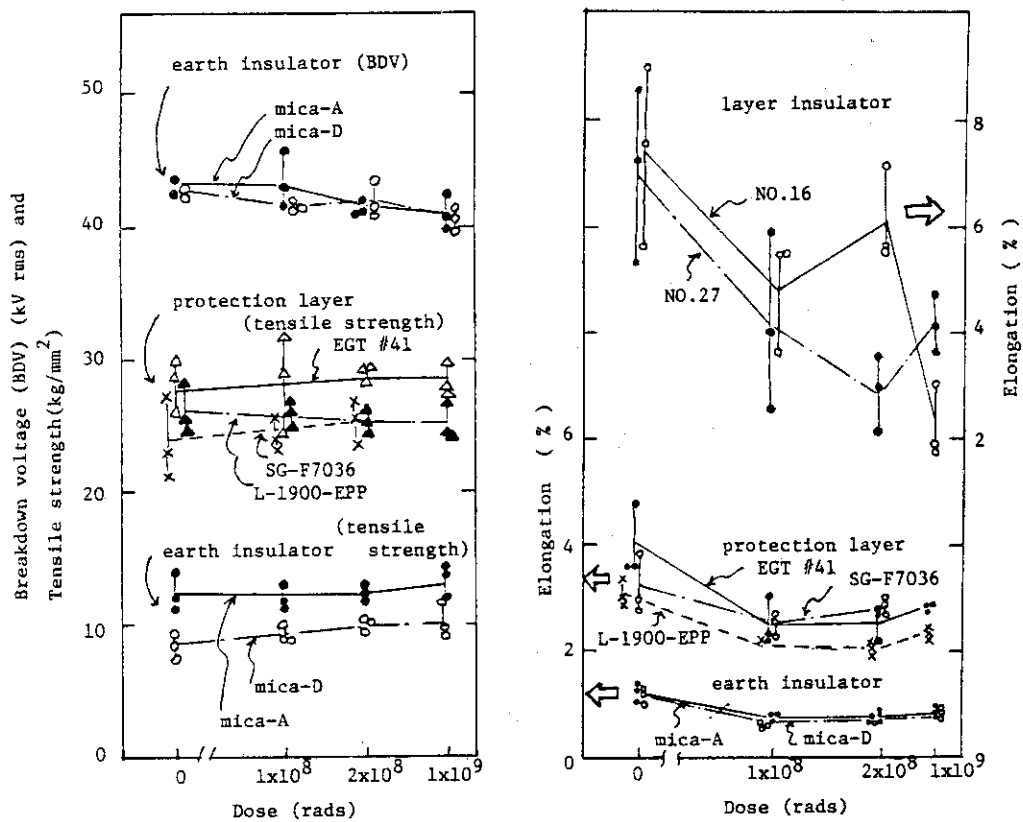


Fig. X.3-4 Poloidal field coil configurations

Fig. X.3-5 Mechanical and electrical characteristics of layer insulator, each insulator and protection layer before irradiation and after <sup>60</sup>Co gamma-ray irradiation.

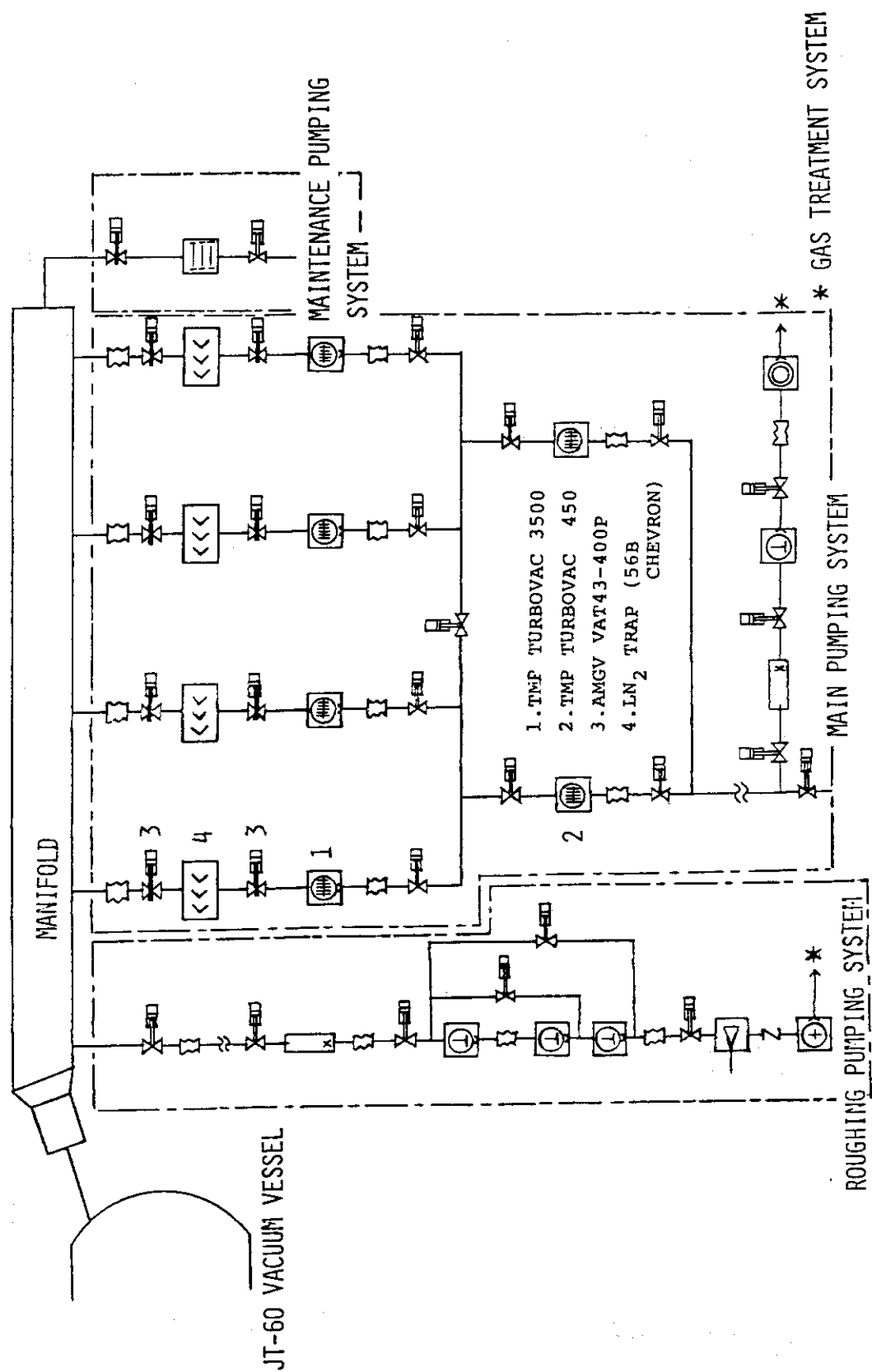


Fig. X.3-6 JT-60 vacuum pumping system configuration (1/4)

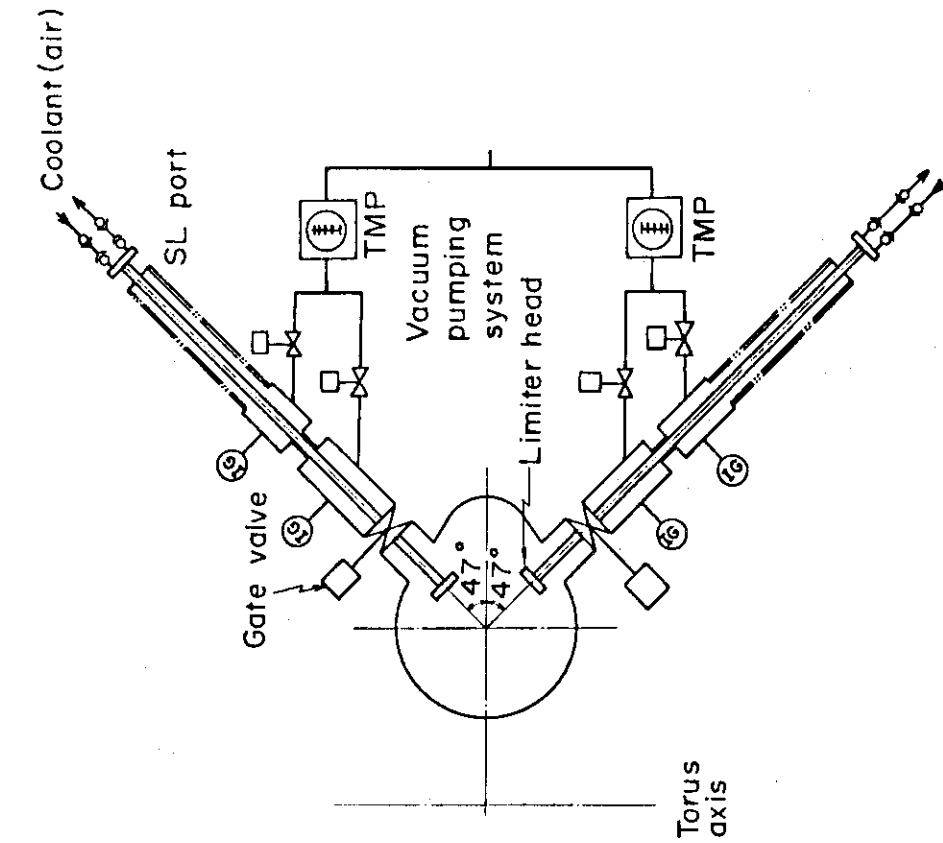


Fig. X.3-8 Schematic view of adjustable movable limiter

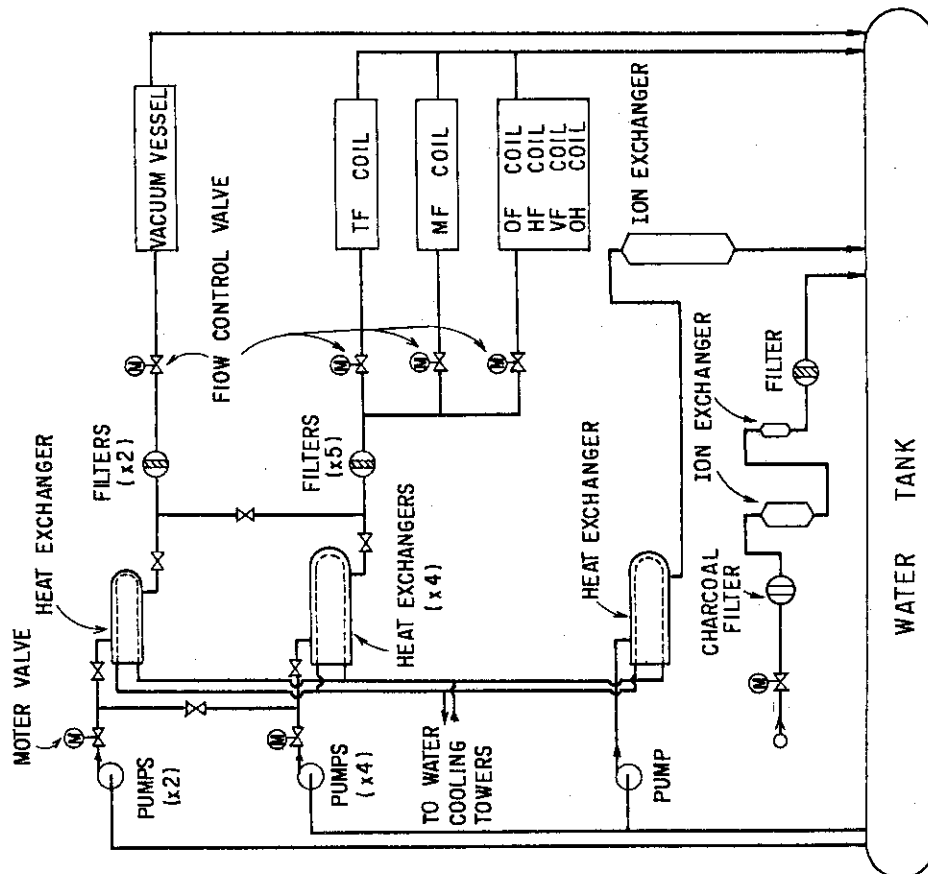


Fig. X.3-7 Primary cooling system

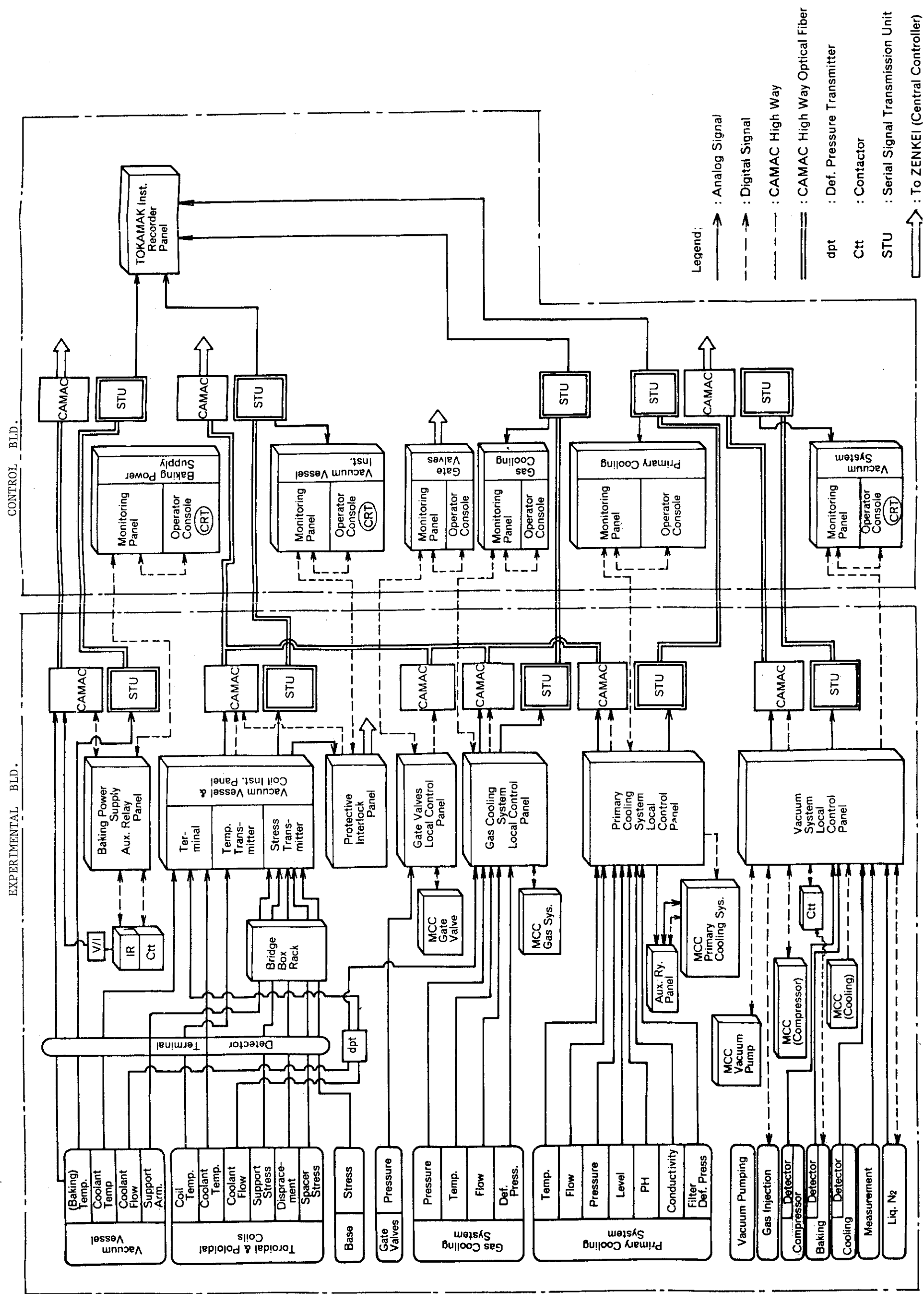


Fig. X.3-9 Machine-I control system configuration

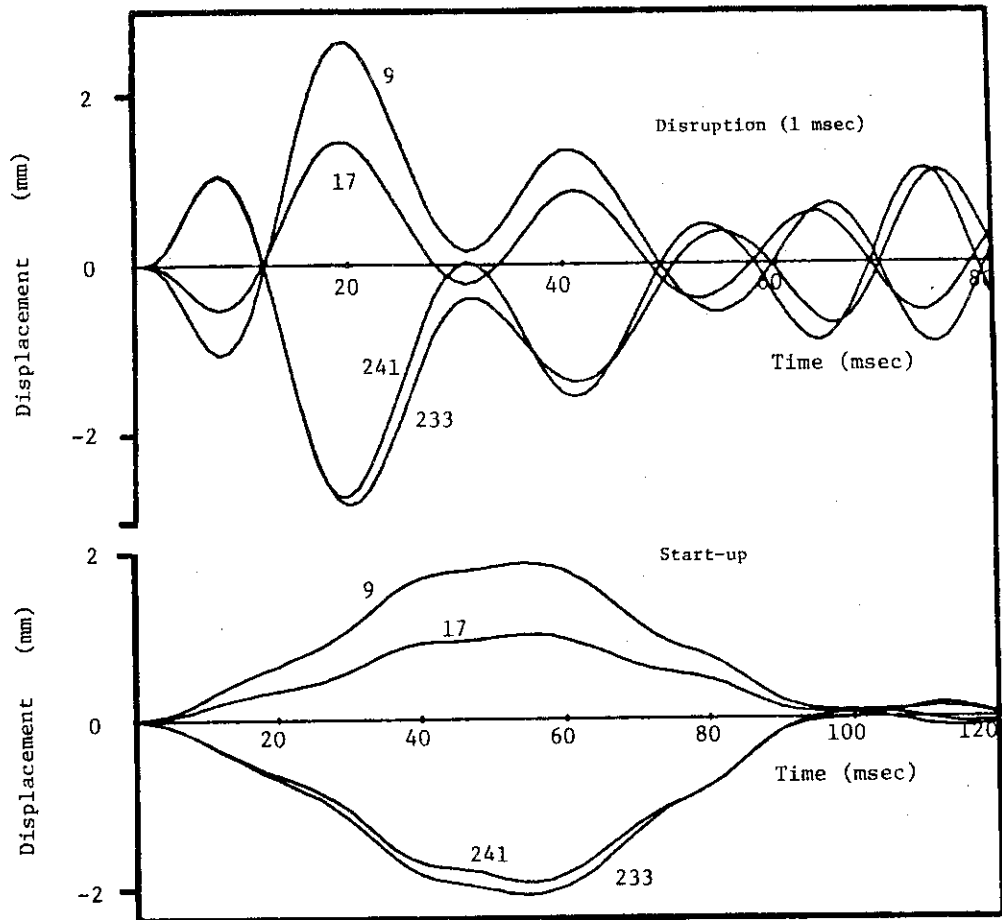


Fig. X.3-10 Displacement revolution of the rigid ring in case of plasma disruption on (1 msec) and start-up

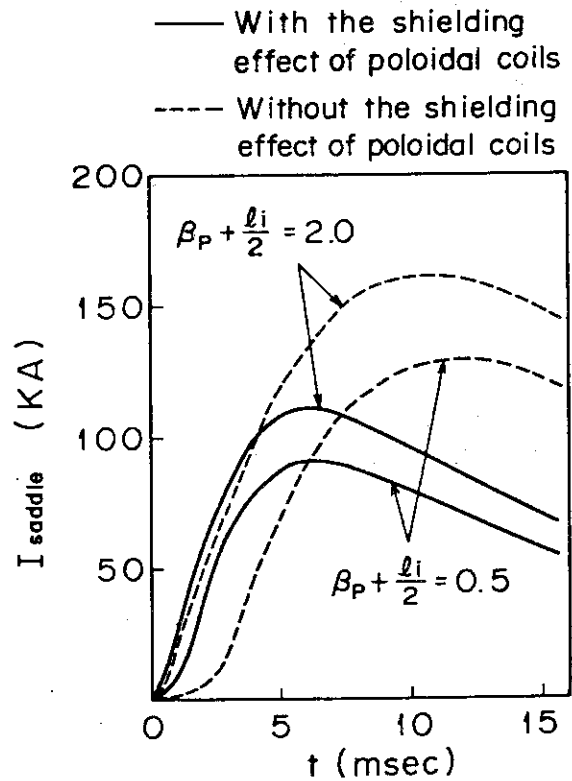


Fig. X.3-11 Saddle-like current due to the rapid disruption

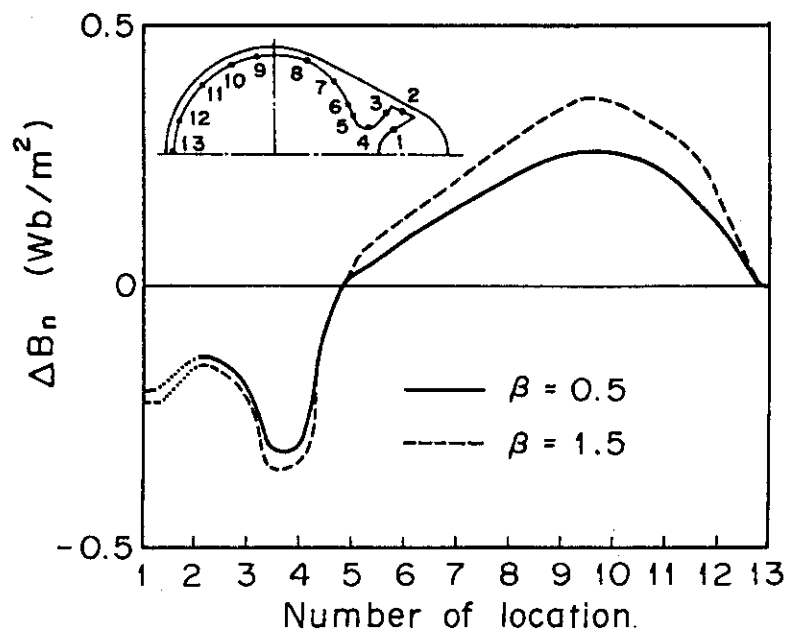


Fig. X.3-12 The magnetic field without the shielding effect of vacuum vessel

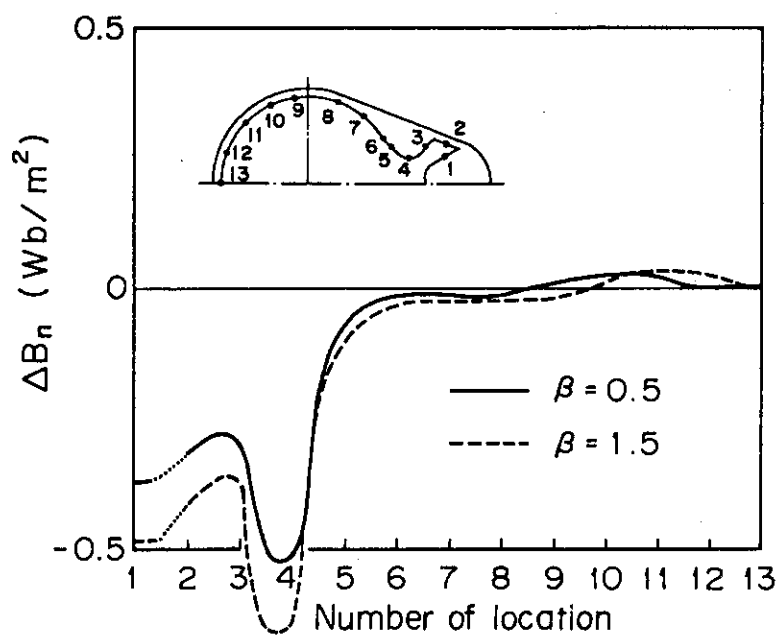


Fig. X.3-13 The magnetic field with the shielding effect of vacuum vessel



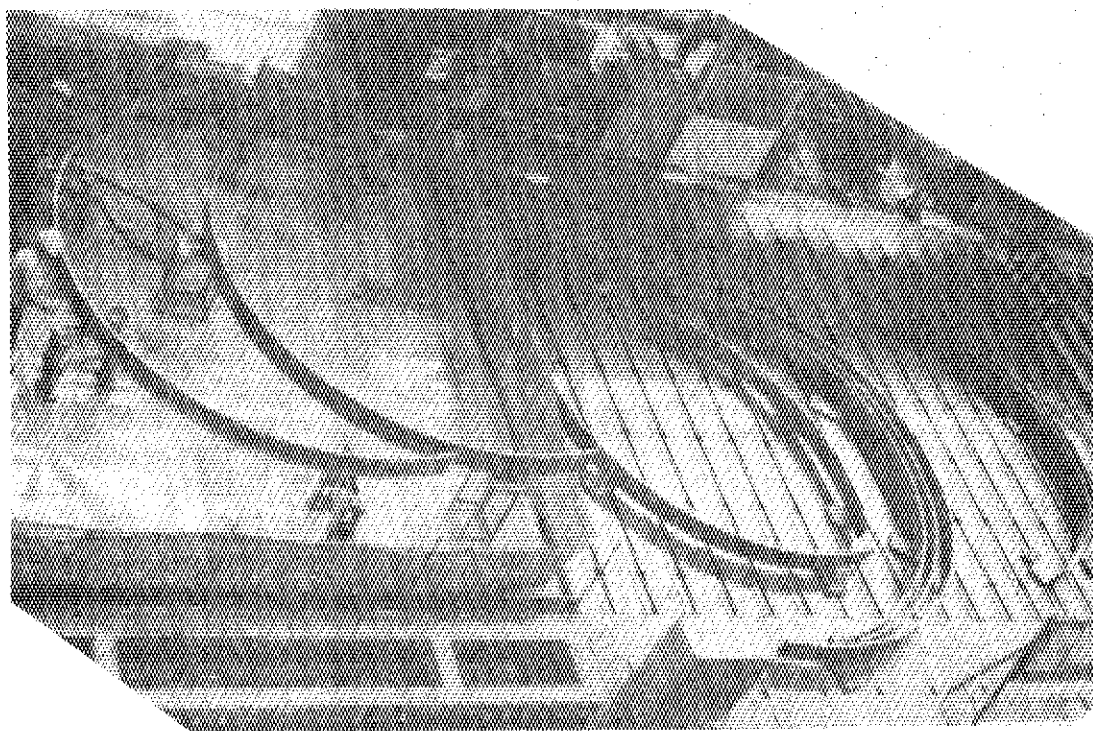


Photo. X.3-1 Bended conditions

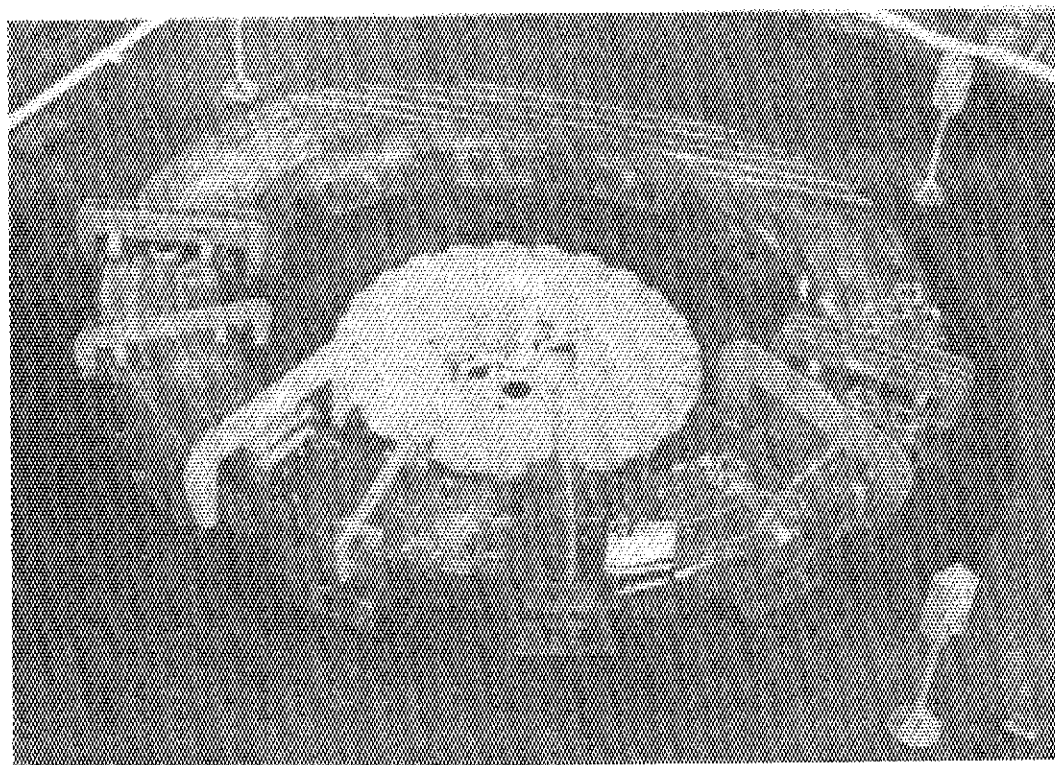


Photo. X.3-2 A pancake coil waiting for ground insulation process

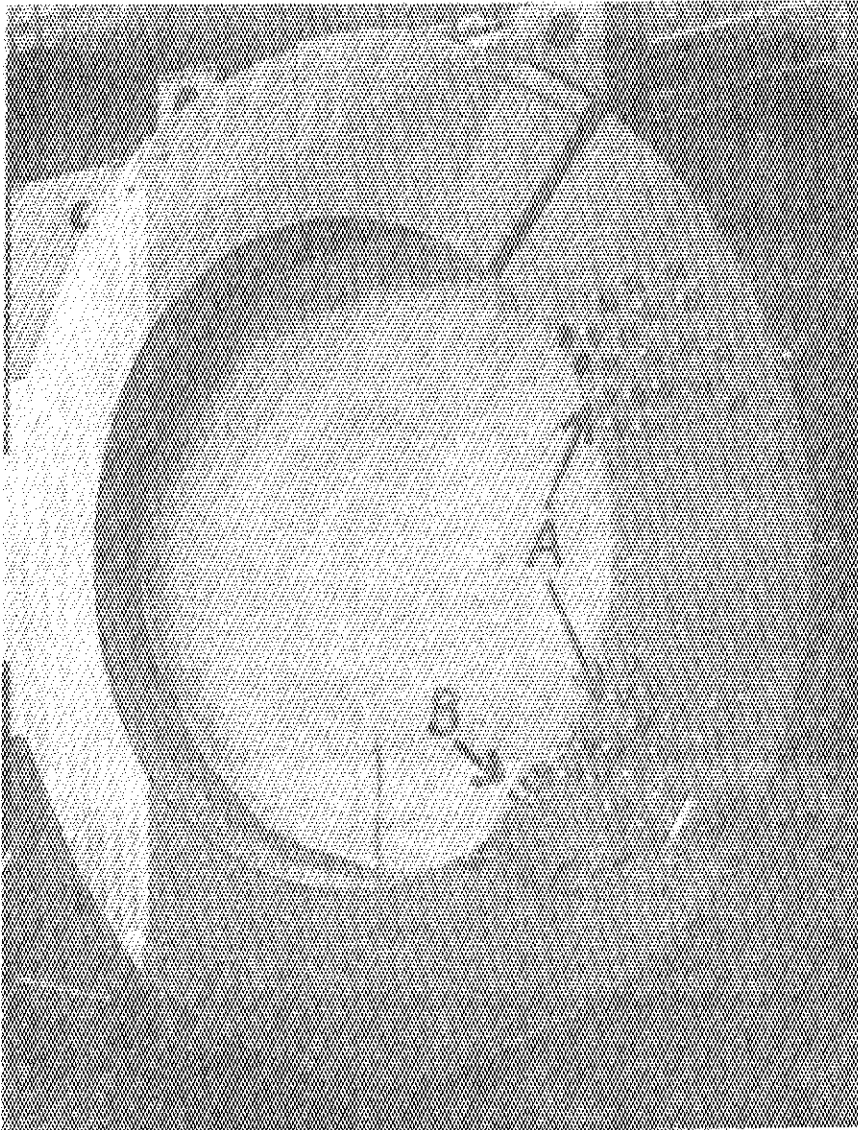


Photo. X.3-3

One fabricated coil  
A: Inlet and outlet  
for cooling water  
B: Connection between  
two pancake coils  
C: Lead wire



Photo. X.3-4 Welding process in making space box between TF coils

#### 4. Status of Power Supplies

The status of JT-60 power supplies is described with emphasis on the progress made since the last review period.

The contract for the manufacture of the poloidal field power supply was awarded to Toshiba Corporation in March 1979. The fabrication of a prototype thyristor convertor unit including high-precision current measurement transformers and others was completed and their tests have been well progressed.

The contract for the toroidal field power supply was also concluded with Mitsubishi Electric Corporation in March 1980.

The systems design of the whole JT-60 electrical power systems has been continued to examine and establish their overall consistency and unification.

The design of the grounding system of the JT-60 systems was completed, and its construction is started with the construction working at the new site.

Table X.4-1 shows the major milestones related to the JT-60 power supplies and our progress to date.

##### 4.1 Poloidal field power supply

The poloidal field power supply of JT-60 is shown schematically in Fig. X.4-1. A motor generator supplies the necessary electric power for all the poloidal field coils, namely, the ohmic heating field coil, the vertical field coil, the horizontal field coil, the quadrupole field coil, and the magnetic limiter coil. In addition to the ohmic build up coil, an inductive energy storage coil is used to make a stepped build up of plasma current and is also energized by the generator as shown in Fig. X.4-1. Each of these coils is independently powered and controlled by respective thyristor banks to meet various operational requirements of the poloidal field system.

The specifications of the generator are summarized in Table X.4-2 and a cross-sectional view is shown in Fig. X.4-2. Detailed reexamination of the electrical and the mechanical design of the generator was completed, and the manufacture is now started. The design and the specifications of the ohmic heating power supply and other poloidal field power supplies (thyristor convertor systems) were also fixed (Table X.4-2). No major modification was introduced into the design described in the last report.

The manufacture of a prototype unit of thyristor convertors and some related equipment for the ohmic heating power supply (see Fig. X.4-3) has been completed, and their tests are being carried out.

#### 4.2 Toroidal field power supply

A composite electrical system which consists of a generator with flywheel and the utility power network system was adopted for the toroidal field power supply. The generator and the utility network system are connected electrically at the dc circuit through rectifier equipment as shown in Fig. X.4-4. A typical operation pattern of the toroidal field power system is shown in Fig. X.4-5.

The specifications are summarized in Tables X.4-3 and X.4-4. A major modification was made on the generator system; the driving system of the generator was changed to a static starting system using thyristors from an induction motor of the previous design. This change was motivated by a closer examination of the overall energy efficiency of the generator system and cost consideration including the operation cost. No engineering problem seems to exist in the fabrication and operation of the static starting system.

#### 4.3 Control system of power supplies

The control system of JT-60 power supplies controls its own objective devices and equipment of the poloidal field and the toroidal field power supplies, and is controlled by the central control system of JT-60. As shown in Fig. X.4-6, CAMAC system is used for interfacing all devices and equipment to be controlled to the computer system of the central controller.

The systems design of CAMAC systems is almost completed and function tests of CAMAC crates including a microprocessor crate controller are being made.

#### 4.4 Systems design of JT-60 electrical power system

The ac supply and distribution system for JT-60 is shown by the simplified diagram of Fig. X.4-7. The electrical power required for the operation of the entire JT-60 systems is supplied from the utility power network at 275 kV, 50 Hz. It is then transformed to proper voltage levels and distributed to various JT-60 loads through three distribution

systems. The largest pulsed load is the toroidal field system which requires 160 MW from the network. The second major loads are the three generator systems and require about 20 MW during operation. A quasi-steady power is also needed for the auxiliary devices and equipment to support the operation of JT-60 facilities.

The design of the ac supply and distribution system has been almost settled, and work is now being done on the design of protection system which is compatible with the design of 275 kV substation at the new site. Interferences to the utility power network induced by the pulsed operation of JT-60 have been analyzed carefully on the basis of the presumed power demand against the power network at the time of planned operation of JT-60. It has been confirmed that the operation envisaged in the JT-60 electrical power system on the present design basis is possible under the limitations which is laid down in the technical provisions between JAERI and The Tokyo Electric Power Company Incorporated.

The layout design of various devices and equipment of power supplies is now almost completed. The three generator systems together with auxiliary switchgear equipment, generator control equipment and others are housed in the motor generator building (Fig. X.4-8). The rectifier systems for the toroidal field power supply, the thyristor convertor systems for the poloidal field power supply, the dc circuit interrupters, and the control systems (CAMAC systems and auxiliary equipment) are placed in the separate rectifier building. The transformer yard intervenes between these two buildings.

Table X.4-1 JT-60 power supplies time schedule

| 1976 | 1977                            | 1978                                       | 1979  | 1980                  | 1981                  | 1982 | 1983                               | 1984                  |
|------|---------------------------------|--|---|-----------------------|-----------------------|------|------------------------------------|-----------------------|
| ▲    | COMPLETE PRECONSTRUCTION DESIGN |  |   |                       |                       |      |                                    |                       |
|      | ▲                               | COMPLETE R & D FOR DC CIRCUIT INTERRUPTERS |   |                       |                       |      |                                    |                       |
|      |                                 | ▲  | ORDER TOKAMAK SYSTEM-TF & PF COILS, VAC. VES.         |                       |                       |      |                                    |                       |
|      |                                 | ▲  | COMPLETE DESIGN REEXAMINATION (P.S. & CONTROL SYSTEM) |                       |                       |      |                                    |                       |
|      |                                 | ▲  | COMPLETE GROUNDING SYSTEM DESIGN                      |                       |                       |      |                                    |                       |
|      |                                 |  | ▲   | ORDER PF POWER SUPPLY |                       |      |                                    |                       |
|      |                                 |  |   | ▲                     | ORDER TF POWER SUPPLY |      |                                    |                       |
|      |                                 |  |   | ▲                     | ORDER CONTROL SYSTEM  |      |                                    |                       |
|      |                                 |  |   |                       |                       | △    | COMPLETE P.S. BLDG.                |                       |
|      |                                 |  |   |                       |                       | △    | START P.S. INSTALLATION            |                       |
|      |                                 |  |   |                       |                       | △    | COMPLETE 275 KV SUBSTATION         |                       |
|      |                                 |  |   |                       |                       | △    | START INTEGRATED JT-60 SYSTEM TEST |                       |
|      |                                 |  |   |                       |                       |      | △                                  | COMPLETE JT-60 SYSTEM |
|      |                                 |  |   |                       |                       |      |                                    | FIRST PLASMA          |

Table X.4-2 Specifications of major components of the poloidal field power supply

|                          |   |  |                    |
|--------------------------|---|--|--------------------|
| Generator                | Vertical shaft salient pole type        | 1  | set                |
|                          | pole                                    | 16   | poles              |
|                          | Capacity                                | 500  | MVA                |
|                          | Voltage                                 | 18   | KV                 |
|                          | Current                                 | 16   | KA                 |
|                          | Frequency                               | 78 - 54  | HZ                 |
|                          | Xd, Xq                                  | 1.84, 1.18   | p.u                |
|                          | Xd"                                     | 0.24   | p.u                |
|                          | Power factor                            | more than 0.45   |                    |
|                          | Flywheel effect                         | 5,500  | ton-m <sup>2</sup> |
|                          | Revolution                              | 585 - 405  | RPM                |
|                          | Energy yield                            | 1.3  | GJ                 |
| Induction motor          | Wound rotor three-phase induction motor | 1  | set                |
|                          | pole                                    | 10   | pole               |
|                          | Capacity                                | 7  | MW                 |
|                          | Voltage                                 | 11   | KV                 |
|                          | Revolution                              | 585 - 405  | RPM                |
|                          | Speed-up time                           | 10   | Min.               |
|                          | Control                                 | Stationary scherbius system and Water rheostat               |                    |
| D.C. circuit breaker     | Vacuum circuit breaker                  | 2  | sets               |
|                          | Voltage                                 | 25   | KV                 |
|                          | Current                                 | 92   | KA                 |
|                          | Commutation capacity                    | 1.0  | mF                 |
|                          | di/dt, dv/dt                            | 450A/ $\mu$ s, (mean)120A/ $\mu$ s(at zero)<br>300v/ $\mu$ s |                    |
| I.E.S. coil              | Reactor of Iron core with air gaps      | 3  | sets               |
|                          | inductance                              | 1.12 / 2.32 / 4.56   | mH                 |
|                          | Connection                              | Series   |                    |
|                          | Total inductance                        | 8  | mH                 |
|                          | Peak current                            | 92   | KA                 |
|                          | Resistance                              | 7.5  | m $\Omega$         |
|                          | R.M.S. current                          | 92KA 2.9   | sec                |
|                          | Rated voltage                           | 25   | KV                 |
| Time constant controller | Resistance                              | 0.072 - 1.0  | $\Omega$           |
|                          | Variable                                | in 20 steps  |                    |
|                          | Maximum energy dissipation              | 78   | MJ                 |
|                          | Rated energy dissipation                | 50   | MJ                 |
|                          | Allowable temperature rise              | 70   | $^{\circ}$ C       |
| Thyristor converter      | OH coil and IES coil PSF1               | SCR 24 pulse   | 92KA-2500V         |
|                          | PSF2                                    | SCR 24 pulse   | 92KA-2500V         |
|                          | Vertical field coil PSVF1               | SR 24 pulse  | 58.0KA-5KV         |
|                          | PSVF2                                   | SCR 24 pulse*  | 58.0KA-5KV         |
|                          | PSVR                                    | SCR 24 pulse*  | 8.6KA-5KV          |
|                          | Quadru-pole field coil PSQ              | SCR 12 pulse*  | $\pm$ 25KA-1800V   |
|                          | Horizontal field coil PSH               | SCR 12 pulse*  | $\pm$ 22KA-500V    |
|                          | Magnetic limiter coil PSM               | SCR 12 pulse   | 95KA-1000V         |
|                          |   | * bi-polar   |                    |

Table X.4-3 Specifications of the toroidal field power supply generator

|                            |                         |
|----------------------------|-------------------------|
| Required Energy            | 4,020 MJ                |
| Maximum Speed              | 600 RPM                 |
| Minimum Speed              | 420 RPM                 |
| GD <sup>2</sup> of MG Set  | 16,000 T-M <sup>2</sup> |
| Repetition Time            | 10 Min.                 |
| Generator:                 |                         |
| Output Power (Peak Value)  | 215 MVA                 |
| Output Voltage             | 18 kV                   |
| Power Factor               | 0.85 lagging            |
| Pole Number                | 16 poles                |
| Output Frequency           | 80 ~ 56 Hz              |
| GD <sup>2</sup>            | 1,400 T-M <sup>2</sup>  |
| Static Starting Equipment: |                         |
| Capacity                   | 19,000 kW               |
| Input Voltage              | 11 kV                   |
| Input Frequency            | 50 Hz                   |
| Starting Time              | 20 Min.                 |
| Flywheel:                  |                         |
| GD <sup>2</sup>            | 14,600 T-M <sup>2</sup> |
| Weight                     | 600 Tons                |
| Diameter                   | 6.6 M                   |
| Length                     | 2.9 M                   |



Table X.4-4 Specifications of major components of the toroidal field power supply

| RECTIFIER | RATING             | NUMBER OF PULSES | NUMBER OF UNITS | UNIT RATING       | CONSTITUTION OF ONE UNIT | RATING OF ELEMENT  | CAPACITY OF TRANSFORMER | %   | NUMBER OF TRANSFORMERS |
|-----------|--------------------|------------------|-----------------|-------------------|--------------------------|--------------------|-------------------------|-----|------------------------|
| SRL1      | 730 V<br>53.0 KA   | 24               | 4               | 730 V<br>13,250 A | 1S-3P-6A                 | 2,500 V<br>3,500 A | 28 MVA                  | 12% | 2                      |
| SRL2      | "                  | "                | "               | "                 | "                        | "                  | "                       | "   | "                      |
| SRL3      | "                  | "                | "               | "                 | "                        | "                  | "                       | "   | "                      |
| SRL4      | "                  | "                | "               | "                 | "                        | "                  | "                       | "   | "                      |
| TSG1      | 1,730 V<br>53.0 KA | 24               | 4               | 865 V<br>26,500 A | 1S-6P-6A                 | 2,500 A<br>3,500 A | 60.2 MVA                | 25% | 2                      |
| TSG-2     | "                  | "                | "               | "                 | "                        | "                  | "                       | "   | "                      |

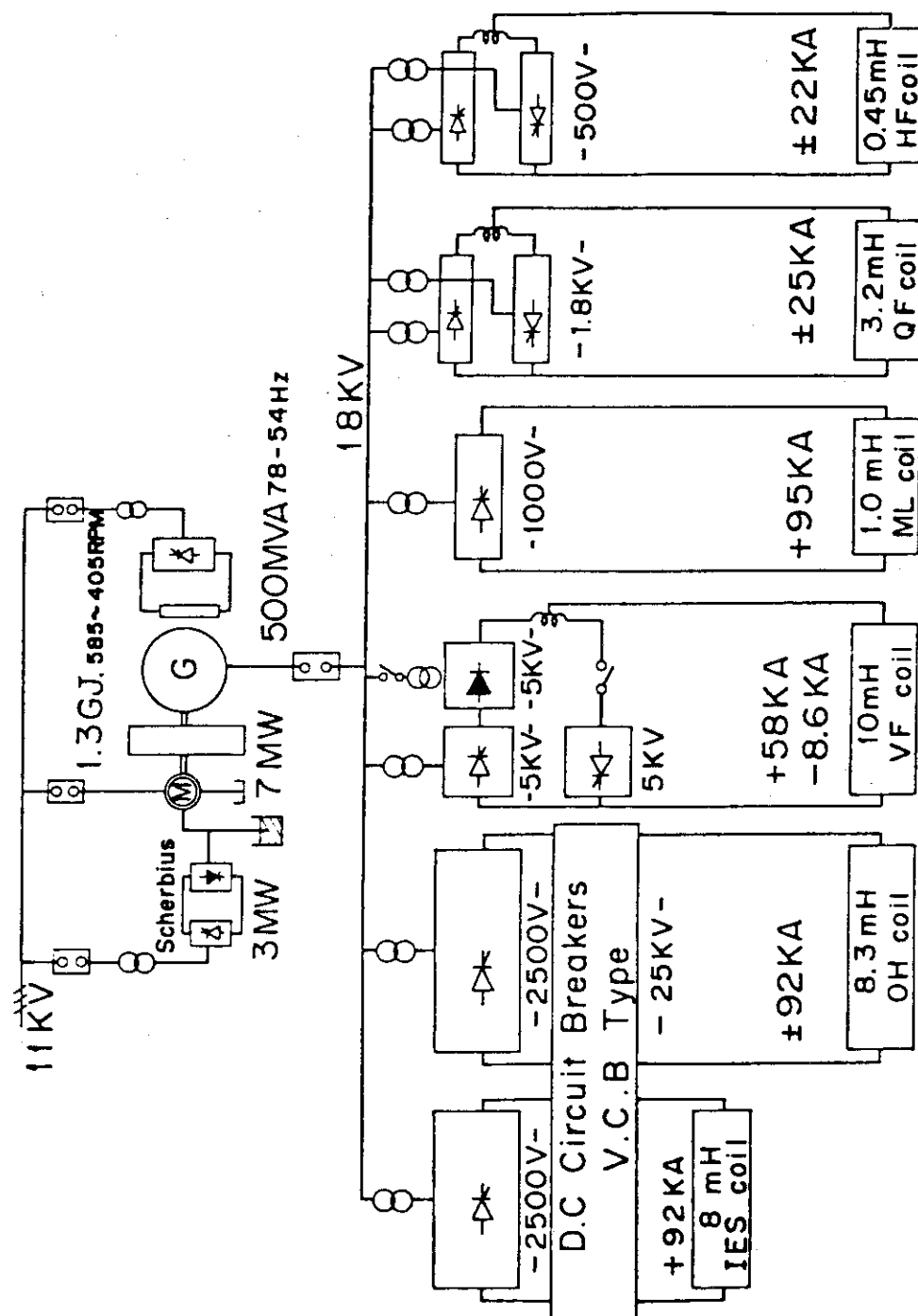


Fig. X.4-1 Schematic diagram of the poloidal field power supply

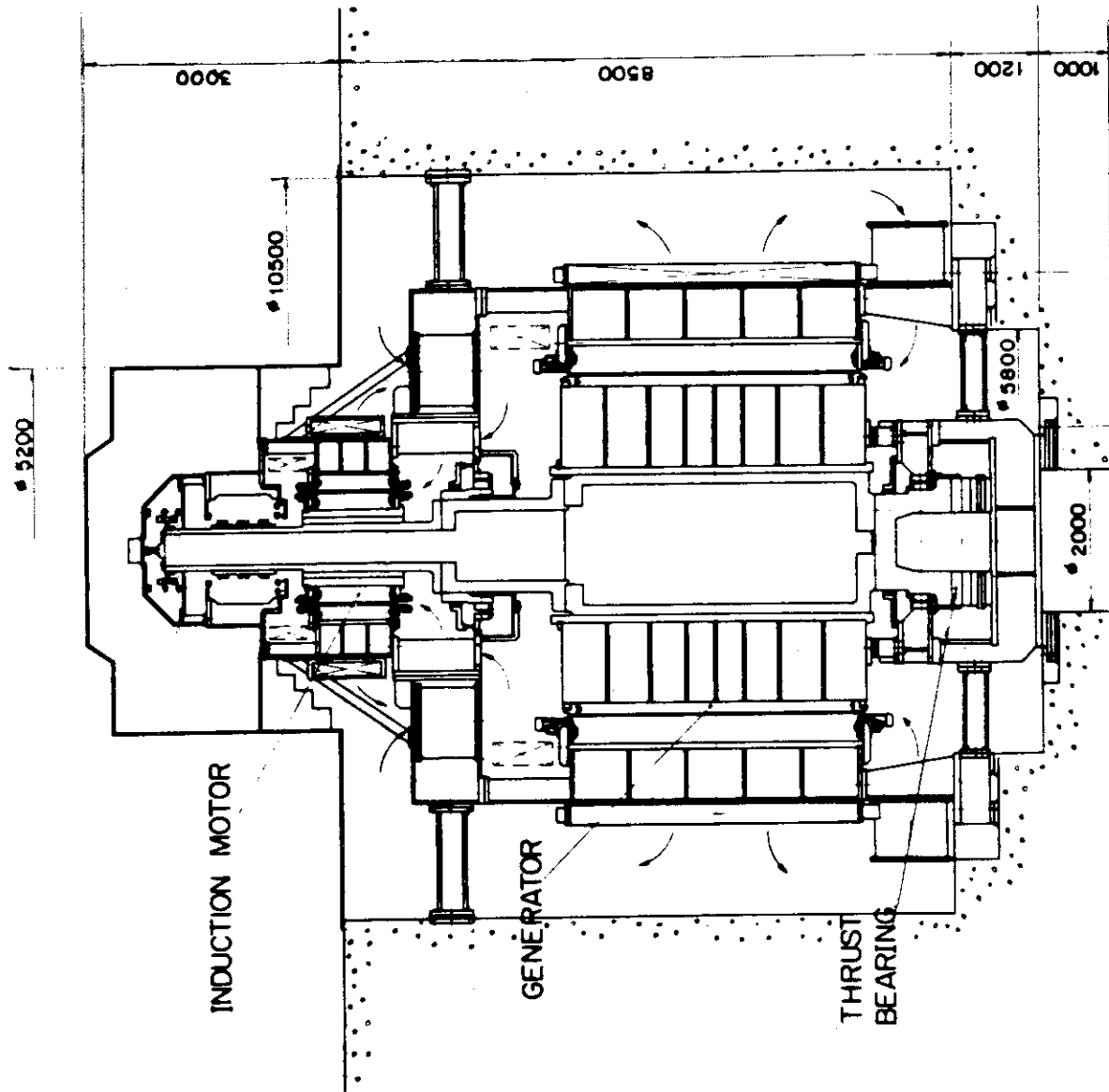


Fig. X.4-2 Cross-sectional view of the poloidal field power supply generator

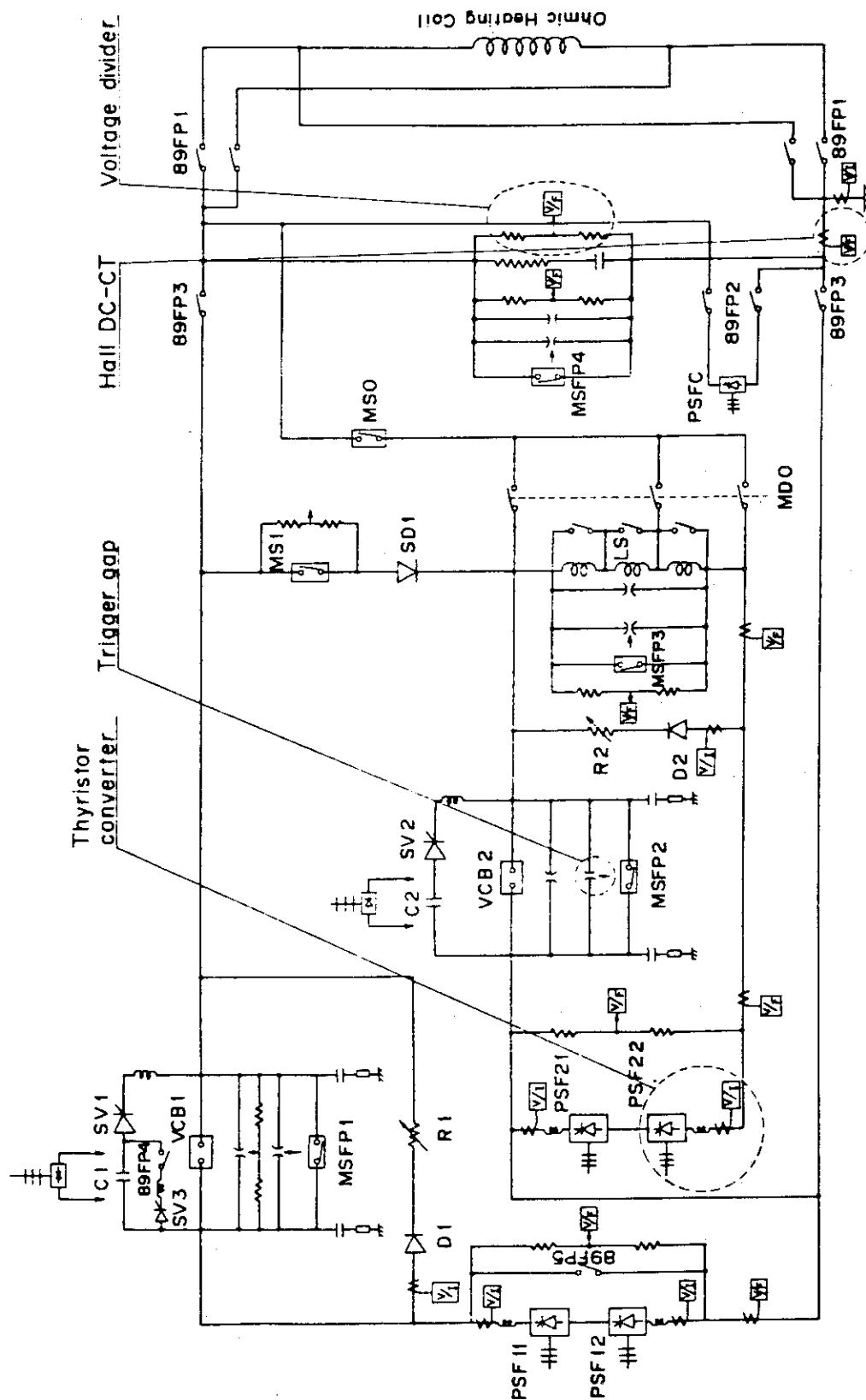


Fig. X.4-3 Ohmic heating circuit of JT-60

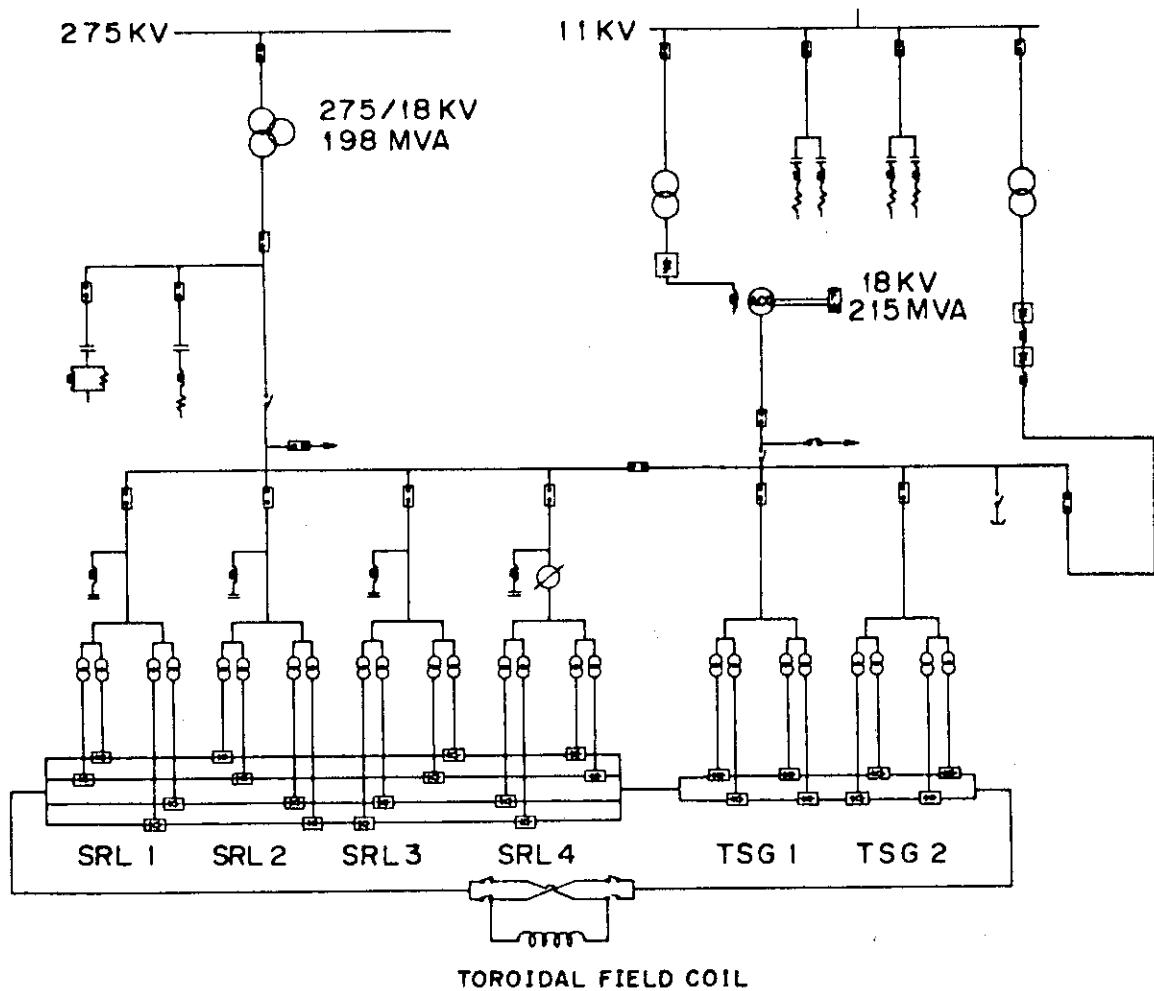


Fig. X.4-4 Circuit diagram of the toroidal field power supply

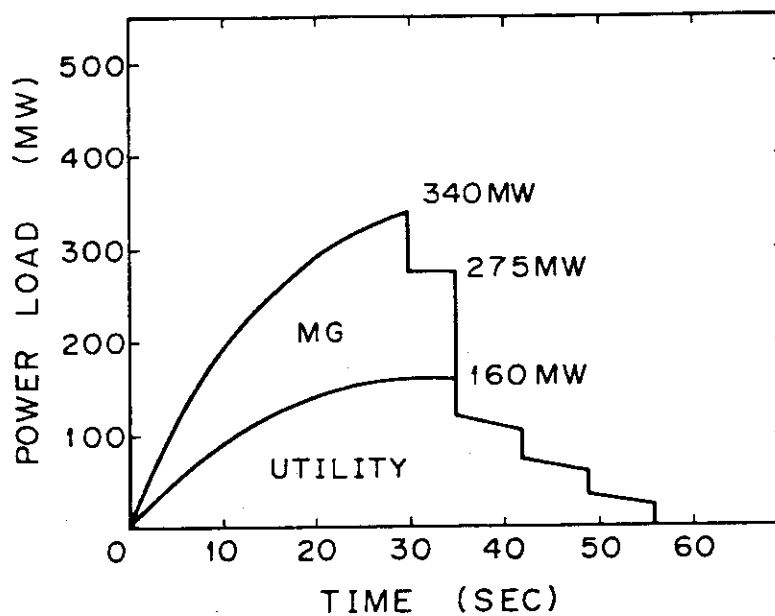


Fig. X.4-5 Load pattern of the toroidal field power supply

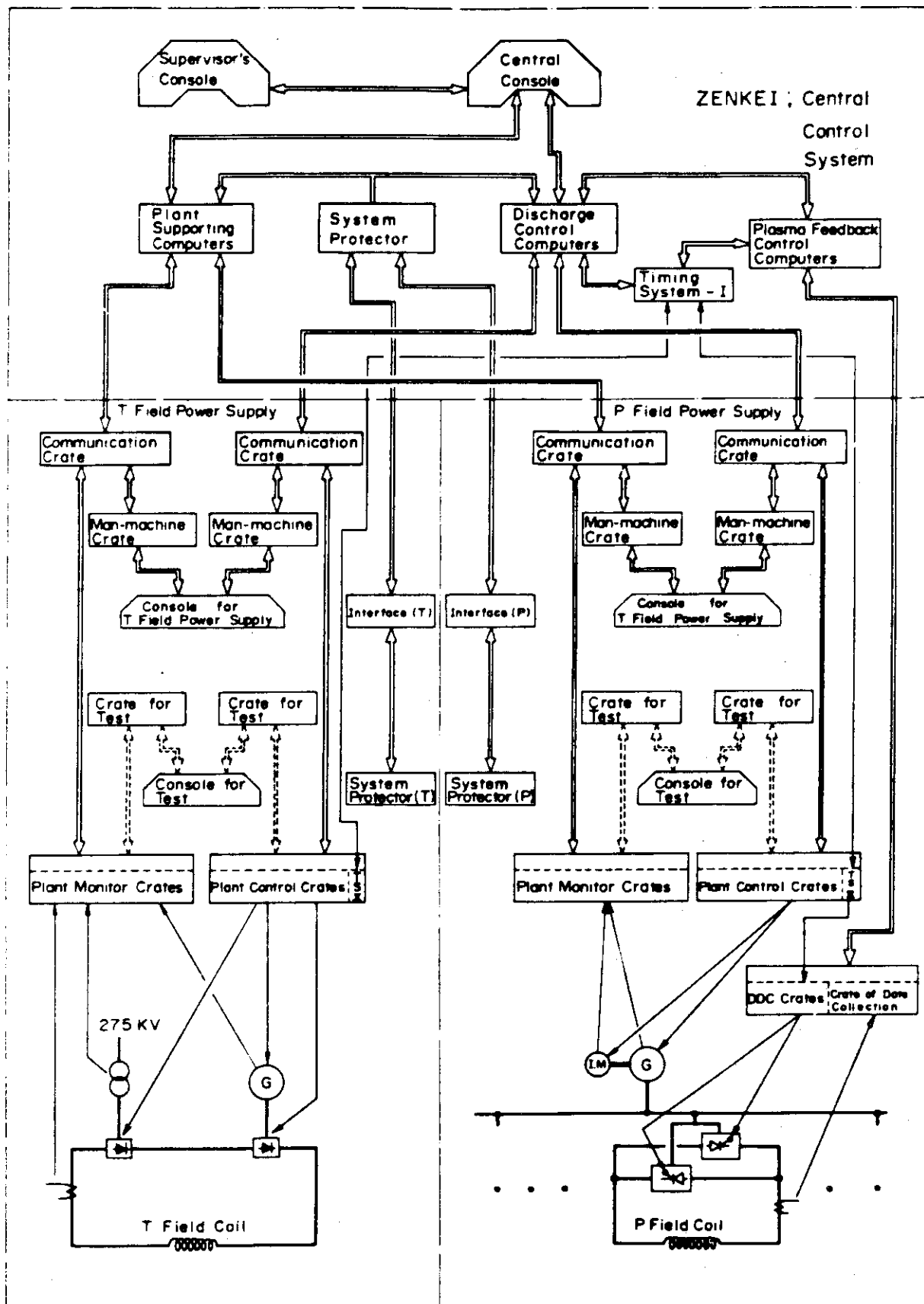


Fig. X.4-6 Control system of the JT-60 power supplies

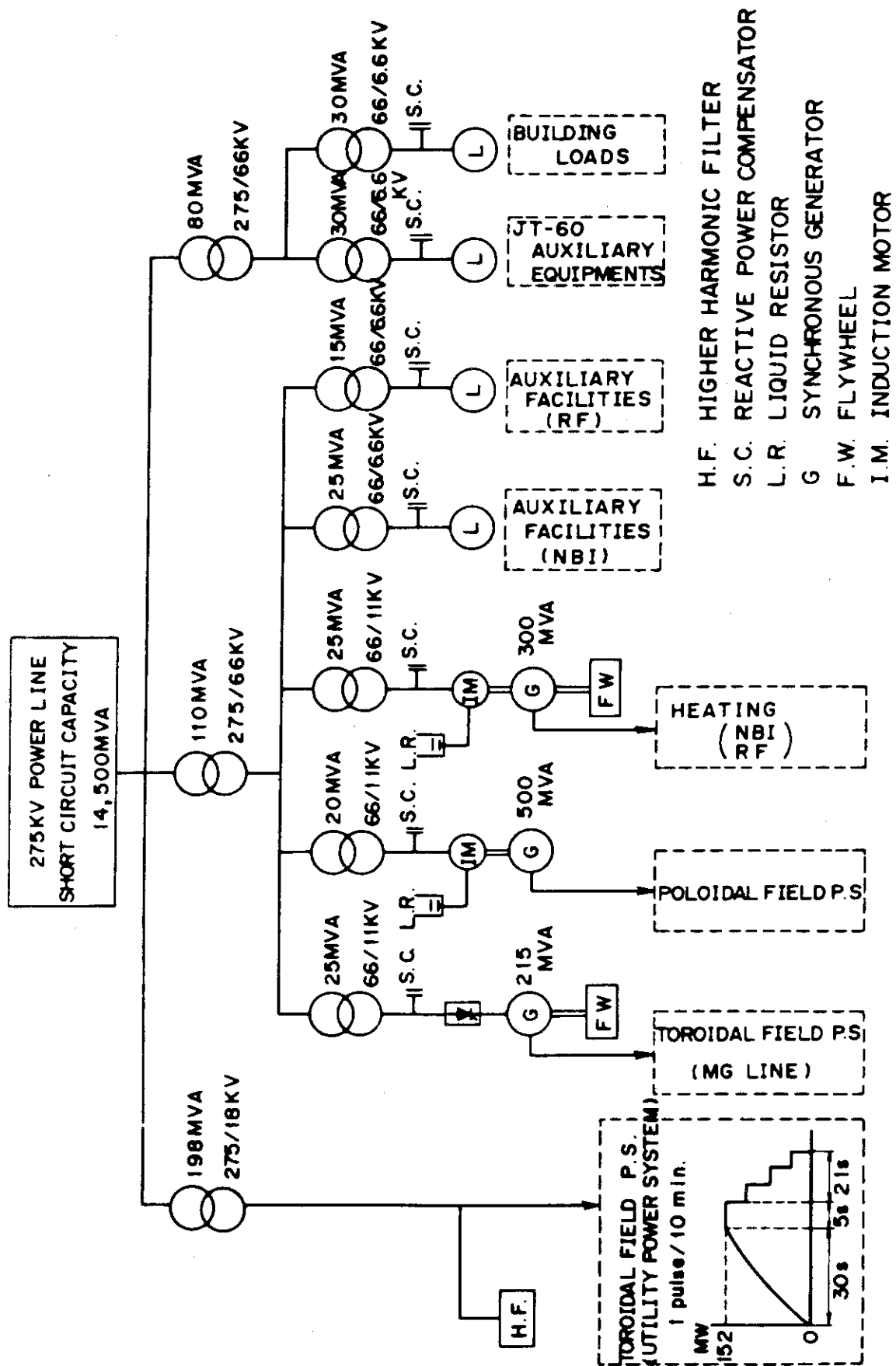


Fig. X.4-7 AC supply and distribution system of JT-60

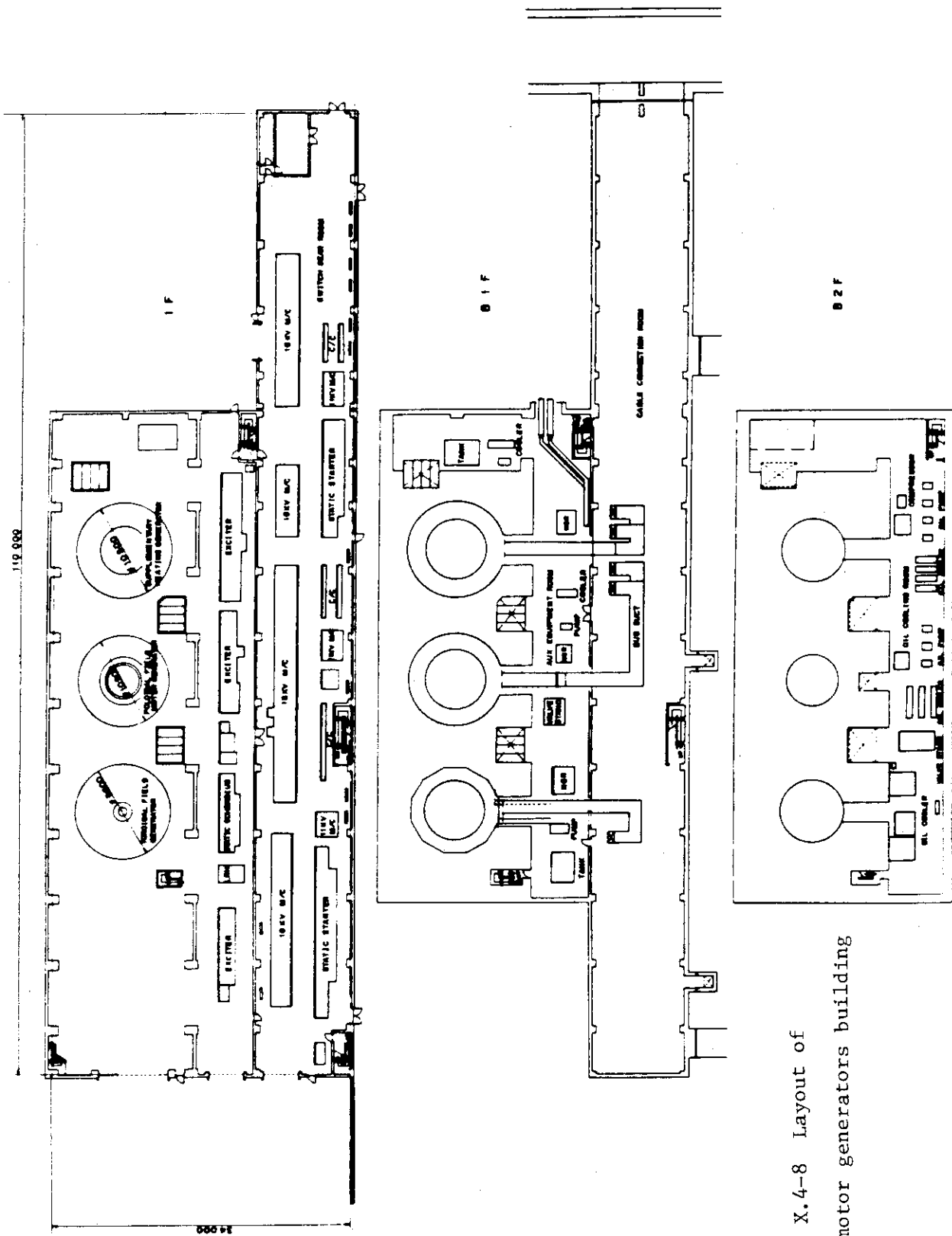


Fig. X.4-8 Layout of the motor generators building



## 5. Status of Control and Diagnostic systems

### 5.1 Major activities of control and diagnostic systems

Major efforts for the construction of the JT-60 Central Controller, Zenkei, were concentrated on the completion of the ordering specification. On the basis of the work made in the last year, we added the readjustment of the function and operation boundaries between Zenkei and sub-control systems, and the results were reflected on the ordering specification. The contract to construct Zenkei was concluded with Hitachi, Ltd. at the end of March 1980. By this contract, total system of Zenkei were entered into the stage of manufacture.

As for the diagnostic systems, the executive plan for the whole diagnostic system was made, considering both the experimental plan of JT-60 and the fabrication status of JT-60 device. The technical specifications have been studied and several developmental items were extracted and executed through the year.

### 5.2 Present design of control system

#### 5.2.1 System design

Control and monitoring system of the JT-60 is required to have large data handling capacity, flexibility, future expansibility and maintainability, because it is for the experimental device. Another requirement is imposed to the system for easy implementation. The JT-60 is composed of several subsystems; a mechanical structure, a toroidal field coil power supply, a poloidal field coil power supply, etc. Each complete subsystem, including its controller, is contracted with a respective industry separately, so it must work well not only as one of a centralized system during experiment but also as a decentralized system during test, commissioning and maintenance.

Hierarchical computer system utilizing CAMAC standards is adopted as a solution for these requirements. The upper level of the system is composed of several minicomputers and the lower level is microprocessor-based distributed intelligence system. The consoles are driven by computers.

All protection sequences are realized by hardwired logics, except the termination of poloidal field in certain cases where the computer control is applied to minimize shock on the JT-60 machine. A timing signal is transmitted directly in real-time to proceed with sequence control during a shot.

Figure X.5-1 shows the architecture topology of the JT-60 computer system which includes computers for data processing. The control system, shown in left-hand of Fig. X.5-1 is grouped into three computer subsystems. The first is to monitor continuous status of plant equipments such as vacuum pumps, cooling facilities, motor generators for poloidal field coil power supply etc. The second is to control and monitor such equipments to perform discharges as a toroidal field coil power supply, a poloidal field coil power supply, a preionization system, a gas injection system etc. The third is to perform feedback-control during discharges. Power supplies of air-core transformer, vertical field coil, horizontal field coil and quadrupole field coil, the gas injection system and auxiliary heating systems are controlled via this loop.

Three computer subsystems are assigned to functions above mentioned. Each computer has its own CAMAC highway to connect nodal crates of the subsystems. The nodal crates contain microprocessors and serial drivers for driving their subsystem highways. Furthermore, the subsystem highway are possible to drive device highways in multi-level hierarchy.

A transversal highway is provided in each subsystem to perform test, commissioning and maintenance. It connects those crates which belong to different highway loops.

The computer proposed for the central controller is HIDIC 80E, whose major characteristics are given in Table X.5-1. Actual structure of computer system is given in Fig. X.5-2, where seven CPUs are used. Five of them are positioned in the control building, while two are positioned in the power supply building to be used exclusively for the feedback control. Shared memories connect five and two CPUs, respectively.

#### 5.2.2 Man-machine interface

The features of the man-machine interface in the JT-60 control system are as follows:

- (1) hierarchical structure. As the control system of JT-60 has a hierarchical structure<sup>1)</sup>, the man-machine interface will be provided corresponding to each hierarchy, whose role is assigned according to operation stage.
- (2) centralization. In the control room independent operation of each sub-system will be carried out for preparation of the experiments. Then, discharge control will be performed for plasma experiments. Nine sub-

system consoles for independent operation of each sub-system are provided and a centralized and computerized console for the operation of discharge control.

In the structure of JT-60 control system the man-machine interface, i.e., control consoles and panels, is shown by thick lines in Fig. X.5-3. At the top of the system a supervisor's console is provided for monitoring the overall status of the JT-60 equipments. During the normal operation a central console is provided for discharge control. To back up the above two consoles, a hard-wired auxiliary graphic panel is installed. Sub-system consoles are provided for independent operation and test of each sub-system. Local panels, which are not shown in this figure, are installed for local operation of equipments and devices. Besides these consoles and panels, a number of consoles will be provided for plasma diagnoses.

As the organization for operation and experiment has not been decided yet, the layout of consoles and panels in the control room has been planned on the following assumptions:

First, the operation and monitoring for discharge control can be carried out by several operators at the central console. Each sub-system console is limited to be used for independent operation of test and preparatory operation before discharge. Secondly, the operators at the central console have to communicate closely with experimentalists at the diagnostic consoles in order that the experiments may be carried out smoothly. Finally, the flexibility and the expansibility are considered for the control consoles and panels of additional heating equipments because their control systems have not been designed yet.

One possible layout scheme for the control room is shown in Fig. X.5-4. The area of this room is about 900 m<sup>2</sup>. The central console is located in the center of the room, where the operators will set the control parameters for discharge and monitor the equipment status and the discharge results. This console is connected to the plant support computer and the discharge control computer. It is composed of twelve unit desks with CRT displays, keyboards and push button switches and some corner desks as shown in Fig. X.5-5. The central console is surrounded with nine sub-system consoles, such as consoles for machine systems I, II, toroidal coil power supply, etc. The supervisor's console with two CRT displays is located at the position where the shift supervisor can oversee the ...

activities of operators working at the central console. The graphic panel is located in the same row where the sub-system consoles are situated. The overall plant status, such as operation stage, shot number, stage of discharge sequence, is displayed with hard-wired devices and the summarized annunciation for each sub-system is displayed on this panel. In addition to these, ten ITV sets and a wired radio system are prepared for monitoring the entrance and inside of JT-60 machine room, etc. and for announcing the information on the operation, respectively. The rest area is used for racks involving control devices of the sub-systems, such as relays and CAMAC crates, and the power distribution boards.

### 5.2.3 CAMAC system

An actual CAMAC system for control and monitoring is shown in Fig. X.5-6. The central highways made of dual serial highways of the plant support computer and the discharge control computer connect several nodal crates which belong to various subsystems. Optical fiber cable shown by dashed lines are employed in the subsystem highways between the control building and the power supply building or the experimental building. Each subsystem has a man-machine crate to perform test, commissioning and maintenance locally, which is commonly connected to the nodal crates for the plant support computer and the discharge control computer by its local highway. Device highways dedicated to various subsystems such as a baking device, a vacuum pumping device, etc. are not fully shown in Fig. X.5-6. Byte serial highways are applied to data transfer paths for the real-time control.

Module configuration of a nodal crate used in the central highways of the plant support system and the discharge control system is shown in Fig. X.5-7. Dataway control of the crate is shared by three intelligences. The first priority is given to the crate controller driven by the local test highway, the second is assigned to the ACD (auxiliary controller with D-port) connected to the central highway and the third is assigned to the microprocessor housed in the ACM (auxiliary controller with micro-processor).

An efficient protocol in the central serial highways is defined in conjunction with function of the ACD. As the data transfer is featured to be exclusively between a buffer memory module and an upper computer, single command can be followed by a block of data with variable length. The data transfer protocol is thus liberated from the CAMAC standard in

spite of using the standard D-port for hardware compatibility. This data transfer can obtain the speed 2.5 times faster than the case of the standard protocol.

A lot of optical fiber cables are employed for data transfer among buildings of the JT-60 and among devices in the experimental building for the reason of its immunity from the difference of the ground level and the influence of the electromagnetic field. Data transfer by using single cable of the optical fiber pair is applied not only to the serial highway but also to the byte serial highway defined in the serial CAMAC standard.

#### 5.2.4 Timing system

Timing signals delivered from the central system to various subsystems proceed with the control sequences and synchronize the diagnostic measurements.

Figure X.5-8 shows a system configuration of the JT-60 timing system. The central timing generators are controlled by the discharge control computer and several timing receivers housed in CAMAC crates of the various subsystems, which are connected directly by optical fiber cables or twisted pair cables to the central timing generators. Another timing generator placed in the power supply building is controlled by both of the central timing generator and the feed-back control computer linked to the discharge control computer.

As the timing signals control large and powerful devices, reliable timing transfer systems are required. Handshaking and error recovery procedure are shown in Fig. X.5-9 together with the outlined block diagram and data format of the timing signal. The encoded signal with destination channel bits and a parity bit is generated by the timing transmitter, and the timing receiver in a subsystem crate decodes the signal to distribute it to subsystem devices. The receiver checks the parity bit and generates response signal upon the correct parity to the transmitter. In the case of no response, the transmitter can try the signal generation again. Input and output lines of the timing receiver are isolated by optical couplers.

#### 5.2.5 Safety and protection system

Briefly, four kinds of systems are considered; (a) a soft ware protection system, (b) hardwired interlock systems, (c) back-up systems

and (d) alarm systems.

These kinds of systems are in the central system and/or in the subsystems as observed in Table X.5-2. Among them, the first two are being mentioned in this section.

The protection interlock system (hard wired) of the central system takes signals from the subsystems, the building devices, the plasma monitors and the discharge control computer in which the software protection system is being established.

#### (a) Software protection system

It is being designed as one of the function of the central computer system. It functions for failure diagnosis, pre-shot checks, post-shot checks and operation mode transit checks.

##### i. Failure diagnosis:

As observed in Fig. X.5-10, the function of failure diagnosis is triggered by a signal from the hardwired interlock system which informs a failure to the computer system when it takes place. After triggered, the computer takes informations about the conditions of subsystems and diagnostics from the status of the hardwired interlock system and the data obtained through CAMACs. The diagnosis will be performed in the way as given in Table X.5-3.

##### ii. Pre-shot checks:

The computer system checks the following items;

- (1) Find miss settings of discharge conditions,
- (2) Conditions of the devices and equipments of subsystems,
- (3) Prediction of a failure with present discharge conditions.

The last item is given because the probabilities that a runaway electron mode or an unusual stress, vibration and temperature at the tokamak machine would takes place are still left after the former two items are cleared.

##### iii. Post-shot checks:

During discharge, subsystems are inhibited to be operated independently. To release the condition after discharge has finished, it is to be performed on the items; (1) confirm the finish of discharge, (2) logging of the alarms which have taken place during discharge.

The confirmation is performed by comparing the table which gives the

conditions of the discharge finish with the monitored data.

(b) Hardwired interlock system

The organization of the hardwired interlock system is that follows the conception of hierarchy as well as the computer control system.

To make up the total hardwired interlock system, isolations according to the respective groundings to keep off noise and protection of propagation of the ground fault of a magnetic field coil at the tokamak machine are under consideration. For isolations, signals are sent by input terminations.

Table X.5-4 represents the failure which would take place associated with the discharge operation, the sensors to catch the phenomena and the way to terminate the discharge operation. It is found to be important to establish proper combinations of the terminating modes of the coil power supplies to minimize the electro-magnetic stress on the tokamak machine.

The terminating modes of the power supplies are present in Table X.5-5. In the table, C-stop is a termination of poloidal field coil power supply with an optimum computer control; it is ruled out of the principle of the "hardwired" protection system, however, considering the importance of minimizing damage on the tokamak, this compromise is considered to be acceptable.

#### 5.2.6 Plasma control

Analytical study based on modern control theory is made on plasma control upon the following conditions<sup>2)</sup>:

- 1) Parameters to be controlled include plasma density, electron and ion temperatures, major radius, etc.
- 2) Actuators to control those parameters are power supplies and neutral beam injectors.
- 3) Only program control is applicable to the neutral beam injectors, while real-time feedback control is superposed on the program control in the operation of power supplies.
- 4) The program control can be corrected during intervals between two successive shots.

Control rules are derived in the following manner. A linearized state description is derived from circuit equations, particle balance equation,

energy balance equation, and equation of motion. Penalty is given for the controlled plasma parameters in cost functional to avoid the regime where instabilities are easy to occur. The model adaptive technique is applied to improve the state description during shot intervals.

References

- 1) "Status of JT-60 Program", 3rd IAEA Technical Committee Meeting on Large Tokamak Equipment, Sept. 1-6, 1978, Paris.
- 2) A Ogata and H. Ninomiya: Proc. 8th Symp. Engng. Problems Fusion Research (San Francisco, 1979) p.1979.



### 5.3 Present design of diagnostic system

#### 5.3.1 System design

In this year, we have reexamined the first plan of diagnostics and selected optimal diagnostic instruments, in the light on the fabrication status of JT-60 device and the experimental schedule and purposes. In the large tokamak experiments, the diagnostics should work not only for the understanding of plasma behavior but also for the control of plasmas in a broad sense, that is, for production of plasmas of high quality. The diagnostics should be also the sensors of safety protection because the thermal and electrical interactions will be large between plasma and tokamak machine. On the other hand, the high accessibility of the diagnostics to the plasma is not obtained in the large tokamaks and the duty cycle of the discharge is very low; one discharge per 10 minutes in JT-60 case. So, each diagnostics should obtain the useful data with highly temporal and spatial resolution simultaneously and the data processing system should work efficiently.

Diagnostic instruments for the JT-60 can be classified as follows: for phase I experiments, Group A is diagnostics to use basic physical information and control. This group is divided into nine classes as shown in Table X.5-6. The second group (Group B) is advanced diagnostics to be developed for phase II experiments as shown in Table X.5-7.

The greater part of the diagnostic ports have been assigned to the diagnostic instruments and the space and the setting method are presently under consideration. Figure X.5-11 shows the example of the arrangement of diagnostic devices.

We have many items of experiments during short time but discharge frequency is very low. So, the efficient use of every discharge shot is essential. On the other word, the control devices and data processing are essential. Figure X.5-12 is a flow chart of the decision process of the experimental conditions of experiment. There will be four loops to let the diagnostic data reflect on the experimental procedures, such as real time feedback loop, shot by shot loop, day-unit loop and week-unit loop, in which different analysis processes may exit. Diagnostics and data processing system should be useful for each analysis process. We are going to realize this experimental scheme with the hierarchical computerized system of control and data processing so that these control loops may work actively, systematically, and efficiently. Fig. X.5-1 shows the computer system of

JT-60 control and data processing. The data reduction system (the right hand side of this figure) is composed of computers of three ranks: the first is center computer system which is composed high level large universal computers which service as a processor system of week-unit loop, the second is inter-shot data processors which are located in the computer room of JT-60 control building and act as processor system of day-unit and shot by shot loops. This computer system is composed of large universal computer or multi-minicomputers. The third is real time data processor which can be connected to the device control system. This processor will be composed of array processor or pipe line microprocessor. The data acquisition computers are composed of micro-computers incorporated in the CAMAC modules.

### 5.3.2 Electron density and temperature measuring systems

The electron density ( $n_e$ ) measuring system (A-1) contains mm wave and sub-mm wave interferometers, which is intended to obtain the spatial distribution by performing the Abel inversion and to obtain the wide monitoring capability of density range from pre-ionized low density plasma to additional heated high dense plasma. The final object of this system is considered to measure the absolute electron density and to use as the sensor of density control by the real-time data processing. The mm waves are used for the monitoring the density during pre-ionization period and the peripheral plasma density, because of their high density resolution and low cut off density. The sub-mm wave applied for the 5 independent chordes is provided for the measurement of dense main plasma, and another for the divertor. The  $\text{CH}_3\text{OH}$  optically pumped sub-mm wave ( $119 \mu\text{m}$ ) laser oscillator is optimized according to the needs of high cw power availability (about 100 mW) and the frequency of high cut off density (over  $10^{15} \text{ cm}^{-3}$ ).<sup>1)</sup>

The sufficient capability for measuring electron density is ensured by the time responsible interferometers combined with a multipulse laser scattering apparatus which is included in the (A-2) system. Mechanical vibration monitoring interferometer, which is aimed at elimination of mechanical vibration signals generated from JT-60 device, were developed and completed successfully in this year.

The electron temperature ( $T_e$ ) measuring system (A-2) contains the cyclotron radiation measurements (FIR spectrometer and heterodyne radiometer) and Thomson scattering measurement (multipulse laser scattering apparatus)

as shown in Table X.5-6. The cyclotron radiation measurements are prepared mainly to estimate the time evolution of  $T_e(r)$  of the thermal equilibrium plasma, and the Thomson scattering measurement is used as a precise calibration system for the cyclotron radiation measurements and local  $T_e$  with high spatial resolution over the peripheral low density region. The soft X-ray measuring system (A-5) will also be used as auxiliary  $T_e$  measuring system.

The cyclotron radiation measurement will be performed by the following two complimentary methods in respect to time and spatial resolution.

- 1) Fourier Spectrometer of Rapid Scanning Michelson Interferometer
- 2) mm Wave Heterodyne Radiometer

For the Thomson scattering measurement, the conceptual specifications of the scattering apparatus are as follows:

- 1) Multi-pulse laser; 5300 Å, 1.5 J/pulse, 20 pps,
- 2) Optical system; fiber optics + spectrometer, alignment optics,
- 3) Detector; 2-D gated detector array.

We have been under developing some components, such as YAG laser oscillator, low loss optical fiber and gated ICCD, for the multipulse laser scattering apparatus.

### 5.3.3 Ion temperature and impurity measuring systems

The ion temperature measuring system (A-3) consists of neutral particle analysers, an active beam probing apparatus, and neutron counters. The specifications of these diagnostic instruments to be required are shown in Table X.5-6. Two kinds of neutral particle analysers will be installed with an electrostatic energy analyser and with a magnetic momentum analyser and electrostatic analyser. The former which is settled at the tangential access port (T-port) can be used for the measurement of parallel component of ion temperature through the divertor region, and the latter which is placed at the vertical access port ( $U_4$ -port) can be used for the normal component. An active method can be prepared for the measurement of central ion temperature. By injecting a monoenergetic atomic beam into a plasma and measuring the energy spread of the beam particle scattered through a fixed small angle by particle collisions the energy distribution of the neutrals or ions in the plasma can be determined. The PHA system with SSD array or the E//B type 2-D detector will be installed in the oblique access

port ( $\text{IN}_2$ ) for the measurement of radial distribution of high energy neutrals (10~200 keV) escaped from a plasma relevant to neutral beam injection and radio frequency wave heating. The SSD for the neutral particle measurement is now under research and development. The mass resolved PHA system with SSD array can be used as an analyser for the small angle scattering method because the primary neutrals have high energy ( $\leq 200$  keV).

Neutron counters such as a  $\text{BF}_3$  proportional counter and a liquid plastic scintillation counter, will be prepared for the neutron flux measurement in the first phase experiments. Although JT-60 is primarily designed for non D-T experiments, D-D discharge may be carried out to be limited to a small number of shots. The neutron counters will be used for the measurement of photo neutrons due to the  $\gamma$ -n reaction by runaway electrons. The photo neutrons must be distinguished from fusion neutrons even in the future reactor. Moreover, in the next step machine and a reactor the neutron measurement is one of the most important diagnostics for the D-T burning control. As we recognized the importance of the neutron measurement, the neutron diagnostic instruments will be prepared for the second phase experiments considering the energy analysis.

The impurity measuring system (A-4) consists of spatial distribution spectrometers (for VIS, VUV and USX ranges), standard spectrometers (to be used for impurity control and calibration) and doppler broadening spectrometers (for VUV and USX ranges). Polychromators with array detectors will be used extensively in JT-60, which will permit us simultaneous observation of the whole wavelength region covered by each of the polychromator. Combination of several polychromators will give us spatially resolved informations of the impurity lines, which is indispensable for impurity control experiment by divertor. To ensure the polychromator design several mounting methods have been examined and several gratings suitable for each of the mounting have been manufactured. Test pieces of array detectors with intensifying device have been manufactured. From even only one array detector of  $100 \times 100$  elements enormous amount data (10 Mbit/sec) are produced. Memories with fast writing speed and large capacity is required. At present, Video-Tape-Recorder is the most hopeful candidate for such memory.

Doppler broadening spectrometry for impurities is also one of the useful methods for the measurement of ion temperature. Two kinds of

spectrometers can be prepared corresponding to the wave length. One is a normal incidence vacuum spectrometer in VUV range ( $1000\sim 3000 \text{ \AA}$ ), and the other is a crystal polychromator in USX range ( $0.1\sim 10 \text{ \AA}$ ). The former is for the line spectra of light impurities in the outer region of plasma and the latter for metal impurities in the hot core region.

#### 5.3.4 Radiation flux and peripheral plasma measuring systems

The radiation flux measuring system (A-5) consists of high counting rate PHA and X-ray wave measuring apparatus. Up to the present time, PIN diode array and bolometer array are planned to be used for wave measurement. A-Type PIN array will be used for the analysis of the radial distribution of the X-ray emissivity, and B-Type PIN array will be used for the mode analysis. A pair of two type array will be mounted one port ( $\text{IN}_2$ ) and two pairs will be mounted in one toroidal section. From PIN array data, modes up to  $m < 4$ ,  $n < 3$  will be expected to be resolved. Thin film bolometers responding to  $0.5 \text{ W/cm}^2$  within 1 ms have been developed in JFT-2. Bolometers of the same type will be used in JT-60. Table X.5-6 shows the conceptual characteristics of MHD measurement. The electromagnetic probing system (A-7) is also used to measure MHD oscillations. About 24 pick up coils are arranged in the poloidal divertor both inside and outside the vacuum vessel. From the arrangement of coils modes at least  $m < 6$ ,  $n < 2$  will be expected to be resolved. The coils outside the vacuum vessel will measure the eddy current.

The peripheral plasma and wall surface measuring system (A-6) consists of probes, thermocouples, TV, gas analyzers and wall surface analyzers. For the power balance studies of the peripheral plasma, floating liner, limiter, magnetic limiter, and various types of probes will be used extensively as in usual divertor experiment. Several liners, limiters, and magnetic limiter plates are specially designed to be floating in JT-60. Particle flux to the first wall will be monitored by such electrodes. Several probes will be mounted on the so called moving probe scanning plasma periphery at a speed of 1 m/sec. IR-TV cameras altogether will view whole area of the inner surface of the vacuum chamber. Periscopes or optical fibers with heat proof structures will be required for all the IR-TV cameras. At present various combination of periscope materials and detectors is being examined. For the ion temperature measurement in the divertor region, various kinds of probes will be used together with the charge exchange neutral particle analysers. The probes are divided into

two types, i.e. a movable probe and a fixed one. The movable probe, which will be placed at the oblique access port (IN<sub>3</sub>), is suitable for the scanning the divertor region. Langmuire probes, Katsumata probes and a Faraday cup with retarding grids will be mounted on the head of the movable probes.

### 5.3.5 Data processing and diagnostic support systems

Primary design of the JT-60 diagnostic data processing system (A-8) was made in 1977. It had a structure of three level hierarchy; i.e., a large computer, mini computers and a CAMAC system. The present design aims at two destinations. The first is to enable any diagnostic signal to be fed back to machine operation in order to produce a better plasma. The second is to reproduce an experimental shot without help of a machine operation. Though these are not fully attained, we believe that they are improved over the preceding design. Some new hardware devices, video tape recorders and a real-time processor, are introduced for these destinations. Detail of the data processing system is shown in Fig. X.5-13. It consists of the inter-shot processor, the real-time processor and the CAMAC system<sup>2)</sup>. The inter-shot processor is either a general purpose computer or of linked midi computers, while the real-time processor consists of pipelined signal processors. The CAMAC system has microcomputers and pre-processors in its modules. Locations of these components are as follows; the inter-shot processor itself is settled in the computer room of the control building, but most of its terminals are put in the control room of the same building and a few of them are distributed in the diagnostic rooms of the experimental building. The CAMAC system has two level hierarchical structure. Crates at the higher level, or upstairs crates, are put in the diagnostic rooms. While crates at the lower level, or downstairs crates, which directly interface diagnostic devices, are put in the torus hall. The real time processor is put in the diagnostic room. One of features of the system is equipment of the real-time processor. Conventional scheme has been data gathering during a shot and processing during a shot interval.<sup>3)</sup> However, the real-time processor processes signals during a shot, so its processing procedure finishes at the moment when a shot finishes. The whole system consequently has an unusual hierarchical structure; i.e., though the inter-shot processor occupies the top level during a shot interval, it surrenders the position to the real-time processor during a shot.

The diagnostic support system (A-9) consists of various diagnostic stages and carriers, cables and pipes, vacuum connecting instruments, shielding cases and diagnostic system control in construction and fabrication phase. The detail design of these interface devices has not been carried out yet.

#### 5.3.6 Phase II diagnostics (B Group)

Conceptual designs of the B group diagnostic systems have not been carried out yet. However, the spectrum of far-infrared (FIR) laser scattering for a high temperature plasma was analyzed in application of the FIR-laser scattering method to measurement of ion temperature in a large Tokamak plasma.<sup>4)</sup>

#### References

- 1) Y. Yamanaka, J. Fujita, et al.: Int. J. of Infrared and Millimeter Waves, Vol.1, No.1 (1980) 57.
- 2) T. Kumahara, A. Ogata, T. Matoba, I. Kondo and Y. Suzuki: IEEE Trans. on Nucl. Sci., Vol.NS-27, No.1 (1980) 637.
- 3) A. Ogata and K. Yuasa: Computer Phys. Communications, 19 (1980) 35.
- 4) T. Kanamori, T. Matoba, A. Funahashi and Y. Suzuki: "Spectrum Analysis of Far-Infrared Laser Scattering for a High Temperature Plasma", JAERI-M 8777 (1980) (in Japanese).

Table X.5-1 Performance of HIDIC 80E

| Item               | Contents                       | Specifications                                       |
|--------------------|--------------------------------|--|
| Main memory        | Device                         | IC   |
|                    | Capacity                       | 64K to 512K words                                    |
|                    | Expansion unit                 | 32K words/64K words                                  |
|                    | Access width                   | 32 bits  |
|                    | Cycle time                     | 0.48 $\mu$ sec                                       |
|                    | Interleave                     | 2 ways   |
| Global memory      | Device                         | Magnetic core  |
|                    | Capacity                       | 32K to 256K words                                    |
|                    | Cycle time                     | 0.75 $\mu$ sec                                       |
| Arithmetic unit    | Number of instructions         | Standard, 137  |
|                    |                                | Single-precision floating option, 14                 |
|                    |                                | User firmware, 64 max.                               |
|                    | Arithmetic registers           | Standard, 2  |
|                    |                                | Floating registers, 8                                |
|                    | Base registers                 | 3  |
|                    | Index registers                | 3  |
|                    | Address modification           | Base index duplex modification                       |
| Operation time     | Addition                       | 0.48 $\mu$ sec (register-memory)                     |
|                    | Multiplication                 | 1.36 $\mu$ sec (register-memory)                     |
|                    | Floating addition              | 0.75 $\mu$ sec (register-register)                   |
|                    | Floating multiplication        | 1.44 $\mu$ sec (register-register)                   |
| Address conversion | Number of mapping registers    | 1,024  |
| I/O control        | Number of input/output devices | 255  |
|                    | DMA transfer rate              | MAX 4M words/sec (Read),<br>MAX 3M words/sec (Write) |
|                    | PCMA transfer rate             | 40K words/sec  |
| Interrupt control  | Number of levels               | 4  |
|                    | Number of sublevels            | 4 $\times$ 256                                       |
|                    | Distinction of interrupt       | Hardware vectoring                                   |



Table X.5-2 Classification of safety and protection systems

| Central system             | Subsystems                  |
|----------------------------|-----------------------------|
| Software protection system |                             |
| Hardwired interlock system | Hardwired interlock systems |
|                            | Back-up Systems             |
|                            | Alarm systems               |

Table X.5-3 Failure diagnosis

|                             |  |
|-----------------------------|--|
| A. Data compilation         | Alarm record<br>Interlock behavior record<br><br>History of data concerning failure                          |
| B. Cause analysis           | Identification of failure source<br><br>Cause analysis in simple case<br><br>Display prediction of influence |
| C. Instruction to operators | Display points to check or repair<br><br>Display items to do for safety and protection                       |

Table X.5-4 Interlocks relating to plasma behavior

| Failure                         | Sensor           | Number of sensors | Interlock behavior |   |
|---------------------------------|------------------|-------------------|--------------------|---|
|                                 |                  |                   | T F V H Q M        | Devices other than power supplies       |
| Too high plasma current         | Rogowski coil    | 3                 | N E C C C C        | Stop sequence, shut down gas injection. |
| Too high hard X-ray flux        | X-ray probe      | 1                 | N N C C C C        | Stop sequence, shut down gas injection  |
| Too high neutron flux           | Neutron detector | 1                 | N N C C C C        | Stop sequence, shut down gas injection  |
| Too high temperature at limiter | Thermo-couple    | 1                 | N N C C C C        | Stop sequence                           |

Table X.5-5 Termination modes of coil power supplies

|        |   | Coil-power supplies |      |
|--------|---|---------------------|------|
|        |   | T                   | F, V |
| E-stop | E1-stop Highest emergency stop                    | T                   |      |
|        | E2-stop Emergency stop                            | T                   |      |
| F-stop | Stop plasma current by force (Inverter operation) | F, V, H, Q, M       |      |
| N-stop | Normal stop                                       | T, F, V, H, Q, M    |      |
| C-stop | Termination with control                          | V, H, Q, M          |      |

Table X.5-6 JT-60 diagnostics (A group) (part 1)

| System  | Symbol | Diagnostics                                    | Specification  |
|---|--------|--|--|
| A-1<br>Electron Density<br>Measuring System     | A-1-a  | Sub-mm Wave Interferometer                     | Main Plasma<br>$\Delta \bar{n}_e \geq 10^{12} \text{ cm}^{-3}$ , $\Delta t \sim \mu\text{S}$<br>Divertor Chamber<br>$\Delta \bar{n}_e \geq 4 \times 10^{12} \text{ cm}^{-3}$ , $\Delta t \sim \mu\text{S}$ |
|   | A-1-b  | 1-mm Interferometer                            | $\Delta \bar{n}_e \geq 4 \times 10^{11} \text{ cm}^{-3}$ , $\Delta t \sim \mu\text{S}$   |
|   | A-1-c  | 2-mm Interferometer                            | $\Delta \bar{n}_e \geq 2 \times 10^{11} \text{ cm}^{-3}$ , $\Delta t \sim \mu\text{S}$   |
|   | A-1-d  | 4-mm Interferometer                            | $\Delta \bar{n}_e \geq 1 \times 10^{11} \text{ cm}^{-3}$ , $\Delta t \sim \mu\text{S}$   |
|   | A-1-e  | Mechanical Vibration Monitoring Interferometer | $\Delta \tilde{X} \sim 1 \mu\text{m}$  |
| A-2 Electron<br>Temperature<br>Measuring System | A-2-a  | FIR Spectrometer                               | $\Delta t \sim 10 \text{ mS}$ , $\Delta X: 20/R$   |
|   | A-2-b  | Heterodyne Radiometer                          | $\Delta t \sim \mu\text{S}$ , $\Delta X: 10/R$   |
|   | A-2-c  | Multipulse Laser Scattering Apparatus          | $\Delta t \sim 20/\text{sec}$ , $\Delta X: 20/R$   |
| A-3<br>Ion Temperature Measuring System         | A-3-a  | Neutral Particle Analyzer (E.S.)               | $E = 0.1 - 30 \text{ keV}$ , $\frac{\Delta E}{E} = 0.05 - 0.1$<br>$\Delta t = 10 - 100 \text{ mS}$   |
|   | A-3-b  | Neutral Particle Analyzer (E.S., M.A.)         | $E = 0.1 - 30 \text{ keV}$ , D & H,<br>$\Delta E/E = 0.1$ : electrostatic<br>with mass analyzer<br>$\Delta t = 50 - 500 \text{ mS}$  |
|   | A-3-c  | Neutral Particle Analyzer Array                | $E: 10 - 200 \text{ keV}$ , $\Delta E/E = 0.1 - 0.3$<br>$\Delta t = 1 - 100 \text{ mS}$ , $\Delta X: 20/R$   |
|   | A-3-d  | Neutral Particle Detector (PHA, M.A.)          | $E = 10 - 200 \text{ keV}$ , H, D & He,<br>$\Delta E/E = 0.1$ , $\Delta t = 10 - 100 \text{ mS}$   |
|   | A-3-e  | Active Beam Probing Apparatus                  | see "A-3-d"  |
|   | A-3-f  | Neutral Beam Source                            | $E_b = 30 - 200 \text{ keV}$ , H, D & He<br>( $< 0.1 \text{ A}$ ) beam pulse: 10sec,<br>choppable $\sim \mu\text{S}$   |
|   | A-3-g  | Neutron Counter                                | $E_n = E_{th} \sim 2.45 \text{ MeV}$<br>$\Delta t = 1 - 100 \text{ mS}$  |

Table X.5-6 JT-60 diagnostics (A group) (part 2)

| System                                 | Simbol | Diagnostics                                       | Specification   |
|--|--------|---|---|
| A-4<br>Impurity Measuring System       | A-4-a  | Light Impurity Spectrometer (Spatial Resolution)  | $\lambda = 10 - 500\text{\AA}$ , $\Delta X: 20$ points/R<br>$\Delta t: \sim \text{lms}$                                   |
|  | A-4-b  | Light Impurity Spectrometer (Doppler)             | $\lambda = 1000 - 3000\text{\AA}$ , Grating<br>$\Delta t: \sim \text{lms}$  |
|  | A-4-c  | Heavy Impurity Spectrometer (Spatial Resolution)  | $\lambda = 0.1 - 10\text{\AA}$ , $\Delta X: 20/R$<br>$\Delta t: \sim \text{lms}$  |
|  | A-4-d  | Heavy Impurity Spectrometer (Doppler)             | $\lambda = 0.1 - 10\text{\AA}$<br>$\Delta t: \sim \text{lms}$   |
|  | A-4-e  | Spectrometer for Periphery                        | $\lambda = 1000 - 3000\text{\AA}$ , $\Delta t: \sim \text{lms}$<br>$\Delta X: \text{several points/periphery}$<br>Grating |
|  | A-4-f  | see "A-4-e"                                       | see "A-e-e"   |
|  | A-4-g  | Spectrometer for Divertor                         | $\lambda = 20 - 300\text{\AA}$ , near X points<br>Grating<br>$\Delta t: \sim \text{lms}$                                  |
|  | A-4-h  | Visible Spectrometer (Spatial Resolution)         | $\lambda = 2000 - 8000\text{\AA}$ , $\Delta X: 20/R$<br>Grating<br>$\Delta t: \sim \text{lms}$                            |
|  | A-4-i  | Visible Spectrometer (Standard)                   | $\lambda = 2000 - 8000\text{\AA}$   |
|  | A-4-j  | Grazing Incidence Spectrometer (Standard)         | $\lambda = 10 - 1300\text{\AA}$   |
| A-5<br>Radiation Flux Measuring System | A-5-a  | High Counting Rate PHA                            | Si(Li) or Ge(I), $E = 1-200\text{keV}$<br>$\Delta t \sim \text{lms}$ , $\Delta X: 3/R$                                    |
|  | A-5-b  | High Counting Rate PHA Array (Spatial Resolution) | Si(Li) or Ge(I), $E = 1-200\text{keV}$<br>$\Delta t \sim \text{lms}$ , $\Delta X: 10 - 20/R$                              |
|  | A-5-c  | PIN Diode Arrays                                  | PIN Diode or SSD<br>$\Delta t \sim \mu\text{s}$ , $\Delta X: 20/R$  |
|  | A-5-d  | Bolometer Arrays                                  | $\Delta t \sim \text{lms}$ , $\Delta X: 20/R$   |
|  | A-5-e  | Hard X-ray Monitor                                | Hard X-ray, $\Delta t: \text{lms}$  |
|  | A-5-f  | Runaway Monitor                                   | see "A-5-f"   |

Table X.5-6 JT-60 diagnostics (A group) (part 3)

| System  | Symbol | Diagnostics  | Specification  |
|---|--------|--|--|
| Peripheral Plasma<br>A-6 and Wall Surface<br>Measuring System | A-6-a  | Moving Probe   | Speed 1m/s<br>{ Langmuire Probe<br>Directional Double Probe<br>Katsumata Probe |
|   | A-6-b  | Probe  | { Faraday Cup<br>Magnetic Probe<br>Target Probe                                |
|   | A-6-c  | Visible TV   |  |
|   | A-6-d  | IR-TV  |  |
| A-7<br>Electro-<br>Magnetic<br>Probing<br>System              |        | (1) Magnetic probes<br>(2) Rogowski coils<br>(3) One turn coils<br>(4) Diamagnetic loops   |  |
| A-8<br>Data Process-<br>ing System                            |        | (1) Inter-shot data processor<br>(2) Real time data processor<br>(3) CAMAC systems   |  |
| A-9<br>Diagnostic<br>Support<br>System                        |        | (1) Diagnostic stages<br>(2) Carriers<br>(3) Cabling and piping<br>(4) Vacuum connecting instruments<br>(5) Shielding cases<br>◦ Magnetic shield<br>◦ Radiation shield |  |

Table X.5-7 JT-60 diagnostics (B group)

| DIAGNOSTIC SYSTEM                                  | DIAGNOSTIC INSTRUMENTS                 |
|--|--|
| B-1<br>Neutron Measuring<br>System                 | (1) Energy analysis                    |
| B-2<br>Ion Density Measuring<br>System             | (1) Beam probing                       |
| B-3<br>FIR Scattering System                       | (1) Ion temperature<br>(2) Fluctuation |
| B-4<br>Current Density Profile<br>Measuring System | (1) FIR polarimeter                    |
| B-5<br>Resonance Scattering<br>System              |  |

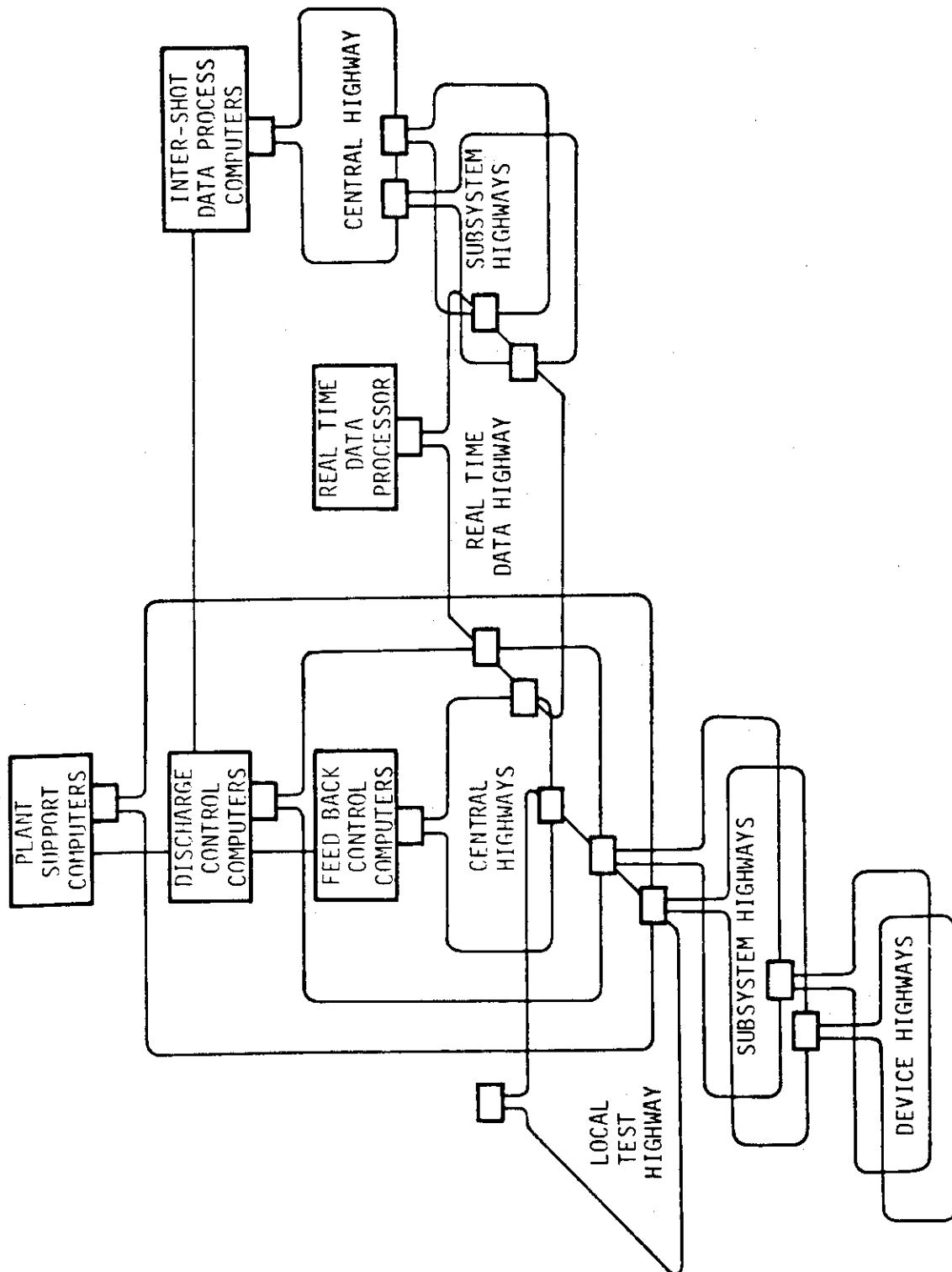


Fig. X.5-1 Architecture topology of JT-60 control and data processing systems

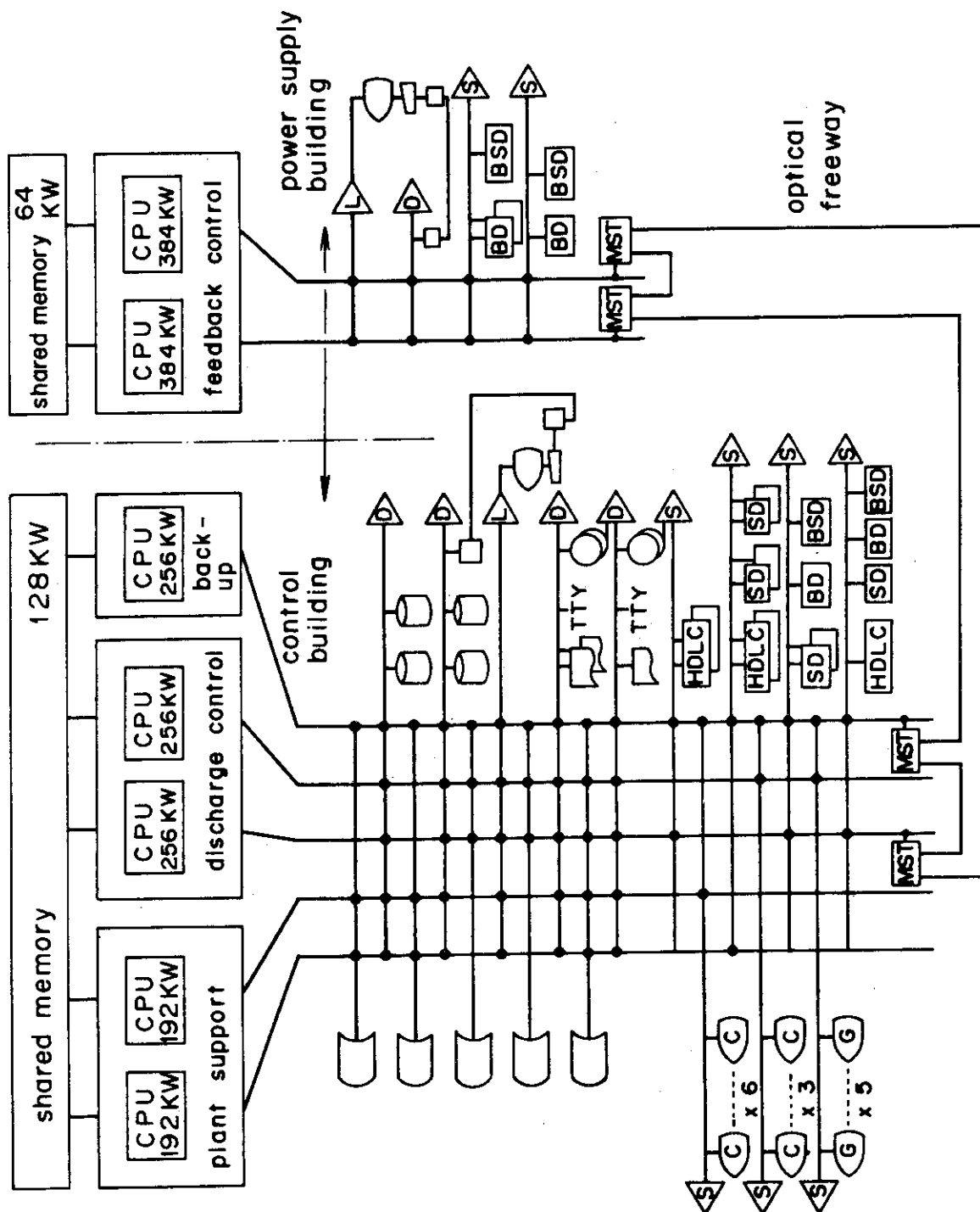


Fig. X.5-2 Structure of computer system



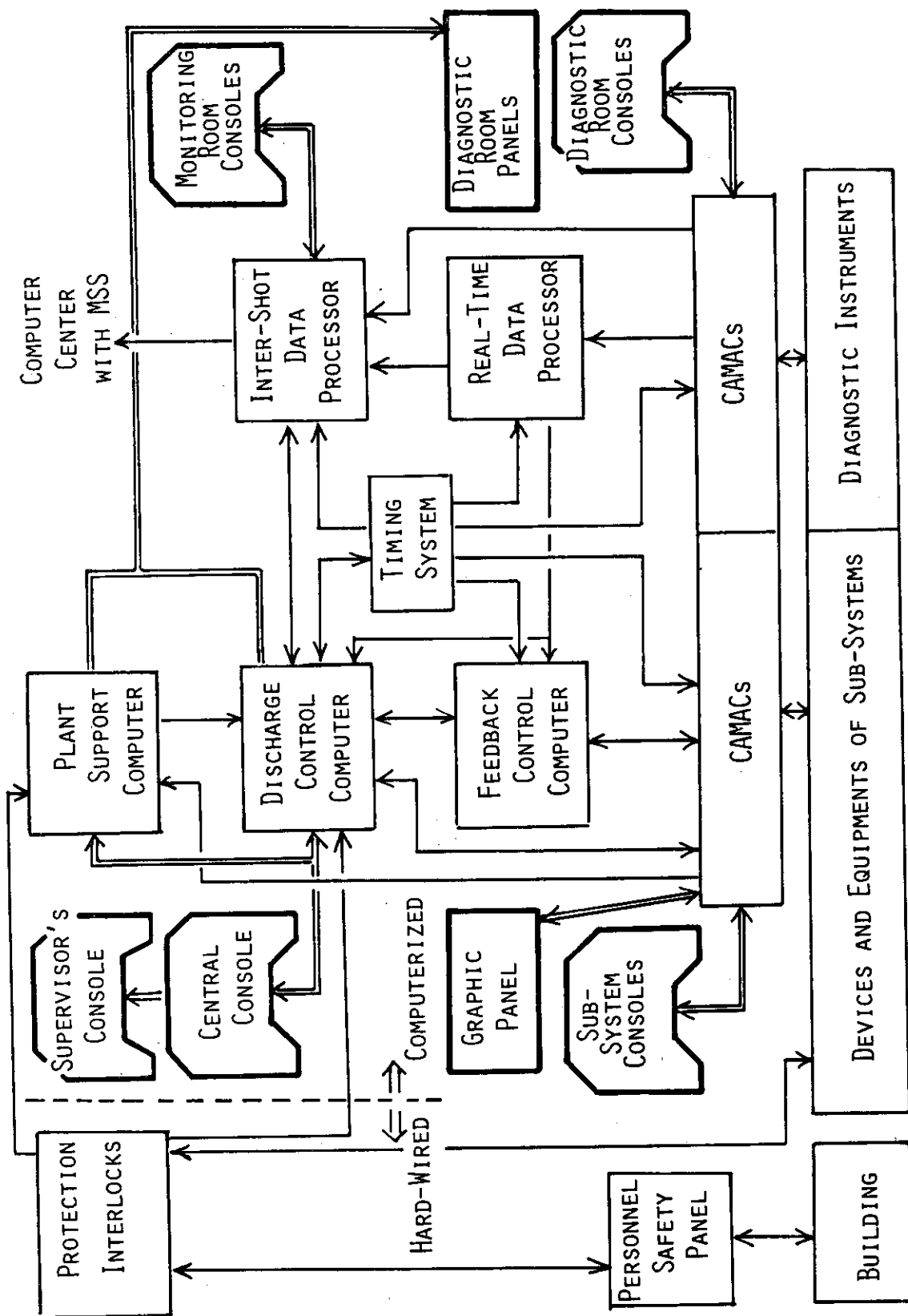


Fig. X.5-3 Structure of JT-60 control system

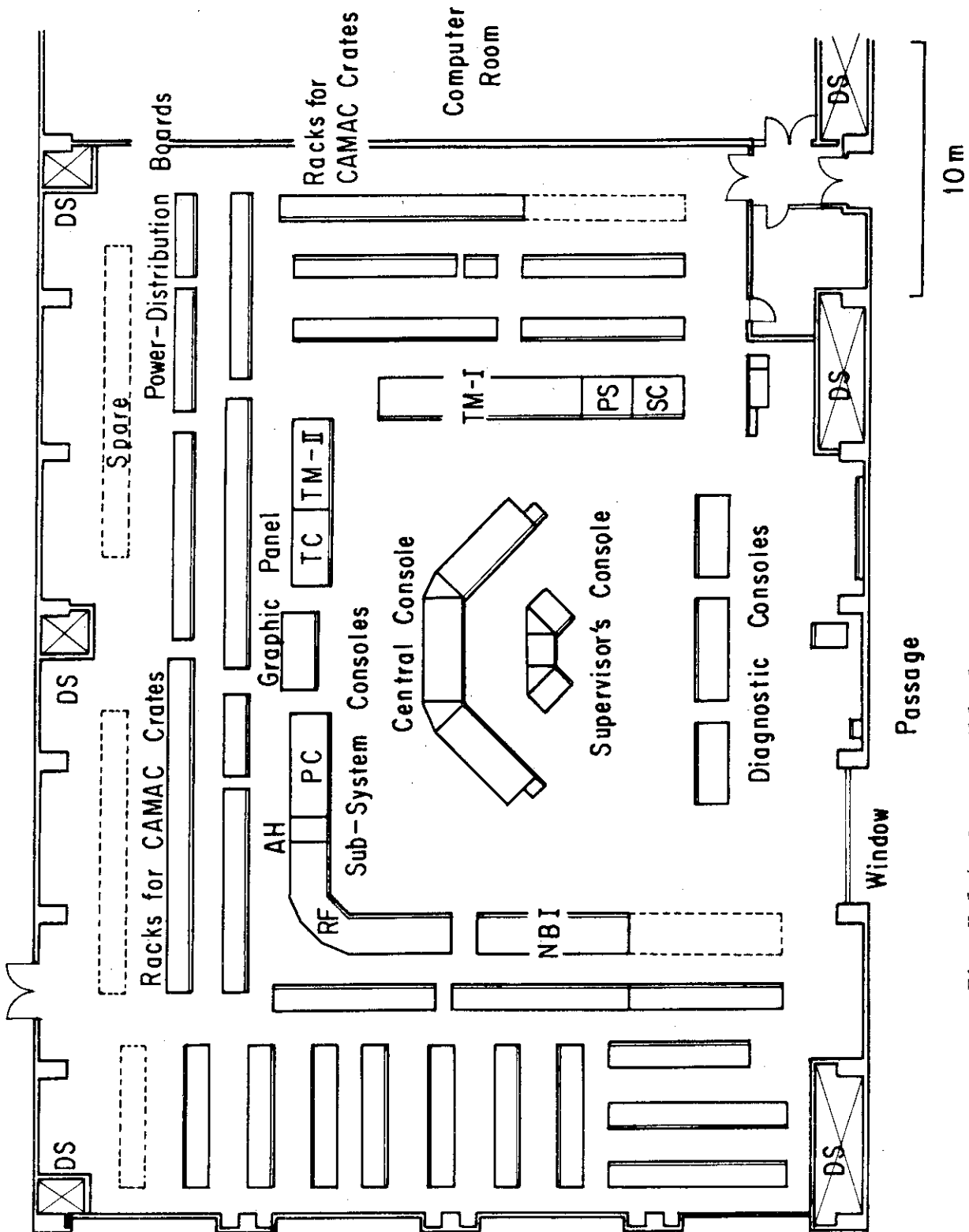


Fig. X.5-4 One possible layout scheme for the control room

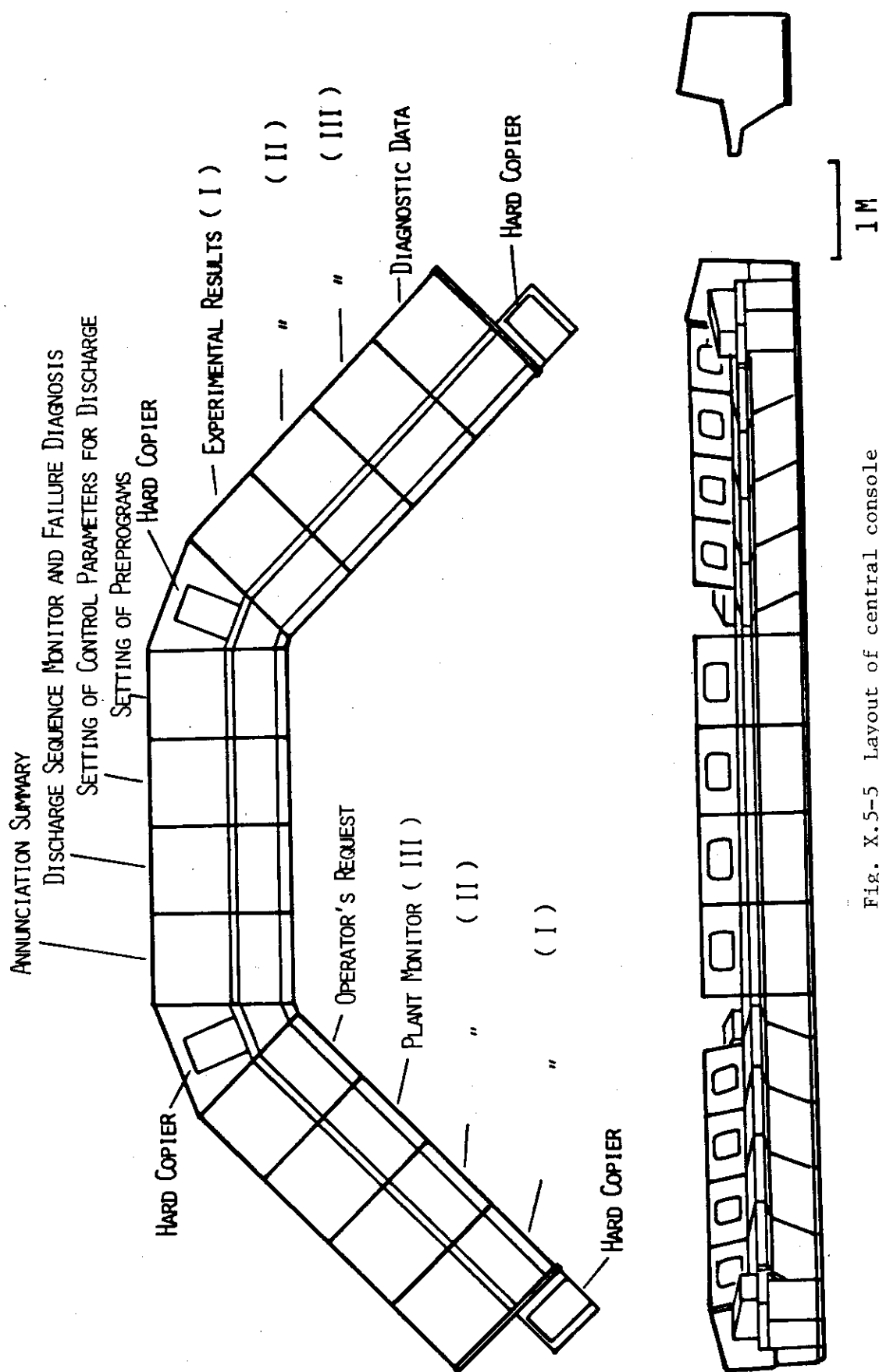


Fig. X.5-5 Layout of central console

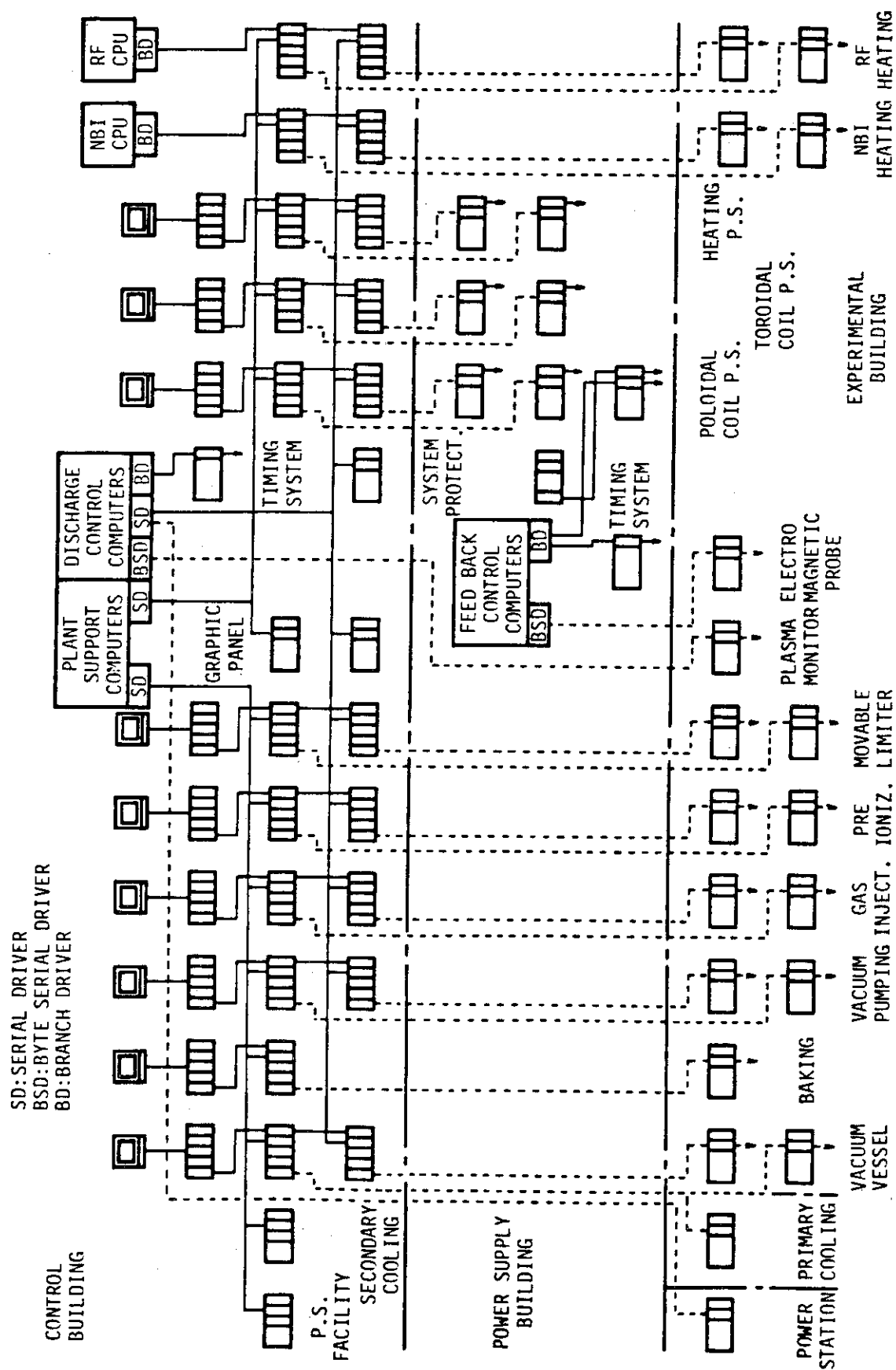
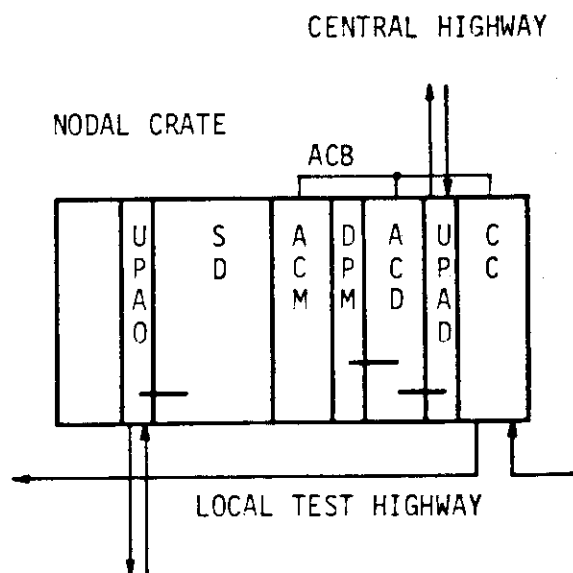


Fig. X.5-6 CAMAC system



CC:CRATE CONTROLLER  
 ACD:AUXILIARY CONTROLLER WITH D-PORT  
 UPAD:U-POR ADAPTOR FOR DUAL HIGHWAY  
 DPM:DUAL PORT MEMORY  
 ACM:AUXILIARY CONTROLLER WITH  
 MICROPROCESSOR  
 SD:SERIAL DRIVER  
 UPAO:U-POR ADAPTOR FOR OPTICAL FIBER

Fig. X.5-7 Module configuration of a nodal crate

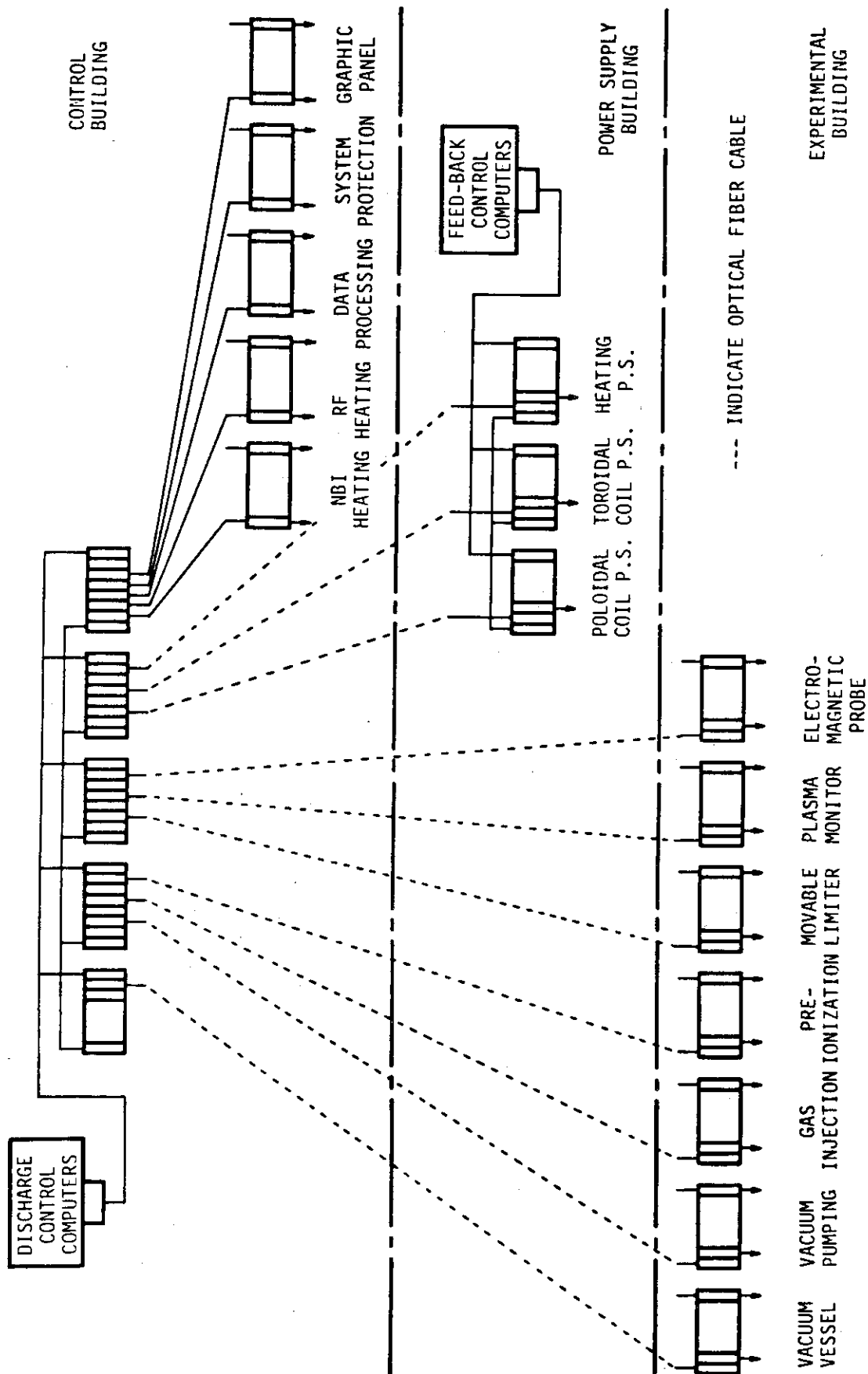
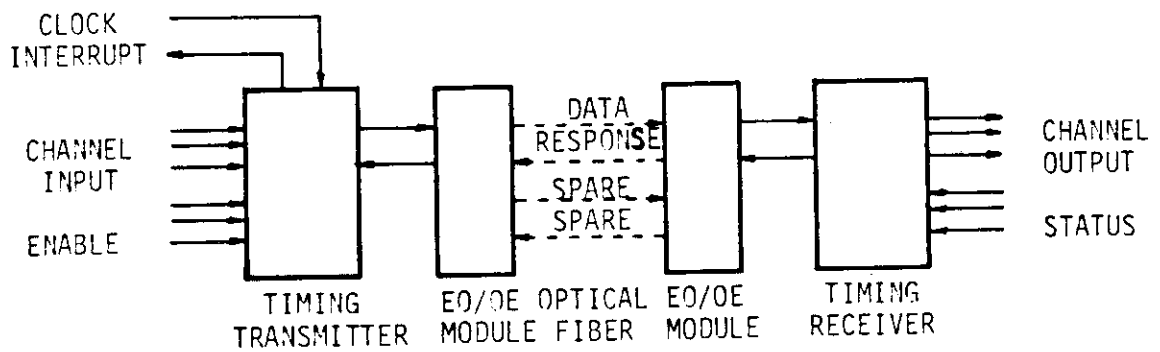
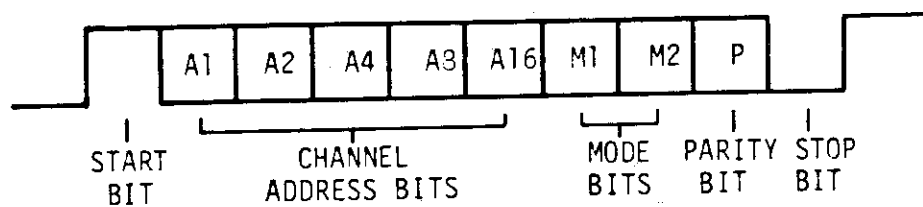


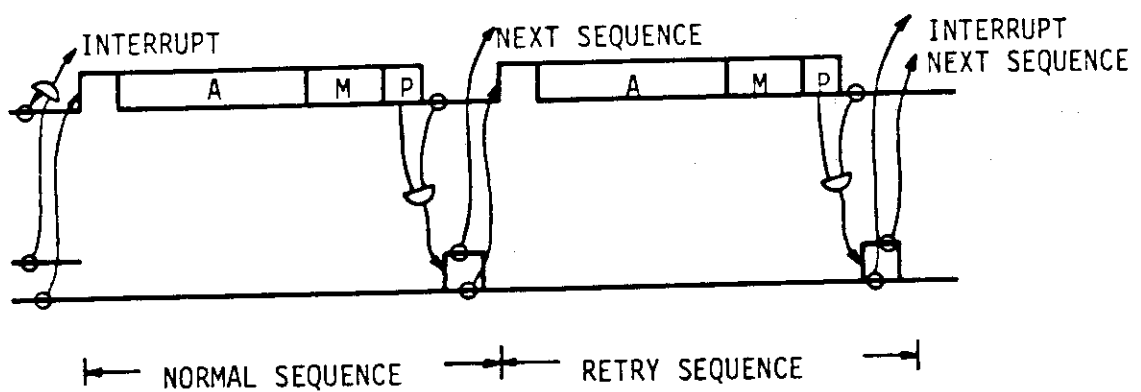
Fig. X.5-8 Timing system



(a) CONFIGURATION



(b) BIT ARRANGEMENTS



(c) ERROR RECOVERY

Fig. X.5-9 Transmission of timing signals

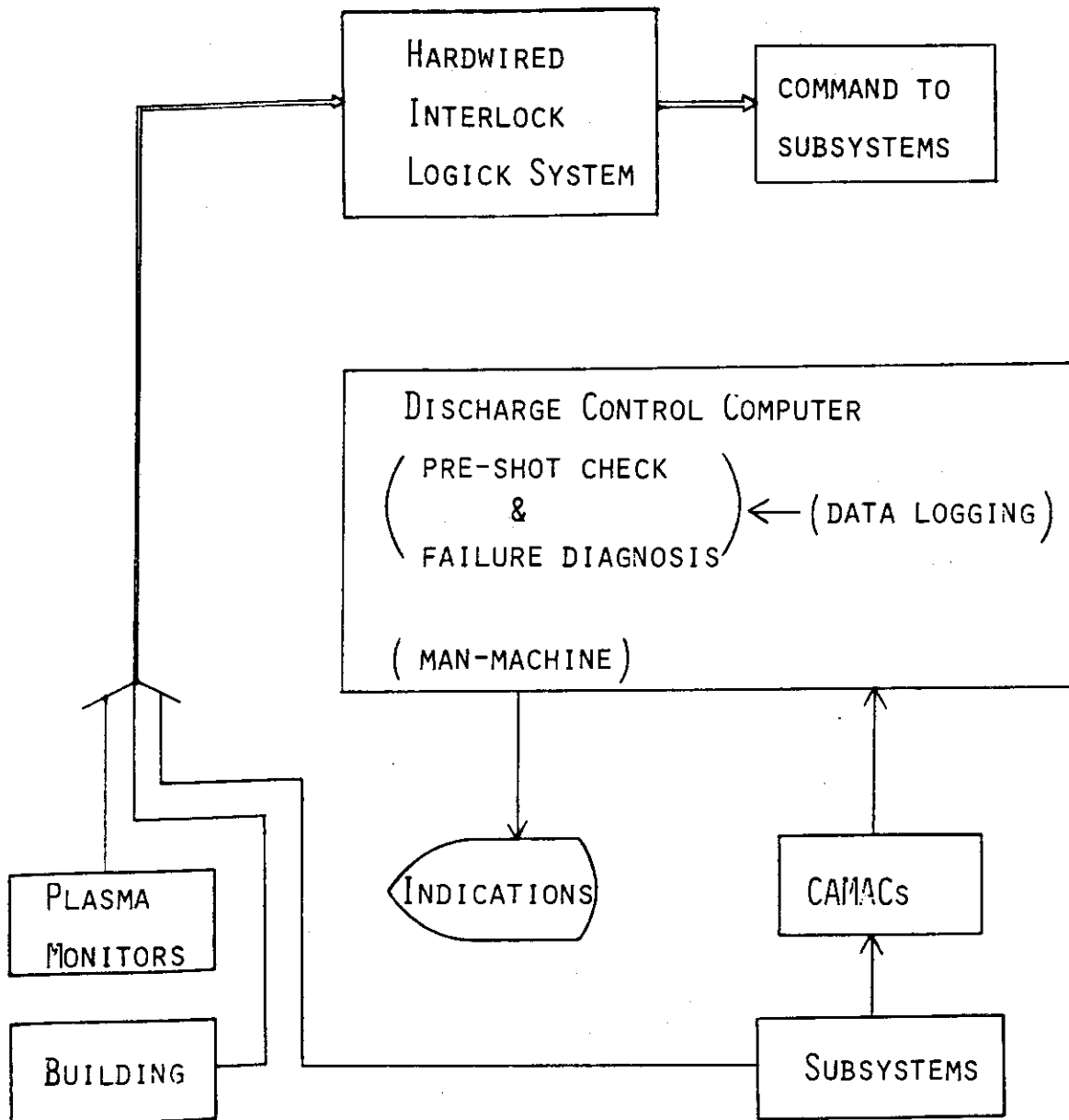


Fig. X.5-10 Signal flow for safety and protection



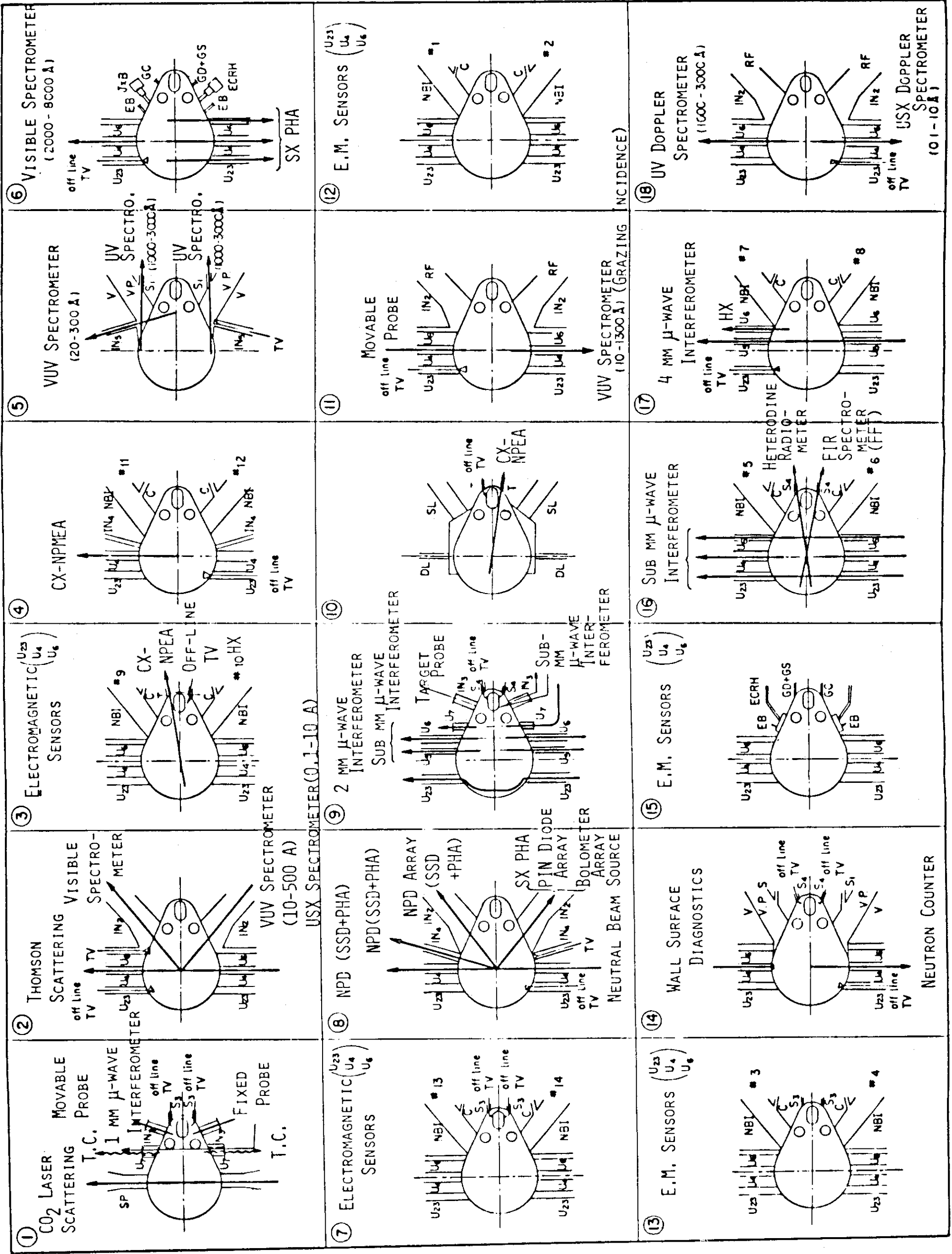


Fig. X.5-11 Allocations of diagnostics.

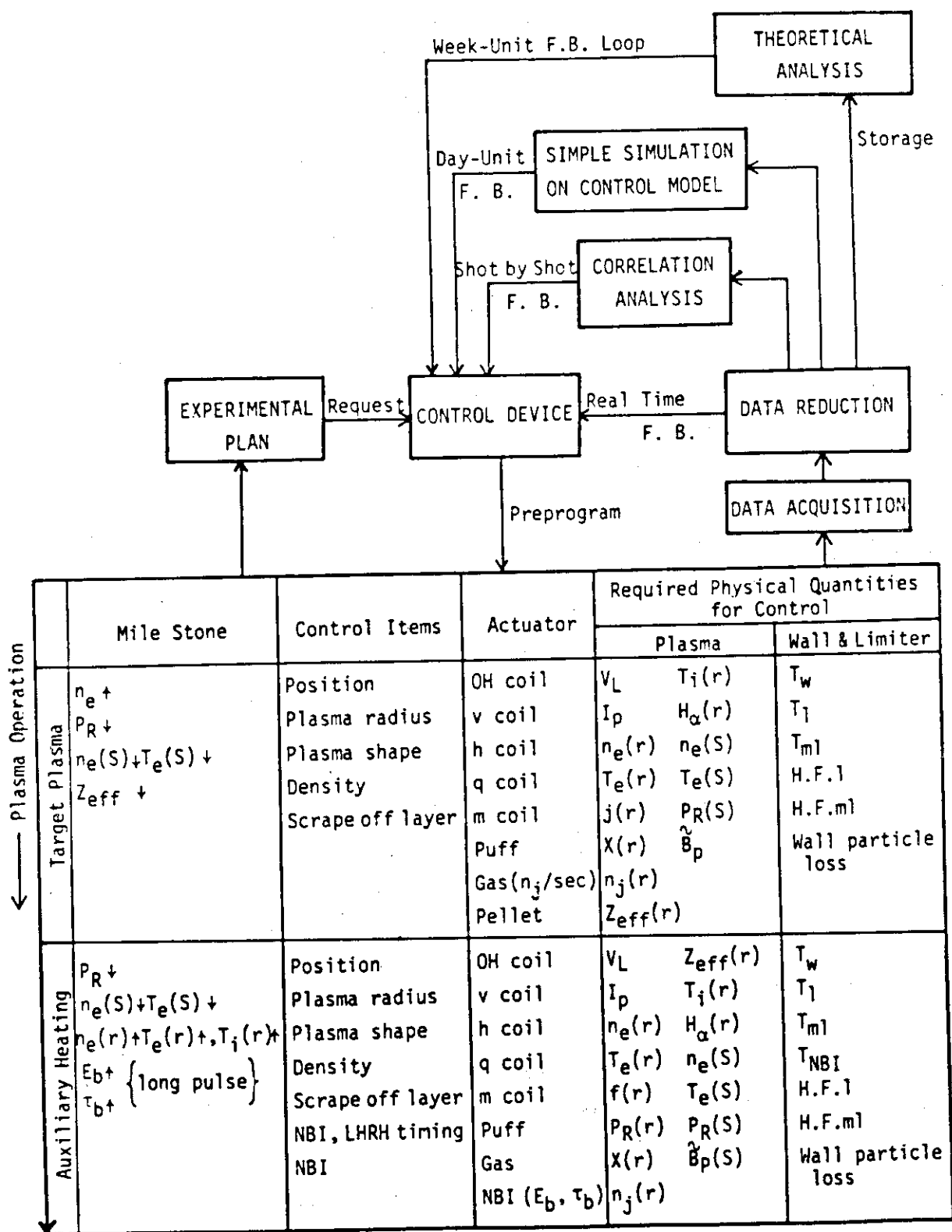


Fig. X.5-12 Flow chart of the decision process of the experimental conditions of experiment

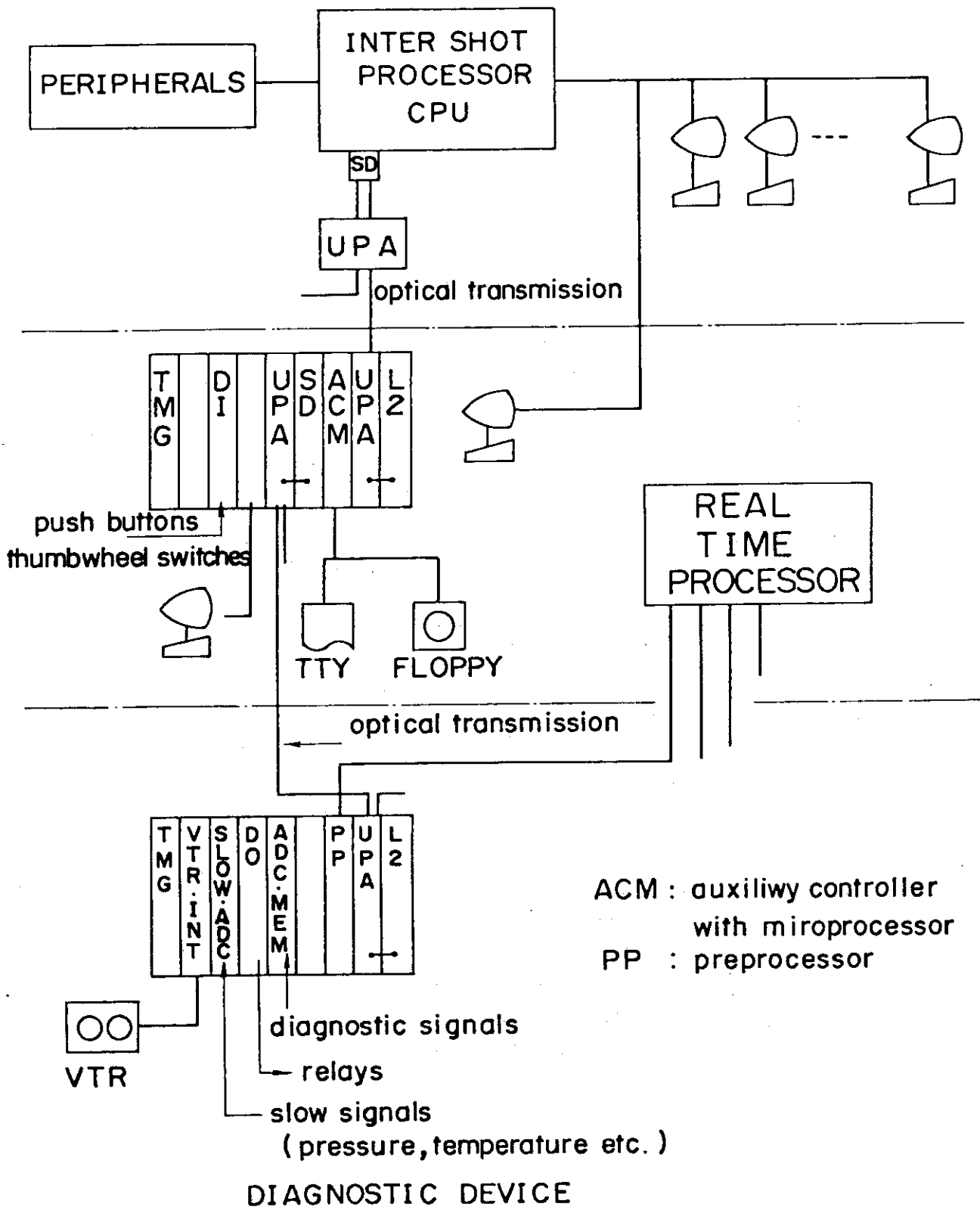


Fig. X.5-13 Detailed structure of the data processing system

## 6. Status of Auxiliary Systems

### 6.1 Secondary cooling system

The secondary cooling system is to remove and dissipate heat generated and transferred through its heat exchanger in each system of JT-60. Major components of the system are a cooling tower, water pumps, valves and pipes, water treatment device and water processing units.

The design was made under the following conditions; maximum wet thermometer temperature 26.5 °C, maximum temperature of make up water 30 °C, and its maximum allowable water supply 130 m<sup>3</sup>/hr. Some of the characteristic values of the system are summarized below:

|   |                             |
|---|-----------------------------|
| Total circulation of water              | 9,850 m <sup>3</sup> /hr    |
| Inlet temperature at exchanger          | 31 °C                       |
| Maximum outlet temperature at exchanger | 37 °C                       |
| Concentration coefficient number        | 4                           |
| Make up water                           | 130 m <sup>3</sup> /hr      |
| Average heat removed                    | 4.7×10 <sup>7</sup> kcal/hr |

### 6.2 Power distribution system

The power distribution system receives electric power from the central power station and distributes the power directly to the toroidal and the poloidal field coil power supply and through power distribution subsystems to the vacuum pumping, secondary cooling, and other systems and to the buildings. The distributed power is as follows:

1. Toroidal field coil power supply:
 

|                     |         |
|---------------------|---------|
| to motor-generator  | 25 MVA  |
| to the oil directly | 200 MVA |
2. Poloidal field coil power supply:
 

|                    |        |
|--------------------|--------|
| to motor-generator | 20 MVA |
|--------------------|--------|
3. Supplementary heating power supply:
 

|                    |        |
|--------------------|--------|
| to motor-generator | 25 MVA |
|--------------------|--------|
4. Operation distribution subsystem: 20 MVA
5. Building distribution subsystem: 15 MVA

## 7. Vacuum Technological Development for JT-60

In June 1979 Vacuum Technology Group was started in the Large Tokamak Development Division. This group has the responsibility for vacuum technology and component development for the JT-60 construction and experiment.

In FY 1979, two vacuum experimental facilities named JVX-I and JVX-II were being designed and constructed. Their completion is expected in August 1980.

JVX-I is intended to use mainly for the optimization of in-situ coatings of low-Z materials and for the demonstration of the surface cleaning procedures for JT-60 including high temperature bakeout, chemical treatment in oxidizing and/or reducing atmosphere, and discharge cleaning. It will consist of a cylindrical vacuum vessel made of Inconel 625, 0.36 m in diameter and 1.5 m long, a molybdenum liner which will be bakeable to 550 °C, an in-situ coating device, an RF discharge equipment, an atomic hydrogen source, diagnostics, and a turbomolecular pumping system with a 20 K cryopump. The surface monitor station will be capable of exposing a sample substrate to the wall position. After coating or cleaning, the sample can be retracted to an attached UHV system for SEM observation and Auger and secondary ion mass analysis.

JVX-II is intended to use mainly for the development of the leak detection and location system in JT-60 and for the testing of vacuum components such as gate valves and vacuum seals. It will consist of a bakeable vacuum vessel made of stainless steel, 1.0 m in diameter and 1.5 m long, a movable mechanism for leak sensors in three dimensional vacuum space, various kinds of leak detection instruments, and a turbomolecular pumping system.

In JT-60, locating a leak to a specific seal will be accomplished by introducing a tracer gas into each joint. This approach is typical of all vacuum seals on the diagnostic, pumping and neutral beam ports, and some welded joints on the vacuum vessel. Leak location would also be done by detecting a local pressure rise within the vacuum vessel due to gas influx from a leak. In this case a small pressure sensor must be moved inside the vacuum vessel by a skilful manipulator. We also studied the possibility of detecting only directional beams from leak points by using a molecular beam detector under a contract with Institute of Industrial Science, The University of Tokyo.

Metal-sealed gate valves are needed to isolate the diagnostic, pumping and neutral beam systems from the torus vacuum vessel. For the procurement of the valves for diagnostic ports, we have been testing samples from domestic and foreign manufacturers in cooperation with Hitachi, Ltd. The test items include opening and closing operation up to 2000 cycles with 350 °C bakeout at open position and 250 °C bakeout at closed position. Valves with polyimide gate seals were ruled out because of a difficulty in procuring the material.

## 8. JT-60 Experimental Planning and Plasma Considerations

### 8.1 Experimental program and schedule

Plasma experimental program were reviewed and revised in view of recent status of tokamak research as well as the JT-60 project. The revised schedule is shown in Fig. X.8.1-1. Since JT-60 is one of the major critical paths for Japanese fusion program, high efficient operation is required as well as well considered preparation. To realize the high efficient operation, it is necessary to obtain reliable heating devices as well as the reliable main machine including the control and diagnostic system, and it is also necessary to operate the machine during 24 hours a day. Concerning the preparation, training of excellent many staffs is very important as well as preparation of excellent numerical codes.

Following experiments are scheduled.

#### 1) Preliminary experiment

In the first phase of this experiment, plasmas only with ohmi heating are studied. A suitable target plasma for heating has to be obtained with and without the divertor (magnetic limiter). Discharges, however, will not be intensively studied in a wide range of plasma parameters because installation and/or test of heating devices, diagnostics and the real time control system will be more important. A  $Q^* = 1$  plasma will be easily obtained with 20 - 30 MW heating because the plasma will have been obtained in the other large tokamak devices. The main objective in this phase is to confirm the results in the other large tokamak projects and to prepare the following experiments.

#### 2) Basic experiment

In this experiment, the standard operation with 30 MW & 10 sec heating is investigated with following items.

##### i) Build-up phase of $Q^* \approx 1$ plasmas

Clean and stable current raising by using the poloidal divertor, control coils, dynamic limiter, gas puff and/or heating devices is investigated. Heating experiment with 20 MW NBI and 10 MW RF with and without the poloidal divertor will be done. 14 Injectors and 4 sets of RF devices are independently operated. It will be necessary to control the scrape-off layer plasma as well as the main plasma.

ii) Confinement characteristics of reactor grade plasmas

Detailed parameter study with and without the poloidal divertor.

iii) Steady state operation

Control of a long pulse plasmas by the real time control system is studied. Not only the plasma position and shape but also the major plasma parameters are controlled by employing various actuators shown in 9.2.1-b with and without the poloidal divertor.

iv) High  $\beta$  operation

The maximum  $\beta$  value will be obtained and high  $\beta$  plasmas are maintained during 5 ~ 10 sec. Build-up process will be intensively investigated as well as characteristics of the high  $\beta$  plasma with and without the poloidal divertor. Very-low-q operations are also investigated.

v) First wall and impurity experiment

In order to obtain first wall data for a reactor, various kinds of wall materials including low-z, middle-z and high-z materials are tested as the first wall. The first wall material to be used in a reactor will be intensively investigated with various wall temperature upto 500 °C. Impurity control by cooling the scrape-off layer plasma is investigated as well as by using the poloidal divertor.

vi) Plasma operation to mitigate engineering difficulty

The following items will be studied: Disruption control; slow current raise and shut down; slow heating; reducing the heat flux density by using swinging divertor; edge cooling and/or vibrating the plasma column; conventional wall material; impurity control without the poloidal divertor; systematic study of stress of coils, vacuum chamber and so on; easy cleaning method; simulation of easy ash exhaust system such as the simple poloidal divertor and/or mechanical divertor; high efficient RF heating; very-low-q operation free from disruption.

vii) High efficient heating

The maximum RF power into the torus is 23 MW. If the scrape-off layer plasma can be controlled, the heating efficiency can be increased.

viii) Development of a control system for a reactor core

It is necessary to develop a reliable real time control system



especially simple sensors for controlling plasma parameters including temperature, density,  $\beta$ , impurity, heat flux and heating. This problem is also planned to be studied.

### 3) Advanced experiment

After increasing NBI power upto 30 MW and RF heating efficiency, the total heating power will be 40 ~ 50 MW. A  $Q^* \approx 3$  plasma will be obtained, and is very similar to the reactor core plasma. The each experiment listed in 2) will be also done with this condition. Extremely long pulse operation will be also studied if it will be required.

### 4) PROTO ETR experiment

After finishing the detailed design of a reactor, JT-60 is planned to be modified to a device similar to the reactor. Before operating the reactor, the similar operation will be tested in the modified JT-60.

In order to do these experiments, following characteristics were incorporated into JT-60: 1) high- $\beta$  operation; 2) real time data processing and real time control of heating devices as well as poloidal coil currents and gas influx: Therefore, the major characteristics of JT-60 are as follows:

- 1) Hydrogen machine
- 2) plasma volume ( $60 \text{ m}^3$ ),
- 3) long pulse operation with additional heating (30~50 MW, 10 sec),
- 4) high- $\beta$  plasma with  $B_t = 4.5 \text{ T}$  (4%, 5~10 sec),
- 5) poloidal divertor with a short and wide throat, and
- 6) easy changeability of the first wall material.

These characteristics are related with the research objectives and a brief description of the each characteristics are shown below.

#### 1) Hydrogen machine

It is important to demonstrate D-T burning, to study  $\alpha$ -particle heating and to investigate neutronics in a D-T machine. The D-T operation, however, induces various problems due to the activation. For example, the first wall replacement after activation is difficult in a D-T machine,

and numbers of shots are limited. There are, on the other hand, many items of research to be studied in a hydrogen machine as discussed below. From this point of view, the hydrogen plasma is planned in JT-60.

## 2) Plasma volume ( $60 \text{ m}^3$ )

It is reasonable to consider that the size of JT-60 is similar to that of a reactor from plasma engineering point of view.

## 3) Long pulse operation with additional heating ( $30\sim 40 \text{ MW}$ , $10 \text{ sec}$ )

The duration  $10 \text{ sec}$  is enough long to study a heating phase, a steady state and plasma control by using a real time control system with a reactor like conditions. Heating power is also enough to obtain a reactor grade plasma.

## 4) High- $\beta$ plasma with $B_t = 4.5 \text{ T}$

In JT-60, behaviors of a reactor like circular plasma near critical  $\beta$  will be examined in detail. Combining the experiment in JT-60 and the experiment in a D-shape device, e.g. D-III or JFT-2M, it is easy to picturize a reactor core plasma.

## 5) Poloidal divertor with a short and wide throat

In a reactor, it is expected that a magnetic divertor is not required. However it is not clear whether a magnetic divertor is necessary or not. A simple poloidal divertor with a short and wide divertor throat is the most reliable divertor concept in a reactor. From this point of view, it is very important to study the simple poloidal divertor in JT-60.

## 6) Easy exchangeability of the first wall material

By this time, it is impossible to decide the first wall material of a reactor. Therefore it is very important to study various kinds of wall materials in a large device. Neutron effects have to be studied in another programme. The first wall of JT-60 is easily demounted or the surface material is easily exchanged by using an in-situ coating method.

These characteristics of JT-60 are mainly given from design studies of reactors. In order to make good use of these characteristics the following diagnostic system and real time control system are being developed.

## a) Diagnostic system

In addition to measurement of conventional plasma parameters, heat flux and particle flux on each surface and peripheral plasma are also measured. All the diagnostics are planned to be arranged so that they may acquire spacial and time resolved informations within one shot.

Priority is given in the adoption of diagnostics to those which do not require complicated data processing. For example, we appreciate cyclotron radiation method best among electron temperature measurements, because it gives spacial and time resolved information straight forwardly without any processing.

## b) Real time control and data processing system

Certain diagnostic informations are gathered, processed and fed to the control system during a shot in real time.

Control items are plasma position, radius, shape, current, density, radiation loss power, scrape-off layer, heating power and timing, temperature,  $\beta$  &  $\beta_p$ , heat flux and so on. Actuators are the poloidal coil system including the magnetic divertor coils, hydrogen and impurity gas supply system, 14 NBI injectors, 4 units of RF systems, the dynamic limiter and so on.

In addition to these characteristics of the device, numerical codes including divertor analysis, high- $\beta$  operation analysis and so on are being developed. Various first wall materials and coating methods are also being tested.

## 8.2 Plasma considerations

## 8.2.1 Predictions of plasma parameters

Principal parameters of JT-60 are summarized in Table X.8-1. First wall (liner and limiter) is made of molybdenum. Some low- $z$  material such as carbon, titanium, or other composites will possibly be coated on the molybdenum base. JT-60 features a magnetic limiter for the control of plasma current and impurity content.

Heating power required in JT-60 is predicted by a simple consideration of power balance, and is given in Fig. X.8-2 in terms of energy confinement time  $\tau_E$ . Power input in ohmic heating is presumed  $P_{OH} = 2 \sim 3$  MW.

Additional heating power of 20 - 40 MW is probably adequate for achieving the expected parameters in JT-60 target region. The machine design permits the poloidal beta up to 2.5 for standard operation mode and up to 1.5 for magnetic limiter operation mode. The later can be improved to 2.5 for specific divertor plasma behaviors.

A hybrid heating of NBI and RF wave is provided for the JT-60 additional heating. Power deposited on plasmas are expected 20 MW of neutral beams and 10 MW of RF waves. Further increase up to 30 MW in neutral beam power is being considered as an advanced program.

Evolution of parameters on  $\bar{n}_E\bar{\tau}_E$ - $\bar{T}$  diagram is shown in Fig. X.8-3, where the Alcator law

$$\tau_E = 5 \times 10^{-21} \sqrt{q_a} \cdot n_e (m^{-3}) \cdot a^2 (m)$$

is presumed as a scaling law of energy confinement and the density limited by neutral beam penetration is defined as

$$\bar{n}_e (m^{-3}) \leq \frac{1}{9} \frac{E_b (eV)}{A_b L (m) \sigma_{eff}} \times 10^{16}.$$

Here  $E_b$  is the beam energy,  $A_b$  the atomic number of injected beam atom, and  $L$  the beam path from the plasma surface to the plasma center, respectively.  $\sigma_{eff}$  is an enhanced beam trapping factor due to ionization and charge-exchange by impurity ions and  $\sigma_{eff} = 1$  for  $Z_{eff} = 1$ . For the heating powers of 75 keV - 20 MW NBI and 10 MW RF, it can be expected that  $\bar{n}_E\bar{\tau}_E = 3 \sim 4 \times 10^{19} m^{-3} \cdot sec$  and  $\bar{T} = 8 \sim 10$  keV, which are in the JT-60 target region. Then the fusion energy gain  $Q^*$  equivalent to D-T plasmas can be reached unity and the breakeven condition is fulfilled even though the beam fusion effect is not anticipated. If fusion enhancement is expected by deuterium beams with the same penetration as 75 keV hydrogen beams, the equivalent fusion gain reaches  $Q^* \sim 2$ .

Further improvement of parameters corresponding to  $Q^* \geq 3$  would be achieved by increase of the beam energy (75-100 keV: operational in the present design), heating power (30-40 MW) and wave heating efficiency (50%→70~80%).

### 8.2.2 Operation scenarios

Because JT-60 features a magnetic limiter, two types of operation

mode are typically possible: standard mode and magnetic limiter mode. Major parameters associated with these two modes are summarized in Table X.8-1.

For desirable current build-up, various operation scenarios<sup>1-2)</sup> are taken into accounts in the design, as shown in Table X.8-2 (a). They are related principally to the control of plasma current distribution and impurity content during the current build-up.

The plasma current is realised in stepwise with aid of inductive energy transfer technologies, as shown in Table X.8-2 (b). Plasma control fields can be follows these step rampings of the plasma current. The rising time of the plasma current is changeable between 0.1 sec and 2 sec. Optimum flux swing can be attained by the double-step or triple-step ramping of the current. Schematic view of plasma during current build-up is shown in Fig. X.8-4 for respective operation modes.

During the flat top with duration of 5 - 10 sec, the plasma current and the plasma position and shape are controlllyd by feedback or pre-programming system in accordance with the changes of plasma beta and current profile in both cases of standard mode and magnetic limiter mode. Heating by NBI and RF wave can sustain reactor-grade plasmas during 10 sec.

Configurations of the equilibrium magnetic field are investigated for high beta operation of both standard and magnetic limiter modes.

At the shutdOwn of plasma, the plasma current and position are feedback-controlled so that the plasma current decreases with a decay time of about 1 sec. The device itself is designed to withstand the electro-magnetic force, heat deposition and induced voltage associated with major current disruption of 1 msec. However, control of current decay time is also beam investigated.

### 8.2.3 Neutral beam injection heating

The injected neutral atoms are stripped to produce fast ions via impact ionization and charge-exchange interaction with plasma particles; electrons, protons and impurity ions. In respect to the charge-stripping interaction between hydrogen atom and impurity ion, an empirical relation<sup>3)</sup>,

$$\sigma_z = Z^{1.4}(\sigma_p + \sigma_{cx}),$$

is used here for the calculations of beam attenuation, where  $\sigma_z$  is the

effective stripping cross section of an impurity ion for hydrogen atom (including impact ionization and charge-exchange),  $Z$  the impurity ion charge,  $\sigma_p$  the proton impact ionization cross section,  $\sigma_{cx}$  the proton-hydrogen atom charge-exchange cross section, respectively.

The beam power deposition profiles are calculated as shown in Fig. X.8-5 for various electron densities<sup>4)</sup>. When the 75 keV beam is injected into a low density plasma with  $n_e \leq 2 \times 10^{19} \text{ m}^{-3}$ , the untrapped beam power exceeds 20 % of the injected beam power. In the meanwhile the beam injected into a high density plasma causes surface trapping of the beam as shown in Fig. X.8-5 : for  $n_e \leq 1 \times 10^{20} \text{ m}^{-3}$  the trapped beam power in the plasma surface ( $0.8 \leq r/a \leq 1$ ) becomes larger than 40% of the injected power.

#### (1) Loss of fast ions

To make detailed treatments of the fast ion behavior in a toroidal plasma and the reionization effect on escaping charge-exchange neutrals. Monte-Carlo techniques are employed as the most useful method to simulate the collisional processes.

Three kinds of loss processes are accounted for the fast ions during their slowing-down process; orbit loss, ripple loss and charge-exchange loss. Quantitative studies of these losses have been made by the Monte-Carlo simulation code. The radial profile of neutral atoms has been calculated by solving a one-dimensional integral equation<sup>5)</sup>. Then the Alcator law is taken as the particle confinement time  $\tau_p$ <sup>6)</sup>.

The choice of quasi-perpendicular injection results in a possible enhancement of fast ion loss due to the effect of toroidal field ripple<sup>7)-8)</sup>.

Drift orbit and collisional process have major influences on the fast ion behavior in the ripples. One of important features is the collisionless ripple-trapping. The ripple trapping zones are illustrated in Fig. X.8-6(a). The central zone corresponds to the direct ripple-trapping region defined by  $(v_{||}/v)^2 < \delta_{eff}$ , where  $\delta_{eff}$  is the ripple well depth and  $v_{||}$  the longitudinal component of the ion velocity  $v$ . Side bands appear even though collisionless, owing to the finite banana size effect associated with the ripple well inhomogeneity.

The existence of ripple results in significant enhancement of banana drift, which is much larger for fast ions than that predicted by earlier investigations<sup>9)</sup>. The radial drift step of banana for a half bounce time is shown in Fig. X.8-6(b) with the fast ion initial pitch angle. The radial

step discontinuity occurs at the fast ion pitch angle of ripple trapped-untrapped boundary.

The total energy loss of fast ions is examined and its density dependence is shown in Fig. X.8-7, where the parabolic profiles are taken for parameters and  $\bar{T}_e = 5$  keV,  $Z_{eff} = 2$  and  $q_a = 3.5$  are assumed here. If we choose the plasma density in the range  $3 \times 10^{19} \text{ m}^{-3} \leq n_e \leq 1 \times 10^{20} \text{ m}^{-3}$ , the total loss power can be held less than 10-15 % of the injected power.

It is expected that the ripple-trapped loss of fast ions  $G_{rt}$  is sufficiently small even though a quasi-perpendicular injection geometry is taken in JT-60. However it should be noted that the ripple-trapped loss ions possibly concentrates on specific areas and causes a large heat deposition on the first wall. Fig. X.8-8 shows the maps of heat deposition due to the banana orbit loss ions and the ripple-trapped loss ions. Because JT-60 employs toroidal limiters, the banana orbit loss ions hits the limiters. On the other hand the ripple trapped loss ions enter localized areas of liner.

## (2) Impurity evolution by neutral beam injection

The impurity evolution associated with beam injection is one of serious problems in the present-day Tokamaks. Here we focus our considerations on the sputtering effect as the impurity origin and do not refer in detail to other processes such as evaporation, erosion and arcing.

Three types of beam-associated particles can incident onto the wall and sputter the wall material. They are

- (a) uptrapped beam particles,
- (b) escaping fast neutrals,
- (c) escaping fast ions.

The escaping fast neutrals have a broad energy spectrum and their population is large in the energy range where the hydrogen sputtering yield exhibits its peak (1-10 keV). On the other hand, fast ions due to banana drift loss and ripple-trapped loss, although their energy profile is expanded during slowing down, have a small fraction in the 1-10 keV range. In the expected parameter range ( $\bar{n}_e = 2 \sim 10 \times 10^{19} \text{ m}^{-3}$  and  $\bar{T}_e = 2 \sim 10$  keV), it is obtained conclusively that the molybdenum fractions sputtered by respective beam-associated loss particles become as follows:

$$\begin{aligned} Y_{ut} &\leq 5 \times 10^{-5} && \text{(by untrapped beam)} \\ Y_{fn} &= 1 \sim 7 \times 10^{-4} && \text{(by fast neutrals)} \\ Y_{fi} &= 0.3 \sim 1.5 \times 10^{-4} && \text{(by fast ions).} \end{aligned}$$

By the summation of  $Y_{ut}$ ,  $Y_{fn}$  and  $Y_{fi}$  the cumulated molybdenum flux becomes  $Y_B = 4 \sim 8 \times 10^{-4}$ , the major of which comes from the fast neutral bombardment. The absolute flux of molybdenum atoms sputtered by fast particles is  $y_b = 0.8 \sim 1.6 \times 10^{16}$  atoms/m<sup>2</sup>·sec.

In turn we need to predict the amount of molybdenum atoms sputtered by plasma particles. For this, three kinds of processes are considered. They are

- (d) wall bombardment by thermal (hot) neutrals,
- (e) wall bombardment by boundary plasma ions,
- (f) self-sputtering by molybdenum ions.

The outflow of the hot neutrals and its energy spectrum can be calculated by the one-dimensional integral equation code for neutrals<sup>3)</sup>. The molybdenum flux sputtered by hot neutrals is estimated as  $y_{hn} = 4 \sim 8 \times 10^{16}$  atoms/m<sup>2</sup>·sec. The molybdenum flux  $y_{pi}$  and  $y_{self}$  caused from processes (e) and (f) are somewhat difficult to estimate, and therefore we will give here roughly the orders of them.

$y_{pi} = 0.2 \sim 2.0 \times 10^{16}$  atoms/m<sup>2</sup>·sec,  
and  $y_{self} = 5 \sim 15 \times 10^{16}$  atoms/m<sup>2</sup>·sec

for the boundary plasma temperature of 50-500 eV and the molybdenum ion concentration in boundary plasma  $\bar{n}_Z/\bar{n}_e = 0.05$  %. From these estimations, it can be seen that  $y_{hn} \sim y_{pi} \sim y_{self}$  and the summation of them  $y_p (= y_{hn} + y_{pi} + y_{self})$  is around  $10^{17}$  atoms/m<sup>2</sup>·sec.

It appears that the impurity influx induced by beam injection  $y_b$  is smaller by one order of magnitude than that by plasma particles  $y_p$ . This situation is not changed in case of low-Z first wall material. It should be noted however that the escaping fast ions due to the banana drift loss or the ripple-trapped loss concentrate on specific areas of the first wall, resulting in a possible erosion or evaporation of the wall surface especially in case of the injection into high density plasmas.

#### 8.2.4 Radio frequency heating

Both of LHRF and ICRF heating schemes are considered in the scope of JT-60 wave heating program. At present, however, priority is placed of LHRF heating scheme and technological efforts are mainly devoted to design and development of LHRF heating system.

LHRF heating scheme has appreciable advantages in engineering aspects: the hardware required for reactor grade tokamaks such as JT-60 is already



state of the art and a simple waveguide coupling system is used favorably. Hence JT-60 employs phased-array-waveguides (Grill) as the LHRF wave coupling system, and aims to achieve effective heating of high density plasmas ( $\bar{n}_e \sim 10^{20} \text{ m}^{-3}$ ) at the power deposition of 10 MW on plasma.

## (2) Plasma-wave coupling characteristics

Brambilla's theory<sup>10)</sup> was employed for studying coupling characteristics. Relation of power reflection coefficient  $R$  versus phase difference was calculated and is shown in Fig. X.8-9(a) for a few values of density gradient  $\partial n / \partial x$ . Power reflection is expected to be less than 20 % for possible density gradient  $\partial n / \partial x \leq 10^{20} \text{ m}^{-4}$  and for controlled phase difference  $\Delta\phi = 90^\circ \sim 180^\circ$ . According to the high power LHRF heating experiment in JFT-2 ( $P_{rf} = 100 \sim 200 \text{ kW}$ ), power reflection was reduced considerably less than that predicted by Brambilla's theory, especially in a range of  $\Delta\phi = 0^\circ \sim 90^\circ$ . It probably comes from a non-linear coupling of the wave with plasmas. Thereby the coupling efficiency 80 % can be expected in JT-60.

Power spectra of  $N_z$ , where  $N_z$  is the refractive index parallel to the magnetic field, are shown in Fig. X.8-9(b) in cases of the pump wave frequency  $f_0 = 1.7 \text{ GHz}$  and  $2.0 \text{ GHz}$ . Then the phase difference  $\Delta\phi$  is set at  $180^\circ$  and density gradient  $\partial n / \partial x = 10^{20} \text{ m}^{-4}$  is assumed. Major part of the wave power is associated with slow waves with  $N_z = 1.4 \sim 3$  for both pump wave frequencies.

## (3) Accessibility and wave propagation

The slow wave, which satisfies the accessibility condition  $N_z^2 > N_{ZA}^2$   $1 + \omega_{pe}^2 / \omega_{ce}^2$ , can propagate toward the higher density region of plasma. Contours of  $N_{ZA}$  are shown by dotted lines on a diagram of toroidal magnetic field  $B_t$  and electron density  $n_e$  in Fig. X.8-10. The perpendicular wave number increases as the wave with constant  $N_z$ , satisfying the accessibility condition, travels radially toward the plasma center. Then two fluid equations were solved in the electrostatic approximations. The wave goes through plasma with increase of perpendicular wave number and is reflected at a turning point. The reflected wave moves toward the lower density region of plasma. This reflected wave is trapped between two ion cyclotron harmonics layers after mode conversion into ion Bernstein mode. Turning point of each wave is traced by solid lines on  $B_t$ - $n_e$  diagram in Fig. X.8-10 for  $f_0 = 1.7$  and  $2.0 \text{ GHz}$ .

When a parabolic profile is assumed for plasma parameters as shown in Fig. X.8-10, the accessibility condition becomes  $N_z \geq 1.4 \sim 1.5$ . Then the slow waves with  $N_z = 1.4 \sim 3$  possibly propagate into a high density region, and the power deposition area is predicted by the hatched zone. This zone moves outward radially as the density increase and/or the frequency decrease.

#### (4) Wave power absorption

The slow wave propagating toward its turning point suffers from an electron Landau damping and the wave energy is absorbed into plasma electrons. On the other hand ion Bernstein wave trapped between the two ion cyclotron harmonics layers converges finally to surface with stronger magnetic field and its energy is absorbed by ions via ion cyclotron damping.

Wave power deposition profiles are shown in Fig. X.8-11(a), (b), and (c). It becomes apparent that the power deposition region moves outward with increase of density and/or temperature. The overall deposition rate of the transmitted power ( $P_{\text{dep}}/P_{\text{rf}}$ ) is estimated as about 90 % in these three cases of plasma parameters.

According to the recent results in JFT-2, effective ion heating has been observed over a wide range of electron densities and its efficiency has become 50 ~ 70 %.<sup>11)</sup> These results predict that effective ion heating is possible even when turning points do not locate near the plasma center. From these considerations, effective heating of high density plasma will be expected in JT-60.

#### 8.2.5 Impurity control

In recent years, impurity control has become one of most important problems in Tokamak research. Impurity control are classified typically into two groups, i.e., light impurity control and wall material impurity control.

##### (1) Light impurity control

Most of light impurities come from the wall surface on which gaseous impurities such as C, N and O are adsorbed and absorbed. These kinds of impurities can be reduced less than acceptable limits by providing proper treatments of the wall surface before assembly and by in-situ conditioning after assembly.

## (2) Wall material impurity control

Control of wall material impurity is essentially important in large tokamaks such as JT-60 to achieve a reactor-grade plasma and maintain it during a long discharge. Evaporation, arcing and sputtering cause the origin of wall material impurity in actual tokamaks. Evaporation can be excluded by spreading the heat flux. Arcing is serious in dirty, unstable discharge and in an early stage of plasma formation. In the steady-state of discharge, however, sputtering by neutral particles, plasma ions and impurity ions become the dominant process of wall material impurity generation.

We consider a simple model of impurity accumulation only due to the sputtering<sup>12)</sup>, which is described by

$$\frac{d\bar{n}_z}{dt} = -\frac{\bar{n}_z}{\tau_z} + (1-\lambda_1)\left(\xi_p \frac{\bar{n}_e}{p} + \xi_z \frac{\bar{n}_z}{\tau_z}\right) + \frac{S_p}{V_p} (1-\lambda_2)(y_{hn}+y_b)$$

where  $\lambda_1$  is the shielding factor for impurity sputtered by plasma ions and impurity ions,  $\lambda_2$  the shielding factor for impurity sputtered by hot neutrals and fast neutrals,  $\xi_p$  the plasma ion sputtering yield,  $\xi_z$  the impurity ion sputtering yield,  $\bar{n}_z$  the average impurity ion density,  $\tau_p$  the plasma ion confinement time,  $\tau_z$  the impurity ion confinement time,  $S_p$  the plasma surface area, and  $V_p$  the plasma volume, respectively. Notations  $y_{hn}$  and  $y_b$  are defined in 8.2.3(2) and their magnitudes are estimated for molybdenum.

In addition to the above equation, a simplified particle balance equation

$$\frac{d\bar{n}_e}{dt} = -\frac{1-\gamma}{\tau_p} \bar{n}_e + \Pi_e$$

is introduced, where  $\gamma$  is the plasma particle recycling ratio and  $\Pi_e$  the particle source such as gas-puffing and injected beam.

By solving these two equations, the impurity accumulation time  $\tau_{zs}$  and the saturation level of the impurity concentration  $(\bar{n}_z/\bar{n}_e)_s$  are derived as:

$$\tau_{zs} = \frac{\tau_z}{1-(1-\lambda_1)\xi_z - (1-\gamma)\frac{\tau_z}{\tau_p} + \frac{\Pi_e}{\bar{n}_e} \tau_z}$$

and

$$\left[\frac{\bar{n}_z}{\bar{n}_e}\right]_s = \left\{ (1-\lambda_1) \frac{\xi_p}{\tau_p} + \frac{S_p}{V_p} (1-\lambda_z) \frac{y_{hn}+y_b}{\bar{n}_e} \right\} \tau_{zs}$$

The impurity accumulation time  $\tau_{zs}$  is estimated as  $(1\sim 5) \times \tau_z$  for the 75 keV-20 MW injection. Long saturation times are associated with low values of  $\lambda_1$  and  $\gamma$ . Assuming that  $\gamma = 0.8$ ,  $\tau_p = \tau_z = 3 \times 10^{-21} \sqrt{q_a} n_e a^2$  and  $\Pi_e = 4.6 \times 10^{19} \text{ m}^2 \cdot \text{sec}$  (corresponding to 75 keV-20 MW injection including cold gas inflow), the saturated impurity concentrations  $(\bar{n}_z/\bar{n}_e)_s$  are calculated in cases of typical wall materials; molybdenum, titanium and carbon.

Then the modification of the sheath potential owing to the secondary electron emission is taken into account.<sup>13)</sup> The results are summarized in Table X.8-3 for molybdenum, Table X.8-4 for titanium and Table X.8-5 for carbon, respectively. The upper limits of impurity concentrations are set at 0.1 % for molybdenum ions, 0.4 % for titanium ions and 10 % for carbon ions from a view point of radiation loss.<sup>14)</sup> The boundaries defined by these limits are illustrated by dark lines in respective tables. From Table X.8-3 and X.8-4 similar results are obtained for the molybdenum and titanium walls: low boundary temperature and high shielding factor are indispensable to reduce the metallic impurity concentration without magnetic limiter. These results indicate that the plasma boundary should be cooled strongly by some method<sup>15)</sup> to obtain a low metallic impurity plasma.

On the other hand, when the magnetic limiter is operated with achievable shielding factors of  $\lambda_1 = 0.9\sim 0.99$  and  $\lambda_2 = 0.9$ ,<sup>16)</sup> the metallic impurity concentration can be held less than the acceptable limits even if the boundary plasma temperature reaches 1000 eV. This boundary plasma can be formed with a low energy conversion rate  $((P_{cx}+P_r)/P_{in} \leq 0.5)$ . Conclusively the employment of magnetic limiter is essential for achieving an impurity free plasma and maintain it through a long discharge.

Sengolu, et al. investigated in detail the behavior of self-sputtered molybdenum ions in JT-60,<sup>17)</sup> by using Monte-Carlo techniques. They obtained relations of impurity growth rate  $\kappa$  versus boundary plasma electron temperature  $T_b$ . The impurity growth rate with magnetic limiter does not exceed unity in a range of  $T_b = 0\sim 400$  eV, which confirms the investigation in the present report. In the mean while  $\kappa$  becomes unity at  $T_b = 50$  eV in case of no magnetic limiter and this critical temperature is somewhat smaller than that given in Table X.8-3. They investigated it further taking into account of the effect of secondary electron emission and suggested that the critical temperature with  $\kappa = 1$  would be 80-140 eV without magnetic limiter.

This result corresponds well to the case of  $\lambda_1 = \lambda_2 = 0.6$  ( $T_b=130$  eV) in Table X.8-4.

Carbon seems most favorable among three materials investigated here as the JT-60 first wall. Table X.8-5 indicates that carbon impurity concentrations do not exceed the permissible level ( $(\bar{n}_z/\bar{n}_e) \leq 10\%$ ) even though the magnetic limiter is not operated. This situation can not be changed by introducing the chemical sputtering effects at 500 °C into the impurity evolution considerations if the boundary plasma temperature  $T_b$  is less than about 1000 eV.

#### 8.2.6 One-dimensional transport simulation

##### (1) Long pulse operation

A long pulse D-T burning is considered as the essential feature of practical fusion reactor. Long pulse operation of a Tokamak is attended with a number of plasma-physical and technological problems such as ash-exhaust, fueling, impurity control, and others. JT-60 intends to simulate some of these problems with hydrogen plasmas by 10-second operation of both the Tokamak and heating devices. Among them two problems, impurity control and density control, are important, in terms of the JT-60 long pulse operation. We treat here the problem concerning density control.

When the 20 MW beam injection is performed, the particle inflow becomes  $\Pi_e = 4.6 \times 10^{19} \text{ m}^{-3} \text{ sec}^{-1}$  in which the cold gas flow from the injectors is included, too. Density increase associated with beam injection results in the surface trapping of the beams. JT-60 has no divertor although a magnetic limiter is provided for impurity control. Then density increase can be controlled by the surface pumping of first wall material.

1-D simulation has been carried out with the 75 keV = 20 MW NBI by taking account of the recycling effect. Density control operation starts at 2 sec and is made by canceling the recycling particle flux corresponding to the efflux from NBI. Some of results are shown in Fig. X.8-12. Although the electron density at the plasma center increases gradually during the 10-sec NBI (Fig. X.8-12(c)), the average density is maintained at about  $(7.5 \sim 8.5) \times 10^{19} \text{ m}^{-3}$ . In the meanwhile the average ion temperature can be sustained beyond 5 keV (Fig. X.8-12(a)). The boundary density is rapidly eroded by the enhanced recycling effect, because of a small diffusion particle flux from the plasma central region, where confinement is

improved with the increase of  $n_e$ . Therefore, it may be most important to clarify the particle transport in the NBI-heated, long pulse operation plasmas.

(2) Surface cooling by low-z impurities

According to DIVA experiment, the mean electron temperature of a plasma in the scrape-off layer can be given by

$$\bar{T}_{es} = 0.2 \frac{P_{in} - P_{cx} - P_r}{P_{in}} (\bar{T}_e + \bar{T}_i),$$

where  $P_{in}$ ,  $P_{cx}$ ,  $P_r$ ,  $\bar{T}_e$  and  $\bar{T}_i$  are the input power, cx-loss power, radiation-loss power, mean electron temperature of the main plasma, and mean ion temperature, respectively. This result indicates that effective cooling near the plasma surface ( $P_r \sim P_{in}$ ) should be essentially required for attaining high temperature bulk plasmas ( $\bar{T}_e + \bar{T}_i = 10 \sim 20$  keV) with a material limiter.

In order to consider the possibility of edge cooling by means of light impurities, calculations were carried out in the case of impurity carbon (6%) taking account of impurity radiation and diffusion. Then the radial profiles of temperature and density were fixed. Temperature and its gradient were low and moderate in the boundary region, but high and steep in the central region. For these profiles, significant amount of partially ionized impurity ions is distributed near the plasma boundary region and excitation loss in this region is much larger than bremsstrahlung loss from the central region (see Fig. X.8-13). We see that radiated power density averaged over the edge region (arbitrarily taken to be 20 cm wide) can be of order  $0.42 \text{ W/cm}^3$ , whose value would correspond to a mean input power density in the case of 20 MW injection in JT-60. It may, indeed, be possible to radiate a substantial fraction of the power by means of edge-region impurity radiation. This result can be reduced essentially from temperature-screening effect: strong inward diffusion of impurities must be suppressed by temperature gradient of plasma ions.

References

- 1) H. Nonomiya, A. Kameari and Y. Suzuki, JAERI-M 6656 (1976)
- 2) T. Kobayashi, T. Tazima, K. Tani and S. Tamura, JAERI-M 7014 (1977)
- 3) R.E. Olson and A. Salop, SRI Annual Report, MP-77-59 (1977).
- 4) K. Tani, et al., Proc. Int. Symp. Heating in Toroidal Plasmas, Varenna, Vol.1, 31 (1978)
- 5) T. Kobayashi, et al., JAERI-M 7014 (1977) (presented in Japanese).
- 6) DIVA Group, Nuclear Fusion, 18, 1619 (1978).
- 7) K. Tani, H. Kishimoto and S. Tamura, Proc. 9th European Conf. on Controlled Fusion and Plasma Physics, Oxford, (1979), p.157.
- 8) K. Tani, H. Kishimoto and S. Tamura, to be presented in 8th IAEA Conference on Plasma Physics and Controlled Nuclear Fusion Research, Brussels (1980) CN-38/W-2-2.
- 9) K.T. Tsang, ORNL/TM-5630, 1976.
- 10) M. Brambilla, Nuclear Fusion, 16, 47 (1976).
- 11) T. Imai and T. Nagashima, private communication.
- 12) K. Tani, et al., IAEA Technical Committee Meeting and Workshop on the Plasma Physics of Intense Neutral Beam Heating in Tokamaks, ORNL, (1979).
- 13) C.F. Barnet, et al., ORNL Report, ORNL-5207 (1977).
- 14) R.V. Jensen, et al., Nucl. Fusion 17 (1977) 1187; T. Tazima, JAERI-M 7717 (1978).
- 15) Y. Shimomura, et al., Nucl. Fusion 17 (1977) 626.
- 16) M. Nagami, et al., Nucl. Fusion 18 (1978) 1347.
- 17) S. Sengoku, et al., Nucl. Fusion 19 (1979) 1327.
- 18) H. Ohtsuka, et al., J. Nucl. Mat. 76&77 (1978) 188.
- 19) P. Sigmund, Phys. Rev. 184 (1969) 383.
- 20) J. Roth, J. Bohdanský and W. Ottenberger, IPP 9/26 (1979).
- 21) D.L. Smith, J. Nucl. Mat. 75 (1978) 20.
- 22) R. Yamada, et al., to be published.

Table X.8-1 Plasma parameter of JT-60

|            | STANDARD<br>OPERATION MODE | MAGNETIC LIMITER<br>OPERATION MODE |
|------------|----------------------------|------------------------------------|
| $I_p$ (MA) | 2.7                        | 2.1                                |
| R (M)      | 3.0                        | 3.2                                |
| A (M)      | 0.95                       | 0.9                                |
| $B_T$ (T)  | 4.5                        | 4.5                                |
| $B_V$ (T)  | 0.38                       | 0.32                               |
| $\beta_P$  | 2.5                        | 1.5 (2.5)                          |

Table X.8-2(a) Operation modes of JT-60

| CURRENT BUILD-UP   | FLAT TOP                           | ADDITIONAL HEATING       |
|--|------------------------------------|--------------------------|
| STANDARD OPERATION<br>MODE   | STANDARD<br>OPERATION<br>MODE      | NBI 20MW<br>&<br>RF 10MW |
| DYNAMIC LIMITER<br>OPERATION MODE                                  |                                    |                          |
| MAGNETIC LIMITER<br>OPERATION MODE                                 | MAGNETIC LIMITER<br>OPERATION MODE |                          |
| ROOM TEMPERATURE OPERATION MODE<br>OR<br>HOT LINEAR OPERATION MODE |                                    |                          |

Table X.8-2(b) Varieties of current build-up

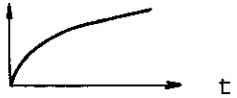


|                     | $I_p$ PATTERN  | VOLT·SEC |
|---------------------|--|----------|
| SINGLE STEP RAMPING |  | 12.7     |
| DOUBLE STEP RAMPING |  | 25.4     |
| TRIPLE STEP RAMPING |  | 25.4     |



Table X.8-3 Molybdenum impurity concentrations with and without magnetic limiter. Conditions marked with \* have no steady state solution in the present model.

| $T_b$ (eV) | Without magnetic limiter |        |        | With magnetic limiter             |         |         |
|------------|--------------------------|--------|--------|-----------------------------------|---------|---------|
|            | $\lambda_1 = \lambda_2$  |        |        | $\lambda_1$ ( $\lambda_2 = 0.9$ ) |         |         |
|            | 0.6                      | 0.7    | 0.8    | 0.9                               | 0.95    | 0.99    |
| 50         | 0.015%                   | 0.01%  | 0.006% | 0.0025%                           | 0.0024% | 0.0023% |
| 100        | 0.044%                   | 0.017% | 0.008% | 0.0029%                           | 0.0026% | 0.0023% |
| 200        | 0.55%                    | 0.031% | 0.01%  | 0.0036%                           | 0.0028% | 0.0024% |
| 400        | *                        | 0.173% | 0.03%  | 0.0096%                           | 0.0053% | 0.0028% |
| 800        | *                        | 2.077% | 0.13%  | 0.031%                            | 0.0135% | 0.0042% |

Proton sputtering yield: H.Ohtsuka et al.<sup>18)</sup>

Self sputtering yield: P.Sigmund.<sup>19)</sup>

Table X.8-4 Titanium impurity concentrations.  
Otherwise, similar to Table X.8-3.

| $T_b$ (eV) | Without magnetic limiter |       |       | With magnetic limiter             |        |        |
|------------|--------------------------|-------|-------|-----------------------------------|--------|--------|
|            | $\lambda_1 = \lambda_2$  |       |       | $\lambda_1$ ( $\lambda_2 = 0.9$ ) |        |        |
|            | 0.6                      | 0.7   | 0.8   | 0.9                               | 0.95   | 0.99   |
| 50         | 0.066%                   | 0.06% | 0.05% | 0.01%                             | 0.01%  | 0.01%  |
| 100        | 0.163%                   | 0.11% | 0.08% | 0.013%                            | 0.01%  | 0.01%  |
| 200        | 4.6%                     | 0.34% | 0.18% | 0.019%                            | 0.013% | 0.015% |
| 400        | *                        | *     | *     | 0.073%                            | 0.028% | 0.034% |
| 800        | *                        | *     | *     | 0.25%                             | 0.147% | 0.055% |

Proton sputtering yield: J. Bohdansky et al.<sup>20)</sup>

Self sputtering yield: D.L.L Smith<sup>21)</sup>

Table X.8-5 Carbon impurity concentrations.  
Otherwise, similar to Table X.8-3.

(a) Physical sputtering( no chemical sputtering)

| Without magnetic limiter |                         |       |       | With magnetic limiter             |        |        |
|--------------------------|-------------------------|-------|-------|-----------------------------------|--------|--------|
| $T_b$ (eV)               | $\lambda_1 = \lambda_2$ |       |       | $\lambda_1$ ( $\lambda_2 = 0.9$ ) |        |        |
|                          | 0.6                     | 0.7   | 0.8   | 0.9                               | 0.95   | 0.99   |
| 50                       | 0.46%                   | 0.34% | 0.23% | 0.11%                             | 0.07%  | 0.038% |
| 100                      | 0.47%                   | 0.35% | 0.24% | 0.11%                             | 0.07%  | 0.039% |
| 200                      | 0.48%                   | 0.36% | 0.24% | 0.12%                             | 0.075% | 0.039% |
| 400                      | 0.48%                   | 0.36% | 0.24% | 0.12%                             | 0.075% | 0.039% |
| 800                      | 0.42%                   | 0.31% | 0.21% | 0.10%                             | 0.067% | 0.037% |

(b) Physical sputtering and chemical sputtering(500°C)

| Without magnetic limiter |                         |       |       | With magnetic limiter             |       |       |
|--------------------------|-------------------------|-------|-------|-----------------------------------|-------|-------|
| $T_b$ (eV)               | $\lambda_1 = \lambda_2$ |       |       | $\lambda_1$ ( $\lambda_2 = 0.9$ ) |       |       |
|                          | 0.6                     | 0.7   | 0.8   | 0.9                               | 0.95  | 0.99  |
| 50                       | 1.66%                   | 1.1%  | 0.83% | 0.4%                              | 0.21% | 0.07% |
| 100                      | 1.75%                   | 1.17% | 0.88% | 0.44%                             | 0.24% | 0.07% |
| 200                      | 1.80%                   | 1.20% | 0.90% | 0.51%                             | 0.27% | 0.08% |
| 400                      | 2.1%                    | 1.40% | 1.05% | 0.70%                             | 0.36% | 0.10% |
| 800                      | 2.8%                    | 1.87% | 1.4%  | 0.78%                             | 0.41% | 0.11% |

Proton sputtering yield: J. Bohdanský et al.<sup>20)</sup>

Self sputtering yield: D.L. Smith<sup>21)</sup>

Chemical sputtering yield: R. Yamada et al.<sup>22)</sup>

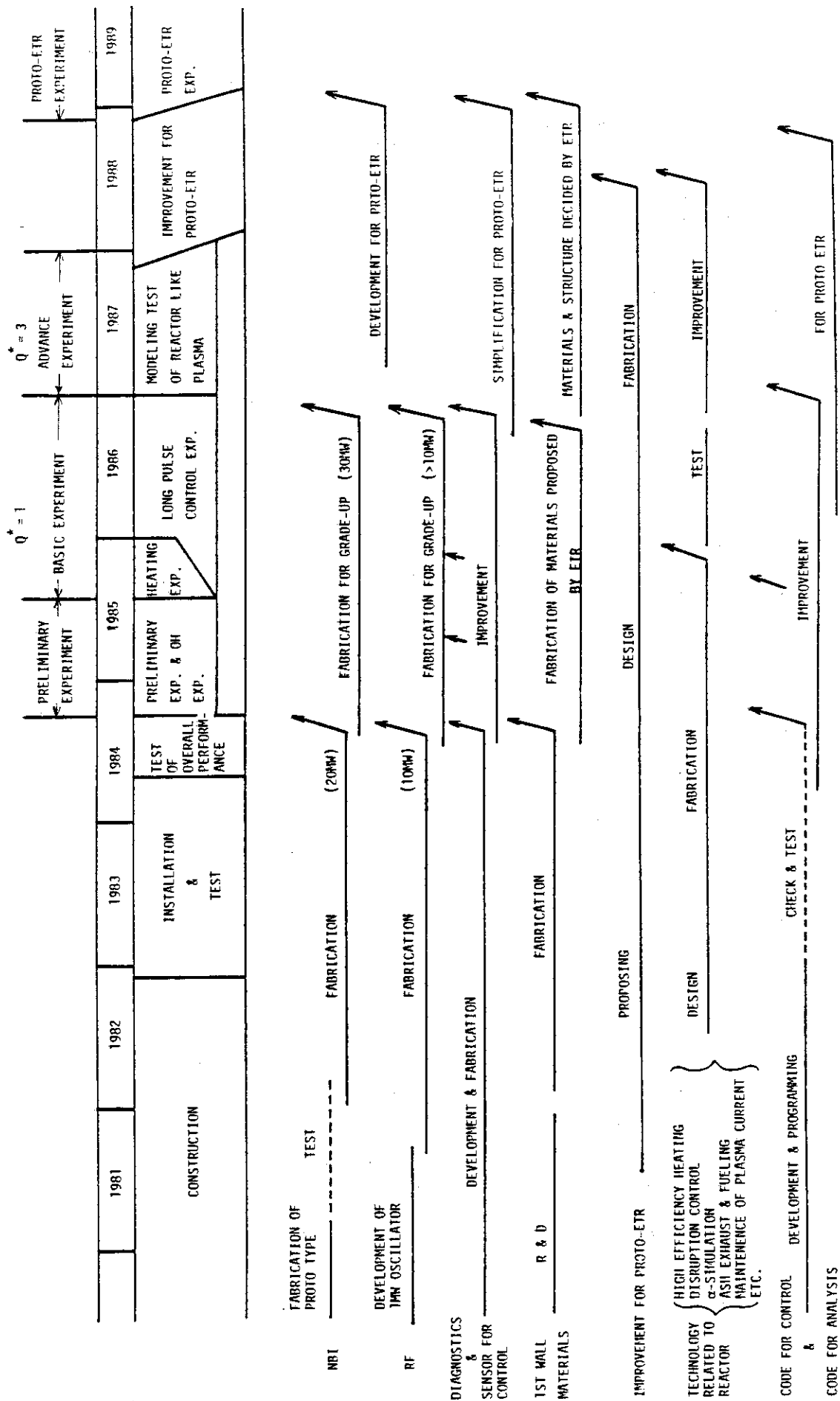


Fig. X.8-1 Experimental program and schedule of JT-60

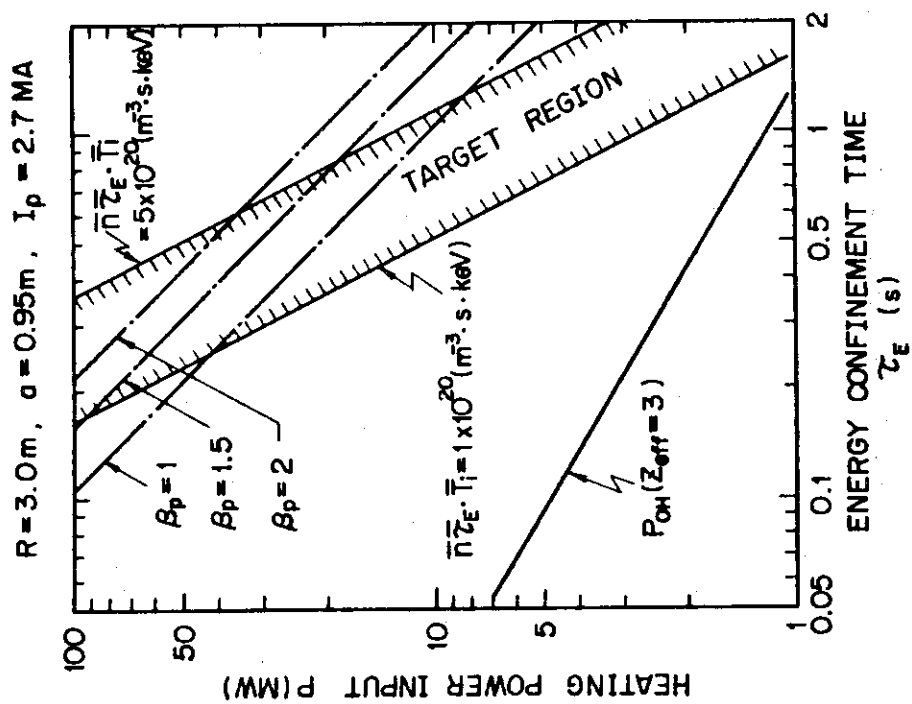


Fig. X.8-2 Power requirement versus energy confinement time

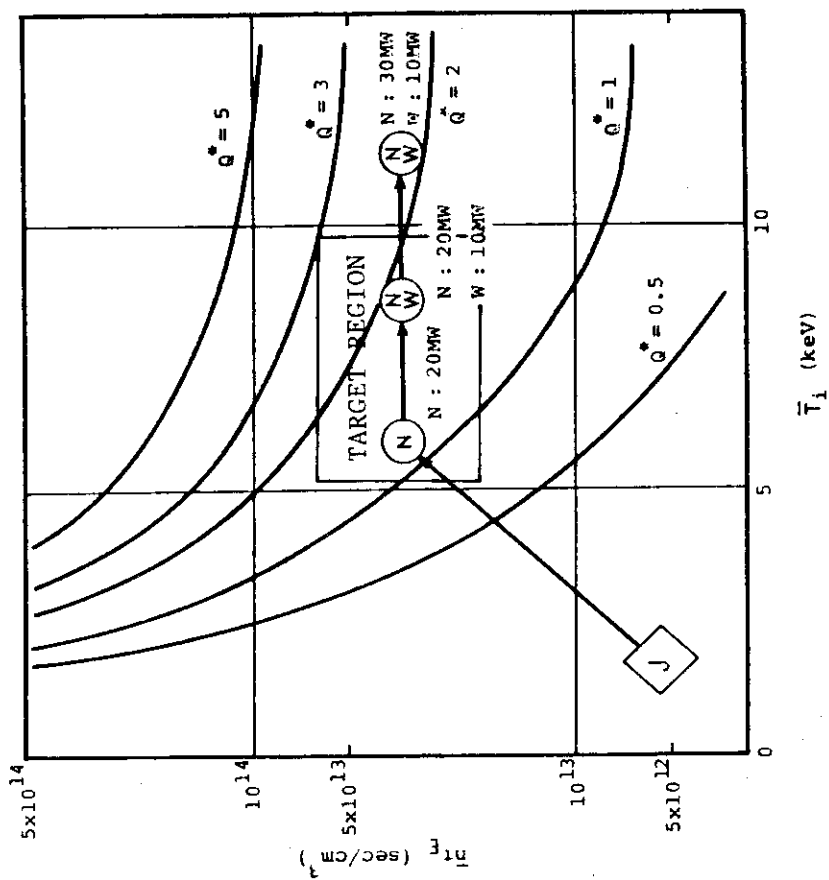


Fig. X.8-3  $\bar{n}\tau_E - \bar{T}_i$  diagram

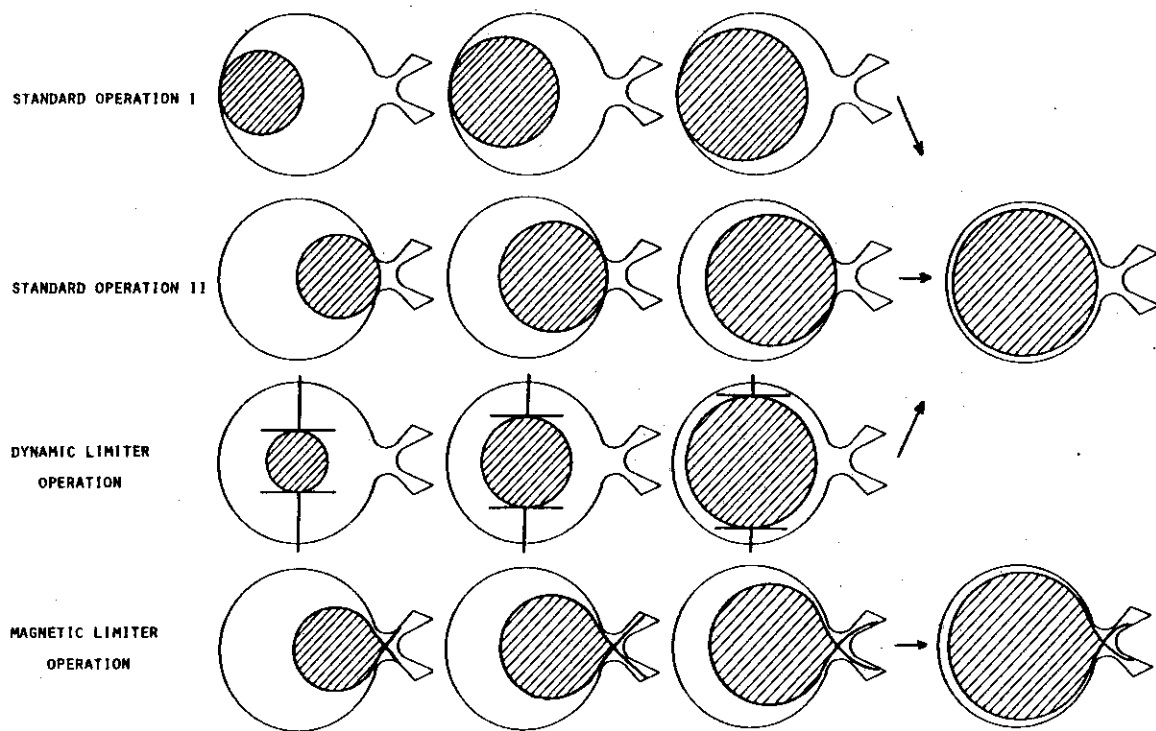


Fig. X.8-4 Schematic view of plasma during current build-up

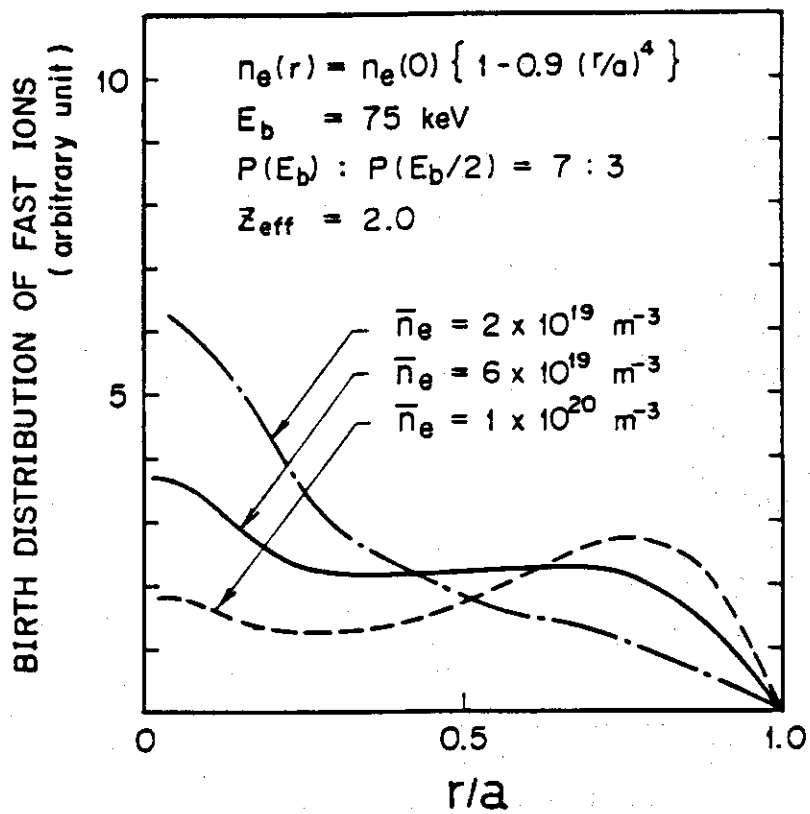


Fig. X.8-5 Birth distribution of fast ions

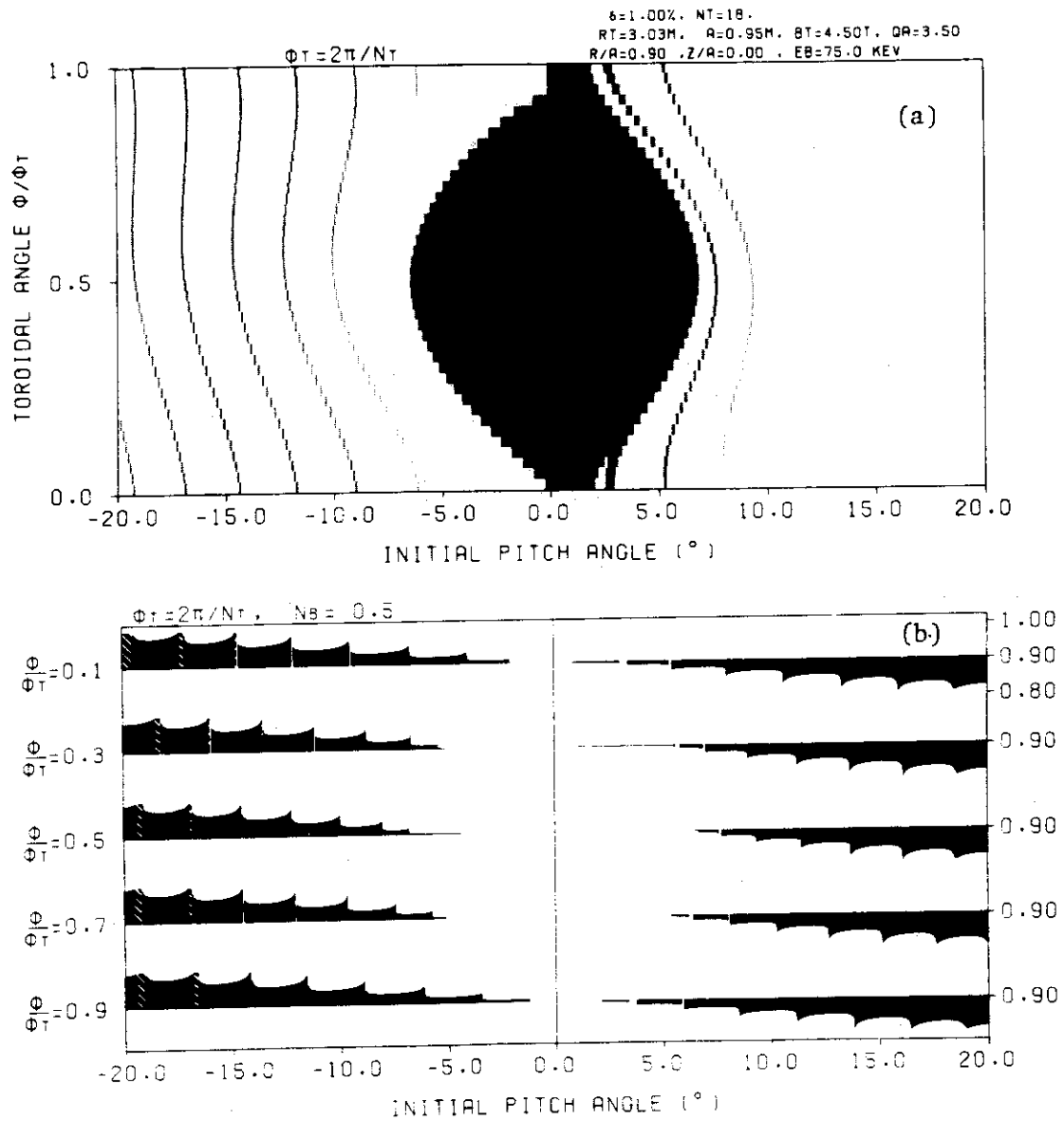


Fig. X.8-6 Collisionless ripple trapping zone (a) and radial banana drift step (b) for fast ions at initial position of  $r/a=0.9$  in JT-60 neutral beam injection.

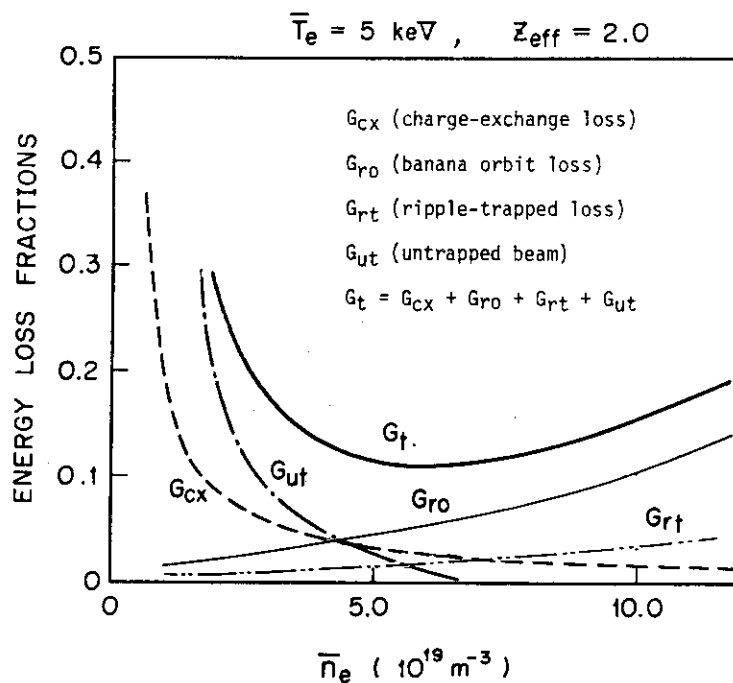
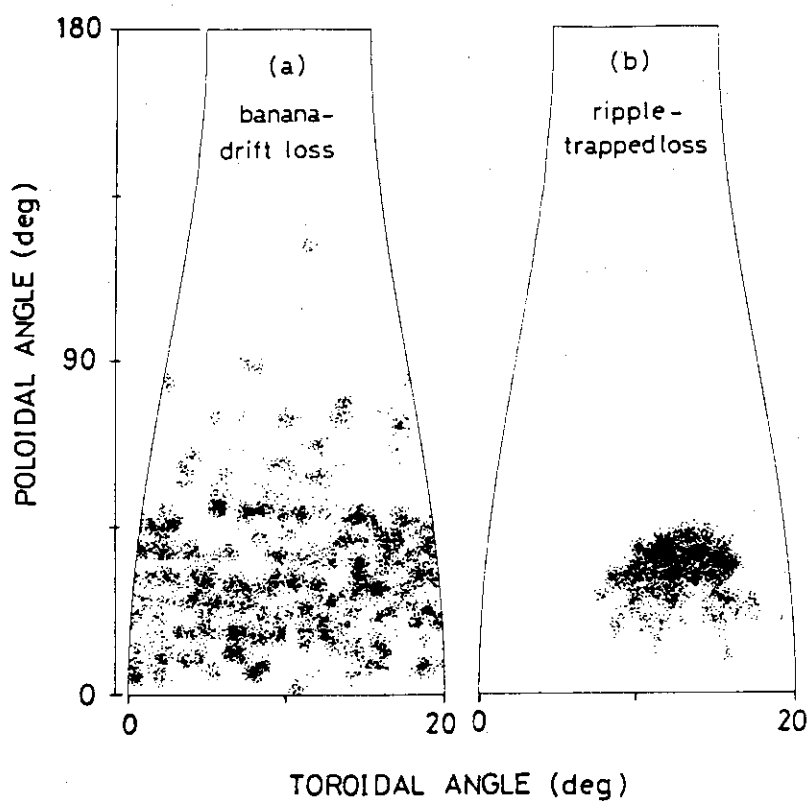


Fig. X.8-7 Total beam energy loss as a function of plasma density

Fig. X.8-8 Energy flux profiles of banana-drift loss particles (a) and of ripple-trapped loss particles (b) at plasma surface in JT-60 neutral beam injection. The injection angle  $\theta_{\text{inj}}$  is  $\pm 73^\circ$  with respect the magnetic axis.

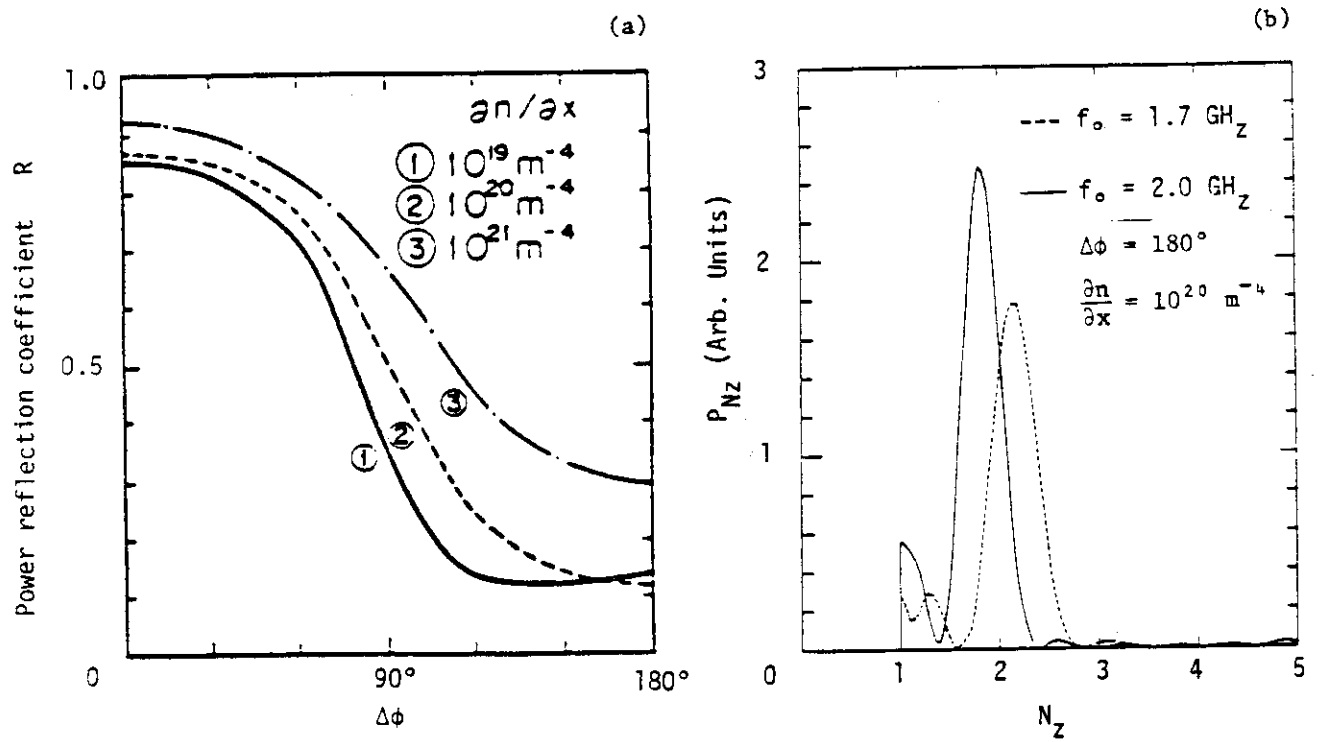


Fig. X.8-9 Plasma-wave coupling characteristics:  
 (a) power reflection coefficient vs. phase difference ( $f_0=1.7 \text{ GHz}$ )  
 (b) power spectrum of  $N_z$ .



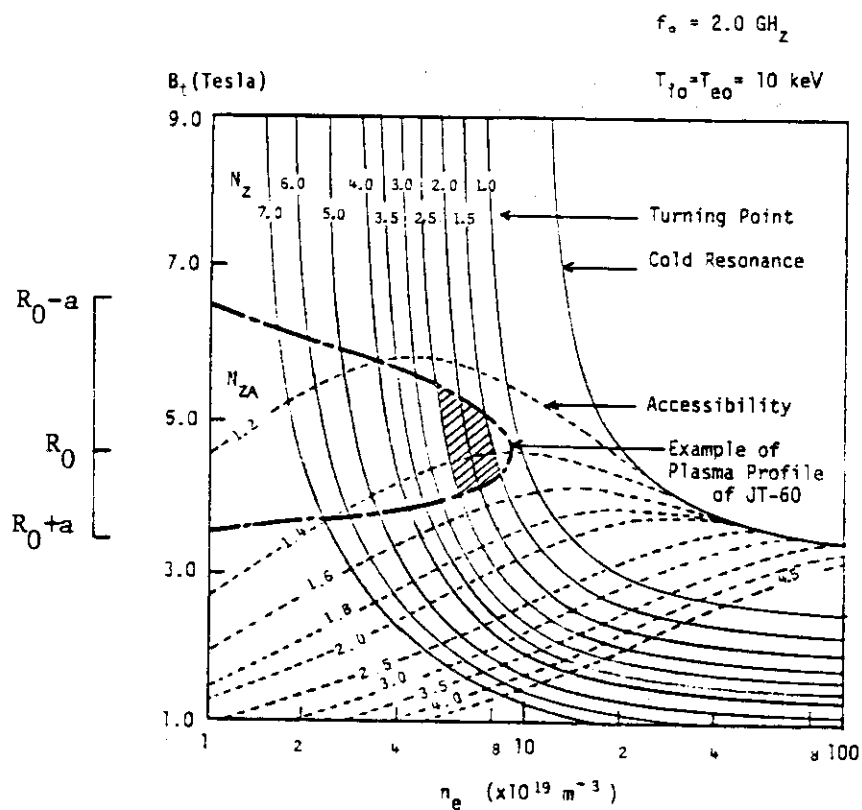
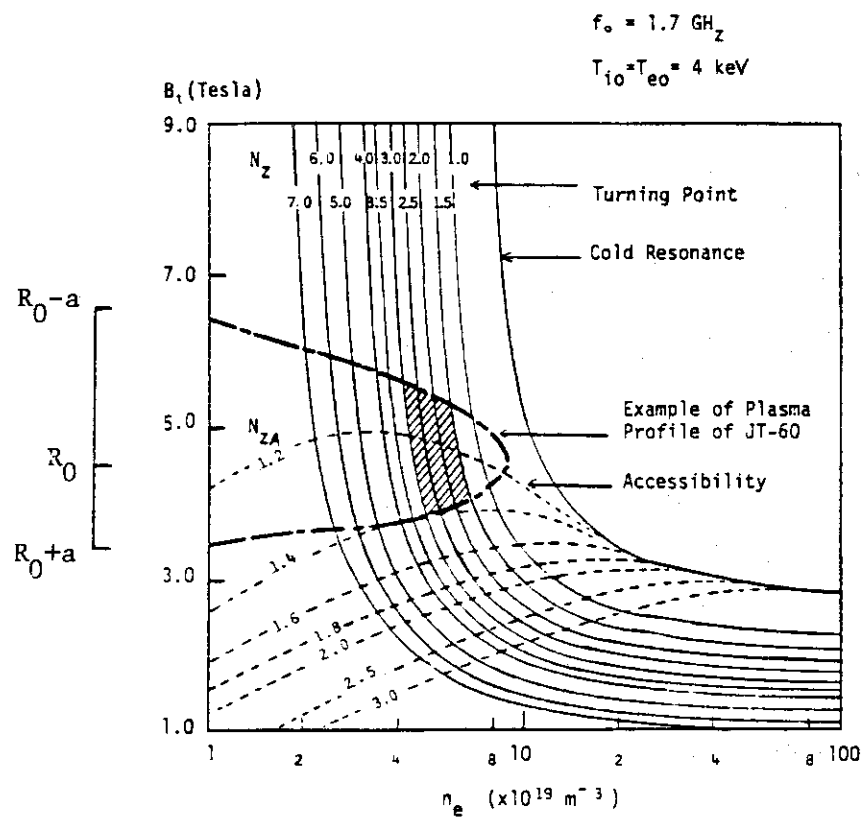
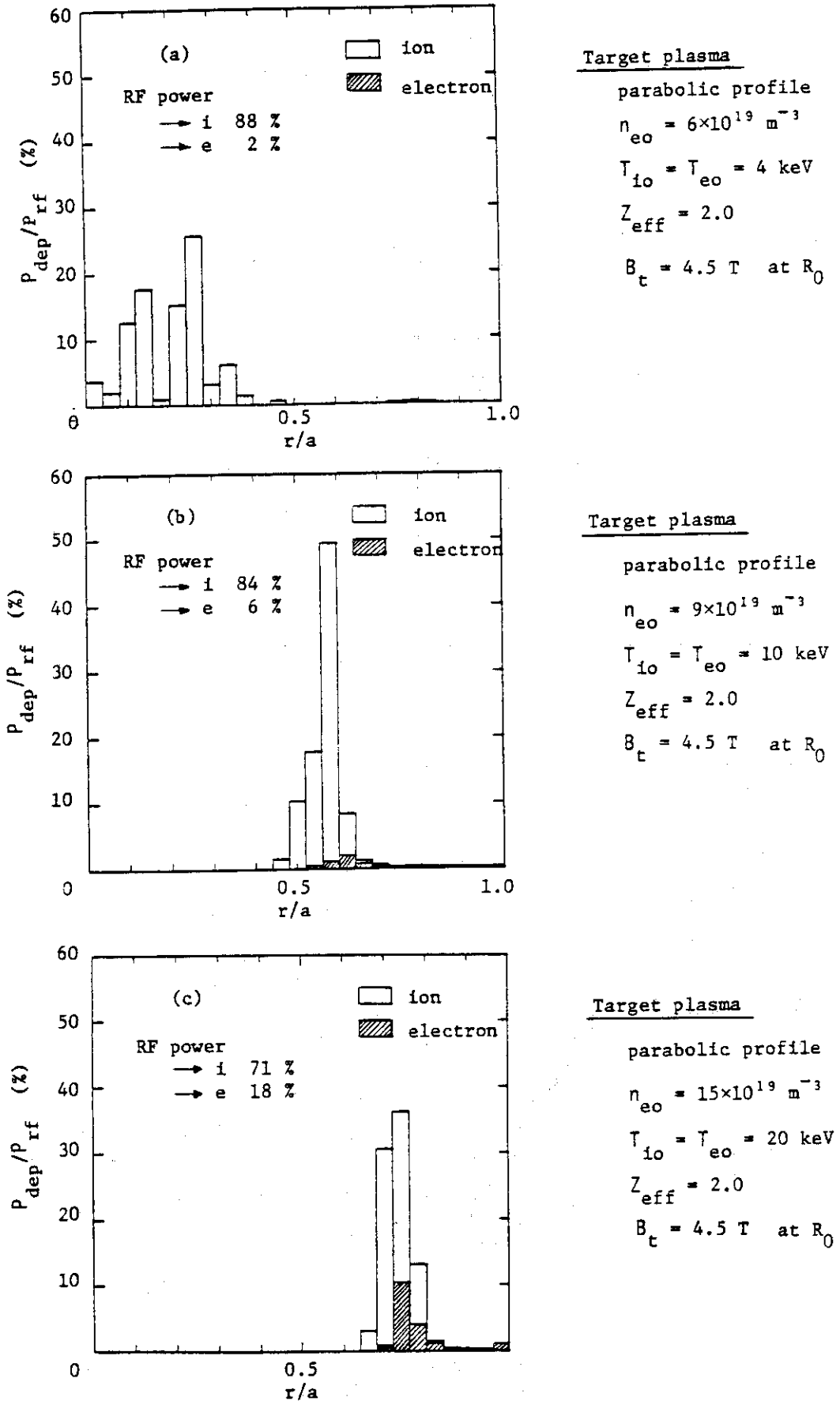


Fig. X.8-10  $B_t$ - $n_e$  diagram for accessibility condition and wave propagation

Fig. X.8-11 Deposition profile of RF power ( $f_0=2.0 \text{ GHz}$ ,  $\Delta\phi=180^\circ$ )

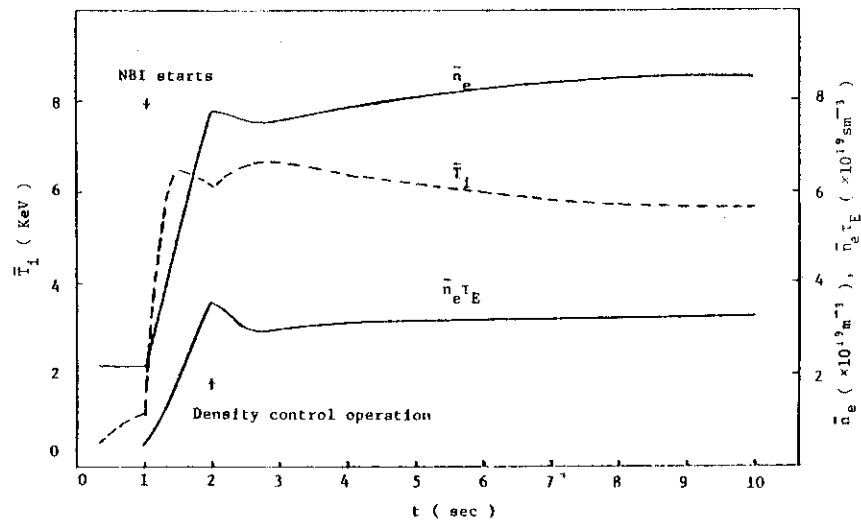


Fig. X-8-12(a) Time evolutions of averaged ion temperature, averaged ion density and  $\bar{n}_e \tau_E$ . Density control operation is made after 2 sec.

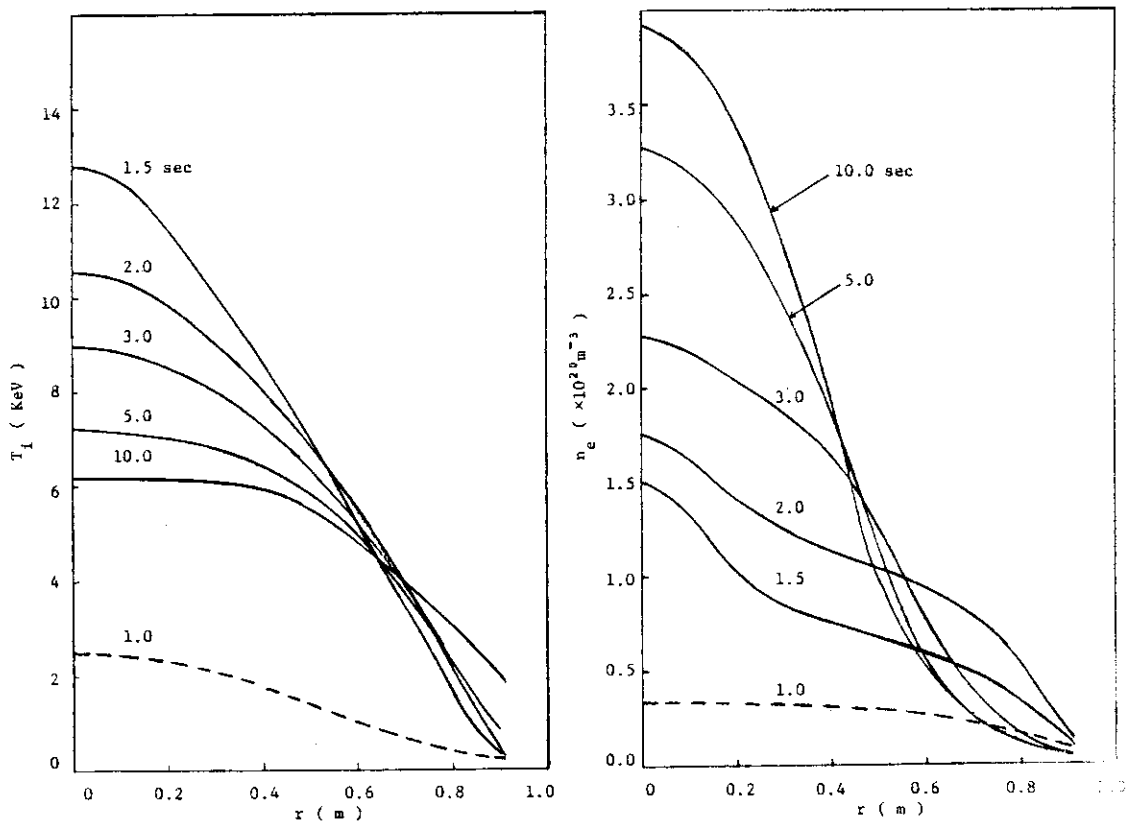


Fig. X-8-12(b),(c) Temporal development of ion temperature and electron density profiles. Otherwise similar to Fig. X-8-12(a).

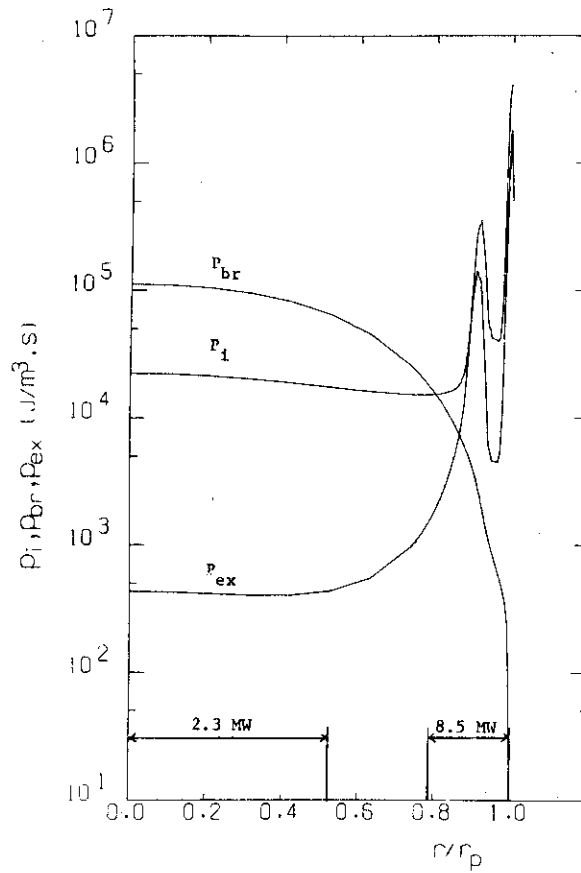


Fig. X.8-13 Radial profile of carbon (6%) impurity radiation from a plasma with its parameter distributions (a), where  $P_{br}$ : bremsstrahlung loss,  $P_{ex}$ : excitation loss,  $P_i$ : ionization loss. 2.3 MW is the total radiated power over the central region of 50 cm, and 8.5 MW over the edge region (arbitrarily taken to be 20 cm wide).

## XI. DEVELOPMENT OF THE NEXT LARGE TOKAMAK MACHINE

### 1. INTOR Activity

The most prominent activity on the next generation tokamak to JT-60 in the fiscal year of 1979 is the activities concerned with INTOR Workshop.

Hitherto, as the next generation machine, Plasma Engineering Test Facility (PETF) has been proposed three years ago on rather conservative standing point both in physics and engineering with the aims to achieve the self-ignition condition and to demonstrate the feasibility of plasma engineering.

In these years, the step of development of plasma physics is large as shown in possible applicability of the experimental scaling law to the higher plasma temperature region, improvement of beta-value, establishment of low  $q$  operation or feasibility of divertor function. The progress of engineering was also large as seen in superconducting coil technology and neutral beam injection technology. A tendency has been generated to aim the maximum reasonable step at the next generation machine by the developments. One of such movement is INTOR activity. INTOR (International Tokamak Reactor) workshop is an international activity to assess a tokamak reactor assumed to be built as a next generation machine by EC, Japan, USA and USSR. Workshop was initiated in September, 1978 and got through its Zero Phase of Data-base Assessment by the end of 1979. From January, 1980, Workshop is in First Phase to accomplish its conceptual design by June, 1981.

The scopes of INTOR are expected as:

- (1) to be a maximum reasonable step from the present status towards future reactors
- (2) to consists of all essential reactor elements
- (3) to be a test facility for future reactor development

INTOR activity in Japan was promoted by JAERI with intimate collaboration with universities and industries. About 70 people of JAERI, 5 peoples of universities and about 60 people of industries were directly involved. In JAERI, it was performed by cooperation of Fusion Research and Development Center (Division of Large Tokamak Development and Div. of Fusion Research), Div. of Reactor Fuel, Div. of High Temperature Engineering, Div. of Physics, Div. of Reactor Engineering and Div. of Health Physics. Big contributions

from industries made engineering design of INTOR so successful. They are from Mitsubishi Group, Toshiba Co., Hitachi, Ltd., Kawasaki Heavy Industry Co. Ltd., NAIG, Fuji Electric Co. Ltd. JAERI could get cooperation from Atomic Energy Research Laboratory of Kyoto University and Institute of Plasma Physics of Nagoya University. INTOR activities in Japan in Zero Phase are integrated in a compiled report.<sup>1)-14)</sup>

At Workshop, Japan proposed a conceptual design of INTOR called INTOR-J. Many Japanese contributions were taken into INTOR concepts especially about physical engineering surveys of divertors, engineering studies of the reactor structure design of power supply systems.

The concepts of INTOR are as follows:

- (1) Achievement of self-ignition condition
- (2) Long burning more than 100 seconds
- (3) Neutron wall loading more than  $1 \text{ MW/m}^2$
- (4) Basically, nonbreeding blanket with possibility of its installation
- (5) Superconduction coil systems
- (6) Installation for test zone
- (7) Neutral beam injection heating with very probable alternative of RF heating
- (8) High duty cycle ( $\sim 70 \%$ ) and availability (more than 25 %, max. 50 %)
- (9) Demonstration of electricity generation ( $10 \text{ MW}_e$ )

## 2. Study of INTOR Reactor Plasma

### 2.1 Particle and energy confinement

Data base assessments for INTOR plasma have been made on the empirical scaling laws, detailed studies on INTOR parameters by zero and one-dimensional model, heat and particle flux to the first wall and divertor plate, effects of impurities on plasma, effects of toroidal field ripple on plasma performance, confinement of alpha particles, level of synchrotron radiation, and consideration of INTOR parameters.<sup>2)</sup>

### 2.2 Impurity control, fueling and exhaust

The data bases of impurity control, fueling and exhaust of INTOR plasma are assessed. They include permissible levels of impurities, experimental results of plasma-wall interactions, specific means for decreasing plasma contamination, impurity control and ash exhaust with

and without divertor (a kind of mechanical divertor), fueling by gas puffing and pellet injection, and related surface phenomena.<sup>3)</sup> Especially, to simplify the structure of the tokamak reactor, an idea of the simplified poloidal divertor was proposed.<sup>15)</sup> All coils of divertors can be located outside of toroidal field coils without big increase of their ampere-turns.

### 2.3 Heating

On neutral beam injection heating, the required heating power, the penetration of injected beam, and the ripple injection were evaluated. On RF heating, its technical status and feasibility of lower hybrid frequency heating at INTOR were assessed.<sup>4)</sup>

### 2.4 Stability control

The theoretical beta-limits, experimental results of current distribution in DIVA, wide range of parameter study of plasma shaping, effect of conduction shell on positional and ballooning mode, and the method of disruption control have been assessed. Good shell effect of the SS blanket was examined. Also shown was the possibility of the equilibrium control of minor radius expansion. Design of hybrid poloidal coil system with exterior coils was carried out.<sup>5)</sup>

### 2.5 Start-up, burn and shutdown

Number of problem areas from the generation of a plasma to the termination of the discharge were investigated, which should be assessed to develop a scenario for sustaining a plasma for the whole duration of a pulse. The reactor relevant burn pulse was also assessed.<sup>6)</sup>

## 3. Design Study of INTOR-J<sup>13),14)</sup>

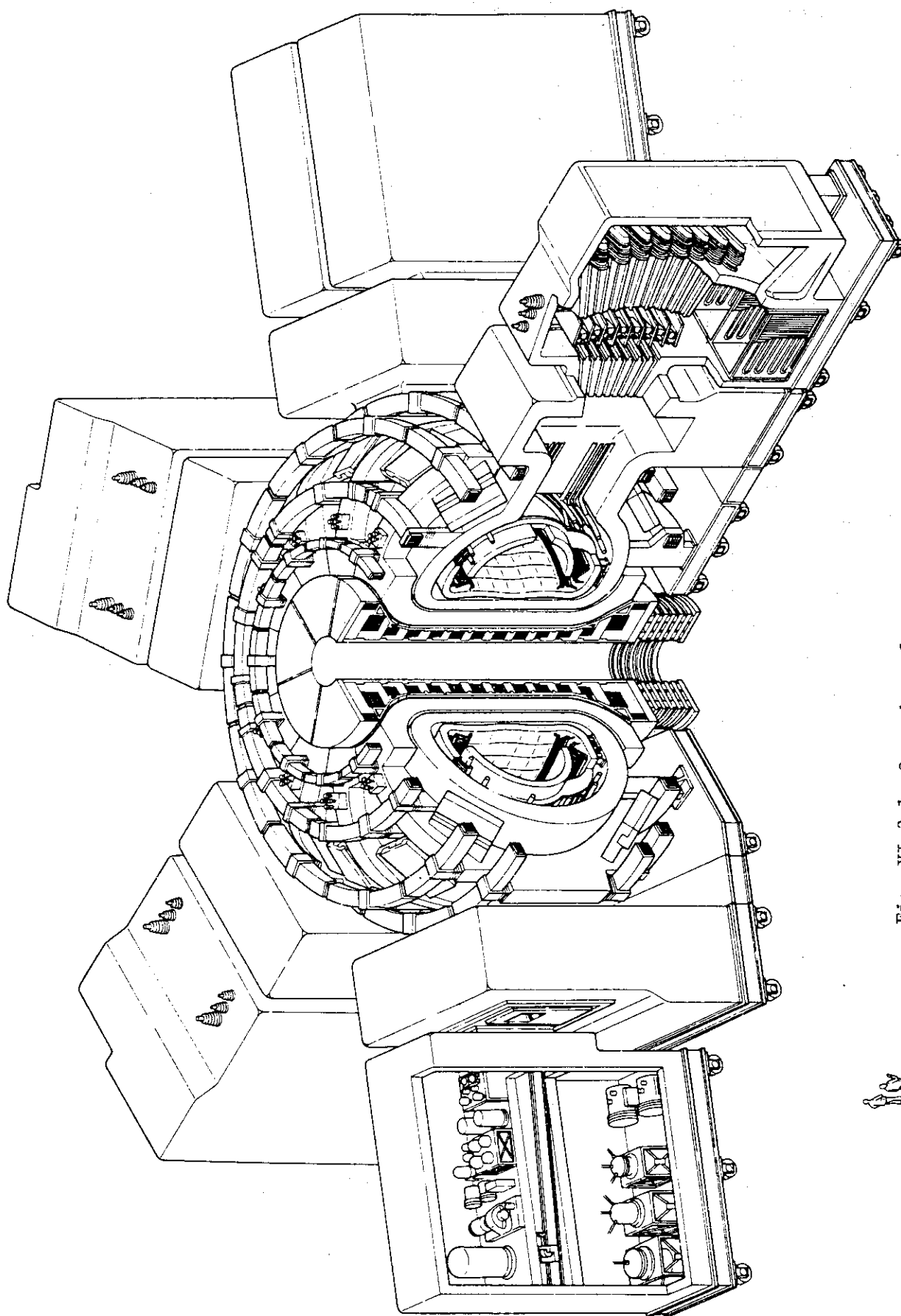
In order to assess the INTOR design data base, consistent discussion based on a systematic reactor design is required. Isolated surveys for individual components tend to lack balance among them. Therefore we have performed a fairly detailed reactor design based on the guiding parameters which had gained a preliminary agreement in the second Workshop Session. The result of the design is presented in this report which we hope will be used as a reference in the Workshop Session III. The main objective of the study is to evaluate and assess the following five items.

- (1) Validity of the guiding parameters (especially those related to reactor size),
- (2) Feasibility of a reactor with poloidal divertors,
- (3) Design problems and R&D items of each component,
- (4) Feasibility of repair and maintenance, and
- (5) Design of test sections for tritium breeding and electric power generation.

Fig. XI.3-1 shows overview of INTOR-J. The design study of the following items are carried out. Design problems and R&D items were enumerated simultaneously with the design.

- (1) Overall concept of reactor with poloidal divertor
- (2) Neutronics design
- (3) Blanket design (breeding and non-breeding)
- (4) Shielding design
- (5) Divertor design
- (6) TF magnet design (for concept A and B)
- (7) PF magnet design (for concept A and B)
- (8) NBI design
- (9) Main vacuum pump design
- (10) Repair & maintenance of reactor, concept A and B
- (11) Repair & maintenance of divertor
- (12) Reactor cooling system
- (13) Blanket test section





## 4. Related Technologies

### 4.1 Materials

For materials data base assessment, selected properties of the materials important in INTOR were evaluated on the basis of data obtained in Japan. Materials covered were austenitic steels, non-magnetic steels, and titanium alloys as structural materials; helium and water for coolant; lithium oxide for breeder; aluminum and copper for stabilizer and organic insulator as magnet materials; graphite for non-metallic materials.<sup>8)</sup>

### 4.2 Power supply and transfer

Current variation each superconducting coil of the hybrid poloidal coil system located outside of the toroidal field coils was calculated from the plasma start-up, through burning and to shut-down. Following this evaluation, a new system for the poloidal field power supply for INTOR was proposed. Its overall power supply system has been evaluated including the operation scheme of generators.<sup>9)</sup>

### 4.3 Tritium

Tritium inventory of INTOR's fuel circulation system and recovery of tritium from solid blanket of  $\text{Li}_2\text{O}$  were investigated. Chemical properties of  $\text{Li}_2\text{O}$  and the results of tritium recovery from neutron-irradiated were summarized. Simulation codes for cryogenic distillation of hydrogen and water distillation of hydrogen isotopic water was developed.<sup>10)</sup>

### 4.4 Vacuum

Vacuum systems data base assessment and evaluation of the principal vacuum parameters for INTOR-J concepts were made. It covered torus vacuum vessel and its pumping system including vacuum wall location, pumping means, available maximum pumping speed, and vacuum wall cleaning. Emphasis in the conceptual studies was on helium pumping by cryopumps. Regeneration cycle and tritium inventory of the cryopumps were evaluated from the published data. Radiation effects on vacuum systems and remote leak detection were also studied.<sup>11)</sup>

#### 4.5 Diagnostics, data acquisition and control

Data assessment was made to consider diagnostics and reactor instrumentations of INTOR. Also considered was how the diagnostics, data acquisition and control should be for the next generation tokamak. Especially, as one of the data assessments of radiation damage problems, data of radiation damage of cables were compiled.<sup>12)</sup>

References

- 1) Fusion Reactor Laboratory, Evaluation of INTOR Size, JAERI-M 8710, Feb., 1980.
- 2) Fusion Research and Development Center, IEAE INTOR Workshop Report, Group 1 - Energy and Particle Confinement, JAERI-M 8621, Jan. 1980.
- 3) Fusion Research and Development Center, IAEA INTOR Workshop Report, Group 3 - Impurity Control, Fueling and Exhaust, JAERI-M 8622, Jan. 1980.
- 4) Fusion Research and Development Center, IAEA INTOR Workshop Report, Group 4 - Heating, JAERI-M 8623, Feb. 1980.
- 5) Fusion Research and Development Center, IAEA INTOR Workshop Report, Group 11 - Stability Control, JAERI-M 8624, Jan. 1980.
- 6) Fusion Research and Development Center, IAEA INTOR Workshop Report, Group 12 - Start-up, Burn and Shutdown, JAERI-M 8625, Jan., 1980.
- 7) Fusion Research and Development Center, IAEA INTOR Workshop Report, Groups 2, 5, 7, 9, 10, 15 - First Wall/Blanket/Shield, Magnetics, Systems Integration and Support Structures, Assembly and Remote Maintenance, Radiation Shielding and Personnel Accessibility, Safety and Environment, JAERI-M 8711, Feb. 1980.
- 8) Shiraishi, K., et al., IAEA INTOR Workshop Report, Group 6 - Materials, JAERI-M 8510, Oct. 1979.
- 9) Fusion Research and Development Center, IAEA INTOR Workshop Report, Group 8 - Power Supply and Transfer, JAERI-M 8511, Oct., 1979.
- 10) Tanaka, K., et al., IAEA INTOR Workshop Report, Group 13 - Tritium, JAERI-M 8512, Oct. 1979.
- 11) Fusion Research and Development Center, IAEA INTOR Workshop Report, Group 14 - Vacuum, JAERI-M 8513, Oct. 1979.
- 12) Fusion Research and Development Center, IAEA INTOR Workshop Report, Group 16 - Diagnostics, Data Acquisition and Control, JAERI-M 8514, Oct. 1979.
- 13) Sako, K., et al., Engineering Aspects of the JAERI Proposal for INTOR (I), JAERI-M 8503, Oct. 1979.
- 14) Fusion Research and Development Center, Engineering Aspects of the JAERI Proposal for INTOR (II), JAERI-M 8518, Nov., 1979.
- 15) Seki, Y., et al., Numerical Calculations of Helium Ash Enrichment and Exhaust by a Simple Divertor, Nuclear Fusion 20 (1980) 1213.

## APPENDIXES

## A.1 Publication List

## A.1.1 List of JAERI-M Report

- 1) Yamamoto S.: "Experimental Studies on an Axisymmetric Divertor in DIVA (JFT-2a)", JAERI-M 8151 (Mar. 1979) (in Japanese)
- 2) Hosoda Y.<sup>\*14</sup>, Shimamoto S.: "Eddy Current Loss Analysis for the Helium Vessel of the IEA-LCT Coil", JAERI-M 8204 (Apr. 1979) (in Japanese)
- 3) DIVA Group: "Study on Very-Low-q Discharges in DIVA", JAERI-M 8205 (Apr. 1979)
- 4) Nagami M.: "Divertor Experiment for Impurity Control in DIVA", JAERI-M 8215 (Apr. 1979)
- 5) Yamauchi M.<sup>\*11</sup>, Nakayama M.<sup>\*13</sup>, Minami K.<sup>\*13</sup>, Seki Y. and Iida H.: "Two-Dimensional Sensitivity Calculation Code : SENSETWO", JAERI-M 8247 (May 1979) (in Japanese)
- 6) Sako K., Tone T., Seki Y., Iida H., Yamato H.<sup>\*11</sup>, Maki K.<sup>\*3</sup>, Ioki K.<sup>\*5</sup>, Yamamoto T.<sup>\*1</sup>, Minato A.<sup>\*4</sup>, Yamauchi M.<sup>\*11</sup> and Shiraishi K.: "Second Preliminary Design of JAERI Experimental Fusion Reactor (JXFR) (Interim Report)", JAERI-M 8286 (Jun. 1979)
- 7) Iida H., Kawasaki H.<sup>\*15</sup>: "TOPIC : A Debugging Code for Torus Geometry Input Data of Monte Carlo Transport Code", JAERI-M 8289 (Jun. 1979) (in Japanese)
- 8) Shimomura Y., Sako K. and Shinya K.<sup>\*11</sup>: "Some Considerations of Ash Enrichment and Ash Exhaust by a Simple Divertor", JAERI-M 8294 (Jun. 1979)
- 9) Takatsu H., Shimizu M., Okumura M.<sup>\*17</sup>, and Kawakami M.<sup>\*17</sup>: "Seismic Analysis of the JT-60 (II) — Dynamic response analysis", JAERI-M 8350 (Jul. 1979)
- 10) Ohara H.: "Two-Stage Acceleration of an Ion Beam for High Power Ion Source", JAERI-M 8357 (Jul. 1979)
- 11) Nakamura H., Kuriyama M.: "Engineering Problems of JT-60 First Wall under NBI Fast Neutral Particle Bombardment", JAERI-M 8359 (Aug. 1979)
- 12) Ando T., Tanaka R., Hirao T., Tamura N., Ohkubo M., Iijima T., Ieda M.<sup>\*\*2</sup>, Nagao M.<sup>\*\*2</sup>, Aki F.<sup>\*3</sup>, Sato T.<sup>\*3</sup>, Goto K.<sup>\*3</sup> and

- Watanabe T.<sup>\*3</sup>: "Flashover Characteristics of Poloidal Field Coils under Gamma-ray Irradiation", JAERI-M 8360 (Aug. 1979)
- 13) Fusion Reactor System Laboratory : "Design Studies on Diagnostic Instrumentation and Control Systems for the JAERI Experimental Fusion Reactor", JAERI-M 8411 (Sep. 1979)
  - 14) Yamamoto T.<sup>\*1</sup>: "MHD Equilibrium Analysis of JAERI Experimental Fusion Reactor", JAERI-M 8413 (Sep. 1979) (in Japanese)
  - 15) Kimura H., Odajima K., Sengoku S., Iizuka S.<sup>\*\*5</sup>, Sugie T., Takahashi K., Yamauchi T., Kumagai K., Takeuchi H., Matsumoto H., Matsuda T., Ohasa K., Nagami M., Yamamoto S., Nagashima T., Maeda H. and Shimomura Y.: "ICRF Heating in DIVA : Parameter Survey and Very High Efficiency Ion Heating Experiment", JAERI-M 8429 (Sep. 1979)
  - 16) Sengoku S., Matsuda T., Matsumoto H., Ohtsuka H., Arai T., Ohasa K., Yamamoto S., Odajima K., Kimura H. and Shimomura Y.: "Characteristics of Carbon-Limiter Surface and Suppression of its Chemical Sputtering", JAERI-M 8465 (Sep. 1979)
  - 17) Sako K., Tone T., Seki Y., Iida H., Yamato H.<sup>\*11</sup>, Maki K.<sup>\*3</sup>, Ioki K.<sup>\*5</sup>, Yamamoto T.<sup>\*1</sup>, Minato A.<sup>\*4</sup>, Sakamoto H.<sup>\*7</sup> and Shinya K.<sup>\*11</sup>: "Engineering Aspects of the JAERI Proposal for INTOR (I)", JAERI-M 8503 (Oct. 1979)
  - 18) Shiraishi K., Kondo T., Nasu S., Takamura S., Oku T., and Murakami Y.: "IAEA INTOR Workshop Report, Group 6 — Materials —", JAERI-M 8510 (Oct. 1979)
  - 19) Shimada R., Miya N.<sup>\*\*3</sup>, Shinya K.<sup>\*11</sup>, Kishimoto H., and Tamura S.: "IAEA INTOR Workshop Report, Group 8 — Power Supply and Transfer —", JAERI-M 8511 (Oct. 1979)
  - 20) Tanaka K., Matsuda Y., Kinoshita M., Naruse Y., Nasu S., Kudo H., Katsuta H., Sanokawa K., Tachikawa E., Yoshida Y., and Obata Y.: "IAEA INTOR Workshop Report, Group 13, Tritium", JAERI-M 8512 (Oct. 1979)
  - 21) Murakami Y., Nakamura K., Abe T., and Obara K.: "IAEA INTOR Workshop Report, Group 14 — Vacuum —", JAERI-M 8513 (Oct. 1979)
  - 22) Iida H., Seki Y., Yamamoto T.<sup>\*1</sup>, and Kawasaki H.<sup>\*15</sup>: "Poloidal Distributions of Neutron Flux, Radiation Damage and Nuclear Heating Rate in a First Wall System of INTOR-J", JAERI-M 8517 (Oct. 1979)
  - 23) Fusion Reactor System Laboratory : "Design Study of Blanket Structure for Tokamak Experimental Fusion Reactor", JAERI-M 8470 (Nov. 1979)

- 24) Fusion Reactor System Laboratory : "Engineering Aspects of the JAERI Proposal for INTOR (II)", JAERI-M 8518 (Nov. 1979)
- 25) Itoh T., Horiike H., Kawai M., Kondoh U.<sup>\*8</sup>, Ohga T., Matsuda S., Shirakata H., and Tanaka S.: "Injector Test Stand ITS-3 for Large-Current Ion Source Development", JAERI-M 8537 (Nov. 1979)
- 26) Iizuka S.<sup>\*\*5</sup>, Odajima K., Kimura H., Sengoku S., Sugie T., Takahashi K., Yamauchi T., Kumagai K., Kawakami T., Takeuchi H., Matsumoto H., Matsuda T., Ohasa K., Nagami M., Yamamoto S., Nagashima T., Maeda H., and Shimomura Y.: "Propagation and Absorption of the Fast Magnetosonic Wave near a Two-ion Hybrid Resonance Layer", JAERI-M 8595 (Nov. 1979)
- 27) Kinoshita M., Matsuda Y. and Naruse Y.: "Preliminary Design Study of Catalytic Oxidation Reactor in Tritium Removal System", JAERI-M 8612 (Dec. 1979) (in Japanese)
- 28) Tsunematsu T., Takeda T., Matsuura T.<sup>\*13</sup>, Azumi M., Kurita G. and Takizuka T.: "Stability Analysis by ERATO Code", JAERI-M 8616 (Dec. 1979)
- 29) Sugihara M., Hirayama T., Nagami M., Shimomura Y., etc.: "IAEA INTOR Workshop Report, Group 1 — Energy and Particle Confinement —", JAERI-M 8621 (Jan. 1980)
- 30) Tazima T., Abe T., Sone K., Yamada R., etc.: "IAEA INTOR Workshop Report, Group 3 — Impurity Control, Fueling and Exhaust —", JAERI-M 8622 (Jan. 1980)
- 31) Takeda T., Kurita G., Matsuura T.<sup>\*13</sup>, Ninomiya H., Tsunematsu T., Shimada R. and Shinya K.<sup>\*11</sup>: "IAEA INTOR Workshop Report, Group 11 — Stability Control —", JAERI-M 8624 (Jan. 1980)
- 32) Tone T. (ed) : "IAEA INTOR Workshop Report, Group 12 — Start-up, Burn and Shutdown —", JAERI-M 8625 (Jan. 1980)
- 33) Kinoshita M., Matsuda Y. and Naruse Y.: "Preliminary Design Study of Tritiated Water Adsorber in Tritium Removal System", JAERI-M 8648 (Jan. 1980) (in Japanese)
- 34) Horiike H., Kishimoto H., Matsuda S., Nagashima T., Ohara Y., Shibata T., Yoshida H. and Shirakata H.: "IAEA INTOR Workshop Report, Group 4 — Heating —", JAERI-M 8623 (Feb. 1980)
- 35) Tanaka Y., Azumi M., Tsunematsu T. and Takeda T.: "High-speed Numerical Code AEOLUS-R1 for Resistive MHD Instability with Single Helicity", JAERI-M 8656 (Feb. 1980) (in Japanese)

- 36) Yamauchi T., Kumagai K., Funahashi A., Matoba T., Sengoku S., Kawakami T. and Shoji T.: "Equipment of Thomson Scattering Measurement on DIVA Plasma", JAERI-M 8677 (Feb. 1980)
- 37) Fusion Reactor System Laboratory : "Evaluation of INTOR Reactor Size", JAERI-M 8710 (Feb. 1980)
- 38) Sako K., Tone T., Seki Y., Iida H., et al.: "IAEA INTOR Workshop Report, Groups 2, 5, 7, 9, 10 and 15 — First Wall/Blanket/Shield, Magnetics, Systems Integration and Structure, Assembly and Remote Maintenance, Radiation Shielding and Personnel Access, Safety and Environment. —", JAERI-M 8711 (Feb. 1980)
- 39) Arakawa Y., Akiba M.<sup>\*\*1</sup>, Sakuraba J.<sup>\*9</sup>, Matsuda S. and Tanaka S.: "Theoretical Study of the Source Plasma of Ion Source for a Neutral Beam Injector", JAERI-M 8741 (Feb. 1980)
- 40) Fusion Reactor System Laboratory : "Design Study of Superconducting Magnets for Tokamak Experimental Fusion Reactor (I)", JAERI-M 8640 (Mar. 1980)
- 41) Fusion Reactor System Laboratory : "Design Study of Superconducting Magnets for Tokamak Experimental Fusion Reactor (II)", JAERI-M 8666 (Mar. 1980)
- 42) Oka K.<sup>\*2</sup>: "Study of Electric Phenomena in Energy Dumping of LCT Coil", JAERI-M 8726 (Mar. 1980)
- 43) Yamauchi M.<sup>\*11</sup>, Seki Y. and Iida H.: "Sensitivity Analysis of Neutronics Calculations in the Preliminary Design of JAERI Experimental Fusion Reactor (Revised)", JAERI-M 8739 (Mar. 1980)
- 44) Sakuraba J.<sup>\*9</sup>, Akiba M.<sup>\*\*1</sup>, Arakawa Y., Araki M., Horiike H., Itoh T., Kawai M., Kuriyama M., Matsuda S., Matsuoka M., Mizutani Y.<sup>\*8</sup>, Ohara Y., Ohga T., Okumura Y., Shibata T., Shirakata H. and Tanaka S.: "Development of Bucket and Lambdatron Ion Source", JAERI-M 8740 (Mar. 1980)
- 45) Fusion Reactor System Laboratory : "Design Study of a Neutral Beam Injection System for JAERI Experimental Fusion Reactor", JAERI-M 8743 (Mar. 1980)
- 46) Fusion Reactor System Laboratory : "Design Study of a RF Wave Heating System for JAERI Experimental Fusion Reactor", JAERI-M 8744 (Mar. 1980)
- 47) Nishi M., Ando T. and Shimamoto S.: "Heat Transfer Characteristics of Large Superconductor with Different Surface Condition" JAERI-M 8771 (Mar. 1980) (in Japanese)



- 48) Tada E., Ando T., Oka K.<sup>\*2</sup> and Shimamoto S.: "Optimum Heat Treatment Condition for Multifilamentary Nb<sub>3</sub>Sn", JAERI-M 8772 (Mar. 1980) (in Japanese)
- 49) Kawai M., Ohga T., Okumura Y. and Shibata T.: "A Multi-channel Optical Beam Monitor of High Power Neutral Beams", JAERI-M 8778 (Mar. 1980)
- 50) Yoshida K., Tada E., Koizumi K. and Hiyama T.: "Mechanical Verification Test for the Japanese LCT Coil (1)" JAERI-M 8784 (Mar. 1980) (in Japanese)
- 51) Tada E., Ando T., Oka K.<sup>\*2</sup> and Shimamoto S.: "Superconducting Characteristics of Nb-Ti alloy in High Magnetic Field", JAERI-M 8785 (Mar. 1980) (in Japanese)
- 52) Nagami M.: "Divertor Experiment for Impurity Control in DIVA", JAERI-M 8215 (Apr. 1979)
- 53) Hiraoka T., Tajima T., Sugihara M., Kasai M.<sup>\*5</sup>, Shinya K.<sup>\*11</sup> and Sakamoto H.: "Conceptual Studies of Plasma Engineering Test Facility", JAERI-M 8198 (June 1979)
- 54) Tajima T. and Sugihara M.: "Wall Lapping Plasma with Rotating Helical Resonant Islands for Impurity Control and Mechanical Values for Ash Exhaust in a Reactor-Grade Tokamak without a Divertor", JAERI-M 8390 (Aug. 1979)
- 55) fusion Research and Development Center: "IAEA INTOR Workshop Report, Group 16, --- Diagnostic, Data Acquisition and Control", JAERI-M 8514 (Oct. 1979)
- 56) Fusion Research and Development Center: "IAEA INTOR Workshop Report, Group 17, --- Cost, Schedule and Manpower Assessment", JAERI-M 8515 (Oct. 1979)
- 57) Fusion Research and Development Center: "IAEA INTOR Workshop Report, Group 11, --- Stability Control", JAERI-M 8624 (Jan. 1980)
- 58) Fusion Research and Development Center: "IAEA INTOR Workshop Report, Group 3, --- Impurity Control, Fueling and Exhaust", JAERI-M 8622 (Jan. 1980)
- 59) Fusion Research and Development Center: "IAEA INTOR Workshop Report, Group 12, --- Start-up, Burn and Shutdown", JAERI-M 8625 (Jan. 1980)
- 60) Fusion Research and Development Center: "IAEA INTOR Workshop Report, Group 4, --- Heating", JAERI-M 8623 (Feb. 1980)
- 61) Fusion Research and Development Center: "IAEA INTOR Workshop Report, Group 1, --- Energy and Particle Confinement", JAERI-M 8621 (Mar. 1980)

## A.1.2 List of Papers Published in Journals

- 1) Itoh K.<sup>\*\*4</sup>, and Inoue S.<sup>\*\*6</sup>: "Radio-Frequency Flux Control of Toroidal Plasmas", Comments Plasma Phys. Cont. Fusion 5 (1979) 203.
- 2) Inoue S.<sup>\*\*6</sup>, Tange T.<sup>\*\*6</sup>, Itoh K.<sup>\*\*4</sup>, and Tuda T.: "Anomalous Ion Loss Due to Low-Frequency Instabilities", Nucl. Fusion 19 (1979) 1252.
- 3) Okamoto M.<sup>\*22</sup>, Azumi M., Takizuka T., and Fukuyama A.<sup>\*\*7</sup>: "Numerical Simulation of Lower Hybrid Wave Propagation in a Plasma", J. Phys. Soc. Jpn. 46 (1979) 1333.
- 4) Itoh K.<sup>\*\*4</sup>, Tuda T., and Inoue S.<sup>\*\*6</sup>: "Toroidal Effect on Nonlocal Collisionless Drift Instability", J. Phys. Soc. Jpn. 48 (1980) 258.
- 5) Inoue S.<sup>\*\*6</sup>, Itoh K.<sup>\*\*4</sup>, and Terashima Y.<sup>\*\*2</sup>: "A Scaling Law for High Density Tokamaks and Its Application to J.I.P.P. T-II device", J. Phys. Soc. Jpn. 48 (1980) 264.
- 6) Naitou H.<sup>\*\*2</sup>, Tokuda S., and Kamimura T.<sup>\*\*2</sup>: "On Boundary Condition for a Simulation Plasma in a Magnetic Field", J. Comput. Phys. 33 (1979) 86.
- 7) Inoue S.<sup>\*\*6</sup>, Itoh K.<sup>\*\*4</sup>, and Yoshikawa S.<sup>\*\*8</sup>: "Critical Conditions for Drift, Drift-Alfven, Drift-Tearing Instabilities of Finite-Beta Plasma in Shered Magnetic Field", J. Phys. Soc. Jpn. 48 (1980) 973.
- 8) Gomei Y.<sup>\*11</sup>, Konoshima S., Fujisawa N., Kasai S., Maeno M., Hirayama T., Suzuki N., and Shimada M.: "Molybdenum, Carbon and Silicon Carbide Limiter Experiment in the JFT-2 Tokamak", Jpn. J. Appl. Phys. 18 (1979) 1317.
- 9) Maeno M., Kawamura K., Gomei Y.<sup>\*11</sup>, Fujisawa N., Suzuki N., Konoshima S., Yamamoto T., Hirayama T., and Shimada M.: "Measurement of Surface Temperature of a Limiter and a Study on Plasma Confinement Characteristics", Jpn. J. Appl. Phys. 18 (1979) 1549.
- 10) Kawamura H., Seki M., and Maeno M.: "Development of Thin Film Thermometer and its Application to Radiation Loss Measurement in JFT-2 Tokamak", J. Nucl. Sci. Technol. 16 (1979) 847.
- 11) Yamamoto T., Imai T., Shimada M., Takeuchi H., Uehara K., Konoshima S., Suzuki N., Hirayama T., Maeno M., Fujii T., Nagashima T., and Fujisawa N.: "Parametric Heating by Radio-Frequency near the Lower Hybrid Frequency in the JFT-2 Tokamak", J. Phys. Soc. Jpn. 48 (1980) 4349
- 12) Kasai S., Funahashi A., Nagami M., and Sugie T.: "Radiation due to Pseudo-Continuum from High-Z Impurities in Upgraded DIVA Tokamak"

- Plasma", Nucl. Fusion 19 (1979) 195.
- 13) Ohasa K., Maeda H., Yamamoto S., Nagami M., Ohtsuka H., Kasai S., Odajima K., Kimura H., Sengoku S., and Shimomura Y.: "Origin of Metal Impurities in DIVA", J. Phys. Soc. Jpn. 46 (1979) 1635.
  - 14) Maeda H., Sengoku S., Kimura H., Ohasa K., Nagami M., Odajima K., Yamamoto S., Azumi M., Shimomura Y., etc.: "Experimental Study of Magnetic Divertor in DIVA", Plasma Physics and Controlled Nuclear Fusion Research 1978 1 (1979) 397.
  - 15) Kimura H., Odajima K., Sengoku S., Ohasa K., Sugie T., Takahashi K., Nagami M., Yamamoto S., Yamauchi T., Shoji T., Takeuchi H., Nagashima T., Maeda H., and Shimomura Y.: "ICRF Heating of a  $D^+$  Plasma with a Minority  $H^+$  Component in DIVA", Nucl. Fusion 19 (1979) 1499.
  - 16) Sengoku S., Azumi M., Matsumoto Y.<sup>\*\*7</sup>, Maeda H., and Shimomura Y.: "The Effects of Metal Impurity Recycling in the Scrape-off Plasma of a Large Tokamak", Nucl. Fusion 19 (1979) 1327.
  - 17) Kimura H., Odajima K., Sugie T., and Maeda H.: "Application of Multigrid Energy Analyzer to the Scrape-off Layer Plasma in DIVA", Jpn. J. Appl. Phys. 18 (1979) 2275.
  - 18) Matoba T., Funahashi A., Itagaki T., Kumagai K., Shoji T., Suzuki N., and Yamauchi T.: "Thomson Scattering Measurements on Ohmically Heated Plasma in the JFT-2 Tokamak", Jpn. J. Appl. Phys. 18 (1979) 611.
  - 19) Imai T., Nagashima T., Yamamoto T., Uehara K., Konoshima S., Takeuchi H. et al.: "Parametric Instabilities in Lower-Hybrid-Frequency Heating of a Tokamak", Phys. Rev. Letters 43 (1979) 586.
  - 20) Imai T.: "Parametric Instabilities during Lower Hybrid Resonance Heating in JFT-2 Tokamak", Kakuyugo-Kenkyu 42 Suppl. 4 (1979) 23 (in Japanese).
  - 21) Uehara K., Fujisawa N., Imai T., Yamamoto T., and Nagashima T.: "Particle and Heat Transport during Lower Hybrid Heating in JFT-2 Tokamak", Kakuyugo-Kenkyu 42 Suppl. 4 (1979) 27 (in Japanese).
  - 22) Tamura S.<sup>\*\*10</sup>, and Kuriyama M.: "Magnetic Specific Heat and Debye Temperature of  $(La_{0.8}Ca_{0.2})MnO_{3+y}$ ", Phys. Letters 70A (1979) 469.
  - 23) Matsuoka M., Ohkubo K.<sup>\*\*2</sup>, and Matsuura K.<sup>\*\*2</sup>: "Propagation of the Lower Hybrid Wave in a Toroidal Plasma", Kakuyugo-Kenkyu 41 Suppl. 6 (1979) 97 (in Japanese).

- 24) Horiike H., Kondoh U.<sup>\*8</sup>, Morita H.<sup>\*7</sup>, Shirakata H., Sugawara T.<sup>\*11</sup>, and Tanaka S.: "Cooling of Extraction Electrode of an Ion Source in Long-Pulse Operation", Rev. Sci. Instrum. 50 (1979) 1453.
- 25) Yamada R., Saidoh M., Sone K., and Ohtsuka H.: "Dose and Microstructural Effects on Surface Topography Change and Sputtering Yield in Polycrystalline Molybdenum for the Bombardment with 2 keV Ne<sup>+</sup> Ions", J. Nucl. Materials 82 (1979) 155.
- 26) Yamada R., Sone K., and Saidoh M.: "Surface Microstructural Effects on Angular Distribution of Molybdenum Particles Sputtered with Low Energy Ne<sup>+</sup> Ions", J. Nucl. Materials 84 (1979) 101.
- 27) Yamada R., Sone K., and Saidoh M.: "Surface Microstructural Effects on Angular Distribution of Molybdenum Particles Sputtered with Low Energy Ne<sup>+</sup> Ions", Kakuyugo-Kenkyu 41, Suppl. 5 (1979) 19 (in Japanese).
- 28) Seki Y., Iida H., and Yamauchi M.<sup>\*11</sup>: "Applicability of Two-Dimensional Sensitivity Calculation Code : SENSETWO", J. Nucl. Sci. Technol. 16 (1979) 530.
- 29) Tone T.: "Effects of Particle Confinement and Recycling on Thermally Stable Regions in D-T Tokamak Plasma", J. Nucl. Sci. Technol. 16 (1979) 453.
- 30) Ogata A., and Ninomiya H.: "Optimal Feedback Control of Plasma Parameters in a Tokamak", Jpn. J. Appl. Phys. 18 (1979) 825.
- 31) Matoba T., Itagaki T., Yamauchi T., and Funahashi A.: "Analytical Approximations in the Theory of Relativistic Thomson Scattering for High Temperature Fusion Plasma", Jpn. J. Appl. Phys. 18 (1979) 1127.
- 32) Tamura S.: "Large Tokamak Experiments / Report on the Third IAEA Technical Committee Meeting, Power Supplies", Nucl. Fusion 19 (1979) 523.
- 33) Tamura S., Shimada R., Kito Y.<sup>\*\*2</sup>, Kanai S.<sup>\*11</sup>, Koike H.<sup>\*11</sup>, Ikeda H.<sup>\*11</sup>, and Yanabu S.<sup>\*11</sup>: "Parallel Interruption of Heavy Direct Current by Vacuum Circuit Breakers", IEEE pes, Summer Meeting 1979 (Paper F79, 706-3).
- 34) Shimada R., Tani K., Kishimoto H., Tamura S., Yanabu S.<sup>\*11</sup>, Ikeda H.<sup>\*11</sup>, Tamagawa T.<sup>\*11</sup>, and Sasaki T.<sup>\*11</sup>: "The Life Test of a DC Circuit Breaker of Tokamak Device JT-60 for a Nuclear Fusion Research", J. Ins. Electrical Engineers Japan 99 (1979) 425 (in Japanese)

- 35) Kito Y.<sup>\*\*2</sup>, Kaneko E.<sup>\*\*2</sup>, Miyamae K.<sup>\*\*2</sup>, and Shimada R.: "Current Sharing between Two Vacuum Circuit Breaker Units in Parallel Operation for Large Direct Current Interruption", J. Ins. Electrical Engineers Japan 99 (1979) 593 (in Japanese).
- 36) Tani K., Kishimoto H., Hoshino K., Yoshida H., Tamura S.: "Neutral Beam Injection for JT-60", Kakuyugo-Kenkyu (special supplement) 42, No.4 (1979) 85 (in Japanese).
- 37) Shimada R., Tani K., Kishimoto H., Tamura S., Ikeda H.<sup>\*11</sup>, Tamagawa T.<sup>\*11</sup>, Yanabu S.<sup>\*11</sup>, Matsushita T.<sup>\*11</sup>: "Symthetic Test Methods of High-Direct-Current Circuit Breaker", Proc. IEEE 126 (1979) 965.
- 38) Shimada R., Tani K., Kishimoto H., Tamura S., Yanabu S.<sup>\*11</sup>, Tamagawa T.<sup>\*11</sup>, Takahashi N.<sup>\*11</sup>, Kanai Y.<sup>\*11</sup>: "Analysis and Full Scale Test of DC Circuit Breaker for Tokamak Device JT-60", J. Ins. Electrical Engineers Japan 99 (1979) 773 (in Japanese).
- 39) Shimada M.: "Behavior of Fast Ions during Lower Hybrid Heating in JFT-2", Kakuyugo-Kenkyu 41 Suppl. 6 (1979) 17 (in Japanese)
- 40) Kimura H., Odajima K., Sengoku S., Ohara K., Sugie T., Takahashi K., Nagami M., Yamamoto S., Yamauchi T., Takeuchi H., Shoji T., Nagashima T., Maeda H. and Shimomura Y.: "ICRF Heating of a  $D^+$  Plasma with a Minority  $H^+$  Component in DIVA", Nucl. Fusion 19 (1979) 1499.
- 41) Nagami M. and Shimomura Y.: "The Recent Tokamak Research", Butsuri 35 (1980) 107 (in Japanese)
- 42) Maeno M., Suzuki N., Konoshima S., Yamamoto T., Shimada M. and Fujisawa N., "Experimental Study on Limit of the Safety Factor in JFT-2 Tokamak", J. Phys. Soc. Jpn. 48 (1980) 273.
- 43) Sugihara M., Kasai M.<sup>\*5</sup> and Hiraoka T.: "Ignition Approach by Neutral Beam Injection Heating in Impurity Contaminated Tokamak Reactor", J. Nucl. Sci. Tech. 16 (1979) 305.
- 44) Gomei Y.<sup>\*11</sup>, Konoshima S., Fujisawa N., Kasai M.<sup>\*5</sup>, Maeno M., Suzuki N., Hirayama T. and Shimada M.: "Molybdenum, Carbon and Silicon Carbide Limiter Experiment in the JFT-2 Tokamak", Jpn. J. Appl. Phys. 18 (1979) 1317.
- 45) Maeno M., Kawamura ., Gomei Y.<sup>\*11</sup>, Fujisawa N., Suzuki N., Konoshima S., Yamamoto T., Hirayama T., Shimada M. and Uehara K.: "Measurement of Surface Temperature of a Limiter and a Study on Plasma Confinement Characteristics", Jpn. J. Appl. Phys. 18 (1979) 1549.

## A.1.3 List of Papers Published in Conference Proceedings

- 1) Azumi M., and Nelson O.B.<sup>\*\*9</sup>: "FCT Heating of Free Boundary Equilibria", 1979 Sherwood Meeting (April 1979, Mount Pocono) 1C32.
- 2) Azumi M., Kurita G., Matsuura T.<sup>\*13</sup>, Takeda T., Tanaka Y.<sup>\*13</sup>, and Tsunematsu T.: "A Fluid Model Numerical Code System for Tokamak Fusion Research", Proc. Fourth Int. Symp. on Computing Methods in Applied Sciences and Engineering (Dec. 1979 Versailles).
- 3) Imai T., Nagashima T., Suzuki N., Fujii T., Fujisawa N., Funahashi A., Iizuka S.<sup>\*\*5</sup>, Kasai S., Kumagai K., Maeno M., Sugie T., Takeuchi H., Uehara K., Yamamoto T., Yamauchi T., Yoshida H., Shiina T., and Shoji T.: "LHRF Heating Experiments on the JFT-2 Tokamak", US-Japan Workshop on Physics of High Power RF Heating (Kyoto, 1980).
- 4) Funahashi A., and Suzuki N.: "Titanium Gettered Wall Experiments on JFT-2", Proc. US-Japan Workshop on Divertors, First Wall Materials and Impurity Control (Tokai, 1980).
- 5) Matsuzaki Y., Fujisawa N., Suzuki N., Maeno M., Yamamoto T., and Tani T.: "Direct Digital Control of Plasma Position in JFT-2 Tokamak without Shell", Proc. 8th Symp. on Engineering Problems of Fusion Research (San Francisco, 1979).
- 6) Fujisawa N., and Mori S.: "Progress in Japanese Tokamak Research", 9th European Conf. on Controlled Fusion and Plasma Physics, (Oxford, 1979).
- 7) Suzuki N., Fujisawa N., Konoshima S., Maeno M., Shimada M., Yamamoto T., Kasai S., and Uehara K.: "Impurity Ion Sputtering for Introducing Metal Impurity in JFT-2 Tokamak", 9th European Conf. on Controlled Fusion and Plasma Physics, (Oxford, 1979).
- 8) Yamamoto T., Funahashi A., Fujisawa N., Iizuka S.<sup>\*\*5</sup>, Kawakami T., Kumagai T., Maeno M., Maeller C.<sup>\*\*16</sup>, Lahaye R.<sup>\*\*16</sup>, Roh T.<sup>\*\*16</sup>, Shoji T., Sugie T., Suzuki N., Takeuchi H., Tanaka Y., Toyama H.<sup>\*\*4</sup>, and Yamauchi T.: "Electron Cyclotron Heating Experiments on the JFT-2 Tokamak", US-Japan Workshop on Physics of High Power RF Heating (Kyoto, 1980).
- 9) Maeda H.: "Improvement of Plasma Characteristics by Metallic Coating in the JAERI Tokamak", Intern. Conf. on Metallurgical Coatings (San Diego, 1979).
- 10) Shimomura Y.: "Poloidal Divertor Experiment in DIVA/JFT-2a", Japan-USSR Joint Seminar on Plasma Diagnostics, (Nagoya, 1979).

- 11) Odajima K., Nagami M., Yamamoto S., Sengoku S., Kimura H., Yamauchi T., Funahashi A., Maeda H., and Shimomura Y.: "Very Low-q Discharge Free from Major Disruption in DIVA", Proc. IAEA Sym. on Current Disruption in Toroidal Devices (Garching, 1979).
- 12) Ohasa K., and DIVA Group: "Research in Method of Obtaining Metallic Impurity Free Plasma in DIVA", IAEA Technical Committee Meeting on Impurities in Tokamak (Alushta, U.S.S.R., 1979).
- 13) Ohasa K., and DIVA Group: "Divertor Experiment in DIVA", IAEA Technical Committee Meeting on Impurities in Tokamak (Alushta, U.S.S.R., 1979).
- 14) Ohasa K., and DIVA Group: "Investigation of Impurity Behaviour in a Boundary Plasma", IAEA Technical Committee Meeting on Impurities in Tokamak (Alushta, U.S.S.R., 1979).
- 15) Ohasa K., and DIVA Group: "Summary of DIVA Experiment", IAEA Technical Committee Meeting on Impurities in Tokamak (Alushta, U.S.S.R., 1979).
- 16) Yamamoto S.: "The DIVA Experiment (I)", Proc. US/Japan Workshop on Divertors, First Wall Materials and Impurity Control, (Tokai, 1980).
- 17) Sengoku S.: "The DIVA Experiment (II)", Proc. US/Japan Workshop on Divertors, First Wall Materials and Impurity Control, (Tokai, 1980).
- 18) Shimomura Y., and Sako K.: "Divertor Concept for INTOR-J and its Engineering Feasibility", Proc. US/Japan Workshop on Divertors, First Wall Materials and Impurity Control, (Tokai, 1980).
- 19) Ohara Y., Akiba M.<sup>\*\*1</sup>, Arakawa Y., Horiike H., Kawai M., Matsuda S., Mizutani Y.<sup>\*8</sup>, Ohga T., Okumura Y., Sakuraba J.<sup>\*9</sup>, Shibata T., Shirakata H., and Tanaka S.: "Ion Source Development at JAERI", Proc. 8th Symp. on Engineering Problems of Fusion Research (San Francisco, 1979) p.198
- 20) Isobe S.<sup>\*3</sup>, Uede T.<sup>\*3</sup>, Shibata T., Shirakata H., and Matsuda S.: "Black Coating Materials for Chevron Baffles of Cryogenic Pumping Panels", Proc. 8th Symp. on Engineering Problems of Fusion Research (San Francisco, 1979) p.533
- 21) Matsuda S., Araki M., Horiike H., Itoh T., Kawai M., Kuriyama M., Matsuoka M., Morita H.<sup>\*7</sup>, Ohara Y., Ohga T., Sakuraba J.<sup>\*9</sup>, Shibata T., Shirakata H., and Tanaka S.: "Prototype Injector Unit For JT-60", Proc. 8th Symp. on Engineering Problems of Fusion

- Research (San Francisco, 1979) p.1383
- 22) Okamoto M.<sup>\*\*2</sup>, Imai T., and Nagashima T.: "Estimation of LHFR-Heating in JFT-2 Tokamak by Numerical Simulation", US-Japan Workshop on Physics of High Power RF Heating (Kyoto, 1980).
  - 23) Murakami Y.: "Review of Fundamental Impurity Studies in JAERI", Proc. US/Japan Workshop on Divertors, First Wall Materials and Impurity Control (Tokai, 1980).
  - 24) Saidoh M., Sone K., Yamada R., and Nakamura K.: "Simultaneous and Continuous Observation of Solid Surfaces under Helium Ion Bombardment", Proc. US/Japan Workshop on Divertors, First Wall Materials and Impurity Control (Tokai, 1980).
  - 25) Yamada R., Nakamura K., Sone K., and Saidoh M.: "Measurement of Chemical Sputtering Yields of Various Types of Carbon", Proc. US/Japan Workshop on Divertors, First Wall Materials and Impurity Control, (Tokai, 1980).
  - 26) Abe T., Obara K., and Murakami Y.: "Conditioning of Graphite Surface by Atomic Hydrogen", Proc. US/Japan Workshop on Divertors, First Wall Materials and Impurity Control (Tokai, 1980).
  - 27) Shimamoto S., Ando T., Hiyama T., Tsuji H., Yoshida K., Tada E., Nishi M., Okuno K., Koizumi K., and Yashukochi K.<sup>\*\*3</sup>: "Cluster Test Facility Construction and Its Future Perspective", Proc. of 8th Symp. on Eng. Problems of Fusion Research, San Francisco, (1979) vol. I, p.269.
  - 28) Ando T., Nishi M., Yoshida K., Tada E., Tsuji H., Hiyama T., Koizumi K., and Okuno K.: "1/4 Cross Section Conductor Test of Japanese LCT Conductor", Proc. of 8th Symp. on Eng. Problems of Fusion Research, San Francisco, (1979) vol. III, p.1436.
  - 29) Shimamoto S., Ando T., Hiyama T., Tsuji H., Yoshida K., Tada E., Nishi M., Okuno K., Koizumi K., Oka K.<sup>\*2</sup>, and Yashukochi K.<sup>\*\*3</sup>: "Japanese Design of a Test Coil for the Large Coil Task", Proc. of 8th Symp. on Eng. Problems of Fusion Research, San Francisco, (1979) vol. III, p.1174.
  - 30) Tsuji H., Shimamoto S., and Yashukochi K.<sup>\*\*3</sup>: "Superconducting Toroidal Magnet for the Next Engineering, Workshop of High Field Superconductor, Tokyo, (1980).
  - 31) Shimamoto S., Ando T., Hiyama T., Tsuji H., Nishi M., Tada E., Yoshida K., Okuno K., Koizumi K., and Yashukochi K.<sup>\*\*3</sup>: "High Field Investigation with the Cluster Test Facility", Workshop of



- High Field Superconductor, Tokyo, (1980).
- 32) Tada E., Nishi M., Ando T., and Shimamoto S.: "Realization of 10 T Multifilamentary Nb<sub>3</sub>Sn Magnet, Workshop of High Field Superconductor, Tokyo, (1980).
  - 33) Takatsu H., Shimizu M.: "Seismic Analysis of the JT-60", Proc. 8th Symposium on Engineering Problems of Fusion Research (San Francisco, 1979).
  - 34) Ogata A., and Ninomiya H.: "Optimal Feedback Control of Plasma Parameters in a Tokamak", IEA Workshop on Computer Control and Data Acquisition, (Tokai, Japan, April, 1979).
  - 35) Yoshikawa M.: "JT-60 project", *ibid.*
  - 36) Ogata A.: "System design", *ibid.*
  - 37) Aikawa H.: "Man-Machine Interface I", *ibid.*
  - 38) Kimura T.: "Man-Machine Interface II", *ibid.*
  - 39) Kondo I.: "Safety and Protection Systems and Instruments", *ibid.*
  - 40) Kumahara T.: "CAMAC System in Control and Data Acquisition of JT-60", *ibid.*
  - 41) Ninomiya H.: "Plasma Control in JT-60", *ibid.*
  - 42) Ogata A., and Ninomiya H.: "Program Control of Current Build-up of a Tokamak", *ibid.*
  - 43) Ogata A., and Ninomiya H.: "System Identification for Plasma Control", *ibid.*
  - 44) Matoba T.: "Software Development for JT-60", *ibid.*
  - 45) Ogata A.: "Amount of Data to be Gathnered in the JT-60 Data Processor", *ibid.*
  - 46) Ogata A.: "Real Time Data Processor Based on Pipeline Technique Using Microprocessors", *ibid.*
  - 47) Ogata A.: "Reliability Analysis of Multiprocessors with Hot Standby Redandance in Discrete-Time System", *ibid.*
  - 48) Ogata A., and Ninomiya H.: "Use of Modern Control Theory in Plasma Control at Neutral Beam Injection", Proc. of 8th Symp. on Fusion Technol., (San Francisco, U.S.A., 1979).
  - 49) Ninomiya H., Shinya K.<sup>\*11</sup>, and Kameari A.<sup>\*5</sup>: "Optimization of Currents in Field-Shaping Coils of a Non-Circular Tokamak", *ibid.*
  - 50) Ninomiya H., Nakamura Y., Ozeki T., Suzuki Y., Kameari A.<sup>\*5</sup>, and Tsuzuki N.<sup>\*11</sup>: "Studies of Eddy Currents in JT-60", *ibid.*

- 51) Matoba T.: "Status of JT-60 Diagnostics", IEA Workshop on Tokamak Diagnostics, (Princeton, USA, March 1980).
- 52) Matoba T., Shiho M., Kimura T., Ogata A., Aikawa H., Nagashima A., Kurihara K., Kondo I., and Suzuki Y.: "JT-60 Project", *ibid.*
- 53) Nagashima A., and Matoba T.: "Electron Density and Temperature", *ibid.*
- 54) Matoba T.: "Multi Pulse Laser", *ibid.*
- 55) Matoba T.: "Optical Fiber Array", *ibid.*
- 56) Matoba T.: "CCD Photo-Detector", *ibid.*
- 57) Kimura T.: "Ion Temperature and Distribution" (JT-60), *ibid.*
- 58) Kimura T.: "Silicon Surface-Barrier Detector for Neutral Particle Measurement", *ibid.*
- 59) Kimura T.: "Small Angle Scattering Method by Neutral Beam Injection for Ion Temperature Measurement", *ibid.*
- 60) Shiho M.: "Power Balance Studies in JT-60", *ibid.*
- 61) Shiho M.: "Power Balance Study, Appendix I, Viewing Ports - JT-60", *ibid.*
- 62) Shiho M.: "Power Balance Study, Appendix II, Arrangement of Diagnostics - JT-60", *ibid.*
- 63) Shiho M.: "MHD Studies in JT-60", *ibid.*
- 64) Ogata A.: "Data Processing and Feedback", *ibid.*
- 65) Kimura T.: "Diagnostic/Tokamak Interface Design Problems", *ibid.*
- 66) Tani K., Kishimoto H., and Tamura S.: "Neutral Beam Injection for JT-60", IAEA Tech. Committee Meeting and Workshop on the Plasma Phys. of Intense Neutral Beam Heating in Tokamaks (ORNL. U.S.A., 1979).
- 67) Tani K., Kishimoto H., and Tamura S.: "Ripple Loss of Fast Ions in a Large Tokamaks", Proc. 9th European Conf. on Controlled Fusion and Plasma Physics, Oxford, Vol.1 (1979) 157.
- 68) Tamura S., Shimada R., Shibata T.<sup>\*11</sup>, and Koyanagi K.<sup>\*11</sup>: "AC Voltage Behavior of Poloidal Field Power Supply System for JT-60", 8th Symp. on Engineering Problems of Fusion Research (San Francisco, 1979).
- 69) Tamura S., Shimada R., Sasaki T.<sup>\*11</sup>, Shibata T.<sup>\*11</sup>, Sato Y.<sup>\*11</sup>, and Fuziwara N.<sup>\*11</sup>: "Development of JT-60 DC Power Supply Equipment", *ibid.*
- 70) Arakawa K., Shimada R., Kishimoto H., Tamura S., Yabuno K.<sup>\*3</sup>, Ishigaki Y.<sup>\*3</sup>, and Saito R.<sup>\*3</sup>: "Design of JT-60 Grounding System", *ibid.*

- 71) Arakawa K., Shimada R., Kishimoto H., Tamura S., Yabuno K.<sup>\*3</sup>,  
Ishigaki Y.<sup>\*3</sup>, and Saito R.<sup>\*3</sup>: "Fault Current Analysis in JT-60  
Grounding System", *ibid.*
- 72) Arakawa K., Shimada R., Kishimoto H., Tamura S., Nishimura H.<sup>\*3</sup>,  
Takahashi T.<sup>\*3</sup>, Yabuno K.<sup>\*3</sup>, and Ito S.<sup>\*3</sup>: "Numerical Analysis of  
Potential Rise in JT-60 Grounding System", *ibid.*
- 73) Shimada R., Arakawa K., Ogata A., and Taoka H.<sup>\*11</sup>: "CAMAC System  
for JT-60 Poloidal Field Power Supply Control", *ibid.*
- 74) Nagami M., Seki S., Konoshima S., Kitsunozaki A., Yokomizo H. and  
Shimada M.: "Single Wall Poloidal Divertor Experiment in Doublet-III",  
US/JAPAN Seminar on Divertor Workshop, First Wall Materials and Impurity  
Control (Tokai, 1979)
- 75) Kitsunozaki A., Fujisawa N., Konoshima S., Nagami M., Seki S., Yokomizo H.,  
Shimada M., Ohara Y., et al. "Joule Heating Dee Experiment in Doublet-  
III", DOE Physics Review Meeting (San Diego, USA, 1979)
- 76) Nagami M., Fujisawa N., Yokomizo H., Shimada M., Konoshima S., Ohara Y.,  
et al.: "Divertor Experiment in Doublet-III", *ibid.*
- 77) Kitsunozaki A., Konoshima S., Nagami M., Seki S., Shimada M. and  
Yokomizo H.: "Preliminary Results of Joule Heating Dee-Shaped Plasma  
Experiment in Doublet-III", APS 21'st Annual Meeting, (Boston, USA, 1979)
- 78) Kitsunozaki A., Konoshima S., Seki S., Nagami M., Yokomizo H. and  
Shimada M.: "Dee Experiment IN Doublet-III", DOE Physics Review Meeting  
(San Diego, USA, 1979)

## A.2 Personnel of the Center

## A.2.1 Number of the staff of the Divisions

|                             | FY 1978 | FY 1979 | FY 1980          |
|-----------------------------|---------|---------|------------------|
| Regular staff <sup>*1</sup> | 140     | 162     | 169              |
| Staff on loan               | 27      | 20      | 20 <sup>*2</sup> |
| Guest scientist             | 7       | 3       | 3 <sup>*3</sup>  |
| Scholarship fellow          | 30      | 5       | 5                |

\*1 Including scientists, technicians, and secretaries.

\*2 Two from Hitachi Ltd.

Two from Mitsubishi Atomic Power Ind. Inc.

Two from Mitsubishi Electric Co., Ltd.

Three from Mitsubishi Heavy Ind. Ltd.

One from Nissin Electric Co., Ltd.

Four from Tokyo Shibaura Electric Co., Ltd.

One from ULVAC Co.

One from Hitachi Cable Co.

One from Kawasaki Heavy Ind. Ltd.

One from Tokyo Information System Co., Ltd.

Two from Fuji Electric Co., Ltd.

\*3 Two from the University of Tokyo.

One from Nihon University.

## A.2.2 List of Scientific Staffs and Officers during FY 1979

## Fusion Research and Development Center

MORI Sigeru (Center Director)

## (A) Division of Thermonuclear Fusion Research

OBATA Yukio (Head)

TANAKA Masatoshi (Deputy Head) (June 1979 ~)

AKAMA Kouzou (Administrative Manager (~ June 1979)

HAYASHI Takashi (Administrative Manager) (June 1979 ~)

Plasma Theory Laboratory

AZUMI Masafumi  
ITOH Kimitaka<sup>\*\*4</sup> (Scholarship fellow)  
KURITA Gen-ichi  
NISHIKAWA Ken-ichi<sup>\*\*2</sup> (Scholarship fellow)  
TAKEDA Tatsuoki (Senior Scientist)  
TAKIZUKA Tomonori  
TANAKA Masatoshi (Chief)  
TOKUDA Shinji  
TSUNEMATSU Toshihide  
TUDA Takashi

Experimental Plasma Physics Laboratory

TANAKA Yuji (Chief)

\* JFT-2

FUJISAWA Noboru (Senior Scientist)  
MAENO Masaki  
SUZUKI Norio  
YAMAMOTO Takumi  
IIZUKA Satoru<sup>\*\*5</sup> (Scholarship fellow)

\*JFT-2a/DIVA

KIMURA Haruyuki  
MAEDA Hikosuke  
MATSUDA Toshiaki  
MATSUMOTO Hiroshi  
ODAJIMA Kazuo  
OHASA Kazumi  
SENGOKU Seio  
SHIMOMURA Yasuo (Senior Scientist)  
YAMAMOTO Shin

\* Diagnostics

FUNAHASHI Akimasa (Senior Scientist)  
KASAI Satoshi  
KAWAKAMI Tomohide  
KUMAGAI Katsuaki  
SUGIE Tatsuo

TAKAHASHI Koki

TAKEUCHI Hiroshi

YAMAUCHI Toshihiko

\* JFT-2M

SHOJI Teruaki

KAMOTO Satoru<sup>\*6</sup>

Facility Operation and Engineering Section

ANNO Katsuto

HASEGAWA Kouichi

HIRATSUKA Hajime

ISAKA Masayoshi

KAZAWA Minoru

KIKUCHI Kazuo

KUNIEDA Shunsuke (Chief)

MATSUZAKI Yoshimi

OKANO Fuminori

SHIBATA Takatoshi

SHIINA Tomio

SUNAOSHI Hidenori

SUZUKI Kihachiro (Deputy Chief)

TANI Takashi

TOYOSHIMA Noboru

YOKOKURA Kenji

YOKOYAMA Kenji

Plasma Heating Laboratory

SHIRAKATA Hirofumi (Chief)

\* Neutral Beam Injection Heating

AKIBA Masato<sup>\*\*1</sup> (Scholarship fellow)

ARAKAWA Yoshihiro

ARAKI Masamori

HORIIKE Hiroshi

ITOH Takao

KAWAI Mikito

KURIYAMA Masaaki

MATSUDA Shinzaburo

MATSUOKA Mamoru  
MIZUTANI Yasuhiko<sup>\*8</sup>  
MORITA Hiroaki<sup>\*7</sup>  
OHARA Yoshihiro  
OHGA Tokumichi  
OKUMURA Yoshikazu  
SAKURABA Junji<sup>\*9</sup>  
SHIBATA Takemasa  
TANAKA Shigeru

\* Radiofrequency Heating

FUJII Tuneyuki  
IMAI Tsuyoshi  
NAGASHIMA Takashi (Senior Scientist)  
UEHARA Kazuya

Superconducting Magnet Laboratory

ANDO Toshinari  
HIYAMA Tadao  
KOIZUMI Koichi  
OKA Kouich<sup>\*2</sup>  
OKUNO Kiyoshi  
NISHI Masataka  
SHIMAMOTO Susumu (Chief)  
TADA Eisuke  
TSUJI Hiroshi  
YOSHIDA Kiyoshi

Plasma Engineering Laboratory

MURAKAMI Yoshio (Chief)  
NAKAMURA Kazuyuki  
OHTSUKA Hidewo  
SAIDOH Masahiro  
SONE Kazuho  
YAMADA Rayji

Tritium Engineering Laboratory

KINOSHITA Masahiro  
MATSUDA Yuji  
NARUSE Yuji (Principal Scientist)

OBATA Yukio (Chief)  
SHIMIZU Toku  
TACHIKAWA Katsuhiro  
TANAKA Kichizo (Senior Scientist)  
YOSHIDA Hiroshi

Fusion Reactor System Laboratory

IIDA Hiromasa  
IOKI Kimihiro<sup>\*5</sup>  
MAKI Koichi<sup>\*3</sup>  
MINATO Akio<sup>\*4</sup>  
NISHIDA Hidetsugu<sup>\*10</sup>  
SAKO Kiyoshi (Chief)  
SEKI Yasushi  
TONE Tatsuzo (Senior Scientist)  
YAMAMOTO Takashi<sup>\*1</sup>  
YAMATO Harumi<sup>\*11</sup>

(B) Division of Large Tokamak Development

ISO Yasuhiko (Head)  
YOSHIKAWA Masaji (Deputy Head)

Large Tokamak Administration Section

SAITO Jo (Chief)  
YOSHIKAWA Kiyoshi (Deputy Chief)

JT-60 Program Office

HIRAOKA Toru (Chief)

\* Planning and Coordinating Group

KASAHARA Yuko  
KISHIMOTO Hiroshi (Senior Scientist)  
NINOMIYA Hiromasa  
SUZUKI Kunihiro  
TOKUTAKE Toshikuni

\* Plasma Analysis Group

HIRAYAMA Toshio  
KUROKI Tetsuzan  
TAZIMA Teruhiko



\* Doublet-III Experiment Group

IOKI Kimihiro<sup>\*5</sup>  
KASAI Masao<sup>\*5</sup>  
KONOSHIMA Shigeru  
KITSUNEZAKI Akio  
NAGAMI Masayuki  
OZAKI Norihiko<sup>\*3</sup>  
SAKAMOTO Hiroki<sup>\*7</sup>  
SEKI Shogo  
SHIMADA Michiya  
SHINYA Kichiro<sup>\*11</sup>  
SUGAWARA Toru<sup>\*11</sup>  
SUGIHARA Masayoshi  
YOKOMIZO Hideaki

JT-60 Project Office I

TAMURA Sanae (Chief)  
SUZUKI Yasuo (Deputy Chief)

\* Power Supplies Group

AOYAGI Tetsuo  
ARAKAWA Kiyotsugu  
HOSHINO Katsumichi  
MIYA Naoyuki<sup>\*\*3</sup> (Scholarship fellow)  
SHIBATA Toshiaki<sup>\*11</sup>  
SHIINA Minoru  
SHIMADA Ryuichi  
TAKAHASHI Shunji  
TANI Keiji  
TSUNEOKA Masaki  
YOSHIDA Hidetoshi  
YOSHIDA Yasuo<sup>\*6</sup>

\* Control Group

AIKAWA Hiroshi  
KANAMORI Takahiro<sup>\*3</sup>  
KIMURA Toyoaki  
KONDO Ikuo  
KURIHARA Kenichi  
MATOBA Tohru (Senior Scientist)

NAGASHIMA Akira  
NAGAYAMA Yoshio<sup>\*\*4</sup> (Scholarship fellow)  
OGATA Atsushi (Senior Scientist)  
SHIHO Makoto

JT-60 Project Office II

IIJIMA Tsutomu (Chief)  
TOMIOKA Hideo (Deputy Chief)

\* Machine Group

ANDO Toshiro  
KAWASAKI Kozo  
MIKI Nobuharu  
MIYAUCHI Yasuyuki  
NAKAMURA Hiroo  
NAKAMURA Yukiharu  
NISHIO Satoshi  
OHKUBO Minoru  
OHTA Mitsuru (Senior Scientist)  
OZEKI Takahisa  
SATO Osamu  
SEIMIYA Munetaka  
SHIMIZU Masatsugu  
TAKATSU Hideyuki  
TOYOSHIMA Noboru  
TSURUMI Satoshi<sup>\*3</sup>  
YAMAMOTO Masahiro

\* Auxiliary Facilities Group

AMANO Shigeru<sup>\*12</sup>  
ARAI Takashi  
HIRUTA Kazuharu  
HOSODA Ryujiro  
KODAMA Kozo  
IKAWA Ken<sup>\*1</sup>  
OGIWARA Norio  
OIKAWA Akira

\* Vacuum Technology Group

ABE Tetsuya  
OBARA Kenjiro

(C) Office of Fusion Program

MATSUI Takashi (Administrative Manager)

INOUE Kenji

TAKEDA Takashi

KUROIWA Katsuhiko

TAZIMA Yasuhide

Guest Scientists

IEDA Masayuki (Nagoya University)

MIYAMOTO Goro (The University of Tokyo)

TUZI Yutaka (The University of Tokyo)

YASUKOCHI Ko (Nihon University)

On leave from

- \*1 Fuji Electric Co., Ltd.
- \*2 Hitachi Cable Co.
- \*3 Hitachi Ltd.
- \*4 Kawasaki Heavy Ind. Ltd.
- \*5 Mitsubishi Atomic Power Ind. Inc.
- \*6 Mitsubishi Electric Co., Ltd.
- \*7 Mitsubishi Heavy Ind. Ltd.
- \*8 Nissin Electric Co., Ltd.
- \*9 Sumitomo Heavy Ind. Ltd.
- \*10 Tokyo Information System Co., Ltd.
- \*11 Tokyo Shibaura Electric Co., Ltd.
- \*12 ULVAC Co.
- \*13 Fujitsu Ltd.
- \*14 Sumitomo Electric Co., Ltd.
- \*15 Century Research Center Co.
- \*16 General Atomic Co.
- \*17 Kozo Keikaku Eng. Inc.

- \*\*1 Kyushu University
- \*\*2 Nagoya University
- \*\*3 Nihon University
- \*\*4 The University of Tokyo
- \*\*5 Tohoku University
- \*\*6 Hiroshima University

- \*\*7 Kyoto University  
 \*\*8 Princeton University  
 \*\*9 Oak Ridge National Laboratory  
 \*\*10 National Institute for Researches in Inorganic Materials

## A.3 Budget of the Center

(unit: Million ¥)

|   | FY <sup>*1</sup> 1978 | FY <sup>*1</sup> 1979  | FY <sup>*1</sup> 1980     |
|---|-----------------------|------------------------|---------------------------|
| Scientific program                      | 9,391.8 <sup>*2</sup> | 22,751.2 <sup>*2</sup> | 28,813.9 <sup>*2</sup>    |
| (excluding Staff & administrative cost) | (14,335.7)            | (25,558.7)             | (24,147.0 <sup>*3</sup> ) |
| Building                                | 1,155.5               | 16,900.1               | 19,968.7                  |
| Site                                    |                       | 1,723.0                | 2,520.3                   |

\*1 From April to March.

\*2 Including cashing of the financial obligation in each FY.

\*3 The total financial obligation from FY 1980 to FY 1983 for the construction of part of the components of JT-60 and for the development of plasma heating systems and superconducting magnet.